Université d'Ottawa · University of Ottawa

AXIAL LOAD TESTS AND ANALYSIS FOR OPEN-ENDED STEEL TUBULAR PILES DRIVEN INTO WEATHERED ROCK

by

Yi HAN

A thesis
submitted to the School of Graduate Studies and Research
under the supervision of

Dr. Erman Evgin

in partial fulfillment of the requirements for the degree of
Master in Applied Sciences in Civil Engineering

Department of Civil Engineering
University of Ottawa
Ottawa, Ontario, Canada

October 1999

The Master in Applied Sciences in Civil Engineering is a joint program between Carleton University and the University of Ottawa, which is administered by the Ottawa-Carleton Institute for Civil Engineering.

0-612-46582-9

ABSTRACT

The bearing capacity of tubular, open-ended steel piles driving into weathered rock was investigated using static load tests, finite element analysis and dynamic load tests. Dynamic load tests were carried out by using the Case Method and the CAPWAP Method which were used to determine the bearing capacity of piles. The effects of final set, pile burial length, setup and other factors on the pile bearing capacity were evaluated. In the static load tests, two piles with 0.813 m diameter and one pile with a diameter of 1.0 m were tested. The finite element analysis was performed to back calculate the load-displacement response of piles. A hyperbolic model for soils and an elastic-plastic model for rocks were used in the study. A parametric study was also carried out. The issues, such as the effects of pile installation and soil plug, were discussed.

ACKNOWLEDGMENTS

My special thanks go to Dr. Erman Evgin, the thesis supervisor. Without his support and encouragement, I know that I would never be able to complete the program. His guidance, invaluable suggestions and comments are gratefully acknowledged, and, especially, his warm heart that I could always feel during the entire period of my study at University of Ottawa will never be forgotten.

A word of thanks is also extended to Dr. Saatcioglu and Dr. Tanaka for their help in my education during my graduate study, and to all the supporting staffs in Civil Engineering.

I dedicate this thesis to my daughter, Julia, my son, Eric and my wife, Lanying.

SUMMARY

The ultimate bearing capacity of tubular, open-ended steel piles driving into weathered rock in a foundation project was investigated by static load tests, finite element analysis and pile dynamic load tests. Three piles were selected for the static load tests. Two piles were selected for the finite element analysis. Two groups of piles with different size were selected for the dynamic load tests. All design methods and load testing methods are reviewed.

During the pile installation, dynamic load tests were carried out by using the Case Method as performed by a Pile Driving Analyser (PDA) on the selected piles. The CAPWAP Method was also used in conjunction with the PDA. The dynamic load tests were conducted during the initial driving of piles, and, for small number of piles, during the restriking of piles. The dynamic load tests provided information about the driving force, the integrity of piles, the static bearing capacity at initial pile driving, and the ultimate load bearing capacity of piles at redriving, including shaft resistance and toe resistance. In the investigation, the ultimate resistance by the CASE Method and CAPWAP Method were determined, and the effects of final set, pile burial length, setup and other factors on the pile bearing capacity were evaluated.

The program of static load tests was planned to investigate the bearing mechanism of the open-ended tubular piles driven into the weathered bedrock. Three piles with a diameter of 0.813 m and 1.0 m, respectively, were tested. Vertical compression tests were performed on all three piles, and tension tests were carried out on two piles. The initial plan was to carry out the static load tests on two piles with different diameters. However, the second test pile failed the design criteria in terms of residual displacement, which led to another test on a pile with a diameter of 0.813 meter. The results of the compression load tests and tension load tests were evaluated, in terms of loads, displacements and time. The performance of the piles in the load tests was analysed and the analysis results were provided in the investigation.

The details of the finite element analysis have been presented for the work of the back-calculation of the load-displacement response of open-ended steel tubular piles driven through clay soil layers into weathered bedrock. An attempt was made to assess, qualitatively, the finite-element model as a rational approach to the analysis of pile load-displacement response. A finite-element model for the soil-pile system was designed and simulations were conducted. A hyperbolic model for soils and an elastic-plastic model for rocks were used in the study. All major parameters were obtained based on the results of the field and laboratory tests or from various engineering handbooks. A parametric study was also carried out. The issues, such as the effects of pile installation and soil plug, were discussed.

TABLE OF CONTENTS

LIST OF TABLES

LIST OF FIGURES

Chapter 1

INTRODUCTION

1.1 Background

In deep foundation engineering, piles are used to transfer loads from the superstructure through weak compressible strata or through water, onto stiffer and less compressible soils or onto rock. Pile foundations are widely used in marine structures, tall structures, bridge structures and offshore structures. As foundations, piles are designed to carry axial loads, including compression and uplift loads, as well as lateral loads.

In the pile design, it is necessary to consider an adequate safety margin against ultimate failure of the ground and adequate margin against excessive pile movements that would impair the serviceability of the structure.

In the past, various methods have been developed to evaluate the pile behavior in different situations of loading, pile materials, construction methods and ground conditions. Most of the methods related to driven piles are reviewed in this study, in terms of the axial bearing capacity and displacement of a pile.

In almost all-important projects, the best way to determine pile behavior is to carry out full-scale load tests on representative piles to obtain suitable parameters and to verify the design assumptions.

In this project, most major testing methods were employed to assess the behavior of open-ended steel tubular pile driven through the clay layers into the highly decomposed bedrock. The methods employed include dynamic load tests, static load tests, site investigation and a numerical analysis.

1.2 Objectives

The objectives of the study are:

(1) To evaluate the axial load capacity of open-ended steel tubular piles driven through clay layers into decomposed bedrock; and

(2) To determine the magnitude of pile head displacement at the specified working loads.

These objectives are achieved by dividing the work in two phases.

In the first phase, the axial load capacity of the pile was determined by carrying out various site investigation tests, dynamic load tests and static axial load tests.

In the second phase, the load-displacement response of a single pile was back-calculated by using a non-linear finite element analysis.

The following issues have been reviewed and discussed:

1. Evaluation and determination of the pile bearing capacity from static load tests;
2. Evaluation and determination of the pile bearing capacity from dynamic load tests, including the shaft resistance and toe resistance;
3. Evaluation of the results from site investigation;
4. Back-calculation of the load-displacement response by the finite element method;
5. Comparison of the pile axial bearing capacities determined from different testing methods and numerical analysis;
6. The set-up of the pile bearing capacity after pile installation by dynamic load test;
7. Discussion of the formulation of soil plug and its contribution to the bearing capacity of a pile;
8. Evaluation of time effect of sustained loads on the bearing capacity of a pile;
9. Discussion of the relation of the bearing capacity of a pile and the pile driving equipment.

1.3 Use of Steel Tubular Piles in Practice

Steel pile foundations are frequently used for high-rise buildings, bridges and offshore petroleum production platforms, as well as waterfront structures.

Compared to piles of other materials, steel piles have the advantages of being robust, light to handle, and capable of carrying large compressive loads when driven into a hard stratum. They can be driven deep to reach a hard stratum or to develop a high shaft resistance, although their cost is high. They can be designed as small displacement piles. They can be readily cut down and extended where the level of the bearing stratum varies. The pile head, which usually buckles during driving, can be cut down and re-trimmed for further driving. They have a good resilience and high resistance to bucking and bending forces.

Steel tubular piles are preferred for marine structures where they can be fabricated and driven in large diameters to resist the axial and lateral forces in deep water structures.

This work presents the studies carried out for a real-life project. The project was for the construction of the quay deck of a wharf. The quay deck is composed of more than 1230 steel tubular piles driven into weathered bedrock. More information about the project is presented in Chapter 4, The Foundation Project.

1.4 Scope of the Study

The following outlines the scope of the work:

1. The site investigation, including the in-situ tests and laboratory tests to find out the physical and mechanical characteristics of the ground;

2. The dynamic load tests: Pile Driving Analyzer (PDA) tests and the analysis by CASE and CAPWAP methods;

3. The static axial load tests for three selected piles, and

4. The finite element analysis.

1.5 Outline of Work

Chapter 2 presents a review of literature on the general methods for determining the axial load bearing capacity and displacement of a pile.

Chapter 3 details the background and applications of the dynamic load test method and the static load method in determining the pile axial load capacity.

Chapter 4 provides information about the foundation project in terms of the geotechnical conditions, pile characteristics and piling equipment.

Chapter 5 gives information on the static load tests and provides evaluation of the test results.

Chapter 6 describes the finite element analysis, in which the measured load-displacement response of a pile is back calculated.

Chapter 7 describes the dynamic load tests in this project and provides evaluation of the test results.

Chapter 8 presents the summary and conclusions of the study.

Chapter 2

PILE DESIGN

2.1 General

The pile design should consider the requirements throughout their service life for adequate safety against bearing capacity failure of the ground and adequate margin against excessive pile movements that would impair the serviceability of the structure. The required factor of safety depends on the importance of the structure, consequence of failure, reliability and adequacy of information on ground conditions, sensitivity of the structure, nature of the loading, local experience, design methodologies, number of representative preliminary pile load tests, etc.

Pile design methods can be divided into the following categories:

1. Semi-empirical correlation with in-situ test results,
2. Rational methods based on simplified soil mechanics or rock mechanics theories,
3. Advanced analytical (or numerical) techniques, and
4. Empirical "rule of thumb".

The satisfactory performance of a pile is, in most cases, governed by the limiting acceptable deformation under various loading conditions.

As being defined in the project, this chapter will review the pile design methods in relation to the axially loaded piles.

2.2 Axial Capacity of Pile in Soil

In the evaluation of the ultimate bearing capacity of an axially loaded pile driven in soil, a number of methods are available:

1. Pile driving formulae for driven piles,
2. Wave equation analysis for driven piles,
3. Calculation methods based on simplifying soil and rock mechanics principles,
4. Correlation with in-situ tests, such as Standard Penetration Tests (SPT).

2.2.1 Pile Driving Formulae

Pile driving formulae relate the ultimate bearing capacity of driven piles to the final set (i.e. penetration per blow). Various formulae have been proposed, such as the Hiley

Formula or Dutch Formula, which are generally based on the principle of conservation of energy, not the actual energy. The inherent assumptions made in some formulae pay little regard to the actual forces that develop during driving, or the nature of the ground and its behavior. The approach is fundamentally incorrect, (Geotechnical Foundation Engineering Manual, 1992).

The Hiley Formula has been widely used for the design of driven piles. The formula is as follows:

$$R_d = \frac{\eta_h W_h d_h}{(s^* + \frac{c^*}{2})} \qquad (2\text{-}1)$$

where

R_d = driving resistance

η_h = efficiency of hammer (allowing for energy loss on impact)

W_h = weight of hammer

d_h = height of fall of hammer

s^* = permanent set of pile

c^* = elastic or recoverable movement of pile

A common requirement is that the final set should not be less than 2.5 mm/blow, unless the pile is founded on rock, in an attempt to avoid over-driving.

Like other driving formulae, Hiley's formula does not account for the rate at which the soil is sheared during pile driving and therefore cannot differentiate between cohesive and granular soils. The high strain rates in cohesive soils during pile penetration can cause the viscous resistance of the soil to be considerably greater than the static capacity of the pile. Poskitt (1991) shows that without considering soil damping, the driving resistance can be overestimated by several folds.

Driven piles in dense soils may cause dilation that can result in false sets. This is likely to happen particularly in dense silty sands or sandy silts when dilation causes negative pore water pressures followed by a reduction in toe resistance when they are dissipated.

The final set of a pile, where the piling formula has been calibrated against satisfactory static load test results and corresponding borehole information, will be useful as a site control measure. Experience suggests that driving to a pre-determined target set by a pile driving formula can help to ensure no 'slack' in the pile-soil system compared to the case of driving the pile to a pre-determined length only.

2.2.2 Wave Equation Analysis

A wave equation analysis based on the theory of wave propagation can be undertaken to assess pile behavior during driving. The reliability of the results depends on the appropriateness of the model and the accuracy of the input data, including the ground properties. Generalized information on hammer characteristics is often used in the analysis. Alternatively, site measurements may be made to determine the boundary conditions and calibrate the results for the hammer system and particular geological conditions. Essentially, this approach allows an estimate of pile bearing capacity and an evaluation of pile drivability and assists in hammer selection. Typical solutions from a wave equation analysis are in the form of capacity versus penetration resistance curves, and predicted maximum stresses in the pile.

It should be noted that the rated hammer energy can differ substantially from actual performance, and some soil parameters pertaining to wave equation analysis are 'model dependent' empirical values and may not be measured directly. The analysis should only be used to provide general guidance on likely pile behavior.

More information associated with the wave equation analysis will be provided in the section regarding the dynamic load tests.

2.2.3 Use of Soil Mechanics Principles

The axial capacity of a pile may be assessed using soil mechanics principles. The capacity may be estimated by summing the shaft resistance and toe resistance of the pile (Geotechnical Foundation Engineering Manual, 1992).

$$R = \sum_{z=0}^{L} C\, q_s\, \Delta z + A_t\, q_b \qquad (2\text{-}2)$$

where the pile circumference C and embedded length L is subdivided into segments of length Δz and the pile toe area A_t. q_s is the unit shaft resistance and q_b is the unit toe resistance.

(1) Driven Piles in Cohesionless Soils

Based on plasticity theories, the ultimate unit toe resistance, q_b, for piles in granular soils may be expressed in terms of vertical effective stress, σ_b', at the pile base, and the bearing capacity factor, N_t, as

$$q_b = N_t\, \sigma_b' \qquad (2\text{-}3)$$

The toe bearing capacity factor N_t depends on soil composition in terms of grain size distribution, angularity and mineralogy of the grains, natural soil density, density changes due to pile installation, and other factors. Typical ranges of values for N_t are provided in any pile design handbook.

The unit shaft resistance, q_s, for piles in cohesionless soils may be expressed in terms of effective stresses as follows:

$$q_s = c' + K_s\, \sigma_v' \tan \phi' \tag{2-4}$$
$$q_s = \beta\, \sigma_v' \text{ (when } c' \text{ is assumed to be zero)} \tag{2-5}$$

where

K_s = coefficient of horizontal pressure which depends on the relative density and state of the soil, method of pile installation, and material, length and shape of the pile

c' = adhesion between soil and pile. For cohesionless soils, it can be assumed that $c' = 0$.

σ_v' = mean vertical effective stress

ϕ' = angle of friction along pile/soil interface

β = a combined shaft resistance factor

All pile design handbooks provide means and tables for the values of the factors, K_s, ϕ' and β.

For driven piles, the selection of design parameters should reflect the pile-soil system involving effects of densification and increase in horizontal stresses in the ground due to pile driving.

(2) Piles in Cohesive Soils

Design handbooks recommend that both the undrained and effective stress methods can generally be used for the design of piles in cohesive soil. The effective stress method is the same as used for pile analysis in cohesionless soils. The use of the undrained method relies on an adequate local database of test results. In the case where piles are subject to significant variations in stress levels after installation (e.g. excavation, rise in groundwater table), the use of the effective stress method is recommended, taking due account of the effects on the K_s values due to the stress changes.

The toe resistance for piles in clays is often related to the undrained shear strength of the clay at the pile toe, τ_u, as follows

$$q_b = N_t\, \tau_u \tag{2-6}$$

N_t, bearing capacity factor, is a function of pile diameter. It has values varying from 6 to 9 depending on the pile diameter (Canadian Foundation Engineering Manual, 1992).

The ultimate shaft resistance (γ_s) of piles in stiff over-consolidated clays can be estimated based on the semi-empirical method as follows (GEO, 1996):

$$\gamma_s = \alpha\, \tau_u \tag{2-7}$$

where α is the adhesion factor. In the above equations, the τ_u is generally determined from unconsolidated undrained triaxial compression tests.

2.2.4 Correlation with Standard Penetration Tests

Semi-empirical correlations have been developed relating both shaft resistance and toe resistance of piles founded in granular soils to N values. Such a procedure would provide an approximate means of allowing for variability of the strata across a site in normalizing and extrapolating the results of load tests. In most of the correlation that have been established, the N values generally refer to uncorrected values before pile installation.

Meyerhof (1986) proposed that the ultimate toe resistance of piles in granular soils may be estimated from average SPT N values near pile toe corrected for an effective overburden pressure of 100 kPa using the approximate relationship for both driven and bored piles in granular soils. For piles exceeding 0.5 m base diameter, an empirical reduction factor, r_b, should be used.

As for the skin friction, for piles driven into granular soils, results presented by Meyerhof (1976 and 1986) are scattered and indicate that the average skin friction generally ranges from 1.5 N_1 to 7 N_1 (kPa), for SPT N_1 values up to about 30, where N_1 is the mean SPT N value corrected for an effective overburden pressure of 100 kPa. He suggested that the average skin friction might be taken as 2 N_1 (kPa) for driven piles in sand.

The design method involving correlation with SPT results is empirical in nature, and the level of confidence is not high particularly where the scatter in SPT N values is large. If load tests on preliminary piles are not carried out, this design approach should be checked using the effective stress method based on soil mechanics principles, and the smaller calculated capacity adopted for design.

Piles may, as well, be designed based on correlations with other types of insitu tests such as cone penetration tests, pressuremeter tests and dilatometer tests.

Cone penetration tests are best suited for silts and sands that are loose to medium dense (such as hydraulically-placed fill and alluvial sands) but may meet premature refusal in dense sands and gravels. The test is generally unsuitable in weathered rocks.

Semi-empirical methods have been developed relating results of Static Cone Penetration Tests (i.e. Dutch Cone or piezocones) to the bearing capacity of piles.

2.2.5 Axial Capacity of Piles in Rock

For the ideal model of a long pile constructed through soil and founded on rock, the degree of load transfer in the portion of the pile shaft embedded in soil will depend on the amount of relative movement arising from base deflection and elastic compression of the shaft, i.e. it will be a function of the relative shaft and base stiffness. In a highly weathered rock layer, the distribution of load in the pile is likely to be complex and may be highly variable.

The settlement of piles founded on rock that have been designed on the basis of bearing capacity theories should always be checked as this is generally the governing factor in, for example, weak rocks, closely-fractured rocks and moderately to highly weathered rocks.

Driven Piles on Rock

The capacity of a driven pile in rock should be confirmed based on driving observations, local experience and load tests. When piles are driven onto or into rock, the exact area of contact with rock, the depth of penetration into rock, and the quality of rock at the foundation level is largely unknown. Consequently, the determination of the capacity of such foundations using theoretical or semi-empirical methods cannot be made with certainty.

Where the joints are widely spaced and closed, very high loads can be sustained by the rock mass and the design is unlikely to be governed by bearing capacity of the ground. In such ground conditions, piles driven to refusal can be designed based on permissible structural stresses of the pile section. Where the joints are open or clay-filled, the rock mass below the pile tip may yield under load. The assessment of the load deformation properties of such rock mass can be made using the empirical relationships developed by Barton (1986).

Correlation reported in the literature between SPT results and the toe resistance of a pile could not be used in this study because the piles were driven into the bedrock. For the same reason, the method developed by Fellenius was not applicable in the present study.

2.3 Uplift Capacity Of Piles

2.3.1 Piles in Soil

Some published test results indicate that the shaft resistance in uplift tests is less than the corresponding shaft resistance in compression, possibly by up to 50% less in a granular soil. Fellenius (1989) suggested that this might be due to the influence of the reduction in vertical effective stress in the ground and Poisson's ratio effect under tension loading.

Fleming et al. (1992) considered that the interpretation of many pile load tests took insufficient account of the residual stresses that existed after pile installation, and consequently the toe resistance of the pile was under-estimated and the shaft resistance was over-estimated. They suggested that there is no systematic difference in the shaft resistance that may be mobilized by an unstressed pile loaded in either tension or compression.

Premchitt et al. (1988) observed that the pattern of residual stresses developed after pile driving was complex and erratic. Therefore, it is difficult to generalize for design purposes. It was noted by Premchitt et al. that the residual shaft resistance and toe resistance locked in after pile driving were not associated with well-defined displacements or an applied loading. Furthermore, the consideration of the shaft resistance associated with the applied loading in a load test (i.e. zeroing the instrumentation immediately prior to a load test) represents the condition of actual working piles supporting superstructure loads. With driven piles, a number of researchers have also emphasized the importance of the dependence of radial horizontal stresses and shaft resistance on the relative position of the pile toe as the pile is advanced, based on observations made in instrumented piles (e.g. Lehane, 1992; Lehane et al, 1993).

For design purposes of driven piles, in view of the uncertainties associated with the distribution of residual stresses after driving and the available capacity having already been partially mobilized, it is recommended that the shaft resistance under tension be taken conservatively as 75% of that under compression, unless higher values can be justified by a sufficient number of load tests.

For relatively slender piles, such as mini-piles, the tendency for the pile to contract radially under tension may lead to lower radial stresses and hence reduce shaft resistance. Fleming et al (1992) estimated that this reduction might amount to 10% to 20%.

Any possible suction effects that may develop at the toe of a pile should be disregarded for prudence, as this may not be reliable.

The working load under tension loading, Q_{wt}, is given by the following:

$$Q_{wt} = (Q_s/F_s) + W_p' \qquad (2\text{-}8)$$

where

Q_s = ultimate shaft resistance under tension
F_s = factor of safety
W_p' = effective self weight of the pile

It is recommended that a minimum factor of safety of 2.5 to 3.5 should be provided on the ultimate shaft resistance in tension.

2.4 Settlement of Single Piles

2.4.1 General

Various analytical techniques have been developed to predict settlements of piles. These techniques provide a convenient framework for deriving semi-empirical correlations between equivalent stiffness parameters back-analyzed from load tests and index properties of the ground. Some of the analytical methods can also be extended to evaluate pile interaction effects in an approximate manner, thus enabling an assessment of pile group behavior to be made within the same framework.

2.4.2 Axial Loading

The various approaches that have been proposed for predicting pile settlement can be broadly classified into three categories:

- Load transfer methods,
- Elastic continuum methods, and
- Numerical methods.

In calculating movements, the stiffness of the founding materials at the appropriate stress level needs to be determined. For normal pile working loads (of the order of 40% to 50% of ultimate capacity), Poulos (1989) has shown that the non-linear nature of soil behavior generally does not have a significant effect on the load-settlement relationship for single piles.

(1) Load Transfer Method

In the load transfer method proposed by Coyle and Reese (1966) for piles in soil, the pile is idealized as a series of elastic discrete elements and the soil is modeled by elasto-plastic springs. The load-displacement relationship at the pile head, together with the distribution of load and displacement down the pile, can be calculated using a stage-by-stage approach.

The axial load transfer curves, sometimes referred to as 't-z' curves, for the springs may be developed from theoretical considerations. In practice, however, the best approach to derive the load transfer curves is by back analysis of an instrumented pile test because this takes into account effects of pile installation.

The load transfer method provides a consistent framework for considering the load transfer mechanism and the load-deformation characteristics of a single pile.

(2) Elastic Continuum Method

The elastic continuum method, sometimes referred to as the integral equation method, is based on the solutions of Mindlin (1936) for point load acting in elastic half-space. Different formulations based on varying assumptions of shear stress distribution along the shaft may be used to derive elastic solutions for piles. Solutions using a simplified boundary element method formulation are summarized by Poulos and Davis (1980) in design chart format.

In the method by Poulos and Davis (1980), the pile head settlement (δ_t) of an incompressible pile embedded in a homogeneous, linear elastic, semi-infinite soil mass is expressed as follows:

$$\delta_t = P\ I_s^* \ /\ E_s\ D \qquad (2\text{-}9)$$

where
P = applied vertical load
I_s* = influence factor for pile settlement
E_s = Young's modulus of founding material
D = pile diameter

The pile settlement is a function of the slenderness ratio (i.e. pile length/diameter, L/D), and the pile stiffness factor, K, which is defined as follows

$$K = E_p \; R_A \; / \; E_s \qquad (2\text{-}10)$$

where
E_p = Young's modulus of the pile
R_A = ratio of pile area to area bounded by outer circumference of pile

Influence factor, I_s*, can be applied to allow for the mode of load transfer (i.e. friction or end-bearing piles), effects of non-homogeneity, Poisson's ratio, pile compressibility, pile-soil slip, pile base enlargement, nature of pile cap, etc. Reference should be made to Poulos and Davis (1980) for the appropriate values.

The ratio of short term (immediate) settlement to long term (total) settlement can be deduced from elastic continuum solutions. For a single pile, this ratio is typically about 0.85 to 0.9 (Poulos and Davis, 1980).

In a layered soil where the modulus variation between successive layers is not large, the modulus may be taken as the weighted mean value (E_{av}) along the length of the pile (L) as follows

$$E_{av} = \frac{1}{L}\sum_{1}^{n}(E_i d_i) \qquad (2\text{-}11)$$

where E_i = modulus of layer i
d_i = thickness of layer i
n = number of different soil layers along the pile length

An alternative formulation also based on the assumption of an elastic continuum was put forward by Randolph and Wroth (1978). This approach uses simplifying assumptions on the mode of load transfer and stress distribution to derive an approximate closed-form solution for the settlement of a compressible pile. A method of dealing with a layered soil profile based on this approach is given by Fleming et al. (1992).

It should be noted that the above elasticity solutions are derived assuming the soil is initially unstressed. Thus, pile installation effects are not considered explicitly except in the judicious choice of the Young's modulus. Alternative simplified elastic methods have been proposed by Vesic (1977) and Poulos (1989) including empirical coefficients for driven and bored piles respectively in a range of soils. Similar approximate methods may be used for a preliminary assessment of single pile settlement provided a sufficient local database of pile performance is available.

For piles founded on rock, the settlement at the surface of the rock mass can be calculated by the following formula assuming a homogeneous elastic half space below the pile tip:

$$\delta_b = \frac{q(1-\upsilon_r^2)D_b}{E_r} C_d C_s \qquad (2\text{-}12)$$

where

δ_b = settlement at the surface of the rock mass
q = bearing pressure on the rock mass
C_d = depth correction factor
C_s = shape and rigidity correction factor
ν_r = Poisson's ratio of the rock mass
D_b = pile base diameter
E_r = Young's modulus of rock mass

The depth correction factor, the shape and rigidity factor may be applied.

For piles founded in a jointed rock, Kulhawy and Carter (1992a and b) have also put forward a simplified method for calculating the settlements.

(3) Numerical Methods

Fleming (1992) developed a method to analyze and predict load-deformation behavior of a single pile using two hyperbolic functions to describe the shaft and base performance individually under maintained loading. These hyperbolic functions are combined with the elastic shortening of the pile. By a method of simple linkage, because the hyperbolic functions require only definition of their origin, their asymptote and either their initial slope or a single point on the function, elastic soil properties and ultimate loads may be used to describe the load-deformation behavior of the pile.

The load-deformation behavior of a pile can also be examined using numerical methods including rigorous boundary element analyses (e.g. Butterfield and Bannerjee, 1971a and b) or finite element analyses (e.g. Randolph. 1980; Jardine et al., 1986). Distinct element methods (e.g. Cundall, 1980) may be appropriate for piles in a jointed rock mass.

These numerical tools are generally complicated and time consuming, and are rarely justified for routine design purposes, particularly for single piles. The most useful application of numerical methods is for parametric studies and the checking of approximate elasticity solutions.

Chapter 3

METHODS OF PILE LOAD TESTS

3.1 General

In order to estimate the pile bearing capacity under consideration, many design methods and formulas were developed by using the principles of soil mechanics and site observations. However, given the many uncertainties inherent in the construction of piles and the difficulties involved in the accurate prediction of the performance of a pile, the common practice in engineering projects to establish pile behavior is to carry out a load test.

Static and dynamic load tests are the two types of the mostly adopted pile load tests. Static load tests are generally preferred because they have been traditionally used and because they are perceived to replicate the long term sustained load conditions. Dynamic load tests are usually carried out as a supplement to static load tests.

3.2 Dynamic Load Test

Dynamic load test is generally carried out by driving a pile or redriving the pile after a certain set-up period. The apparatus required for carrying out a dynamic pile load test includes a driving hammer, strain transducers and accelerometers, together with appropriate data recording, processing and measuring equipment.

Dynamic monitoring provides measurements of strain and acceleration in a pile subjected to driving. A significantly higher degree of accuracy can be obtained from wave equation analysis when used in conjunction with these field measurements.

In the dynamic load test, the strain and acceleration measured at the pile head for each blow are recorded. The signals from the instruments are transmitted to a data recording, reducing, and displaying device to determine the variation of force and velocity with time.

Two general types of analysis based on wave propagation theory, namely direct and indirect methods, are available. Direct methods of analysis apply to measurements obtained directly from a (single) blow, whilst indirect methods of analysis are based on signal matching carried out on results obtained from one or several blows.

Examples of direct methods of analysis include CASE, IMPEDANCE and TNO method, and indirect methods include CAPWAP, TNOWAVE and SIMBAT. CASE and

CAPWAP analyses are used mainly for displacement piles, although in principle they can also be applied to cast-in-place piles.

The reliability of the predictions of the dynamic load test methods depends on the adequacy of the wave equation model and the premise that a unique solution exists when the best fit is obtained within the limitation of the assumption of an elastic/rigid plastic soil behaviour (Rausche et al, 1985). In addition, there are uncertainties with the modelling of effects of residual driving stresses in the wave equation formulation.

A more detailed formulation of the wave equations such as CAPWAP or SIMBAT are preferred for analyzing dynamic load tests. These can be applied to non-homogeneous soils or piles with a varying cross-sectional area. The static load-settlement response of a pile can also be predicted. In practice, the wave equation analysis may be used to calibrate the damping coefficients in a CASE analysis to permit more piles to be tested by the less expensive CASE method. This is a reasonable approach in a relatively uniform soil, provided the CASE analyses are also calibrated against site-specific static load tests. As the field data collected for a CASE analysis will be sufficient for a detailed wave equation analysis, the latter should be carried out when the CASE analysis results are in doubt. In complex ground conditions, it is preferable to undertake more detailed wave equation analyses.

The results of dynamic load test may be used for design provided an adequate site investigation has been carried out and the method has been calibrated against static load tests on the same type of pile of similar length cross section and under comparable soil conditions. It should be noted that a proper calibration of the analysis model has to be based on tests on piles loaded to failure. A static load test that is carried out to a pre-set design load is an inconclusive result for assessing the ultimate resistance of the pile.

Dynamic load tests may be used as an indicator of the consistency of the piles and to detect weak piles. By building up a reliable local database of piles tested statically and dynamically, dynamic load tests may be useful with confidence for determining pile capacity without static load tests, particularly for piles in area where access is difficult or on small sites, or when time is limited.

Before introducing CASE Method and CAPWAP Method, which have been used in the project, a brief review of the wave equation and relevant pile and soil models will be presented in the next section.

3.2.1 Basics of Wave Equation and the Models for Pile and Soil

Smith (1960) introduced a comprehensive model to simulate pile driving and to calculate pile capacity and stresses from observations made in the field. The method is based on wave propagation theory, and is since known by the "Wave Equation Analysis of Pile Driving."

Differential Equation of Motion and its Solution

Waves associated with mechanical vibrations are generally a function of space and time. In a solid rod that is straight, homogeneous, elastic, and having constant cross-sectional area, longitudinal wave propagation can be described by the following partial differential equation (Timoshenko and Goodier, 1970):

$$\frac{\partial^2 u}{\partial t^2} = c^2 \frac{\partial^2 u}{\partial x^2} \qquad \text{(3-1a)}$$

or $$\ddot{u} = c^2 u'' \qquad \text{(3-1b)}$$

where,

$\ddot{u}$ = second partial derivative of displacement with respect to time, i.e. acceleration.

u" = second partial derivative of displacement with respect to x, i.e. strain gradient in the x direction.

c= wave speed expressed as: $c^2 = E/\rho$

E = Young modulus of elasticity

ρ = density of the material

The homogeneous differential equation above is referred to as the linear one-dimensional wave equation. Its numerical solution for pile driving purposes is presented by many researchers. By using d'Alembert's integration method (Kreyszig, 1979), its closed form general solution is as follows:

$$u(x,t) = f(x-ct) + g(x+ct) \qquad \text{(3-2)}$$

which implies that a displacement pattern in the rod consists of two components: f and g. The function f describes a wave of magnitude u that is travelling in the positive x direction at a speed c. The function g describes a wave travelling in the negative x direction at a corresponding speed -c. The waves thus described coexist, and are shifting position with time without changing shape.

Wave Equation Application to Pile Driving

For a pile embedded in an elastic medium and subject to soil resistance, and the soil is also modelled as a viscous model, the basic wave equation needs to be modified to account for the soil static resistance and dynamic resistance.

As presented in another convenient format of the above equation, two parts representing the static soil resistance, R_{stat}, and the dynamic component of resistance, R_{dyn}, are added,

$$A\,\rho\,\ddot{u} = A\,E\,u'' + R_{stat} + R_{dyn} \qquad \text{(3-3)}$$

This equation represents the wave equation in an infinitely long elastic pile subject to visco-elastic soil resistance along the entire shaft. Its solution requires elaborate mathematical manipulation and is best-assessed using numerical techniques.

Smith Model

Smith (1960) method of representing the pile analytically is shown in Figure 3.1. Smith modelled the soil as an elasto-plastic material with viscous damping as illustrated in Figure 3.2.

The elasto-plastic load-deformation characteristics of the soil are modelled using frictional springs. Two soil parameters, Quake and R_{MAX}, are defined to determine soil stiffness and the stress level at which plastic flow occurs. The soil quake is the magnitude of elastic deformation taking place before plastic yield. R_{MAX} is the maximum static resistance a soil element can provide against pile movement. Pile ultimate resistance (R_{ult}) is the summation of all static resistance provided by the different soil elements.

The viscous behaviour of the soil accounts for the dynamic resistance encountered during pile movement. Viscosity is traditionally modelled using a dashpot. The corresponding dynamic resistance is assumed linearly proportional to pile element velocity, v, by means of a damping coefficient, j. It should be noted, however, that dynamic resistance is a function of velocity and disappears as soon as the motion stops. Smith argued that toe damping must be greater than shaft damping, because around a pile toe, the soil is being displaced, while along the shaft there is only relative movement between the pile and the soil.

The Wave Equation Analysis Program (WEAP Program)

Smith soil model introduced three major parameters to model soil behaviour: static resistance, damping, and quake. The WEAP program adopted Smith parameters for the soil model and additionally introduced new ones.

The WEAP introduced a dimensionless coefficient, name CASE damping coefficient, to replace Smith damping (Goble and Rausche, 1976). According to Smith (1960), the dynamic soil resistance is proportional to the static soil resistance by means of the product of the pile velocity and a damping factor, j_{smith}, named Smith damping coefficient.

$$R_{dyn} = j_{smith} \, V \, R_{stat} \tag{3-4}$$

where,

R_{dyn}	= dynamic soil resistance
j_{smith}	= Smith damping coefficient
V	= velocity of pile at each segment
R_{stat}	= maximum static resistance of the soil element

Case damping suggests that the dynamic soil resistance is proportional to pile impedance by means of the product of the pile velocity and a dimensionless damping coefficient,

j_{case}, named Case damping coefficient.

$$R_{dyn} = j_{case}\, V\, Z \qquad (3\text{-}5)$$

where,

R_{dyn} = dynamic soil resistance
j_{case} = Case damping coefficient (dimensionless)
V = velocity of at pile tip
Z = pile impedance = $E_p\, A_p\, /c$
E_p = Young's modulus of the pile
A_p = cross sectional area of the pile
c = wave speed through the pile

3.2.2 Case Method Estimate of Pile Capacity

Case Method is a simplified method that uses a closed form solution to estimate pile bearing capacity using the force and velocity measurements. The assumptions behind the Case Method are as follows:

- the pile material is ideally elastic
- the pile is of uniform cross section
- the soil resistance shows rigid plastic behaviour and is concentrated to the pile toe

Based on the above assumptions, and the theory of wave propagation in uniform rods, the total soil resistance mobilised at the pile toe can be computed from the following equation (Goble et al., 1980):

$$R_{total} = \frac{1}{2}(F_1+F_2) + \frac{1}{2}(V_1-V_2)\, Z \qquad (3\text{-}6)$$

where,

F_1 = Force in pile head at impact
F_2 = Force in pile head at time 2L/c
V_1 = Velocity of pile head at impact
V_2 = Velocity of pile head at time 2L/c
Z = Pile impedance expressed as Mc/L
M = Pile mass
c = Wave speed in pile material
L = Pile length.

In words, the above equation states that the mobilised total soil resistance is the average of force measured at the time of impact and at 2L/c later, plus the impedance of the pile times half the difference between the velocity values at impact and 2L/c later.

The soil resistance computed using the above equation is the sum of static and dynamic resistance. The dynamic component of resistance is temporary and is due to soil damping.

The static soil resistance, called Case Method estimate, can only be estimated if the dynamic component is correctly separated from the total soil resistance. The dynamic resistance due to pile toe damping can be expressed as follows,

$$R_{dyn} = j_{case} V_{toe} Z \qquad (3\text{-}7)$$

which has been shown in section 3.2.1.

Therefore,

$$R_{stat} = R_{total} - R_{dyn} \qquad (3\text{-}8)$$

The dimensionless damping factor j_{case} is an operator entered variable. The appropriate j_{case}, is dependent on the type of soil at the pile toe and the actual pile dimensions. A range of j_c values appropriate to different soil types was proposed by Rausche et al. (1985). It should be noted that the recommended values of j_{case}, are predominantly for end-bearing piles. In practice, j_c values can vary significantly, particularly in layered and complex ground conditions, causing potential errors in pile capacity prediction. The results of Case Method depend on the value selected for this parameter.

3.2.3 The CAPWAP Method

The advantages of wave equation analysis and the field measurements taken during dynamic monitoring have been combined in a computer program called CAPWAP (CAse Pile Wave Analysis Program). The CAPWAP analysis method was developed by Rausche et al., 1972. The method is superior to conventional wave equation analysis because it does not require any assumption of soil properties such as damping and quakes. Instead, the field measurements taken during dynamic monitoring are used to compute the soil parameters and ultimate resistance.

The CAPWAP Method

The CAPWAP analysis makes use of the force and velocity measurements obtained by means of dynamic monitoring. The early CAPWAP model used a lumped mass system of masses and springs similar to the model originally proposed by Smith in 1960, as shown in Figure 3.3. Later, Smith's model was replaced by the continuous pile model shown in Figure 3.4.

The analysis commences by identifying the pile properties such as elasticity, mass, and cross-sectional area, as well as variations of these parameters along the pile length to establish the pile impedance profile. The pile is divided into several elements as illustrated in Figure 3.3. Each pile element is about one metre in length. Soil elements are assigned to the pile elements to represent soil resistance and soil resistance distribution along the pile shaft. For each soil element, assumptions are made at first about the soil parameters: damping, quake, and maximum resistance.

The digitised measured velocity is input to the CAPWAP as a loading condition at the pile head. The wave propagation in the pile due to pile head acceleration is subsequently simulated. Time is divided into increments called analysis steps. In every analysis step, the force, velocity, and displacement of every pile element are computed using the concepts of wave equation. The analysis usually covers a time interval of 4L/c to 5L/c following the first peak velocity that identifies hammer impact.

The force trace computed in the pile head element is subsequently compared to the force trace measured in the field. At first, there is a little agreement, only. Guided by the discrepancy between the computed and measured force traces, the user adjusts the input parameters such as soil resistance, quake, and damping. The analysis is repeated and another force trace is computed. When the best possible match between the computed and measured force traces is achieved, the analysis is terminated. The soil parameters used for the last run are considered representative to the actual soil conditions existing in the field during the driving of the pile.

Pile Model

The pile model shown in Figure 3.3 was initially used for CAPWAP analysis. The model consists of a series of masses connected by means of elastic springs. The driving system was eliminated from the CAPWAP model since its role was replaced with actual field measurements.

For uniform homogeneous piles, subdividing the pile into several segments according to the lumped mass approach suggested by Smith results in uniform segments of equal length. For non-uniform piles, or for piles made up of different materials, the equal length segments imposed by the lumped mass model have variable mass, stiffness, and travel time. CAPWAPC (CAse Pile Wave Analysis Program - Continuous Version) is a development of the original program. CAPWAPC uses a continuous pile model, in Figure 3.4, which has several major advantages over the lumped mass model. Primarily, the speed of computation was increased in addition to improving the accuracy of wave propagation analysis.

The pile is divided into a number of segments of equal travel time, i.e. it takes the wave a constant time interval, dt, to travel through any pile element of length dL_i .

$$dL_i = dt\ c_i \tag{3-9}$$

where,

dL_i = length of pile element i.

dt = time increment used for wave equation analysis.

c_i = wave speed through pile element i.

The length of continuous pile segments is varied to conserve a constant time travel, dt.

The CAPWAP, as well as the CAPWAPC, used dashpots to model internal pile material damping.

Soil Model

As described in section 3.3, WEAP program inherits Smith parameter for the soil model and introduces new ones to model soil behaviour. Among which, WEAP introduced a dimensionless coefficient, named CASE damping coefficient, to replace Smith damping (Goble and Rausche, 1976).

$$R_{dyn} = j_{smith} \ V \ R_{stat} \qquad (3\text{-}10)$$

which has been introduced in the section 3.2.1.

The CAPWAP used the soil model of the WEAP and extended it by further including the additional soil parameters. Therefore the parameters in the model include: static resistance, damping, quake, unloading soil parameters, such as unloading soil resistance and unloading soil quakes, reloading resistance, toe gap, soil plug, and toe soil damper.

Matching Techniques

To obtain an agreement between the measured and computed force at pile head, good estimates have to be made. Unless the influence of different parameters is qualitatively known, a CAPWAP match becomes a random search for one combination through an infinite number of permutations. Fortunately, the nature of parametric influence on the calculated traces is readily known. The knowledge can be used to systematically improve the CAPWAP match.

Normally, a CAPWAP analysis is carried out on a trace about 4L/C long in time. A good agreement match should extend at least to about 3L/C in time. A lower agreement quality may be accepted for the last L/C.

A CAPWAP trace can be divided into four periods as shown in Figure 3.5.

Period 1 extends from peak impact to about 2L/C. It is highly governed by shaft resistance. Close to impact, this region traces the early wave reflections. It is the easiest portion of the trace to match.

Period 2 exists in the vicinity of 2L/C, and has duration of about 3 ms plus the rise time of impact, t_r. It is governed by toe properties that are: resistance, damping, quake, gap, and soil plug. All these parameters can be significant in this portion of the trace.

Period 3 has a duration of about 5 ms. It is separated from the time 2L/C by a period equivalent to the rise time of impact t_r. This period is slightly complex, and is mostly governed by damping and ultimate soil resistance. Period 3 overlaps Periods 2 and 4.

Period 4 occurs following Period 2 and extends to the end of the trace. Wave reflections become very complex. The period is usually affected by all program parameters. Most unloading takes place during Period 4 that makes it possible to obtain a good match by adjustment of the unloading parameters.

Input parameters for the analysis include pile dimensions and properties, soil model parameters including the static pile capacity, Smith damping coefficient, j_s, and soil quake (ie. the amount of elastic deformation before yielding starts), and the signals measured in the field. The output will be in the form of distribution of static unit shaft resistance against depth and base response, together with the static load-settlement relationship up to about 1.5 times the working load. It should be noted that the analysis does not model the onset of pile failure correctly and care should be exercised when predicting deflections at loads close to the ultimate pile capacity.

Results of CAPWAP analysis also provide a check of the CASE method assumptions since the ultimate load calculated from the CAPWAP analysis can be used to calculate the CASE damping coefficient. Sound engineering judgement is required in determining whether a satisfactory match has been achieved and whether the corresponding combination of variables is realistic.

3.3 Pile Static Load Test

Static load tests on the working piles are the most reliable method to determine the axial bearing capacity, including compression and tension, as well as lateral capacity of piles. Static load testing is expensive, and while it is not practical to attempt a statistically representative number of tests, usually more than one test is necessary. However, the necessary number of static tests can be significantly reduced if combined with dynamic testing and monitoring, where the static testing will serve essentially as a calibration of the dynamic testing.

3.3.1 Reaction Arrangement and Equipment

For compression tests, three types of reaction system can be used. They are kentledge, tension piles and ground anchors. The tension piles were used in the project.

For uplift tests, the arrangement involving jacking at the centre is preferred because an even load can be applied to the test pile.

A typical load application and measurement system usually consists of hydraulic jacks, a load measuring device, spherical seating and load bearing plates.

Devices used for measuring pile head settlement in a load test include dial gauges (graduated to 0.01 mm), linear variable differential transducers (LVDT) and optical levelling systems.

In a compression or tension test, measurements should be taken by four dial gauges evenly spaced along the perimeter of the pile to determine whether the pile head tilts significantly. The measuring points of the gauges should sit on the pile head or on brackets mounted on the side of the pile with a glass slide or machined steel plate acting as a datum for the stems. Care should be taken to ensure that the plates are perpendicular to the pile axis and that the dial gauge stems are in line with the axis.

3.3.2 Test Procedures

Two types of load testing procedures are commonly used, namely maintained-load (ML) and constant-rate-of-penetration (CRP) tests. The ML method is applicable to compression, tension and lateral load tests, whereas the CRP method is used mainly in compression load tests.

The design working load (WL) of the pile should be pre-determined where WL is defined as the allowable load for a pile before allowing for factors such as negative skin friction, group effects, redundancy, etc.

In a maintained-load test, the load is applied in increments, each being held until the rate of movement has reduced to an acceptably low value before the next load increment is applied. It is usual practice to include a number of loading and unloading cycles in a load test. Such cycles can be particularly useful in assessing the onset of plastic movements by observing development of the residual (or plastic) movement with increase in load. Based on this information, Butler and Morton (1971) deduced critical load ratios for piles in difficult geological formations. This concept can be used to assess the acceptance criteria for load tests on piles as discussed by Cole and Patel (1992).

Different loading procedures have been proposed in the literature (ASTM, 1995). When testing a preliminary pile, where practicable, the pile should be loaded to failure or at least to sufficient movement (say, a minimum of 5 % of pile diameter). If the pile is loaded beyond 2 WL, a greater number of small load increments, of say 0.15 to 0.2 WL as appropriate, may be used in order that the load-settlement behaviour can be better defined before pile failure.

In principle, the same loading procedures suggested for compression tests may be used for tension load tests.

The constant-rate-of-penetration test has the advantage that it is rapid. However, the mobilised pile capacity may be influenced by strain rate effects, particularly in cohesive soils.

A constant strain rate of 0.25 to 1.25 mm/min and 0.75 to 2.5 mm/min is commonly used for clays and granular soils respectively (ASTM, 1995). The load should be supplied by a hydraulic power pack and by regulating the rate of oil flow to the jack and monitoring the pile movement with dial gauges. This procedure can control the rate of pile penetration better. In general, CRP tests are less suitable for piles founded on rock or granular soils and can constitute a safety hazard if the increase in loading becomes excessive.

3.3.3 Interpretation of the Results

There are a wide variety of criteria for interpreting loading test results, which can be divided into two groups:

- Criteria governing the acceptance of the tested pile. In these methods, no consideration is given to the failure load of the pile. In most cases, a pile is deemed acceptable if the observed settlement of the pile head is within specified limits, which are selected independently of the type and length of the pile. These methods overestimate the capacity of a short pile, underestimate the capacity of a long pile, and they should not be used.

- Criteria defining the failure load of the tested pile, from which the allowable load may be computed by applying a factor of safety. Such methods should be used because they provide a better understanding of pile capacity and behaviour.

Many different failure criteria have been proposed in the technical literature, a number of which have been discussed by Fellenius (1975, 1980). The failure loads as evaluated from the different criteria show a range of about 30% from the lowest to the highest.

Chapter 4

THE FOUNDATION PROJECT

4.1 General

This chapter presents the information on a real-life project, in terms of the structures, site geotechnical conditions and laboratory testing results, pile characteristics and piling equipment.

The project is for a construction of a quay deck of a wharf terminal. The quay deck is 940 meters in length with expansion joints 60 meters apart. According to the requirements of operation and stacking layout plan, the width of the quay deck is 35.5 meters. Because both crane rails can be installed on the quay deck, it has the advantage of reducing any differential settlement between the two rails. A cross-section of the structure and the crane load on the structure are given in Figures 4.1 and 4.2, respectively.

The piled quay deck is composed of the superstructure of beam-deck and pile foundations. The piles are at 6.4 m apart in the longitudinal direction and there are six piles under each transverse beam. A typical bay of the pile layout is shown in Figure 4.3. The piles at the front and rear crane beams are 1.0 m in diameter, and the piles in between are 0.813 m in diameter. At the midspan of the two crane beams, there is another batter pile of 1.0 m diameter. Both batter piles are inclined towards the inside. The wall thickness of the steel piles is 18 mm. The longitudinal and transverse beams of the quay structure are cast-in-situ concrete with a depth of 1.6 m. These beams are positioned at the grids. The composite slabs are of precast and cast-in-situ concrete panels placed on top of the beams with a total thickness of 0.45m.

Considering the large working load imposed on the quay structure, especially the wheel load of the quay cranes, and the stringent requirements on settlement of crane rails, the piles were designed such that they were founded in the bedrock to avoid possible uneven settlement of the piled deck. In the areas with higher bedrock level encountered, socketed piles were used and the tips of piles were socketed into competent bedrock to a depth of 3 m to ensure adequate bearing capacity and resistance to horizontal and tensile forces. In the areas where bedrock was at deep level, pile lengths were increased so that the piles were founded on the weathered rock stratum to ensure that the piles have adequate bearing capacity and tolerable settlement.

A total of 1270 open-ended steel tabular piles were driven in the project by a diesel hammer. The major features of the diesel hammer are listed in the Table 4.1. The mechanical properties of three representative piles, i.e. the test piles, are listed in Table

4.2. Dynamic load tests and static load tests were carried out on the three working piles in the project. The static load tests were only carried out to the extent of the design loads, instead of testing the piles to failure. All reaction piles in the static load tests were also working piles in the project. Well-planned records were kept for the test piles in the entire testing process, including the site investigation, pile installation, and dynamic and static load tests.

During the design period, an extensive site investigation was planned and carried out. A total of 121 boreholes were drilled. Boreholes were arranged 20 meter apart. After the piles were installed, more boreholes were drilled at each location of the test piles. Figure 4.4 shows the ground profile at the locations of three test piles. The SPT tests were carried out during the coring process, before the load test work. Figure 4.5 illustrates the SPT results along the depth at the test pile locations.

4.2 Geotechnical Conditions and Results of Laboratory Testing

The distribution of rock and soil layers in the project area is divided into three layers: upper layer, middle layer and bottom layer.

The upper layer is composed of marine sedimentary silt and silty clay. The silt layer is widely and continuously distributed, ranging in colours from dark gray to gray, and containing organic materials and shells. Average depth of this layer is 5 m and the water content is larger than 60%. It is extremely soft and the allowable unit soil resistance is 60 kPa. The silty clay layer is mainly distributed under the silt layer, with a depth less than 2 m. The SPT-N value is less than 1 and the allowable unit soil resistance is about 80 kPa.

The middle layer is composed of clay, clay loam and coarse alluvial gravel. The layer is distributed widely and uniformly, and well developed. It ranges from top to bottom as: The plastic clay contains small amount of cobbles and sand lenses in depth at an average of 1 to 2 m, with a SPT-N value of 7 and an allowable unit soil resistance of 180 kPa. The coarse gravel sub-layer has varying grain sizes and an average thickness of 1 to 2 m, with a SPT-N value of 22 and an allowable unit soil resistance of 240 kPa. The clay loam sub-layer has hard to medium plasticity, uneven sand lenses and cobbles, with a SPT-N value of 11 and an allowable unit soil resistance of 220 kPa.

The bottom layer is composed of bedrock, mainly lapilli bearing coarse ash tuff. The core samples show that it is highly fractured, even in some moderately strong rock layers. The core recovery ratio was very low. The weathered rock can be described as follows:

The rock at the top layer is extremely weak and highly weathered lapilli bearing coarse ash tuff. It is mixed clayey sandy silt with occasional fine quartz gravel and occasional limonite stalined relict joints. In the very weak and highly weathered rhyolitic lapilli bearing coarse ash tuff, the rock layer is distributed widely and varying in depth. The top elevation of the rock layer is at -15.27 m to -27.44 m. The SPT-N value increases significantly with increased depth. At the top, for SPT-N is 50, the depth of penetration, S, is 100 to 200 mm. At the bottom, for SPT-N is 50, the depth of penetration, S, is 10 to 50 mm. The allowable unit soil resistance ranges from 500 kPa to 1000 kPa.

For the moderately weathered rhyolitic lapilli bearing coarse ash tuff, the fissures in the rock layer are well developed. It has very closely spaced joints, highly fractured and with some very narrow sheared cleavages. It also has extremely closely spaced compression joints/cracks and very closely to medium spaced quartz veins (<2mm), dipping at 40° - 50°. The core-recovery is about 50%.

In the slightly weathered rock layer, the rhyolitic lapilli tuff is featured with very closely spaced rough planar and undulating clean joints. The minerals remain basically not weathered, but are usually mingled with broken layers at different depths. The core-recovery rate is about 85%. The depth is from -18.0m to -32.0m.

The laboratory tests were conducted for the soil and rock samples from boreholes, in addition to the tests on site.

In the experimental program for the medium and slightly weathered rock, 43 pieces of core samples were selected for the uniaxial compression tests under wet and dry conditions. The test data show that the results are scattered and the rock has low compressive strength. Table 4.3 shows the summary of the rock test results. The average value of uniaxial compressive strength in dry condition was 64 MPa and was 26 MPa in wet condition. For highly weathered bedrock, three sets of core samples were selected for consolidated-undrained triaxial tests. The results show that the effective cohesion is 21.7 kPa and the effective angle of internal friction is 26.9 degree, on average. The recommended value for unit pile toe resistance is 2300 kPa, and the value for unit pile shaft resistance is 100 kPa.

Major characteristics of physical and mechanical features of the soil are listed in Table 4.4. For sand, the average unit pile shaft resistance is 80 kPa and the unit pile toe resistance is 240 kPa. For alluvium the unit pile shaft resistance is 80 kPa and the unit pile toe resistance is 220 kPa.

4.3 Pile Characteristics and Installation

1. The Pile Characteristics:

The characteristics of piles are summarized in Table 4.2.

2. Pile installation:

The steel piles in the project were driven open-ended. There are various types of driving equipment available in the market for pile installation, such as hydraulic hammer, drop hammer, steam or compressed air hammer and diesel hammer. A diesel hammer, DELMAG D80 diesel hammer (see Table 4.1 for more information), was selected for use in the project. The following summarizes the operational principles and characteristics of the diesel hammer.

For a diesel hammer, the weight is lifted by fuel combustion. The hammer can be either single-acting or double-acting. Usually, only a small crane base unit is required to support the hammer. The driving characteristics of a diesel hammer differ appreciably from those of a drop or steam hammer in that the pressure of the burning gases also acts on the anvil (i.e. the driving cap) for a significant period of time. As a result, the duration of the driving forces is increased. The length of the stroke varies with the driving resistance.

The ram weight of a diesel hammer is generally less than a drop hammer but the blow rate is higher. The actual efficiency is comparatively low because the pressure of the burning gas renders the ram to strike at a lower velocity than if it were to fall freely under gravity. The efficiency is dependent upon the maintenance of the hammer. An efficiency value of 0.6 was assumed in the project. Furthermore, as the hammer needs to exhaust gas and dissipate heat, shrouding to reduce noise can be relatively difficult.

The steel tubular piles, having a diameter of 1.0 m and 0.813 m respectively, were installed into the bedrock. In the piling area, the marine deposit and silt layers were removed before any pile was installed. The seabed soil was checked before the dredging operation completed. This ensured that the entire burial length of a pile could contribute to the pile shaft resistance, as well as to the needed pile lateral resistance. The design elevation of the piling area is at -14 meter local datum. Any difference below this elevation was filled with quarry run rockfill after the piles were installed. The impact of the added rockfill layer on the pile bearing capacity was considered in the design. The driving of each test pile was terminated when the final set was equal to or less than 2.5 mm, and the pile toe penetrated into bedrock at a design elevation below the ground level. If the final set was reached, but the pile toe was above the design elevation, the bearing capacity of the concerned pile was checked. If the pile penetration into the ground was less than expected, the piles were socketed into the moderately strong bedrock for three meters, and, on selective basis, the proving boreholes were drilled to confirm the piles' penetration into the bedrock.

4.4 Discussions

The following aspects are considered important in a pile construction project.

- The loading and operational requirements in a project decide the selection of the pile and the arrangement of the piles.
- The knowledge about the geotechnical conditions at a construction site is very important. It will help in selecting pile type, installation methods and piling equipment.
- The construction methods and pile-driving equipment, to some extent, affect the success of the project.

Chapter 5

STATIC AXIAL PILE LOAD TESTS

5.1 General

Static load tests were conducted on three test piles, designated as A17, F54, and D57. The program of static load tests was planned to investigate the load bearing mechanism of the open-ended tubular piles driven into the highly weathered bedrock. Vertical compression tests were performed on all three piles, and tension tests were carried out on Piles A17 and D57. Pile A17 has a pile diameter of 1.0 meter, and Piles D57 and F54 have a pile diameter of 0.813 meter. The initial plan was to carry out the static load tests on two piles with different diameters. However, the second test pile failed the design criteria in terms of residual displacement. Because of the failure of the second pile, it was decided to conduct another test on a pile with 0.813 meter in diameter.

5.2 Requirements of the Static Load Test

The geotechnical conditions at the pile locations were investigated, prior to pile load tests, by drilling boreholes and using suitable in-situ testing. Such borehole testing was required to at least five times the largest pile dimension or 6m (whichever is the greater) below the pile toe, except where the bearing stratum was sand or gravel, in which case the depth was required to increase to at least 10 times the largest pile dimension below the pile toe.

5.2.1 Compression and Tension Load Tests

For a sustained load test the loading and unloading was carried out in stages as shown in the Table 5.1. It was designed to have two cycles of loading/unloading process for compression and tension tests. Each load increment was 25% of maximum load under consideration. For the compression test, the maximum load was the design load for the first cycle, and the maximum load was two times the design load for the second cycle. For the tension test, the maximum load was the design load plus pile self weight for the first cycle, and the maximum load was 1.5 times the design load plus pile self weight for the second cycle. The maximum load was sustained for 72 hours in the second cycle for both compression and tension tests, while other loading increments were sustained for one hour, in most cases. The sustaining time of unloading was 20 minutes for compression load test, and 10 minutes for tension test, with few exceptions.

Compression Load Test

Following the application of each increment of load, the load was held until the rate of settlement was less than 0.1 mm in 20 minutes, but in no case for a period less than the value shown in Table 5.1.

The load after each stage of unloading was kept constant until the rate of recovery was less than 0.1 mm in 20 minutes with few exceptions in which case the next stage of unloading might proceed after the expiry of the period stated in Table 5.1.

During loading stages, the values of load, time and settlement were recorded immediately after reaching the load level and at 15 minute intervals approximately for 1 hour, at 30 minute intervals between 1 hour and 4 hours, and at 1 hour intervals after 4 hours from the application of the increment of load, as applicable, and immediately before the next increase of load.

During the unloading stages, the load, time and settlement were recorded immediately upon reaching the load, and again upon reaching the end of the period.

A pile would be considered to have failed in a static compression load test when any of the following conditions applies:

- When loaded to and unloaded from 100% of the design load, the residual settlement of the pile head after rebound exceeds 4 mm;
- When loaded to and unloaded from 200% of the design load, the residual settlement of the pile head (including that from the 100% load cycle) after rebound exceeds 8 mm.
- The test loading (compression) as specified in Table 5.1 could not be sustained;
- Under a test load of 200% of the design load, the settlement of the top of the pile exceeds 10% of the least lateral dimension of the pile.

Tension Load Tests

Following the application of each increment of load, the load was held until the rate of displacement was less than 0.03 mm/minute and reducing, but in no case for a period less than the value shown in Table 5.1. The load after each stage of unloading was kept constant until the rate of recovery did not exceed 0.03mm/min.

At the loading/unloading stages, the load, time and settlement were recorded in the same manner as that for the compression load test.

A pile is considered to have failed in a static tension load test when any of the following conditions applies:

- When loaded to pile self weight plus 150% of the design tension load, total upward movement of the pile head exceeds 15mm;

- When unloaded from pile self weight plus 150% of the design tension load, the residual upward movement of the pile head exceeds 8 mm;
- The test load as specified in Table 5.1 cannot be sustained.

5.3 Arrangements of Testing Work

There were four reaction piles and two reference piles surrounding the test pile as shown in Figure 5.1. Based on the results of the dynamic load tests, the ultimate shaft resistance, under compression, of a pile was estimated to be more than 4000 kN. Half of the capacity could be expected to be used for the tension purpose. The sum of the resistance for tension of the four reaction piles was about 8000 kN, which was larger than the maximum test load, 7020 kN.

The capacity of the hydraulic jacks was 9600 kN. The accuracy of the measuring gauge was 0.01 mm and its stroke was 30 mm.

5.4 Static Load Test on Three Piles

Two static load tests were scheduled on a pile with a diameter of 1.0 m and 0.813 m, respectively. However, during the load test for the pile with a diameter of 0.813 m, it was found that the residual displacement did not satisfy the design requirement. It was decided that one more static load test needed to be carried out for another pile with the same diameter. Therefore, three working piles were selected for the static load tests. They were Piles A17, F54 and D57. All piles were tested to the design loads, but not to failure.

5.4.1 Static Load Tests on Pile A17

This was the first of three test piles. The pile had a diameter of 1 meter. It was driven into bedrock, through soil layers, with open-end. The compression load test was conducted 37 days after the pile was installed and the tension load test was conducted 3 days after the compression load test.

A borehole was drilled inside the pile. The length of the pile was 28.38 meters and the pile penetration length into the ground was 11.2 meters and the pile toe was driven into the highly weathered bedrock. The final set was 1.4 mm at the initial pile driving. The dynamic load test was carried out at the initial pile driving, but no redriving was conducted.

Compression Load Test

According to the requirements, two cycles of loading/unloading were conducted in the compression load test. The first cycle was loaded to the maximum design load, i.e. 3348 kN. In the second cycle, the pile was loaded to twice the design load, i.e. 6696 kN. The requirement for each load increment/decrement to be sustained to the extent that displacement rate was less than 0.1 mm/20 minutes, but not less than the specified time duration, was satisfied in the entire testing period. For each increment/decrement, the loading/unloading process only took about 2 minutes. The loads, displacement and time were recorded.

Tension Load Test

According to the requirements, two cycles of loading/unloading were conducted in the tension load test. In the first cycle, the pile was loaded to the self-weight plus maximum design load, i.e. 930 kN. In the second cycle, the pile was loaded to the self-weight plus 1.5 times the design load, i.e. 1230 kN. For each increment/decrement, the loading/unloading process only took about 2 minutes. The loads, displacement and time were recorded.

5.4.2 Static Load Test on Pile F54

This was the second of three tested piles, and it was the only pile that had redriving records associated with CAPWAP results. It has a diameter of 0.813 meter. The compression load test was conducted 75 days after the pile was installed and 32 days after the pile was redriven, respectively. The tension load test was not carried out.

A borehole was drilled inside the pile. The pile length is 32.92 meters and the pile penetration length into the ground was 9.33 meters and the pile toe was driven into the highly weathered bedrock. The final set was 2.5 mm at the initial pile driving. The dynamic load test was carried out at the pile initial driving and the redriving. The final set of redriving was 2.4 mm, and the total pile penetration into the soil at the redriving was 60 mm.

Compression Load Test

According to the requirements, two cycles of loading/unloading were conducted in the compression load test. In the first cycle, the pile was loaded to the maximum design load, i.e. 3346 kN. In the second cycle, the pile was loaded to twice the design load, i.e. 6692 kN. After the sustained period of 72 hours for the maximum load of 6692, the load was increased to 7026.6 kN. For each increment/decrement, the loading/unloading process only took about 2 minutes. The loads, displacement and time were recorded. The residual displacement of the pile head, 22.58 mm, exceeded the limit of 8 mm design requirement. The tension load test was not conducted on this pile.

5.4.3 Static Load Test on Pile D57

After Pile F54 failed the design requirement for the residual displacement, pile D57 was selected for the static load test for the purpose to assess the axial load bearing capacity of piles with a diameter of 0.813 meters. The compression load test was conducted 73 days after the pile was installed and the tension load test was conducted 3 days after the compression load test.

A borehole was drilled inside the pile. The length of the pile was 33.43 meter and the pile penetration length into the ground was 11.95 meters and the pile toe was driven into the highly weathered bedrock. The final set was 2.5 mm at the initial pile driving. The dynamic load test was carried out at the initial pile driving, but no redriving was conducted.

Compression Load Test

According to the requirements, two cycles of loading/unloading were conducted in the compression load test. In the first cycle, the pile was loaded to the maximum design load, i.e. 3510 kN. In the second cycle, the pile was loaded to twice the design load, i.e. 7020 kN.

Based on the previous test results, the increment of 25% of maximum loading at the final stage of load test would cause excessive displacement to the tested pile. Therefore, in this pile test, the load increment was reduced to one half of the scheduled increment value after 150% of the design load was applied at the second loading cycle, i.e. the last two load increments were divided into four load increments, in which each load increment was 12.5% of the test load. For each increment/decrement, the loading/unloading process only took about 2 minutes. The loads, displacements and time were recorded.

Tension Load Test

According to the requirements, two cycles of loading/unloading were conducted in the tension load test. In the first cycle, the pile was loaded to the self-weight plus maximum design load, i.e. 664.3 kN. In the second cycle, the pile was loaded to the self-weight plus 1.5 times the design load, i.e. 869.3 kN. For each increment/decrement, the loading/unloading process took about 2 minutes. The loads, displacement and time were recorded.

5.5 Load Test and Evaluation of the Test Results

5.5.1 General

The pile-soil interaction is evaluated hereafter by means of load/displacement responses. The pile displacement reduced very quickly when the loading process was completed for each load increment. It satisfied the requirement of sustained period of 0.1 mm/20 minutes. Unloading requirements were also met. During the test, the temperature, tide, wind and wave had some impacts on the tests for 72-hour sustained load, especially on the reference beam.

5.5.2 Load-Displacement Response under Compression Load

Figure 5.2 shows the load-displacement relation for the compression load test of Pile A17. In the first loading cycle, the displacement of the pile head was 7.51 mm under the compressive load of 3348 kN. The residual displacement was 0. In the second loading cycle, the displacement of the pile head was 17.95 mm under the compressive load of 6696 kN. The residual displacement was 0.13 mm. For every additional load applied, i.e. 25% of the design load, the displacement of the pile head increased about 2 mm. The last load increment caused about 4 mm displacement due to the 72 hours of sustained load. During the unloading process, when the maximum load was reduced to the next unloading value, the rebound of displacement was relatively small. The rebound rate of displacement increased only after the applied load was less than 2000 kN.

Figure 5.3 shows the load-displacement relation for the compression load test of Pile F54. The results show the excessive displacement at the second loading cycle, which is considered a failure under the design criteria. In the first cycle of the loading, the displacement of the pile head was 11.29 mm under the compressive load of 3346 kN. The residual displacement was 0.42 mm. In the second cycle of the loading, the displacement of the pile head was 49.46 mm under the compressive load of 7026.6 kN. The residual displacement was 22.58 mm, and it is significantly larger than the allowable displacement limit of 8 mm. For every additional load applied, i.e. 25% of the design load, the displacements of the pile head had values ranging from less than 3 mm to about 5 mm. However, the last design load increment, which brought the maximum design load in place, caused more than 23 mm displacement. Among 23 mm of the displacement, 5.6 mm occurred during the time when the load increment was applied, and the rest was due to the 72 hours of the sustained load. In the figure, the fact is represented by an obviously abrupt change in the slope of the load/displacement curve. The 23 mm of the displacement on the pile head caused by the maximum design load did not rebound in the unloading process and it led to the final residual displacement of 22.58 mm. Before the last load increment was applied, the displacement was only about 25 mm, which is about 3% of the pile diameter. When this additional 25% of the design load was applied, the displacement was increased to about 50 mm, which is about 6% of the pile diameter. After the last load increment was applied and the total load was sustained for 72 hours, an additional load of 334.6 kN was proposed and added. The curve shows that it only caused less than 2 mm displacement. It is obvious that the pile gained additional capacity when the pile toe penetrated into new bedrock layer.

Figure 5.4 shows the load-displacement relation for the compression load test of Pile D57. From the figure, it can be seen that the last two load increments, each of which is 25% of the design load, were divided into four load increments. In the first loading cycle, the displacement of the pile head was 11.88 mm under the compressive load of 3510 kN. The residual displacement was 0.45 mm. In the second loading cycle, the displacement of the pile head was 29.06 mm under the compressive load of 7020 kN. The residual displacement was 3.9 mm. For every additional load increment, i.e. 25% of the design load, the displacement of the pile head was about 3 mm, while, for the last four smaller increments, the displacement of the pile head was about 2 mm or less. The last load increment caused about 4.4 mm displacement due to the 72 hours of the sustained load. This time, the sustained load only managed to cause 2.24 mm displacement at the pile head, comparing to 17.4 mm displacement measured for Pile F54. There is an interesting phenomenon in the figure: when the maximum load was decreased according the test schedule with smaller decrements, the rebound of the displacement was relatively small, and it was held on until certain amount of loads was taken away. The rebound rate of displacement only increased after the total remaining load was less than 2000 kN. This is the same as that observed for Pile A17.

Test Data Evaluation

Figure 5.5 presents the load-displacement curves under the compression load for all three tested piles in the second loading cycle. Pile A17 had zero residual displacement after the first loading cycle, while Pile F54 and D57 had 0.42 mm and 0.45 mm residual displacement, respectively. Basically, Pile A17 had less displacement than the two other smaller piles. For Pile A17, when the load was 5859 kN, the displacement on the pile head was 14.07 mm. For comparison, the loads causing the same displacement on the pile head of Piles F54 and D57 were only about 4300 kN, which is about 35% less, or 1500 kN smaller, than that for A17. The curves show that Piles F54 and D57 had very similar displacement values under the same compression load until an accumulated load of 5000 kN. Pile F54 began to show increased displacement after the load of 5000 kN, and it is represented in the curve by an abrupt turning point at the last load increment. For Pile D57, after the accumulated load reached 5000 kN, the load increments were reduced from 25% of the design load to 12.5% of the design load. The displacement of the pile head had smaller values as shown in the figure. At the displacement of 24.5 mm, Pile D57 had a load of 6581 kN, while Pile F54 had only a load of 6142 kN for the same amount of displacement. The difference is about 440 kN, or 7% of the load. At the end of all three load-displacement curves, the "tails" show significant increase of the displacement due to the sustained load, i.e. 72 hours versus 1 hour, in the test. In the static load test, the amount of load increment and the time of the sustained load have significant impacts on the pile settlement.

The Figure 5.6 shows the comparison of the behaviour of three piles under the first compression load cycle. For Pile A17, when having a displacement of 7.51 mm, the load was 3348 kN, while the other two piles had a load of about 1000 kN smaller, which is about one-thirds of the total load. Two smaller piles needed a displacement of about 12 mm, which is about 30% more than that for Pile A17, to mobilize sufficient resistance for the load of 3348 kN.

Figure 5.7 shows the displacement ratio of D57, F54 and A17 in the first and second cycle of loading. In order to compare the performance of Piles F54 and D57 during the first loading cycle, the displacements of Piles D57 and F54 are plotted in Figure 5.7a as a ratio of the displacements of Pile A17. Pile F54 had an excessive displacement at the load of 870 kN, with a value 2.0 of the displacement ratio against Pile A17, while Pile D57 has a value of 1.6. After the load of 1700 kN, two smaller piles have the same displacement ratio against Pile A17. It is about 1.5.

Figure 5.7b shows the ratio of displacement of Piles D57 and F54 against Pile A17 in the second loading cycle. The figure shows that the displacements of Piles F54 and D57 are 2.3 times bigger than that of Pile A17, when the load is smaller than 1000 kN. When the load is between 2000 kN and 5000 kN, the displacement ratios are the same with a value of 1.3. After the load of 5000 kN, Pile D57 began to show less displacement with a smaller displacement ratio against Pile A17. At this stage, the toe resistance of Pile D57 began to play a more important role and the displacement ratio against Pile A17 was reduced to 1.3. After a load of 6000 kN, Pile F54 began to have excessive increase of displacement with a displacement ratio of 2.6 against that of Pile A17.

Figure 5.8 shows the pile head displacement gradient, which is defined as a ratio of increment of displacement versus increment of applied load.

Figure 5.8a shows that Pile F54 had an excessive displacement at the first load increment. However, it followed the normal pattern starting from the second load increment. At the last load increment, Pile D57 shows reduction of displacement. Pile A17 has a displacement pattern of linear increase.

Figure 5.8b shows that all three piles have quite constant displacement gradients when the load is smaller than 6000 kN. Pile F54 shows the biggest increase in the displacement gradient after 6000 kN. Pile F54 regained the strength even after an increment of load was added. Pile D57 curve shows that it had a large amount of displacement increase at the end of the sustained load. Pile A17 curve shows that its gradient did not change very much.

Figure 5.9 shows the relation between the displacement and the ratio of displacement versus the load.

For Pile A17, Figures 5.9a and 5.9b show that the ratio of displacement over load along with the increase of displacement. It shows normal patterns in the two figures for the relationship.

For Pile F54, Figure 5.9c shows very large initial values for the ratio of displacement over load. The first value is 3.7 and the next value is less than 3.3. This observation in the figure can be explained in a number of ways. The first thought should be on the soundness of the pile to see if it was broken or not, since the initial displacement was so excessive. This could not happen in this project due to the steel pile. Then, it is possible that the pile needed a large displacement to mobilize enough resistance to overcome the applied load. There are a few possible answers to the problem. First, the shaft resistance was very small, or it was smaller than expected in the design. Secondly, there was a gap underneath the toe of the pile, due to the rebound of the pile during the pile driving. The last reason is that the bedrock underneath the pile toe was very weak and its strength was not sufficient to resist the applied load.

For Pile F54, Figure 5.9d shows very large final values for the ratio of displacement over load. For the large final displacements, it could be concluded that the bedrock was highly fractured at the pile toe. Excessive gradients at the initial and final loading show possible bedrock structure broken down underneath the pile toe, if other possibilities could be ruled out.

For Pile D57, Figures 5.9f and 5.9g show the normal relationship between the ratio of displacement over load increases and displacement. As in Figure 5.9d, Figure 5.9g shows a slightly higher initial value for the ratio of displacement over load increase. By looking at the curve in Figure 5.9f, one can speculate that it would have a smaller value for the initial load if there were only one cycle of loading.

5.5.3 Load-Displacement Relations under Tension Load

Due to the reason that Pile F54 did not provide satisfactory compression test results, the tension load test did not apply to Pile F54. Therefore, there are only two piles having tension test results.

Figure 5.10 shows the load-displacement relation for the tension load test of Pile A17. In the first loading cycle, the displacement of the pile head was 1.64 mm under the tension load of 930 kN. The residual displacement was 0. In the second loading cycle, the displacement of the pile head was 2.67 mm under the tension load of 1230 kN. The residual displacement was 0.22 mm. For every additional load increment, i.e. 25% of the design load, the displacement of the pile head was about 0.6 mm. The last load increment caused about 1.0 mm displacement due to the 72 hours of the sustained load. When the maximum load was reduced according to the unloading schedule, the rebound of displacement showed a linear recovery.

Figure 5.11 shows the load-displacement relation for the tension load test of Pile D57. In general, the load-displacement relation is normal for both loading cycles, and the residual displacements were very small. In the first loading cycle, the displacement of the pile head was 2.33 mm under the tension load of 664.3 kN. The residual displacement was 0.51 mm. In the second loading cycle, the displacement of the pile head was 3.76 mm under the tension load of 869 kN. The residual displacement was 1.28 mm. For every additional load increment, i.e. 25% of the design load, the displacement of the pile head was about 0.75 mm. The last load increment caused about 1.23 mm displacement due to the 72 hours of sustained load. When the maximum load was reduced according to the unloading schedule, the rebound of displacement showed a good recovery.

Figures 5.12 and 5.13 show the comparison of first and second loading cycle of the tension load for the two tested piles. A17 shows straight lines in both first cycle and second loading cycle.

Figure 5.14 shows the displacement ratio of Pile D57 over Pile A17 under the tension load. In the first loading cycle, Pile D57 had a displacement 1.4 times larger than that of Pile A17 at the load of 100 kN, and the ratio was 2.3 times at the end of loading cycle. In the second loading cycle, Pile D57 had a displacement 1.7 times larger than that of Pile A17 at the load of 100 kN, and the ratio was 2.06 times at the end of loading cycle. It is obvious that the displacement of Pile D57 increased more quickly than that for Pile A17 in the first cycle and the ratio became constant after the load of 400 kN. In the second loading cycle, the ratio shows irregular changes at the beginning, which might be caused by the loading/unloading operation in the test. When making the figure, the residual displacements of the piles from the first loading cycle were deducted.

Figure 5.15 shows the displacement gradient of the two piles under the tension load. It can be seen that the displacement rate under the tension load increased when loads were increased. At second loading cycle, Pile D57 shows a sign of excessive displacement when load exceeded 600 kN.

5.5.4 Displacement and Time

Figures 5.16, 5.17, 5.18 5.19 and 5.20 show the relationship between the pile head displacement and time. The figures only show the displacement after the loads were applied. The results show the change of displacement during the sustaining time. For most of the time, the displacement occurred during the loading process that lasted about 2 minutes without recording. This is why the lines on the figures are not continuous ones. It can be seen that all the lines, except for the last one in each figure, are straight horizontal ones. During one hour of sustained load, the displacement did not change very much. In the figures, it shows that the reading of the sustained load was affected by adverse environment, such as tide, wind, wave and, especially, temperature.

In Figure 5.16, for Pile A17 under the compression load, each load increment caused about 2 mm displacement. Immediately after the maximum load was applied, the displacement was 16.24 mm. At the end of 72 hours of the sustained load, the displacement was 18.44 mm. Application of the load increase produced about 2 mm displacement and 72 hours of the sustained load produced another 2 mm displacement.

In Figure 5.17, for Pile A17 under the tension load, each load increment caused various displacements from 0.3 mm to 0.6 mm. At the maximum load, the displacement was 2.27 mm. At the end of the sustained load, the displacement was 2.67 mm. It can be seen that the application of load increase produced about 0.6 mm displacement and 72 hours of the sustained load produced another 0.4 mm displacement.

In Figure 5.18, for Pile F54 under the compression load, each load increment caused a displacement of about 3 mm, except for the load with 72 hours of sustaining time. At the maximum load, the displacement was 34.13 mm. At the end of 72 hours of the sustained load, the displacement was 47.54 mm. The application of load increment produced about 10 mm displacement and the 72 hours of the sustained load produced another 13.4 mm displacement. Due to the excessive displacement, an additional load of 334 kN was applied to the pile head. 1.92 mm of displacement occurred after the load increment. The final displacement was 49.46 mm. It can also be seen in the figure that, during 72 hours of the sustained load, most of the displacement happened in the first 1,000 minutes, i.e., within first 16 hours.

In Figure 5.19, for Pile D57 under the compression load, each load increment caused about 3 mm displacement. At the maximum load, the displacement was 26.41 mm. At the end of 72 hours of the sustained load, the displacement was 29.06 mm. For this load increment, the application of the load increase produced about 2 mm displacement and 72 hours of the sustained load produced another 2 mm displacement.

In Figure 5.20, for the Pile D57 under the tension load, each load increment caused various displacements from 0.3 mm to 0.7 mm. At the maximum load, the displacement was 3.22 mm. At the end of the 72 hours sustained load, the displacement was 3.76 mm. The application of the last load produced about 0.69 mm displacement and 72 hours of the sustained load produced another 0.54 mm displacement.

5.6 Discussions

1. For piles with diameters of 1.0 meter and 0.813 meter used in the project, the pile capacity is sufficient to carry the design loads. The piles with a diameter of 1.0 meter have a larger bearing capacity than that of the piles with a diameter of 0.813 meter. The piles of both size also have sufficient capacity to resist the uplift loads in the design.

   It is desirable to drive steel tubular piles to virtual refusal on a strong rock stratum, thereby developing its maximum bearing capacity. In this project, the pile penetration was controlled by a pre-determined final set during the pile driving. Both shaft resistance and toe resistance contribute to the total resistance of the piles, especially the shaft resistance of a pile is important for the tension loads in the project. The total pile resistance should be taken as the sum of the external skin friction, the end-bearing on the pile wall annulus, and the total internal skin friction; or the end-bearing resistance of the plug, whichever is less.

2. For Pile F54, all results from the analysis presented in this chapter indicate that it is a pile with a problem. There are a few possible reasons that caused the problem, such as toe gap, weak rock in the toe area, or reduction of the shaft resistance of the pile.

   When open-ended steel tubular piles are adopted, working loads based on the permissible working stress on the steel may result in concentrations of very high loading on the rock beneath the toe of the pile, even if they are helpful in achieving the penetration of layers of weak or broken rock to reach a hard stratum. This causes a high concentration of load on the relatively small area of rock beneath the steel cross-section. The ability of the rock to sustain this loading without yielding depends partly on the compressive strength of the rock and partly on the frequency and inclination of fissures and joints in the rock mass. Very high toe loads can be sustained if the rock is strong. If the horizontal or near-horizontal joints are wide, there will be some yielding of the rock mass below the pile toe but the amount of movement will not necessarily be large since the zone of rock influenced by a pile of slender cross-section does not extend very deep below the toe level.

3. The "tails" at the end of the curves in the figures for the static load test results show the time effect of the sustained loads. In addition to the amount of loads, the time of the sustained load is also an important factor in relation to the pile performance under the design loads.

   Bjerrum (1973) reported if a pile is subjected to a sustained load over a long period the shearing stress in the clay next to the pile is carried partly in effective friction and partly in effective cohesion. This results in a downward creep of the pile until such time as the frictional resistance of the clay is mobilized to a degree sufficient to carry the full shearing stress. If insufficient frictional resistance is available the pile will continue to creep downwards. Tomlinton (1994) pointed out that, for effects of sustained loads on piles driven in stiff clays, there might be a reduction in resistance with time. Surface water can enter the gap and radial cracks around the upper part of the pile caused by the entry of displacement piles, and this results in a general softening of the soil in the fissure system surrounding the pile. The stability of a pile group founded on a rock formation is governed by that of the individual pile. Tomlinson (1994) pointed out that one or more of the piles might yield due to the presence of a pocket of weathered rock beneath the pile toe, but there is no risk of block failure.

Chapter 6

BACK CALCULATION OF LOAD-DISPLACEMENT RELATION BY FINITE ELEMENT ANALYSIS

6.1 General

The purpose of the finite element analysis is to back calculate the pile load-displacement responses under compressive and tension loads.

Due to the availability of high-speed computers and powerful numerical techniques such as the finite element method, it is more desirable now than ever before to evaluate the load-displacement relation of a pile-soil system by using numerical techniques as a supplement to static load tests. In the finite element analysis, after the parameters of material models for one pile have been determined using the results of laboratory tests and static load tests, they can be used to predict the behaviour of any other size of pile under different load levels.

As part of this project, triaxial tests were carried out for the clay soil and the test results were used to prepare the parameters for a nonlinear model in the analysis work. An elastic-plastic model is used for the rock materials in the finite element analysis work. The relevant parameters for the selected models are prepared accordingly.

SIGMA/W, a finite element software product, is used in this study to perform the analysis work. This particular software can be used to perform stress and deformation analysis of earth structures. Its comprehensive formulation makes it possible to analyze simple linear elastic deformation problems as well as nonlinear elastic-plastic effective stress problems.

In the following sections of this chapter, the method used for the determination of the soil and rock parameters and the modeling approach for the pile-soil system are described in detail. At the end, the results from the finite element analysis are presented.

6.2 Pile Selection

There are two types of piles used in the project in terms of pile size. One type has a pile diameter of 1.0 meter and the other has a pile diameter of 0.813 meter. The static load tests were conducted on three piles, one with a diameter of 1.0 meter pile and two tests with a diameter of 0.813 meter. In the work of the finite element analysis, two piles have been selected, i.e. Piles A17 and F54. In the static load tests, Pile A17 has both compression and tension test results, and Pile F54 has only compression test results.

The characteristics of the two piles are listed as follows. Burial lengths of 11 meters and 9.3 meters for A17 and F54, respectively, are used in the making of the finite element mesh of the pile-soil system.

	A17	F54	
Total Length	28.38	32.92	m
Buried Length	11.2	9.33	m
Free Length	17.18	23.59	m
Length in Analysis	11	9.3	m
Pile Weight, in Water	112	104	kN

6.3 Hyperbolic Model for Soils

6.3.1 Model description

The stress-strain behaviour of soil becomes nonlinear, particularly as failure conditions are approached. A procedure for modeling this soil behaviour by varying the soil modulus is addressed in the following sections.

The formulation presented by Duncan and Chang (1970) is used in this section to compute the soil modulus. In this formulation, the stress-strain curve is hyperbolic and the soil modulus is a function of the confining stress and the shear stress that a soil is experiencing. This nonlinear material model is attractive since it requires soil properties that can be obtained quite readily from triaxial tests or the literature (Duncan et al., 1980).

Duncan and Chang's non-linear stress-strain curve is a hyperbola in the shear stress, (σ_1-σ_3) versus the axial strain space as shown in Fig. 6.1. Depending on the stress state and stress path, three soil moduli are required; namely, the initial modulus, E_i, the tangential modulus, E_t, and the unloading-reloading modulus, E_{ur}.

It is found that soil behaviour over a wide range of stresses is non-linear, inelastic, and depends upon the magnitude of the applied confining pressures in the tests. In this section, the hyperbolic stress-strain relationship is described. This relationship takes into account to some extent the nonlinearity, stress-dependency, and inelasticity of soil behaviour.

6.3.2 Formulation of the Model and Parameters

The parameters involved in the non-linear stress-strain relation are as follows:

E_i modulus	Initial soil modulus.
Poisson's Ratio	A constant value is used.
K	Modulus number.
n	An exponent describing the change in soil modulus as a function of the confining stress.

$K_{(ur)}$	Modulus number used during unloading and reloading.
$K_{(bulk)}$	Modulus number used to compute the bulk modulus. The bulk modulus is used in turn to compute the Poisson's ratio.
m(exponent)	A value describing the rate of change of the bulk modulus as a function of the confining stress.
Min. P. Ratio	A minimum value for Poisson's Ratio when it is computed from the bulk modulus. (The computed Poisson's ratio is limited to a maximum of 0.49 and a minimum of 0.01.)
Pa	Atmospheric pressure.
R_f	Ratio between the asymptote to the hyperbolic curve and the maximum shear strength (the ratio is usually between 0.75 and 1.0).
c	Cohesive part of soil strength.
ϕ	Soil friction angle in degrees.

The four parameters K, K_{ur}, n, and R_f are evaluated by using the stress-strain data of the triaxial compression tests, the same tests used to determine Mohr-Coulomb strength parameters c and ϕ.

Kondner et al. (1963a, 1963b, 1963c, 1965) have shown that the non-linear stress-strain curves of both clay and sand may be approximated by a hyperbola with a high degree of accuracy. The proposed hyperbolic equation by Kondner was:

$$(\sigma_1 - \sigma_3) = \frac{\varepsilon}{a + b\varepsilon} \qquad (6\text{-}1)$$

where,

σ_1	Major principal stress
σ_3	Minor principal stress
$(\sigma_1-\sigma_3)$	Stress difference
ε	Axial strain
a	Reciprocal of the initial tangent modulus
b	Reciprocal of asymptotic value of stress difference

Kondner showed that the values of the coefficients a and b could be determined easily if the stress-strain data are plotted on transformed axes, corresponding to the best fit between a hyperbola (a straight line) and the test data, as shown in Figure 6.2. Figure 6.3 shows the variation of initial tangent modulus as a function of σ_3. This allows the determination of K and n.

$$E_i = \frac{1}{a} \qquad (6\text{-}2)$$

$$(\sigma_1 - \sigma_3)_{ult} = \frac{1}{b} \qquad (6\text{-}3)$$

where,

E_i Initial tangent modulus

$(\sigma_1\text{-}\sigma_3)_{ult}$ Asymptotic value of stress difference

The asymptotic value of stress difference is always larger than the compressive strength of the soil by a small amount. This would be expected, because the hyperbola remains below the asymptote at all finite values of strain. The asymptotic value may be related to the compressive strength by means of a factor R_f as shown below.

$$(\sigma_1\text{-}\sigma_3)_f = R_f(\sigma_1\text{-}\sigma_3)_{ult} \qquad (6\text{-}4)$$

where,

$(\sigma_1\text{-}\sigma_3)_f$ Stress difference at failure

R_f The failure ratio

From the results of different soils, the value of R_f has been found to be between 0.75 and 1.00, and is assumed independent of confining pressure.

By expressing the parameters a and b in terms of initial tangent modulus value and the compressive strength, the hyperbolic equation proposed by Kondner, may be written as:

$$(\sigma_1 - \sigma_3) = \frac{\varepsilon}{\dfrac{1}{E_i} + \dfrac{\varepsilon R_f}{(\sigma_1 - \sigma_3)_f}} \qquad (6\text{-}5)$$

This hyperbolic representation of stress-strain curve developed by Kondner et al., has been found to be a convenient and useful means of representing the nonlinearity of soil stress-strain behaviour, and forms an important part of the stress-strain relationship described herein.

Except in the case of unconsolidated-undrained tests on saturated soils, both the tangent modulus and the compressive strength of the soils have been found to vary with the confining pressure applied in the tests. Experimental studies by Janbu (1963) have shown that the relationship between initial tangent modulus and confining pressure may be expressed as

$$E_i = KP_a\left(\frac{\sigma_3}{P_a}\right)^n \qquad (6\text{-}6)$$

where,

P_a Atmospheric pressure (same unit as E_i)

The values of parameters K and n may be determined from the results of series of triaxial compression tests by plotting the values of E_i/P_a against σ_3/P_a on log-log scales and fitting a straight line through the data points. The value of the modulus number K is equal to the intercept of the straight line with a vertical line, where σ_3/P_a is equal to one. The slope of the fitted straight line gives the exponent n, as shown in Figure 6.3.

The bulk modulus is defined as:

$$B_m = \frac{(\Delta\sigma_1 + \Delta\sigma_2 + \Delta\sigma_3)/3}{\Delta\varepsilon_v} \tag{6-7}$$

where,

B_m Bulk modulus

ε_v Volumetric strain

The bulk modulus is related to confining pressure in the same manner as initial modulus to confining pressure.

$$B_m = K_B P_a \left(\frac{\sigma_3}{P_a}\right)^m \tag{6-8}$$

The modulus number K_B and the exponent m may be determined from the results of series of triaxial compression tests or an isotropic triaxial consolidation test by plotting the values of B_m/P_a against σ_3/P_a on log-log scales and fitting a straight line through the data points. The slope of the fitted straight line gives the exponent m. The modulus number K_B is equal to the value on the vertical scale, where σ_3/P_a is equal to one.

The relationship of the bulk modulus to the Poisson's ratio can be defined as follows from the theory of elasticity.

$$B_m = \frac{E}{3(1-2\nu)} \tag{6-9}$$

6.3.3 Determination of Model Parameters

In this section, triaxial test results for soil will be used to determine the hyperbolic model parameters.

Two piles, A17 and F54, were selected for the finite element analysis. One set of parameters was determined using the laboratory test data and the results of the load test on Pile A17. The performance of Pile A17 under the compression and tension loads was analysed. The finite element analysis of Pile F54 used the same parameters as for Pile A17. Accordingly, one set of representative triaxial test results was chosen from the soil test data available for the location. The numbering system used in the triaxial tests has been adopted in the study. Test A113-13 is for the Pile A17. The results are from consolidated-undrained triaxial tests. The process of determining the parameters E_i, $(\sigma_1-\sigma_3)_{ult}$, R_f, K and n is described in the following sections.

For the soil at the location of Pile A17, the stress-strain data obtained from each of the three undrained triaxial compression A111-13 tests are presented in Figure 6.4. In Figures 6.5, 6.6, and 6.7, the data are plotted on transformed axes, in which the hyperbolic stress-strain curves are represented by fitting a straight line to the test data, for confining pressures of 100 kPa, 200 kPa, and 300 kPa, respectively.

The values of constants a and b that are the intercept and the slope of the resulting straight lines, respectively, is determined from the equations of the lines for each test. Using the equations provided in the previous sections, Equation 6-2 and 6-3, the values of E_i and $(\sigma_1-\sigma_3)_{ult}$, are calculated for each test and are listed below.

The failure ratio R_f as described before is independent of confining pressure and relates the compressive strength at failure to the asymptotic value of maximum stress difference. The values of asymptotic stress difference are obtained as described above and the values of compressive strength at failure are found from the test data. Using Equation 6-4 introduced above the failure ratio is calculated for each test and the results are summarised in the following table.

	Test	σ_3, kPa	a	E_i, kPa	b	$(\sigma_1-\sigma_3)_{ult}$, kPa	$(\sigma_1-\sigma_3)_f$, kPa	R_f
1	A111-13	100	5.09E-05	19,646	4.28E-03	234	210	0.89
2	A111-13	200	4.45E-05	22,472	2.17E-03	461	379.9	0.82
3	A111-13	300	3.28E-05	30,488	1.82E-03	549	445.9	0.81

The average value for R_f can be assumed as $R_f = 0.84$ for A111-13.

The values of E_i corresponding to the confining pressures of 100 kPa, 200 kPa, and 300 kPa were determined in the above table. The value of the atmospheric pressure is 101.3 kPa. As shown in Figure 6.8, the values of E_i/P_a and σ_3/P_a are plotted on log-log scales and a straight line is fitted to the three data points. The intercept of this line, where σ_3/P_a is equal to one and the slope, are the values of K and n, respectively, and are presented below:

For A111-13: $K = 200$, $n = 0.18$

For each consolidated-undrained triaxial compression test, the values of R_f and E_i are used in the above-mentioned equations, Equations 6-5 and 6-6, to determine the fitted hyperbolic model to the test data.

An initial value of K_{ur} is taken as 2 times the value of K. Constant values of the Poisson's ratio are used for the materials where required. The bulk modulus and related modulus number $K_{(bulk)}$ are not required in this study.

Mohr-Coulomb strength parameters c and ϕ, in terms of total stress have the following experimental values:

	c, kPa	ϕ, Degree
A111-13:	40	21

As a guideline, the local government provides a typical range of values of Young's Modulus and Poisson's ratio for various soils. The related values are listed in the following table, (GEO, 1993).

	E modulus (MPa)	Poisson's ratio	E modulus (MPa)	Poisson's ratio
			Undrained	Undrained
Soft Clay	1 - 4	0.1 - 0.3	2 - 6	0.1 - 0.5
Firm Clay	3 - 8	0.1 - 0.3	5 - 12	0.1 - 0.5
Stiff Clay	5 - 15	0.1 - 0.3	10 - 20	0.1 - 0.5

Poisson's ratio should have a value of 0.49 for the soil in undrained conditions. All parameters prepared in this section will be listed in a table at the end of the next section.

The time effect will not be considered in this finite element analysis. The 72-hour sustaining time for the maximum loads, which caused some displacements, will not be simulated.

Figures 6.9, 6.10 and 6.11 show the calculated hyperbolic stress-strain relation and the laboratory test data for the soil.

6.4 Parameters of Rock Materials

Initially, the triaxial test data for the highly weathered rock were used to determine the parameters of the hyperbolic model. However, as stated in the previous sections, the hyperbolic model was developed for clay and sand, but not for rock materials. The results of the calculation did not match with those from laboratory tests. Therefore, an elastic-plastic model was used for rock in the analysis. The parameters involved with the model are elastic modulus, Poisson's ratio, cohesion and friction angle.

According to the borehole profile as illustrated in Figure 4.4, there are three types of rock at the locations for the two piles in the study, i.e. highly weathered rock, moderately weathered rock and slightly weathered/intact rock. Since the way the rock parameters are classified in the local engineering handbooks and the site conditions at the pile locations, the moderately weathered rock and intact rock are treated in the same category in this study.

6.4.1 Highly Weathered Rock

Consolidated-undrained triaxial tests were conducted for the highly weathered rock for the cohesion values and friction angles. A summary of the cohesion values and friction angles is shown in the following table.

Tuffs	c', kPa	φ', °
max	30	29
min	13	25.7
Average	21.7	26.9

For highly weathered rock, typical ranges of the shear strength parameters are shown in the following table (GEO, 1993).

	Tuff	
	c', kPa	φ', °
Highly Weathered Tuffs	5 - 10	32 - 38

From the two tables listed above, it can be seen that the values of the shear strength parameters from the test are higher in cohesion and lower in friction angle as compared with those from the local design handbook. Taking the values in the two tables into consideration, it was decided to use, for the highly weathered rock, the cohesion value of 22 kPa, and the friction angle value of 27 degree, for the elastic-plastic model in the finite element analysis. The Poisson's ratio is given a value of 0.25. The value of the elastic modulus is decided by trial and error.

6.4.2 Moderately Weathered Rock and Intact Rock

During the site investigation, tests were carried out for the rock samples. The following table shows the results from uniaxial compression test. The uniaxial compression strength ranged between 10 MPa and 100 MPa.

Uniaxial Compression Stress (MPa)		
Dry	max.	101
	min.	30
	mean	64
Wet	max.	95
	min.	10
	mean	26

For the general guideline, the local government provides the ranges of the parameters for various rocks in different design handbooks.

For moderately weathered rock to intact rock, the following table provides typical range of the values of uniaxial compressive strength, (GEO, 1996). When comparing the values given in the table with the tested values from the above table, it can be seen that the rock samples tested in this project belong to Grade III.

	Tuffs		
Material Decomposition Grade	I	II	III
Uniaxial Compressive Strength, q_c, MPa	150 -350	100 - 200	10 - 150

Note: Grade I - fresh rock; Grade II - slightly weathered; Grade III - moderately weathered.

For moderately weathered rock to intact rock, the following table provides typical range of values of modulus of deformation and Poisson's ratio as determined in the laboratory (GEO, 1996).

	Tuffs		
Material Decomposition Grade	I	II	III
Laboratory Modulus of Deformation, E, GPa	60 - 150	30 - 80	5 - 40
Poisson's ratio		0.2 - 0.5	

Peck summarized the typical rock properties, and it is shown in the following table as a reference, (Peck, 1969).

Rock Type	Compressive Strength q_{um}, kPa		Shear Strength kPa		E, MPa	Lab.	Poisson's Ratio Field	Lab.
Basalt	193,053 to	461,949			24,821 to	40,679	0.30-0.32	0.26-0.28
Granite	68,948 to	266,827	13,790 to	29,372	37,232 to	81,358	0.25-0.27	0.17-0.29
Quartzite	110,316 to	308,885			24,821 to	86,184	0.25-0.30	0.07-0.17
Limestone	16,892 to	195,811	8,274 to	20,546	22,753 to	82,048		0.24-0.27
Marble	54,469 to	186,158	8,825 to	45,023	to			
Sandstone	33,784 to	137,895	1,958 to	20,615	6,895 to	62,053	0.28-0.30	0.07-0.17
Slate	47,919 to	213,737	13,721 to	24,476	36,542 to	57,916	0.30-0.32	0.24-0.25
Shale	3,447 to	44,816			to		0.26-0.27	0.20-0.25
Concrete	13,790 to	34,474	2,758 to	6,895	17,237 to	27,579	0.15	0.15

From the above tables, it can be estimated that the elastic modulus has a value range from 5,000 MPa to 40,000 MPa. By using the values in the above table for the uniaxial compressive strength, the cohesion value of the rock should have a typical range of values between 5,000 kPa and 50,000 kPa, since the cohesion can be estimated as one half of the uniaxial compressive strength. A value of 0.2 will be used for the Poisson's ratio. The friction angle is given an initial value of 32 degree.

Final Parameters

The material properties for the soil and rock from the site investigation and the preparations in the previous sections are listed in the following table. For the parameters that are not included in the table, they will be decided in the work of the finite element analysis, according to the ranges given in the above sections. The value range of undecided parameters is given as follows:

- The elastic modulus for highly weathered rock has a value around 5 GPa and its exact value is determined by trial and error.
- The elastic modulus for moderately weathered/intact rock has a value in the range of 5 GPa to 40 GPa.
- The cohesion for the moderately weathered/intact rock has a value between 5,000 kPa and 50,000 kPa, based on the test results in this project.

Case	E (kPa)	μ	K (kPa)	n	R_f	c (kPa)	ϕ (degree)	K_{ur} (kPa)
Clay		0.49	200	0.18	0.84	40	21	400
Weathered rock	by trial	0.25				22	27	
Intact rock	by trial	0.2				by trial	32	

6.5 Computer Program SIGMA/W

SIGMA/W is a general finite element software product for stress and deformation analyses of geotechnical engineering structures. One can choose to use a variety of different stress-strain constitutive relationships that range from simple linear-elastic, to non-linear elasto-plastic models. Loads can be applied and removed in stages, and SIGMA/W can be used to compute the changes in pore-water pressures that arise from stress state changes.

SIGMA/W is formulated for several elastic and elasto-plastic constitutive soil models. All models may be applied to two-dimensional plane strain and axisymmetric problems. Among all the models, the following models will be used in the analysis of the study:

- Linear Elastic

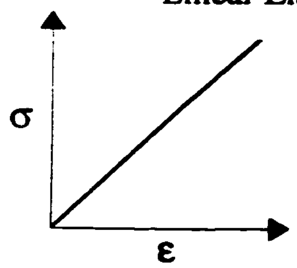

- Nonlinear Elastic (Hyperbolic)

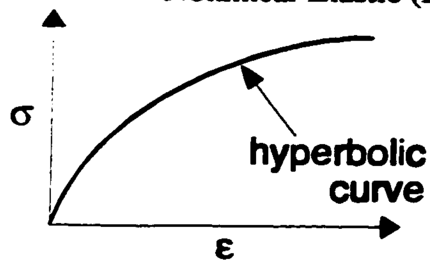

- Elastic Plastic (Mohr-Coulomb or Tresca)

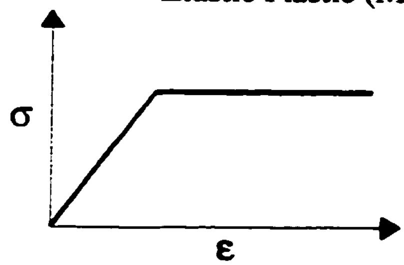

The methods, equations, procedures, and techniques used in the formulation and development of the SIGMA/W are well documented in the reference, (GEO-SLOPE, 1998). SIGMA/W is formulated for either two-dimensional plane strain or axisymmetric problems using small displacement, small strain theory.

The finite element equation used in the SIGMA/W formulation for a given time increment is,

$$\int_v [B]^T [C][B] dv \; \{a\} = b\int_v < N>^T dv + p\int_A < N>^T dA + \{F_n\} \tag{6.10}$$

where:

$[B]$	= strain-displacement matrix
$[C]$	= constitutive matrix
$\{a\}$	= column vector of nodal incremental x- and y-displacements
A	= area along the boundary of an element
v	= volume of an element
b	= unit body force intensity
$<N>$	= row vector of interpolating functions
p	= incremental surface pressure
$\{F_n\}$	= concentrated nodal incremental loads

Summation of this equation over all elements is implied. It should be noted that the SIGMA/W is formulated for incremental analysis. For each time step, incremental displacements are calculated for the incremental applied load. These incremental values are then added to the values from the previous time step. The accumulated values are reported in the output files. Using this incremental approach, the unit body force is only applied when an element is included for the first time during an analysis.

For a two-dimensional plane strain analysis, SIGMA/W considers all elements to be of unit thickness. For constant element thickness, t, Equation 6.10 can be written as:

$$t\int_A [B]^T[C][B]dA\ \{a\} = bt\int_A < N>^T dA + pt\int_L < N>^T dL \tag{6-11}$$

However, in an axisymmetric analysis, the equivalent element thickness is the circumferential distance about the axis of symmetry. Although the complete circumferential distance is 2π radians times the radial distance, R, SIGMA/W is formulated for one radian (unity).

Consequently, the equivalent thickness is R and the finite element equation for the axisymmetric case becomes,

$$\int_A \left([B]^T[C][B]R\right) dA\ \{a\} = b\int_A \left(R < N>^T\right) dA + p\int_L \left(R <N>^T\right) dL + \{F_n\} \tag{6-12}$$

Unlike the thickness, t, in a two-dimensional analysis, this radial distance, R, is not a constant within an element. Consequently, R needs to be evaluated inside the integral.

SIGMA/W solves this finite element equation for each time step to obtain incremental displacements and calculates the resultant incremental stresses and strains. It then sums all these increments since the first time step and reports the summed values in the output files.

SIGMA/W CONTOUR graphically displays the analysis results computed. The results can be presented as contours, graphs, tables of values, or a deformed mesh plot.

More information on the program can be obtained from the reference (GEO-SLOPE, 1998).

6.6 Modeling Approach

A finite element analysis consists of two steps. The first step is to model the problem, while the second step is to formulate and solve the associated finite element equations. Modeling involves designing the mesh, defining the material properties, choosing the appropriate constitutive soil model, and defining the boundary conditions.

6.6.1 Units

The metric system is adopted in a SIGMA/W analysis.

Geometry	Soil Unit Weight	Cohesion	Pressure	Force	E (modulus)
meters	kN/m^3	kN/m^2	kPa	kN	kPa

6.6.2 Mesh Design

Assessment of the Results by Static Load Tests

Chapter 5 provides all static load test results for the relation of load and displacement at the pile heads. Each pile is composed of two sections in terms of its interaction with the surrounding soil layers. The top section of each pile is up in the air/water, and the bottom section is buried in the soil. The finite element analysis work in this Chapter will focus on the latter section.

Assuming that the steel tubular piles are in perfect linear elastic range under the loads applied, the deformation of the free section of each pile is estimated and deducted from the pile displacement results from static load tests. Figure 6.12 to Figure 6.16 show the displacements of Pile A17 and Pile F54 under the compression load and tension load, when only considering the section of pile buried in the soil. The results of two loading cycles are included. The figures show that the maximum settlement for two piles is less than 10 mm, except for the result for the last load applied to Pile F54. This excessive displacement will not be simulated in the analysis. The maximum displacement caused by tension load is less than 1.3 mm.

Mesh Design

The amount of computer processing time required to solve the finite element equations is proportional to the number of nodes in the problem, the difference between node numbers in each element, and the integration order. SIGMA/W does not have specific limitations on the number of nodes and elements in a mesh. The finite element mesh system, as shown in Figure 6.41 for Pile A17, has 1463 elements and 3213 nodes. The one in Figure 6.42 for Pile F54 has 1243 elements and 2667 nodes. The finite element discretization is based on the axisymmetric eight node quadrilateral element.

A linear elastic formulation is used for the steel tubular pile, because the pile material usually remains elastic during the course of loading. It is expected that the soil and rock in the vicinity of piles undergo deformation as shown in the figures from Figure 6.12 to Figure 6.16.

The accuracy and performance of an element is affected to some extent by its shape. For quadrilateral elements, the best performance is achieved when the interior angles are all 90 degrees (a rectangle); for triangular elements, the best performance is achieved when one interior angle is 90 degrees and the other two angles are 45 degrees.

The aspect ratio (length to height) of elements can also affect the performance. The best performance of long, thin elements is achieved by quadrilateral elements with eight nodes and nine-point integration. An aspect ratio of one gives the best performance. Long, thin elements with aspect ratios much greater than five can lead to poor results. SIGMA/W has no restrictions on the aspect ratio.

The above principles have been given the best possible considerations in the mesh design.

The pile-soil system to be analyzed is illustrated in Figure 6.41 and Figure 6.42 for Pile A17 and F54, respectively. The pile is a long thin object for the portion to be considered in the work. However, since it is the perfect elastic material, it is designed to have an aspect ratio of close to five. All other soil and rock elements around the pile have aspect ratio values close to one.

All pile elements and the soil/rock elements around the piles have secondary nodes at the mid-points between the corner nodes. These elements are known as "higher order" elements, since the equations describing the deformation within the element are of a higher order than when there are no secondary nodes. Higher order elements exhibit better behaviour than the ordinary 4-noded quadrilateral and 3-noded triangular elements. Ordinary elements are adequate for the linear-elastic model. For the nonlinear constitutive soil models, the material properties are a function of the computed stresses. Therefore, a reasonable stress distribution within the element is essential, and higher order elements should be used.

The boundaries in the pile center and at the end of right side of the mesh have x-displacement restriction. The bottom boundary of the pile-soil system has both x-displacement and y-displacement restrictions.

Soil Model Selection

For each soil-pile system, the soil layer has the Hyperbolic Model throughout the analysis work. Both highly weathered rock layer and moderately-weathered/intact rock use elastic-plastic model, for each pile. The parameters for different materials have been prepared in the previous sections. The modulus of elasticity for steel is set equal to 200 GPa. Poisson's ratio of the steel is set equal to 0.3 in the elastic range.

Convergence Criteria

In all non-linear analyses, it is necessary to use iterative techniques to compute acceptable solutions. Non-linear analyses exist when a soil property is dependent on the computed results. For example, the tangent modulus E_t depends on the stress state in the ground, but the stresses are dependent on the tangent modulus. This means that the analysis has to be done many times until there is a reasonable match between the soil properties and the computed stresses. When the analysis has produced an acceptable match, the solution is deemed to have converged. SIGMA/W uses two convergence criteria: the displacement criterion and the unbalanced load criterion. The displacement criterion checks the ratio of the vector norm of incremental displacements in iteration to the vector norm of the total displacements in the load step. The unbalanced load criterion compares the unbalanced load in iteration to the applied load in the load step as a percentage ratio. The unbalanced load criterion is usually required when the analysis approaches limit equilibrium.

During the analysis work, both the displacement criterion and the unbalanced load criterion are used. A convergence criterion of 2% and a maximum number of iterations of 35 are assigned for both criteria.

Limiting Loads

The SIGMA/W finite element equations are a set of equilibrium equations. The applied forces are in equilibrium with the resisting forces that arise from the soil strength. The load that can be applied is, therefore, limited by the ultimate resistance of the system. In the terminology of the program, the limiting load is the load that results in a factor of safety equal to 1.0. The modeling consequence of applying loads in excess of the limiting load is usually numerical instability, that is, a lack of convergence and widely varying oscillation in the solution. It is also important to remember that SIGMA/W is not formulated for large displacements or large strains. Therefore, carrying an analysis well past the point of limiting equilibrium may produce unrealistic results.

Effect of Installation

In this project, the piles were installed by driving. The installation affects the soil around the piles. In granular materials, soil density changes around the pile. In cohesive soils, excess pore water pressure is generated during pile driving operations. The dissipation of the excess pore water pressure may take a long time depending on the consolidation characteristics of the cohesive soil. Pile driving changes the stresses in the ground irrespective of the soil type.

Interface elements were used between the pile and soil elements in the finite element analysis. Two-thirds of the soil or rock strength were assigned to the interface elements. However, it was found that the interface elements had very little influence on the load/displacement response of compression piles. Poulus (1980) pointed out that, for piles bearing on a stiffer stratum, the effect of slip is generally less significant.

Among other things, one of the reasons for differences in the displacements determined from calculations and tests may be the residual load. The residual load in a pile is caused during the installation of a pile, by reconsolidation of the soil, and by a previous loading cycle. It manifests itself as a compression in the pile caused by negative skin friction in the upper portion of the pile, which is balanced by positive shaft resistance in the lower portion of the pile plus some toe resistance.

Taking the above factors into consideration, different amounts of loads, such as 25%, 50% and 75% of the design loads, were applied to the pile head, prior to the application of the increments of design loads, in the analysis. The results show that any amount of preloading would significantly reduce the displacements of the pile under the test loads, due to the fact that soil behaves in an elastic manner until it reaches to the max stress level experienced previously.

Effect of Soil Plug in Open-Ended Pipe Piles

For open-ended steel tubes, considerations need to be given to assess whether the pile will act in a plugged mode or unplugged mode. When subjected to compression working loads, the soil around and beneath the open end is not displaced and compressed to the same extent as that beneath a closed-ended pile. After a soil plug is formed, the base resistance increases sharply from that provided by the net cross-sectional area of the pile toe to some proportion (not 100%) of the gross cross-sectional area.

Depending on the pile-soil situations, there are two ways to consider the bearing capacity of open-ended tubular piles. First, it can be taken as the sum of the skin friction along the external perimeter of the shaft and the ultimate base resistance with a reduction factor applied, i.e. ignoring the internal skin friction between soil plug and pile. Alternatively, the bearing capacity of a pile can be taken as the sum of the external and internal shaft friction and the base resistance on the net cross-sectional area of the pile toe; or the end-bearing resistance of the plug, whichever is less.

Tatsunori (1995) suggested that, based on a test on open-ended steel tubular piles driven in soft rock, the total inner shaft resistance is limited to the end-bearing capacity of the ground below the soil plug, when a perfect plug is formed. He described that, in his tests, the ground below the pile toe was compressed by the tubular pile with perfect plug mode in which the inner soil at the bottom 2 meters of the pile was highly compressed sideways, which resulted in a large inner shaft resistance.

In this study, a "perfect" soil plug is assumed. Special considerations were given to the soil layers inside the pile by using interface elements. However, the effects of the interface elements were not significant. At the end, it was decided that the soil inside a pile has the same shaft resistance as that possessed by the soil outside the pile in the full-buried length of the pile.

Considerations for Tension Loads

The tension loads have to overcome the weight of the pile material and the resistance of the interface between the pile and soil/rock before the pile head can be pulled up. In SIGMA/W, body forces are included in an analysis by specifying a non-zero load (or weight) per unit volume. For each element, SIGMA/W computes the volume of the element, multiplies the volume by the specified unit load of the material, and applies the total element body load as forces at the nodes of the elements. The body loads alone will cause the displacement at the pile head. In the analysis, the displacement caused by the body weights of the soil materials alone is calculated. Since this displacement is not considered during the period of the static load tests, it is deducted from the total displacement caused by the combination of tension loads and body weights of the soil materials in the analysis of the soil-pile system. The tension at the pile toe was removed in the analysis.

For materials in water, the unit weight of the steel pile is 71 kN/m^3. The unit weight of soil in water is 10 kN/m^3. For rock, the unit weight in water is 13 kN/m^3 in the project.

6.7 Modeling Results and Comparison with the Results by Static Load Test

The finite element discretizations are illustrated in Figure 6.41 and Figure 6.42 for Pile A17 and F54, respectively. The width of the mesh is 11 meters, and the total height is about 17 meters. It is designed to have, at least, 6 meters of rock thickness underneath the pile toes.

6.7.1 Finite Element Mesh Sensitivity Analysis

Due to the thickness of the pile, the soil around the pile, especial at the pile toe area, has to be designed as fine mesh. In order to get the best results, the size of a soil element adjacent to the pile shaft is designed to have dimensions of 0.15x0.16 meters, and the size of a soil element adjacent to the pile toe is 0.10x0.16 meter. The mesh of Pile A17 is composed of 1463 elements and 3213 nodes, while that of Pile F54 is composed of 1243 elements and 2667 nodes.

The effects of the sizes of soil domain on the load-displacement response are studied. Two additional meshes with soil radii of 8 meters and 5 meters were considered for comparison with the domain used in the calculations, i.e. with the soil radius of 11 meters, for Pile A17. When comparing to the results with soil radius of 11 meters, the pile head displacement for the 5 meters soil radius has values more than one percent starting from the third increment load and the maximum difference is close to 6% for the last three load increments. Whereas, the pile head displacement for 8 meters soil radius is similar to that for 11 meters soil radius. Only the last two load increments have little more than 1% difference, and the maximum difference is only 1.6%, when comparing with the two results. Therefore, the mesh used throughout the analysis can be considered adequate.

6.7.2 Parametric Study

With the parameters discussed in Section 6.3 and 6.4, a parametric study has been conducted for two purposes:

1. To select appropriate parameters in order to relate the analysis results of the displacements of the pile under given loads with that obtained from the static load tests, and

2. To examine the effects of different parameters on the final displacement results calculated by the finite element program.

The principle of selecting different parameters is to have the results of calculated displacements matched with that from the static load tests. For the convenience of the explanation, the table listed in the Section 6.4 is presented here again as follows:

Case	E (kPa)	n	K (kPa)	n	R_f	c (kPa)	ϕ (degree)	K_{ur} (kPa)
Soil		0.49	200	0.18	0.84	40	21	400
Weathered rock	by trial	0.25				22	27	
Intact rock	by trial	0.2				by trial	32	

For the intact rock layer, two appropriate values are assigned to its elastic modulus and cohesion. By trying different values for the elastic modulus of the highly weathered rock, the best possible match for Pile A17 was found, when the three parameters had the following values. Figure 6.18 shows the results.

For weathered rock: E = 2,000,000 kPa
For intact rock: E = 10,000,000 kPa, and c = 1,000 kPa.

The parametric study plan is illustrated in the following table. In the program, one parameter was changed at a time to assess its effect on the load/displacement response. For the clay, all parameters were decided in the previous sections. The soil layers above the rock is regarded as one uniform layer of soil with the same soil properties in order to simplify the preparation work for the analysis.

Soil Type		Value 1	Value 2	Value 3	Unit
Clay	ν =	**0.49**			
Weathered Rock	E =	1,000,000	2,500,000	4,000,000	kPa
	ν =	0.2	**0.25**	0.35	
	c =	15	**22**	30	kPa
	ϕ =	20	**27**	35	degree
Intact Rock	E =	5,000,000	**10,000,000**	20,000,000	kPa
	ν =		**0.20**	0.3	
	c =	500	**1,000**		kPa
	ϕ =		**32**	40	degree

Note: The bold figures are the values in first set of parameters.

6.7.3 Results of the Analysis

Figure 6.18 shows a good match of the results from the calculations and static load test. Figure 6.19 to Figure 6.32 show the results of the finite element analysis for 14 different combinations of the parameters. The values of the parameters related to each case are listed in Table 6.1.

(1) Highly Weathered Rock

Effect of Elastic Modulus

Figure 6.33 shows the results of the analysis, when the elastic modulus of highly weathered rock has different values of 1,000,000 kPa, 2,000,000 kPa, 2,500,000 kPa and 4,000,000 kPa. When the elastic modulus reduces, the displacement increases accordingly. Figures 6.18, 6.19, 6.20 and 6.21 show the effect of each value on the load-displacement response.

Effect of Friction Angle

Figure 6.34 shows the results of the analysis, when friction angle of highly weathered rock has values of 20°, 27° and 35°. When friction angle is in the range from 27° to 35°, the displacement reduces as the friction angle increases a small amount. However, the displacement increases significantly when the friction angle reduces to 20°. Figures 6.18, 6.24 and 6.25 show the details of the effects of different friction angle values. Figure 6.25 shows that, when the friction angle increases, the rock becomes less plastic and is showing linear elastic behaviour.

Effect of Cohesion

Figure 6.35 shows the results of the analysis, when cohesion of highly weathered rock is given values a range of values. It can be seen that, in the given value range, the effect of cohesion values is not significant. Figures 6.18, 6.22 and 6.23 show the details of the effects of different cohesion values.

Effect of Poisson's Ratio

Figure 6.36 shows the results of the analysis, when Poisson's ratio of highly weathered rock has values ranging between 0.2 and 0.35. The figure shows that the displacements increase when the Poisson's ratio increases. Figures 6.18, 6.26 and 6.27 show the details.

(2) Intact Rock

Because the intact rock is deep below the pile toe, the rock properties have little, if any, effects on the load/displacement response in the system, according to the analysis results. Figure 6.28 to 6.32 show the details of analysis results when using different parameters for the intact rock. Figure 6.37 shows the comparison of the results.

(3) Two Final Matches for Pile A17 and F54

Figure 6.18 and Figure 6.40 show the results from finite element analysis, with the parameters listed first in Table 6.1 without a case number. It can be seen that the analysis results for Pile F54 has a good match with the results from the static load test, although the analysis was performed using the parameters prepared for Pile A17. Pile F54 has a smaller diameter than that of Pile A17.

(4) The Results under Tension Loads

Figure 6.38 and Figure 6.39 show the results of the analysis and the static load test under the tension loads for Pile A17. All parameters used in the analysis are the same as that applied for Figure 6.18 under the compression loads for Pile A17. The maximum tension load in the second loading cycle was sustained for 72 hours. It can be seen that it has reasonable matches with the results from the static load test in the first loading cycle and in the second loading cycle.

6.8 Summary

The purpose of this study was to back-calculate, by using finite element analysis, the load-displacement response of open-ended steel tubular piles driven through clay soil layers into weathered bedrock. An attempt has been made to assess qualitatively the finite-element model as a rational approach to the analysis of pile load-displacement responses.

A finite-element model for the soil-pile system was designed and an assessment of the model was conducted. A hyperbolic model for soils and an elastic-plastic model for rocks were used in the study. All major parameters were prepared based on the results of the field and laboratory tests or from various engineering handbooks. A parametric study was carried out. The issues, such as interface elements and soil plug were discussed.

The study should be useful in describing the effect of design loads at the pile head on the behaviour and deformation of the soil and rock, and the extent of this effect in the region around the pile shaft and below the pile toe. The load-displacement response of a pile predicted by the model could be used to improve the existing empirical and rational approaches for pile analysis. From the outcome of the analysis, it is demonstrated that results obtained for the cases analyzed are plausible and consistent with the static load tests.

Chapter 7

PILE DYNAMIC LOAD TEST

7.1 General

Dynamic load tests were carried out by using the CASE Method as performed by a Pile Driving Analyzer (PDA) in the project. The computer programme CAPWAPC, which will be referred as CAPWAP for simplicity hereafter, was also used, in conjunction with the PDA, to verify the PDA output and also to determine the shaft resistance and toe resistance of piles. The dynamic load tests were carried out during the initial driving of piles, and, for a small number of piles, during redriving of piles.

The pile and soil models for the related methods have been described in Chapter 3. It is not the intention of this chapter to study the parameters of those models and their effects. The main purpose, therefore, is to relate the test results produced by the CASE and CAPWAP Methods to the other measured field data, such as setup time, final set and pile burial length, and to investigate and evaluate the effects of these factors on the pile axial bearing capacity estimated by the methods.

This Chapter describes briefly the PDA tests and evaluates the ultimate resistance of the piles and the factors that have effects on the test results.

7.2 Purpose of Dynamic Load Test in the Project

As supplementary information to the static load test, the purpose of the dynamic load tests was to determine:

(1) the driving force, the integrity of the piles and the static soil resistance through driving test,

(2) the ultimate resistance of the piles at redriving.

After the soil recovery from initial driving, the ultimate resistance of the piles was determined through redriving tests. The shaft resistance, the toe resistance and the relationship between the load P and the settlement S, i.e. P-S curve, was obtained through the CAPWAP Method.

7.3 Test Procedure and Requirement

Before the pile installation, holes were drilled on each test pile at the locations that were 1.5 times the pile diameter below the pile head in order to install transducers. At the final stage of pile driving, a few strain transducers and acceleration transducers were installed on both sides of the pile when the pile driving operation was suspended. By installing the transducers on both sides of the pile, the extent of eccentric driving on each side of the pile was measured and the impact of eccentric driving on the test data could be avoided. After the pile driving restarted, the signals of strain and acceleration were transmitted from the transducers to PDA through low noise screened cables and were converted into waves of force and velocity shown in the screen. The results by the CASE Method could be provided on site and the results by the CAPWAP Method could be provided after in-house analysis.

The outcome from the CASE Method is influenced by the striking force, striking energy, cushion etc. In the project, all tests were conducted on the working piles. The initial driving test was carried out during the operation of pile installation. The redriving test was carried out, at least, one week after the completion of the pile installation. The redriving was carried out with two groups of strike, each group should be composed of about 10 strikes. Normally, it is required that the set under each strike is no less than 2 mm. Otherwise the ultimate shaft and toe resistance of the pile could not be fully mobilized, and, therefore, the ultimate resistance of a pile gained from the test would be less than the real one. On the other hand, if the final set is more than 10 mm, the ultimate resistance of a pile gained from the CASE Method and CAPWAP Method could not be accurate, either.

The Pile Driving Analyzer (PDA) manufactured by American Pile Dynamic Inc. was used in the project.

7.4 Pile Driving Results

Before presenting and evaluating the results from the dynamic load test, it would be useful to have a look at the information of pile installation. The data presented below is the summary of the records of the pile installation in the project.

Pile Driving Impacts on Pile Penetration

Figure 7.1 shows the pile penetration as a function of the blow counts during pile driving for the three piles studied.

It took about a total of 400, 500 and 700 blows for Piles A17, F54 and D57 to reach the required final set, respectively. The borehole information shown in Figure 4.4 indicates that the thickness of the overburdens above the highly weathered bedrock are 8.2 m, 6.8 m and 8.5 m for Piles A17, F54 and D57, respectively. Figure 7.1 shows that it took 37 blows, 46 blows and 38 blows for Piles A17, F54 and D57 to sink 8.79 m, 6.52 m and

7.31 m, respectively, at the first batch of blows. These blow counts clearly show that the piles were driven down the bedrock level very easily with the driving hammer used. Piles A17, F54 and D57 were driven into the bedrock for 3.0 m, 2.47 m and 3.5 m, respectively, before they satisfied the final set requirement. Piles A17 and D57 had deeper penetration, while F54 had less penetration, into the bedrock, before the final set reached 2.5 mm or less, as required. It can be seen from the penetration curves shown in Figure 7.1, that most of the penetration, i.e. about 80% of the total penetration, happened during the first 50 to 100 blows.

Figure 7.2 shows a relationship between the pile driving and pile penetration. The design final set was 2.5 mm/blow, which is equivalent to 40 blows/100 mm. The number of blows increased along with the depth of the pile penetration. After reaching about 20 blows per 100 mm, which is equivalent to a set of 5 mm, the speed of pile penetration decreased significantly, under the given pile driving effort. When pile driving reached 5 mm set, the piles could only be further driven about 1.0 meter into the bedrock before meeting the set requirement, which was 2.5 mm.

Figure 7.3 shows a relationship between the average set and pile length embedded in ground. This is another way to explain the observations plotted in Figure 7.2. After the first batches of blows, the piles were deep in the soil. After the pile toes reached the rock layer, the set was less than 20 mm. The figure shows that the Piles A17, F54 and D57 penetrated further into the rock for about 1.4 m, 1.7 m and 2.5 m, respectively, before the requirement for the final set was satisfied. For Pile D57, an abrupt change happened at the set of 5 mm, which implies that a possible weak rock layer was encountered.

7.5 Field Dynamic Load Tests

In the project, a total of 567 piles were tested during the initial pile driving, among which 99 piles were tested during the redriving. Through the CASE Method and CAPWAP Method, the following parameters were determined: driving stress, strike energy, soil resistance of driving, integrity of a pile, ultimate resistance of a pile, shaft resistance and toe resistance of a pile, and simulated P-S curve.

Initial Driving Tests of Piles A17, D57 and F54

Pile A17: During the test of the pile, seven blows were conducted and the pile penetrated into the soil for about 10 mm. The average final set was, therefore, 1.4 mm. The initial results of the pile bearing capacity by the CASE Method were: total load bearing capacity was 8300 kN and the total static load bearing capacity was 6800 kN.

Pile D57: In the test, 16 blows were conducted and the pile penetrated into the soil for about 40 mm. The average final set was 2.5 mm. The initial results of the pile bearing capacity by the CASE Method were: total pile bearing capacity was 6730 kN and the total static bearing capacity was 6140 kN.

Pile F54: In the test, 20 blows were conducted and the pile penetrated into the soil for about 50 mm. The average final set was 2.5 mm. The initial results of the pile bearing capacity by the CASE Method were: total pile bearing capacity was 7550 kN and the total static bearing capacity was 6380 kN.

Redriving Test of Pile F54

The elapsed time for the redriving was 13 days. In the redriving test, 25 blows were conducted and the pile penetrated about 60 mm into the soil. The average final set was about 2.4 mm. The value of the pile ultimate resistance by the CASE Method was 7000 kN. The value of the ultimate resistance by the CAPWAP Method was 7056 kN, among which, the shaft resistance capacity was 4816 kN and toe resistance was 2240 kN. The strength recovery factor K = 7056/6380 = 1.1.

The results of the PDA tests on three piles are shown in Table 7.1.

Initial Driving Tests and Redriving Tests for other Piles

Initial driving tests and redriving tests were carried out for 567 piles and 99 piles, respectively. The elapsed time of pile redriving varied from 2 days to 79 days after the piles were first installed. In order to evaluate the behaviour of the piles under the dynamic load tests, two groups of pile were selected, based on the criteria: having same pile diameters and having test records at both initial driving and redriving. The information of PDA tests about the piles in each group is shown in Table 7.2 for the piles with a diameter of 1.0 meter and in Table 7.3 for the piles with a diameter of 0.813 m, respectively. From the tables, it can be seen that there are 27 piles with a diameter of 1.0 meter, and 10 piles with a diameter of 0.813 meter in the respective group. Two piles in the 0.813 meter group do not have test results at the initial pile driving.

7.6 Evaluation of Dynamic Load Test Results

This section summarizes the results from the dynamic load tests. A discussion is provided to evaluate the results of the ultimate resistance by the CASE Method and CAPWAP Method, and the effect of factors, such as final set, pile burial length, setup and displacement. In the following analysis, the ultimate resistance of a pile is related to its burial length, the final set at pile installation, and the elapsed time after initial driving.

It should be noted that in a few cases the piles with the final set values over 3 mm were due to insufficient pile lengths that led to the suspension of the pile driving operation. The final set of the piles was controlled at around 2.5 mm as required after the piles were lengthened. However, no further dynamic load tests were conducted on these piles after the pile driving operation resumed. The set values larger than 2.5 mm showing in the relevant figures and tables are not the real final set at first driving and, therefore, the ultimate resistance calculated by the CASE method is not the real ultimate resistance of the relevant piles.

7.6.1 Ultimate Resistance by the CASE Method and CAPWAP Method

Piles with a Diameter of 1.0 Meter

Figure 7.4 shows the results of the CASE and CAPWAP methods after initial driving and redriving, respectively. The results of the CASE Method at initial driving show that the smallest ultimate resistance is 5700 kN, the largest ultimate resistance is 7500 kN and the average ultimate resistance is 6706 kN. At redriving, by the CASE Method, the smallest ultimate resistance is 7100 kN, the largest ultimate resistance is 9000 kN and the average ultimate resistance is 7933 kN. According to the CAPWAP Method, the smallest ultimate resistance is 6944 kN, the largest ultimate resistance is 8964 kN and the average ultimate resistance is 7842 kN at redriving.

From the above data, it can be seen that the difference margin between the smallest and largest ultimate resistance is around 2000 kN. At redriving, the CASE and CAPWAP methods gave quite agreeable results for the ultimate resistance, even if the CAPWAP Method had the ultimate resistance values slightly smaller than that by the CASE Method. When comparing with the results by the CASE Method at the initial driving, the values given by the CASE Method and CAPWAP Method at redriving are about 1200 kN larger, on average. By comparing the results by the CAPWAP Method at redriving over the CASE Method at initial driving, the largest recovery rate of the ultimate resistance is 1.23, the smallest recovery rate is 1.06 and the average recovery rate is 1.16.

Piles with a Diameter of 0.813 Meter

Figure 7.5 shows the results of the CASE and CAPWAP methods at initial driving and redriving, respectively. The results from the CASE Method at initial driving show that the smallest ultimate resistance is 6680 kN, the largest ultimate resistance is 7190 kN and the average ultimate resistance is 6802 kN. At redriving, by the CASE Method, the smallest ultimate resistance 7000 kN, the largest ultimate resistance is 8670 kN and the average ultimate resistance is 7538 kN. According to the CAPWAP Method, the smallest ultimate resistance is 7043 kN, the largest ultimate resistance is 8565 kN and the average ultimate resistance is 7477 kN at redriving.

The difference between the smallest and largest ultimate resistance is around 500 kN, 1600 kN and 1500 kN, for the CASE Method at initial driving, and the CASE and CAPWAP methods at redriving, respectively. At redriving, the CASE and CAPWAP methods gave quite agreeable results, and they were about 700 kN, on average, larger than that given by the CASE Method at the initial driving. By comparing the results of the CAPWAP Method at redriving and the CASE Method at initial driving, the largest recovery rate of the pile ultimate resistance is 1.20, the smallest recovery rate is 1.02 and the average recovery rate is 1.11.

Comparison and Discussion

According to the CAPWAP Method, the largest value of the ultimate resistance for 1.0 m diameter piles is about 9000 kN, while the largest value of the ultimate resistance for 0.813 m diameter piles is 8600 kN. The difference is about 400 kN, which is about 4.5% of the total ultimate resistance. Piles with two different diameters gave almost the same smallest ultimate resistance value of 7000 kN. The average values of the ultimate resistance are 7800 kN and 7500 kN, for 1.0 m diameter pile and 0.813 m diameter pile, respectively. It can be seen that the difference is only about 300 kN, which is 4% of the total ultimate resistance.

As for the data variation, 0.813 m diameter piles have a smaller difference between the largest and smallest ultimate resistance by different methods, while 1.0 m diameter piles have a larger difference.

The CASE Method and CAPWAP Method gave agreeable results for the pile ultimate resistance.

Comparing the ultimate resistance measured at first driving and redriving, the larger diameter piles had a higher increase in the bearing capacity. The average value of the ultimate resistance for 1.0 m diameter piles is 6700 kN at first driving, while the average value of the ultimate resistance for 0.813 m diameter piles is 6800 kN. However, after recovery, the average value of the ultimate resistance for 1.0 m diameter piles increased to 7800 kN, while the average value of the ultimate resistance for 0.813 m diameter piles became 7500 kN. The 1.0 m diameter piles had an average increase of 1100 kN in bearing capacity, while the 0.813 m diameter piles had an average bearing capacity increase of 700 kN. It has to be noted that the maximum elapsed time for 0.813 m diameter piles was only 15 days.

7.6.2 Ultimate Pile Shaft Resistance and Toe Resistance

Piles with a 1.0 m Diameter

Figure 7.6 presents the results of the ultimate shaft resistance and toe resistance by the CAPWAP Method at redriving. The largest ultimate shaft resistance is 5954 kN, the smallest ultimate shaft resistance is 3048 kN and the average ultimate shaft resistance is 5234 kN. The largest ultimate toe resistance is 3896 kN, the smallest ultimate toe resistance is 1848 kN and the average ultimate toe resistance is 2608 kN. The ratio of the ultimate shaft resistance over the ultimate toe resistance is between 0.78 and 3.06, and the average ratio is 2.09.

Piles with a 0.813 m Diameter

Figure 7.7 presents the results of the ultimate shaft resistance and toe resistance by the CAPWAP Method at redriving. The largest ultimate shaft resistance is 5103 kN, and the smallest ultimate shaft resistance is 3956 kN and the average ultimate shaft resistance is 4567 kN. The largest ultimate toe resistance is 3702 kN, the smallest ultimate toe resistance is 2240 kN and the average ultimate toe resistance is 2910 kN. The ratio of the ultimate shaft resistance over the ultimate toe resistance is in a range from 1.27 to 2.15, and the average ratio is 1.6.

Comparison and Discussion

The average ultimate toe resistance is 2608 kN for 1.0 m diameter piles. The average ultimate toe resistance is 2910 kN for 0.813 m diameter piles. The results implicate that a soil plug was formed to some extent for every pile in the project. The toe area of a 1.0 m diameter pile is about 0.056 m^2 and the allowable unit toe resistance recommended for the rock in this project is 2300 kPa maximum. The end bearing capacity on the pile wall annulus is therefore about 130 kN.

Piles with a larger diameter had a larger ultimate shaft resistance under the given conditions. 1.0 m diameter piles had, on average, an ultimate shaft resistance more than 700 kN larger than that of 0.813 m diameter piles. The ratio of the average shaft resistance of these two different piles is about 1.15, while their perimeter ratio is 1.23.

On average, 0.813 m diameter piles had a larger toe resistance than that of 1.0 m diameter piles. The difference is about 300 kN, which represents 10% of the average toe resistance for 1.0 m diameter piles. 0.813 m diameter piles had a bigger portion of the ultimate toe resistance in the total bearing capacity than that for 1.0 m diameter piles. It seems that, with the given pile driving equipment and the ground conditions, the toe resistance of piles with 0.813 m diameter was fully utilized. It implies that the ultimate resistance of piles with 1.0 m diameter could have larger values, if their toe resistance were fully utilized. From Figures 7.6 and 7.7, it can be seen that the largest pile ultimate resistance is always associated with the largest toe resistance values.

7.6.3 Impact of Final Set on the Ultimate Bearing Capacity

Piles with a Diameter of 1.0 Meter

Figure 7.8 shows the final set and ultimate resistance by the CASE and CAPWAP methods for 1.0 m diameter piles. The final set is in the range from 1 mm to 2.9 mm at first driving, and from 0.1 mm to 2.9 mm at redriving.

Figure 7.8a shows the ultimate resistance by the CASE Method at initial driving as a function of the final set for the piles with a diameter of 1.0 m. The ultimate resistance increased, when the final set values decreased.

Figure 7.8b shows the ultimate resistance by the CASE Method at redriving as a function of the final set for 1.0 m diameter piles. The values of the ultimate resistance do not show an obvious correlation to the final set values. If any, it can be said that the ultimate resistance had slightly high values when the final set was around 2.0 mm.

Figures 7.8c and 7.8d show the relation between the final set and the ultimate shaft resistance and the ultimate toe resistance by the CAPWAP Method, respectively. It seems that the values of the final set did not have an obvious impact on either the ultimate toe resistance or shaft resistance of the piles in the given final set range. The values of the ultimate toe resistance vary from 2000 kN to 4000 kN, while the values of the ultimate shaft resistance are between 4500 kN and 6000 kN. The ultimate shaft resistance tends to be on the high side when the final set is between 1 mm and 2.5 mm, while the ultimate toe resistance does not show any sign of such advantage.

Figure 7.8e shows the ultimate resistance by the CAPWAP Method as a function of the final set. The final sets of the selected piles were in the range from 0.1 mm to about 3.0 mm. Because the piles were driven into the rock, most of the piles had very small final set values at redriving. It also implicates that the driving equipment used in the project was not sufficient to make a final set of about 2.5 mm for the piles. From the figure, it can be seen that the pile axial bearing capacity is in the range of 7000 kN to 8000 kN, while a few reach 9000 kN. The values of the final set did not have an obvious impact on the axial ultimate resistance of the piles in the given range of final set values. If any, the bearing capacity of the piles was slightly on the higher side, when the final set was around 2 mm.

Piles with a Diameter of 0.813 Meter

Figure 7.9 shows the final set and the ultimate resistance by the CASE and CAPWAP methods for 0.813 m diameter piles. The final set is in the range from 1.7 mm to 3.3 mm at first driving, and from 1.2 mm to 2.4 mm at redriving, respectively.

Figure 7.9a shows the ultimate resistance by the CASE Method at redriving as a function of the final set. Figure 7.9b shows the ultimate resistance by the CASE Method at initial driving as a function of the final set. The final set values in the given range, in the two figures, do not show an obvious effect on the ultimate resistance.

Figures 7.9c and 7.9d show the ultimate shaft resistance and ultimate toe resistance by the CAPWAP Method as a function of the final set. Again, the values of the final set in the given range do not have obvious effects on either the toe resistance or shaft resistance of the piles.

Figure 7.9e shows the ultimate resistance by the CAPWAP Method as a function of the final set. The values of the final set of selected records are in the range between 1.0 mm to about 2.5 mm. The values of final set do not have obvious impacts on the ultimate axial bearing capacity of the piles in the given final set range.

Comparison and Discussion

According to the requirements of PDA test, the final set value shall be controlled at around 2.50 mm. The ultimate resistance would be smaller if the set is smaller than 2.00 mm. However, the results of the analysis presented above do not support the argument.

Generally speaking, in the given range of the final set, the final set has no obvious impact on the ultimate resistance of the piles.

It is obvious that the hammer used in the project is more efficient to drive the 0.813 m diameter piles. The final set for the 0.813 m diameter piles is in the range from 1 mm to 3 mm and most of the values are larger than 1.0 mm, as shown in Figure 7.9. However, the final set for the 1.0 m diameter piles is in the range of 0.1 mm to 3 mm, while most of the values are less than 1.0 mm, as shown in Figure 7.8.

7.6.4 Impact of Burial Length of Pile on Ultimate Resistance

Piles with a Diameter of 1.0 Meter

Figure 7.10 shows the relation between the burial length and the ultimate resistance by the CASE and CAPWAP methods for 1.0 m diameter piles. The studied piles have various burial lengths ranging from 6.88 m to 20.58 m.

Figures 7.10a and 7.10b show the bearing capacity by the CASE Method at both initial driving and redriving as a function of the pile burial length. Figures 7.10a and 7.10b show the increase of the ultimate resistance when the pile burial length is increased, except for the four piles with the burial length of around 20 meters. Table 7.2 shows that the four piles did not have the largest shaft resistance and their ultimate toe resistance had the values slightly higher than an average value from other piles.

Figure 7.10c shows the ultimate toe resistance as a function of the pile burial length. The ultimate toe resistance tends to increase with longer pile burial length. Four piles with about 20 m burial lengths show a slightly higher toe resistance.

Figure 7.10d shows the ultimate shaft resistance as a function of the pile burial length. The ultimate shaft resistance of the piles increased, as the pile burial lengths were longer. Four piles with about 20 m burial lengths show a slightly smaller shaft resistance than the average values.

Figure 7.10e gives the ultimate resistance by the CAPWAP Method, which is in the range of 7000 kN to 9000 kN. On average, the results show that the ultimate resistance increased along with the increase of the pile burial length, except for the piles with burial lengths of about 20 m.

Piles with a Diameter of 0.813 Meter

Figure 7.11 shows the relation between the burial length and the ultimate resistance by the CASE and CAPWAP methods for 0.813 m diameter piles. The studied piles have various burial lengths ranging from 7.81 m to 10.8 m.

Figures 7.11a and 7.11b show the bearing capacity as a function of the pile burial length. The ultimate resistance decreased when the pile burial length was longer.

Figure 7.11c shows the ultimate toe resistance by the CAPWAP Method as a function of the pile burial length. The ultimate toe resistance decreased when the burial length increased, with one exception.

The ultimate shaft resistance of the piles is plotted in Figure 7.11d which shows that the ultimate shaft resistance decreased as the pile burial length increased.

Figure 7.11e shows the ultimate resistance by the CAPWAP Method as a function of the pile burial length. The results show a decrease in the ultimate resistance with an increase in pile burial length. When the pile burial lengths are over 10 meters, the ultimate resistance is stabilized at values of around 7000 kN.

Comparison and Discussion

The ultimate resistance of the 1.0 m diameter piles increased slightly when the pile burial length became longer under the given conditions and the range of pile burial length. The ultimate resistance of the 0.813 m diameter piles decreased, when the pile burial length became longer under the given conditions and the range of pile burial length. The two different piles show contradictory results for the relations between the pile ultimate resistance and the pile burial length.

The ultimate toe resistance of the 1.0 m diameter piles has values ranging from 2000 kN to 3000 kN, with a few exceptions. The ultimate toe resistance of the 0.813 m diameter piles has values ranging mostly from 2500 kN to 3500 kN. The piles with a 0.813 m diameter have a higher ultimate toe resistance than that for the piles with a 1.0 m diameter.

The ultimate shaft resistance of the 1.0 m diameter piles has values ranging mostly from 4500 kN to 6000 kN. The ultimate shaft resistance of the 0.813 m diameter piles has values ranging from 4000 kN to 5000 kN. The piles with a larger diameter have a higher ultimate shaft resistance.

7.6.5 Impact of Setup Rate on the Ultimate Bearing Capacity

Piles with a Diameter of 1.0 Meter

Figure 7.12 shows the setup rate of the piles as a function of the elapsed time. The setup rate is defined by the result from the CAPWAP Method at redriving divided by the result from the CASE Method at the initial driving. The elapsed time is in the range from 2 days to 79 days.

The results clearly indicate that the recovery rate, i.e. the setup, increased with time in the first twenty days or so. This implies that, up to about 15 days, the ultimate resistance increased along with the elapsed time. After fifteen days, the ultimate resistance further increased, but the results also show low values of the recovery rate. The setup time could be as long as up to sixty days, as shown in the figure. For the four piles with more than 70 days of elapsed time, their burial lengths are less than 10 meters, and the shortest one is about 6.88 meters. The recovery rates for these four piles are on low side. Table 7.2 shows that two piles with up to 70-day elapsed time have a setup rate of 1.06 when the pile burial lengths are about 8 m or 9 m.

Figure 7.13 shows a relation between the setup rate and the final set at first driving for 1.0 m diameter piles. It seems that the final set at first driving had no obvious impact on the pile setup. Note that the piles were lengthened and redriven when the set was larger than 4 mm.

Figure 7.14 shows the setup rate for 1.0 m diameter piles as a function of the pile burial length. It is indicated in the figure that the setup value increased as the pile burial length increased.

Figure 7.15 is a plot of the setup rate and the bearing capacity by the CASE Method at first driving for 1.0 m diameter piles. The figure shows that the lower ultimate resistance by the CASE Method at first driving provides higher setup rate.

Piles with a Diameter of 0.813 Meter

Figure 7.16 shows the effect of various factors on the setup rate for 0.813 m diameter piles.

Figure 7.16a shows the setup rate as a function of the pile burial length for 0.813 m diameter piles. It is indicated in the figure that the setup value decreased as pile burial length increased. It is different from that observed in the relevant figure for 1.0 m diameter piles.

Figure 7.16b shows the setup rate of the piles versus the elapsed time. The elapsed time is in the range from 2 days to 15 days. The ultimate resistance increased with the time. Note that the data are very limited for this group of piles.

Figure 7.16c gives the relation between the setup rate and the final set at first driving for 0.813 m diameter piles. The setup rate was slightly smaller when the final set at the initial driving had higher values.

Figure 7.16d illustrates the relation between the setup rate and the bearing capacity by the CASE Method at first driving for 0.813 m diameter piles. The figure shows that the setup rate decreased as the bearing capacity increased, when the bearing capacity values were smaller than 6800 kN. The setup rate increased significantly, when the bearing capacity value was over 6800 kN.

Comparison and Discussion

After initial pile driving, the ultimate resistance of the piles increased along with the time. The recovery time could be as long as sixty days. However, this time period was not verified due to the lack of data between 20 days and 40 days in Figure 7.12. It is also not practical to wait for sixty days to conduct required load test in any real life project. Two-week time, under the given conditions, could be used as a reasonable elapsed time.

For 1.0 m diameter piles, the longer the pile burial length was, the higher the setup rate was. However, for 0.813 m diameter piles, the setup rate decreased when the pile burial length was longer.

7.6.6 Impact of Total Pile Settlement at Redriving

Piles with a Diameter of 1.0 Meter

Figure 7.17 shows the impact of the total pile settlement at redriving. The CAPWAP Method can provide shaft and toe resistance when a pile is tested at redriving. In most cases, the pile settlement was very small at the redriving.

Figure 7.17a shows the ultimate shaft resistance as a function of the pile penetration at the redriving. There is no obvious increase in shaft resistance within 50 mm penetration. The shaft resistance had higher values when the penetration was between 50 mm and 150 mm.

Figure 7.17b shows the ultimate toe resistance as a function of the pile penetration at the redriving. It shows a reverse trend to that observed in Figure 7.17a. When the penetration of the piles was between 50 mm and 150 mm, it gave smaller toe resistance values.

Figure 7.17c shows that the pile penetration at redriving has no obvious impact on the setup rate.

Figure 7.17d shows the ultimate resistance as a function of the pile penetration at redriving. Generally speaking, the ultimate resistance attains slightly higher values when the penetration is higher.

Discussion

When a pile has a larger total penetration at redriving, the ultimate shaft resistance tends to be larger, but the ultimate toe resistance tends to be smaller.

7.7 Summary and Discussion

1. In terms of the ultimate bearing capacity, 1.0 m diameter piles gave the largest value of about 9000 kN, while 0.813 m piles gave a value of 8600 kN. The smallest ultimate resistance of the piles has a value of 7000 kN. The average values of the ultimate resistance were 7800 kN and 7500 kN, for 1.0 meter pile and 0.813 meter pile, respectively. The CASE Method and CAPWAP Method gave agreeable results for the pile ultimate resistance.

2. The results from the dynamic tests show that the piles in the project were solidly plugged and the end-bearing could be assumed to act over the entire cross-sectional area of a pile. Tatsunori (1995) suggested, based on the tests on open-ended steel tubular piles driven in soft rock, the total inner shaft resistance is limited to the end-bearing capacity of the ground below the soil plug, when a perfect plug is formed. He described that, in his tests, the ground below the pile toe was compressed by the tubular pile with perfect plug mode in which the inner soil at the bottom 2 meters of the pile was highly compressed, which resulted in a large inner shaft resistance.

3. After initial pile driving in the project, the bearing capacity of the pile foundation increased along with the time. The recovery time was about two weeks, in the given conditions.

   Pile driving activity will change the properties of the soil surrounding piles from those existing prior to the pile installation. The effects of pile driving in clays were considered by de Mello (1969) as follows: (1) remolding or partial structural alteration of the soil surrounding the pile; (2) alteration of the stress state in the soil in the vicinity of the pile; (3) generation and dissipation of the excess pore pressures developed around the pile; and (4) long-term phenomena of strength regain in the soil.

   Because driving of piles into clay soils, the undrained strength of clay is initially decreased considerably because of driving, but the significant regain of strength occurs with elapsed time between driving and pile testing. The strength usually increases because of two factors: thixotropic regain of undrained strength as the structure bonds destroyed by remolding are at least partially restored, and the increase resulting from local consolidation of the clay produced by dissipation of excess pore-water pressures that arise from the increase in stress in the soil surrounding the pile.

The results of many measurements of pore pressure at the pile face revealed that the excess pore pressure might become equal to or even greater than the effective overburden stress. However, the induced excess pore pressures decrease rapidly with distance from the pile and generally dissipate very rapidly. Tatsunori at al, (1995), observed that positive pore pressures are generated near the pile surface due to pile installation. Large pore pressure is generated in soil plug inside the pile during driving, which may facilitate the installation of pile due to reduced shear strength of soil. He also observed that only imperfect soil plugging occurs during pile driving.

4. Piles with a larger diameter have a larger ultimate shaft resistance in the given conditions. The 1.0 m diameter piles have, on average, an ultimate shaft resistance of 5234 kN, and the largest shaft resistance is 5954 kN and the smallest shaft resistance is 3048 kN. The 0.813 m diameter piles have, on average, an ultimate shaft resistance of 4567 kN, and the largest shaft resistance is 5103 kN and the smallest shaft resistance is 3956 kN. Piles with a smaller diameter have comparatively a larger ultimate toe resistance in the given conditions. The 1.0 m diameter piles have, on average, an ultimate toe resistance of 2608 kN, and the largest toe resistance is 3896 kN and the smallest toe resistance is 1848 kN. The 0.813 m diameter piles have, on average, an ultimate toe resistance of 2910 kN, and the largest toe resistance is 3702 and the smallest toe resistance is 2240 kN. It can be seen that, in the given geotechnical conditions and pile driving equipment, the toe resistance of both sizes of the piles is very close. The portion of toe resistance in the total bearing capacity for 0.813 m diameter piles is bigger than that for 1.0 m diameter piles, in the given conditions. The piles with the highest bearing capacity are always associated with higher values of toe resistance.

5. Generally speaking, in the given range of the final set, the set value has no obvious impact on the ultimate resistance of the piles. The hammer used in the project is more efficient for the 0.813 m diameter piles. It has difficulty to drive the 1.0 m diameter piles at redriving, in terms of proper final set.

Due to a limited number of test data, it is impossible to assess the impact of one factor at a time by making other factors the same. For example, it would be impossible to have all piles with the same burial length in order to assess the impact of the final set on the pile bearing capacity. The ultimate resistance of a pile is affected by many factors, such as pile burial length and setup time, besides the pile driving equipment and the analysis methods. Even if all efforts have been made to ensure the accuracy of the discussions and conclusions presented in the chapter, one should use the results with caution. Because of limited number of test data, the conclusions in this chapter are to be re-affirmed.

Chapter 8

SUMMARY AND CONCLUSIONS

8.1 Summary of Investigation

The ultimate bearing capacity of tubular, open-ended steel piles driving into weathered rock in a foundation project was investigated by static load tests, finite element analysis and pile dynamic load tests. Three piles were selected for the static load tests. Two piles were selected for the finite element analysis. Two groups of piles with different size were selected for the dynamic load tests.

During the pile installation, dynamic load tests were carried out by using the CASE Method as performed by a Pile Driving Analyser (PDA) on the selected piles. The CAPWAP Method was also used in conjunction with the PDA. The dynamic load tests were conducted during the initial driving of piles, and, for small number of piles, during the restriking of piles. The dynamic load tests provided information about the driving force, the integrity of piles, the static bearing capacity at initial pile driving, and the ultimate load bearing capacity of piles at redriving, including shaft resistance and toe resistance. In the investigation, the ultimate resistance by CASE Method and CAPWAP Method were determined, and the effects of final set, pile burial length, setup and other factors on the pile bearing capacity were evaluated.

The program of static load tests was undertaken to investigate the bearing mechanism of the open-ended tubular piles driven into the weathered bedrock. Three piles with a diameter of 0.813 m and 1.0 m, respectively, were tested. Vertical compression tests were performed on all three piles, and tension tests were carried out on two piles. The initial plan was to carry out the static load tests on two piles with different diameters. However, the second test pile failed the design criteria in terms of residual displacement, which led to another test on a pile with a diameter of 0.813 meter. The results of the compression load tests and tension load tests were evaluated, in terms of loads, displacements and time. The performance of the piles in the load tests was analysed and the analysis results were provided in the investigation.

The details of the finite element analysis have been presented for the work of the back-calculation of the load-displacement response of open-ended steel tubular piles driven through clay soil layers into weathered bedrock. An attempt was made to assess, qualitatively, the finite-element model as a rational approach to the analysis of pile load-displacement response. A finite-element model for the soil-pile system was designed and simulations were conducted. A hyperbolic model for soils and an elastic-plastic model for rocks were used in the study. All major parameters were obtained based on the results of the field and laboratory tests or from various engineering handbooks. A parametric study was also carried out. The issues, such as interface elements and soil plug, were discussed.

8.2 Conclusions

Based on the results of the investigation, the following conclusions can be made:

1 The piles were driven to a pre-determined final set in the rock, and they were regarded as having both toe resistance and shaft resistance. Piles with diameters of 1.0 meter and 0.813 meter have adequate bearing capacity, i.e., 6944 kN and 7043 kN, respectively, to resist the design load, i.e., 6696 kN.

2. Pile head displacement at the working load was 17.95 mm for 1 meter diameter pile and 29.06 mm for 0.813 meter diameter pile. These values were obtained from static load tests. The finite element analysis also provided comparable results.

3. For the bearing capacity of piles, it was not possible to make direct correlation between static and dynamic load tests because static load tests were not carried out to failure. However, the dynamic load tests gave values of pile capacities larger than the working loads used in the static load test.

4. For the piles in the project, a soil plug was formed to some extent, due to the large inner shaft resistance. The toe resistance can be assumed to act over the entire cross-sectional area of a pile.

5. For the effect of sustained loads on piles driven in clays, there may be a reduction in shaft resistance with time. This may result concentrations of very high loading on the rock beneath the toe of a pile, which would cause yielding of rock mass below a pile toe.

6. Pile driving activity changed the properties of the soil inside and surrounding piles from those existing prior to the pile installations. Setup was caused mainly by recovery of soil strength after remolding. The setup time in the project is about two weeks.

7. The results of the finite element analysis for the cases analyzed are consistent with the static load tests. The study should be useful in describing the effect of design loads at the pile head on the behavior and deformation of the soil and rock, and the extent of this effect in the region around the pile shaft and below the pile toe. The load-displacement response of a pile calculated by the model could be used to improve the existing empirical and rational approaches for pile analysis. The finite element models and the determined parameters in the project could be used to estimate the load-displacement response for the piles with different sizes and under different design loads.

8.3 Recommendations for Future Research

Based on the experience gained during this study, the following recommendations can be made:

1. Find a relation between the results of static and dynamic load tests based on rate dependent stress-strain relations.

2. Determine the effect of pile driving on the soil density, state of stress and excess pore water pressure using large displacement analysis.

3. Further studies on the effectiveness of a soil plug would be useful.

REFERENCES

American Petroleum Institute (1987). Recommended practice for planning, designing and constructing fixed offshore platforms. *API RP2A*

ASTM (1995). Standard test method for piles under static axial compressive load, D1148-81. *1995 Annual Book of ASTM Standards*, vol. 04.08, American Society for Testing and Materials, New York, pp 87-97.

Barton, N.R. (1986). Deformation phenomena in jointed rock. *Geotechnique*, vol. 36, pp 147-167.

Bjerrum, L. (1973). Problems of Soil Mechanics and Construction in Soft Clay. *Proceedings of the 8th International Conference*, ISSMFE, Moscow, vol. 3, pp 150-7.

Butler, F.G. and Morton, K. (1971). Specification and performance of test piles in clay. *Proceedings of the Conference on Behaviour of Piles*, London, pp 17-26.

Butterfield, R. and Bannerjee, P.K. (1971a). The elastic analysis of compressible piles and pile groups. *Geotechnique*, vol. 21, pp 43-60.

Butterfield, R. and Bannerjee, P.K. (1971b). The problem of pile group-pile cap interaction. *Getoechnique*, vol. 21, pp135-142.

Canadian Geotechnical Society (1992). *Canadian Foundation Engineering Manual. (Third Edition)*. Canadian Geotechnical Society, Ottawa, 512p.

Cole, K.W and Patel, D. (1992). Review of prediction of pile performance in London Clay under the action of service loads. *Proceedings of Conference on Piling - European Practice and Worldwide Trends*, London, pp 80-87.

Coyle, H.M. and Reese, L.C. (1966). Load transfer for axially loaded piles in clay. *Journal of the Soil Mechanics and Foundations Division, American Society of Civil Engineers*, vol. 92, no. SM2, pp 1-26.

Cundall, P.A. (1980). *UDEC - A generalized distinct element program for modeling jointed rock*. Peter Cundall Associates, (Report PCAR-1-80), for European Research Office, US Army, 69 p.

De Mello, V. F. B. (1969). Foundations of buildings on clay. *State of the art report*. Proceedings 7th International Conference. S.M. and F.E., Mexico City. pp 49-136

Duncan, J.M. and Chang, C.Y. (1970). Nonlinear analysis of stress and strain in soils. *Journal of the Soil Mechanics and Foundations Division, ASCE*, vol. 96, no. SM5, pp 1629-1654.

Duncan, J.M., Byrne, P., Wong, K.S., and Mabry, P. (1980). *Strength, Stress-Strain and Bulk Modulus Parameters for Finite Element Analyses of Stresses and Movements in Soil Masses.* Report No. UBC/GT/80-01. Department of Civil Engineering, University of California, Berkeley, California.

Fellenius B.H. (1975). Test loading of piles - Methods, Interpretation, and Proof Testing. *Journal of the Geotechnical Engineering Division, ASCE*, vol. 101, GT9, pp. 855-869.

Fellenius, B.H. (1980). The analysis of results from routine pile load tests. *Ground Engineering*, vol. 13, no. 6, pp 19-36.

Fellenius, B.H. (1989). Unified design of piles and pile groups *Transportation Research Board Record* 1169, pp 75-82.

Fleming, W.G.K., Weltman, A.J., Randolph, M.F. and Elson, W.K. (1992). *Piling Engineering*. (Second edition). Surrey University Press, London, 390 p.

GEO (1993). *Guide to Retaining Wall Design (Geoguide 1). (Second edition).* Geotechnical Engineering Office, Hong Kong, 267p.

GEO (1996). *Pile Design and Construction. (GEO Publication No.1/96).* Geotechnical Engineering Office, Hong Kong, 344p.

GEO-SLOPE. (1998). *SIGMA/W for Finite Element Stress and Deformation Analysis, Version 4.* GEO-SLOPE International Ltd., Calgary, Alberta, Canada.

Goble, G.G., and Rausche, F. (1976). Wave equation analysis of pile driving. *WEAP program. Vol. 1 - Background, Vol. 2 - User's Manual, Vol. 3 - Program Documentation, US Department of Transportation, Federal Highway Administration, FHWA*, Office of Research and Development, Implementation Division, Washington, D.C., 371p.

Goble, G.G., Rausche, F., and Likins, G.E. (1980). The analysis of pile driving. A state-of-the-art. *Proceedings, International Seminar on the Application of Stress-Wave Theory to Piles*, Stockholm, 1980, H. Bredenberg, Editor, A.A. Balkema, Rotterdam, pp. 131-162.

Janbu and Nilmar (1963). Soil Compressibility as Determined by Ocdometer and Triaxial Tests. *European Conference on Soil Mechanics and Foundations Engineering*, Wiesbaden, Germany vol. 1, pp19-25.

Jardine, R.J., Potts, D.M., Fourie, A.B. and Burland, J.B. (1986). Studies of the influence of non-linear str5ess-strain characteristics in soil-structure interaction. *Geotechnique*, vol. 36, pp 377-396.

Kondner, R.L. (1963a). Hyperbolic Stress-strain Response: Cohesive Soils. *Journal of the Soil Mechanics and Foundations Division*. ASCE, vol. 89, no. SM1, Proc. Paper 3429, pp 115-143.

Kondner, R.L., and Zelasko, J.S. (1963b) A Hyperbolic Stress-strain Formulation for Sands. *Proceedings, 2nd Pan-American Conference on Soil Mechanics and Foundations Engineering*. Brazil, vol. I, pp 289-324.

Kondner R.L. and Zelasko, J.S. (1963c). Void Ratio Effects on the Hyperbolic Stress-strain Response of a Sand. *Laboratory Shear Testing of Soils*, ASTM STP no. 361. Ottawa.

Kondner, R.L. and Horner, J.M. (1965). Triaxial compression of a Cohesive Soil with Effective Octahedral Stress Control. *Canadian Geotechnical Journal*. vol. 2, no. 1, pp 40-52.

Kreyszig, E. (1979). Advanced engineering mathematics. *John Wiley and Sons, Fourth Edition*, pp. 468-538.

Kulhawy, F.H. and Carter, J.P. (1992a). Settlement and bearing capacity of foundations on rock masses. Chapter 12 in *Engineering in Rock Masses*, edited by F.G. Bell, pp 231-245. Butterworth-Heinemann, Oxford.

Kulhawy, F.H. and Carter, J.P. (1992b). Socketed foundations in rock masses. Chapter 25 in *Engineering in Rock Masses*, edited by F.G. Bell, pp 509-529. Butterworth-Heinemann, Oxford.

Lehane, B. (1992). *Experimental Investigations of Pile Behaviour Using Instrumented Field Piles*. Ph.D. thesis, University of London, 615 p. (Unpublished).

Lehane, B., Jardine, R.J., Bond, A.J. and Frank, R. (1993). Mechanisms of shaft friction in sand from instrumented pile tests. *Journal of Geotechnical Engineering, American Society of Civil Engineers*, vol. 119, pp 19-35.

Meyerhof, G.G. (1976). Bearing capacity and settlements of piled foundations. *Journal of the Geotechnical Engineering Division, American Society of Civil Engineers*, vol. 102, pp197-228

Meyerhof, G.G. (1986). Theory and practice of pile foundations. *Proceedings of the International Conference on Deep Foundations*, Beijing, vol. 2, pp 1.77-1.86

Mindlin, R.D. (1936). Force at a point in the interior of a semi-infinite solid. *Physics*, vol. 77, pp 195-202.

Peck, G. M. (1969). The rational design of large diameter bored piles founded on rock. *Rock Mechanics. Symp. Institute Engineers*. Australia. Sydney. pp 48-51.

Poskitt, T.J. (1991). Energy loss in pile-driving due to soil rate effects and hammer misalignment. *Proceedings of Institution of Civil Engineers*, Part 2, vol. 91, pp 823-851

Poulus, H.G. (1989). Pile behaviour - theory and application. *Geotechnique*, vol. 39, pp 365-415.

Poulos, H.G. and Davis, E.H. (1980) *Pile Foundation Analysis and Design*. John Wiley and Sons, New York, 41[illegible]

Premchitt, J., Gray, I. and Massey, [illegible]. (1988). Initial measurements of skin friction on some driven piles in reclamat[illegible] Hong Kong Engineer, vol. 16, no. 5, pp 25-38.

Randolph, M.F. (1980). PIGLE[illegible] *A Computer Program for the Analysis and Design of Pile Groups under Ge[illegible]al Loading Conditions*. Cambridge University Engineering Department [illegible]earch Report, Soils TR 91, 33 p.

Randolph, M.F. and Wroth [illegible]P. (1978). Analysis of deformation of vertically loaded piles. *Journal of th[illegible] Geotechnical Engineering Division, American Society of Civil Engineers*, vol. [illegible]04, pp 1465-1488.

Rausche, F., Moses, F., and Goble G. G., 1972. Soil Resistance Prediction from Pile Dynamics. *American Society of Civil Engineers, ASCE, Journal of Soil Mechanics and Foundations Division*, Vol. 98, No. SM9, pp. 917-937

Rausche, F., Goble G. G. and Likins, G. E. (1985). Dynamic determination of pile capacity. *Journal of Geotechnical Engineering, American Society of Civil Engineers*, Vol. 111, pp 367-383.

Rausche, F., Likins, G. E., and Hussein, M., 1986. Dynamic Analysis of Impact Piles by WEAP86 *Report prepared for Office of Implementation Federal Highway Administration*, McLean, Virginia, 40 p.

Smith, E.A.L. (1960). Pile driving analysis by the wave equation. *American Society of Civil Engineers, ASCE, Journal for Soil Mechanics and Foundation Engineering*, vol. 86, No. SM4, pp.35-61. (Discussion in Vol. 87, No. SM1, pp. 63-75)

Tatsunor[illegible] M., Yuji, M. and Tadao, H. (1995). Performance of Axially Loaded Steel Pile Pi[illegible] Driven in Soft Rock. *Journal of Geotechnical Engineering*, vol 121, no. 4, p[illegible] 305-3015.

Timoshenko, S.P., and Goodier, J.N. (1970). Theory of elasticity. *Engineering Societies Monographs, McGraw Hill Book Company, Third edition*, pp. 485-514

Tomlinson, M.J. (1994). *Pile Design and Construction Practice. (Fourth edition)*. Spon, 411 p.

Vesic, A.S. (1977). *Design of Pile Foundations*. National Co-operative Highway Research Program, Synthesis of Highway Practice no. 42, Transportation Research Board, National Research Council, Washington D.C., 41 p.

Table 4.1 D80-23 Hammer Performance Parameter

Item		Unit	Value
Features	total weight	kg	16905
	cylinder weight	kg	8000
	hammer length	m	
	hammer diameter	m	
Performance	blows per minute	1/minute	36 - 45
	max. stroke distance	m	3.4
	explosive energy per time	Nm	266830 - 171085
	max. explosive force	kN	2600

Table 4.2 Features of Steel Tubular Piles A17, F54 and D57

	Item	Notation	Unit	A17	F54	D57
	Ppile Specification					
1	Outer Radius	r_o	mm	1000	813	813
2	Inner Radius	r_i	mm	964	777	777
3	Wall Thickness	t_w	mm	18	18	18
4	Cross-Section Area	A	mm^2	55530.79	44956.19	44956.19
5	Length	L	m	28.38	32.92	33.43
6	Free Length	L_f	m	17.18	21.88	21.48
7	Burial Length	L_b	m	11.2	9.33	11.95
8	Raking		%	0.00%	0.00%	0.00%
	Pile Driving					
9	Total Blow, First Driving		unit	384	492	688
10	Final Set, First Driving		mm/blow	1.4	2.5	2.5
11	Total Blow, Redriving		unit		25	
12	Final Set (average), Redriving		mm/blow		2.4	

Table 4.3 Bedrock Characteristics

Uniaxial Compression Stress (MPa)		
Dry	max.	101
	min.	30
	mean	64
Wet	max.	95
	min.	10
	mean	26

Table 4.4 Soil Physical and Mechanic Characteristic by Layers

Layer	Soil descrip-tion	Water Content W (%)	unit weight γ (kN/m³)	Void ratio (e)	Liquid limit WL (%)	Plastic index I_p (%)	Liquidity index I_L (%)	Quick shear		Consolidated quick shear		Coefficient of compression 100-200kPa (MPa⁻¹)	Permeability coefficient 10^{-6} (mm/s)	Unconfined compressive strength q_u (kPa)	Standard penetration N (63.5) (blow)	Allowable bearing capacity R(kPa)	Ultimate shaft resistance q_s (kPa)	Layer features description
								Φ (degree)	C (kPa)	Φ' (degree)	C' (kPa)							
1-1	Silt	61.8	16.1	1.75	41.3	20.2	2.05	0	7.3	12.0	13.8	1.58	1.25	7.8	<1	60	15	plastic to soft plastic
1-2	Silt clay	48.1	17.1	1.37	37.6	19.2	1.55	0	7	12	15	1.13		10.4	<1	80	20	soft plastic, thickness less than 2m
2-1	Clay	35.9	18.4	1.03	42.9	22.5	0.69	9	36	16.3	34			80.2	7	180	40	plastic, depth 1-2m, widely distributed
2-2	Coarse sand														22	240	80	300m in the east, with good continuity, depth 1-2m, the west is distributed in lens shape
2-3	Clay loam	22.7	19.9	0.69	25.9	12.1	0.74	13.5	32.5	18.1	32.4			99.6	11	220	80	
3-1	completely weathered Tuff														N=50 S=100-200 mm	500~1000	100	decomposed into earth shape, standard penetration increases with depth, heavy decomposed
3-2	medium weathered tuff															1000~2000	150	
3-3	slightly weathered tuff																	fresh rock, not decomposed

TABLE 5.1 SEQUENCE OF TEST LOADING

Sequence Of Compression Loading

Load, % of Design Load	Minimum Time of Holding Load
25	1 hour
50	1 hour
75	1 hour
100	1 hour
50	10 minutes
0	1 hour
25	1 hour
50	1 hour
75	1 hour
100	1 hour
125	1 hour
150	1 hour
175	1 hour
200	72 hours
175	20 minutes
150	20 minutes
125	20 minutes
100	20 minutes
75	20 minutes
50	20 minutes
25	20 minutes
0	1 hour

Sequence of Tension Loading

Loading	Minimum Holding Time
25% of Stage 1 loading	1 Hour
50% of Stage 1 loading	1 Hour
75% of Stage 1 loading	1 Hour
100% of Stage 1 loading	1 Hour
75% of Stage 1 loading	10 Minutes
50% of Stage 1 loading	10 Minutes
25% of Stage 1 loading	10 Minutes
0% of Stage 1 loading	1 Hour
25% of Stage 2 loading	1 Hour
50% of Stage 2 loading	1 Hour
75% of Stage 2 loading	1 Hour
100% of Stage 2 loading	72 Hours
75% of Stage 2 loading	10 Minutes
50% of Stage 2 loading	10 Minutes
25% of Stage 2 loading	10 Minutes
0% of Stage 2 loading	1 Hour

note: Stage 1: Pile self weight plus working friction.
Stage 2: Pile self weight plus 1.5 times working friction.

Table 6.1 Clay and Rock Parameters for Finite Element Analysis

	Pile A17							
	Compression	E (kPa)	v	c (kPa)	ϕ (degree)	K (kPa)	n	Rf
1	Second Loading Cycle							
	clay	10,000	0.49	40	21	200	0.18	0.84
	weathered rock	2,000,000	0.25	22	27			
	intact rock	10,000,000	0.2	1,000	32			
2	Second Loading Cycle Case1							
	weathered rock	**1,000,000**	0.25	22	27			
	intact rock	10,000,000	0.2	1,000	32			
3	Second Loading Cycle Case2							
	weathered rock	**2,500,000**	0.25	22	27			
	intact rock	10,000,000	0.2	1,000	32			
4	Second Loading Cycle Case3							
	weathered rock	**4,000,000**	0.25	22	27			
	intact rock	10,000,000	0.2	1,000	32			
	Second Loading Cycle Case4							
5	weathered rock	2,000,000	0.25	**15**	27			
	intact rock	10,000,000	0.2	1,000	32			
	Second Loading Cycle Case5							
6	weathered rock	2,000,000	0.25	**30**	27			
	intact rock	10,000,000	0.2	1,000	32			
	Second Loading Cycle Case6							
7	weathered rock	2,000,000	0.25	22	**20**			
	intact rock	10,000,000	0.2	1,000	32			
	Second Loading Cycle Case7							
8	weathered rock	2,000,000	0.25	22	**35**			
	intact rock	10,000,000	0.2	1,000	32			
	Second Loading Cycle Case8							
9	weathered rock	2,000,000	**0.2**	22	27			
	intact rock	10,000,000	0.2	1,000	32			
	Second Loading Cycle Case9							
10	weathered rock	2,000,000	**0.35**	22	27			
	intact rock	10,000,000	0.2	1,000	32			
	Second Loading Cycle Case10							
11	weathered rock	2,000,000	0.25	22	27			
	intact rock	**5,000,000**	0.2	1,000	32			
	Second Loading Cycle Case11							
12	weathered rock	2,000,000	0.25	22	27			
	intact rock	**20,000,000**	0.2	1,000	32			
	Second Loading Cycle Case12							
13	weathered rock	2,000,000	0.25	22	27			
	intact rock	10,000,000	**0.3**	1,000	32			
	Second Loading Cycle Case13							
14	weathered rock	2,000,000	0.25	22	27			
	intact rock	10,000,000	0.2	**500**	32			
	Second Loading Cycle Case14							
15	weathered rock	2,000,000	0.25	22	27			
	intact rock	10,000,000	0.2	1,000	**40**			

Note: bolded values are the changed ones in the sets.

Table 7.1 PDA Test Informtion

No.	Item	Unit	A17	D57	F54
	Initial Driving				
1	Pile Length	m	33	36	31
2	Final Set	mm	1.40	2.50	2.50
3	Hammer Energy	kJ	65	85	77
4	Hammer Force	kN	6,100	5,160	5,970
5	Stress in Pile	MPa	110	115	133
6	Total Bearing Capacity	kN	8,300	6,730	7,550
7	Total Static Bearing Capacity	kN	6,800	6,140	6,380
	Redriving				
8	Elapsed Time	day			13
9	Final Set	mm			2
10	Hammer Energy	kJ			130
11	Hammer Force	kN			7,200
12	Stress in Pile	MPa			
13	Pile Bearing Capacity (CASE)	kN			7,000
14	Pile Shaft Resistance (CAPWAP)	kN			4,816
15	Pile Toe Capacity (CAPWAP)	kN			2,240

Table 7.2 Pile Information, 1.0 m Diameter Pile

	Pile	Burial Length	First Drive	First Drive	Set, Redrive	CASE, Redrive	CAPWAP	Shaft Resistance	Toe Resistance	Elapsed Time	K
		m	mm	kN	mm	kN	kN	kN	kN		
1	A70	13.8	5	6200	0.2	8200	8018	5495	2523	19	
2	A74	12.36	4	6000	0.8	7500	7502	5654	1848	19	
3	B7	14.1	1.6	7300	0.12	8200	7966	5240	2726	2	1.09
4	B9	7.9	1.8	6700	0.11	7400	7266	5248	2018	2	1.08
5	B11	10.46	4.4	5700	1.1	7200	6944	3048	3896	39	
6	B13	10.2	1	7200	2	8200	8102	5542	2560	5	1.13
7	B15	11.4	2.3	6800	2	8000	7846	5702	2144	6	1.15
8	B17	10	1.8	6800	2.6	8000	7833	5427	2406	6	1.15
9	B19	6.6	2.9	6900	1.4	8300	8156	5954	2202	10	1.18
10	D5	12.81	1.7	7200	2	8200	8102	5796	2306	48	1.13
11	D9	19.55	4.5	5800	1	7500	7190	4562	2628	43	
12	D11	18.83	2	6400	0.13	7700	7732	4939	2793	44	1.21
13	D13	20.58	2.5	6600	0.04	7900	7842	5010	2832	39	1.19
14	D17	18.62	2.6	6600	0.3	8000	7926	5111	2815	44	1.20
15	D70	9.28	2.5	6600	0.4	7700	7725	4765	2960	14	1.17
16	E9	15.43	2.3	6400	0.1	7900	7764	5460	2304	53	1.21
17	E11	13.67	2	6000	0.15	7600	7402	5290	2112	52	1.23
18	E13	11.42	2.6	6900	0.2	8100	8023	5912	2111	52	1.16
19	E15	12.58	2.2	7300	0.7	8300	8240	5734	2506	50	1.13
20	E17	11.22	2.2	7100	0.7	8100	8121	5298	2823	50	1.14
21	E62	9.4	2.2	6900	0.08	7700	7296	4779	2517	73	1.06
22	E60	8.79	2.8	6500	0.3	7200	7735	5630	2105	73	1.19
23	F9	13.87	2.1	7200	2	8900	8778	5655	3123	47	1.22
24	F11	14.8	1.2	7500	1.2	9000	8908	5098	3810	47	1.19
25	F15	15.16	1.7	7300	0.4	9000	8964	5714	3250	47	1.23
26	F70	8.07	2.5	6800	0.33	7300	7272	4682	2590	77	1.07
27	F74	6.88	2.5	6400	2.9	7100	7093	4570	2523	78	1.11

Table 7.3 Pile Information, 0.813 meter Diameter Pile

	Burial Length	First Drive	CASE, First Drive	Set, Redrive	CASE, Redrive	Shaft Capacity	End Capacity	CAPWAP	Elapsed Time	K, Setup
	m	mm	kN	mm	kN	kN	kN	kN	days	
F54	9.33	2.5	6380	2.4	7000	4816	2240	7056	13	1.11
F59	8.8	2.5	6880	1.5	7070	4242	2805	7047	2	1.02
G51	7.84	2.2	6750	1.2	7030	4734	2309	7043	2	1.04
H52	8.6	2.8	6900	2.2	8210	4882	3245	8127	15	1.18
H53	7.81	2	7120	1.3	8640	4863	3702	8565	15	1.20
H54	8.07	2.5	7190	1.3	8670	5103	3459	8562	14	1.19
H59	9.53	1.7	6640	1.8	7190	4461	2692	7153	13	1.08
I50	10.18	0	0	1.5	7050	4288	2700	6988	13	0.00
I53	10.8	0	0	1.8	7030	3956	3112	7068	10	0.00
N26	9.44	3.3	6560	1.3	7490	4326	2837	7163	3	1.09

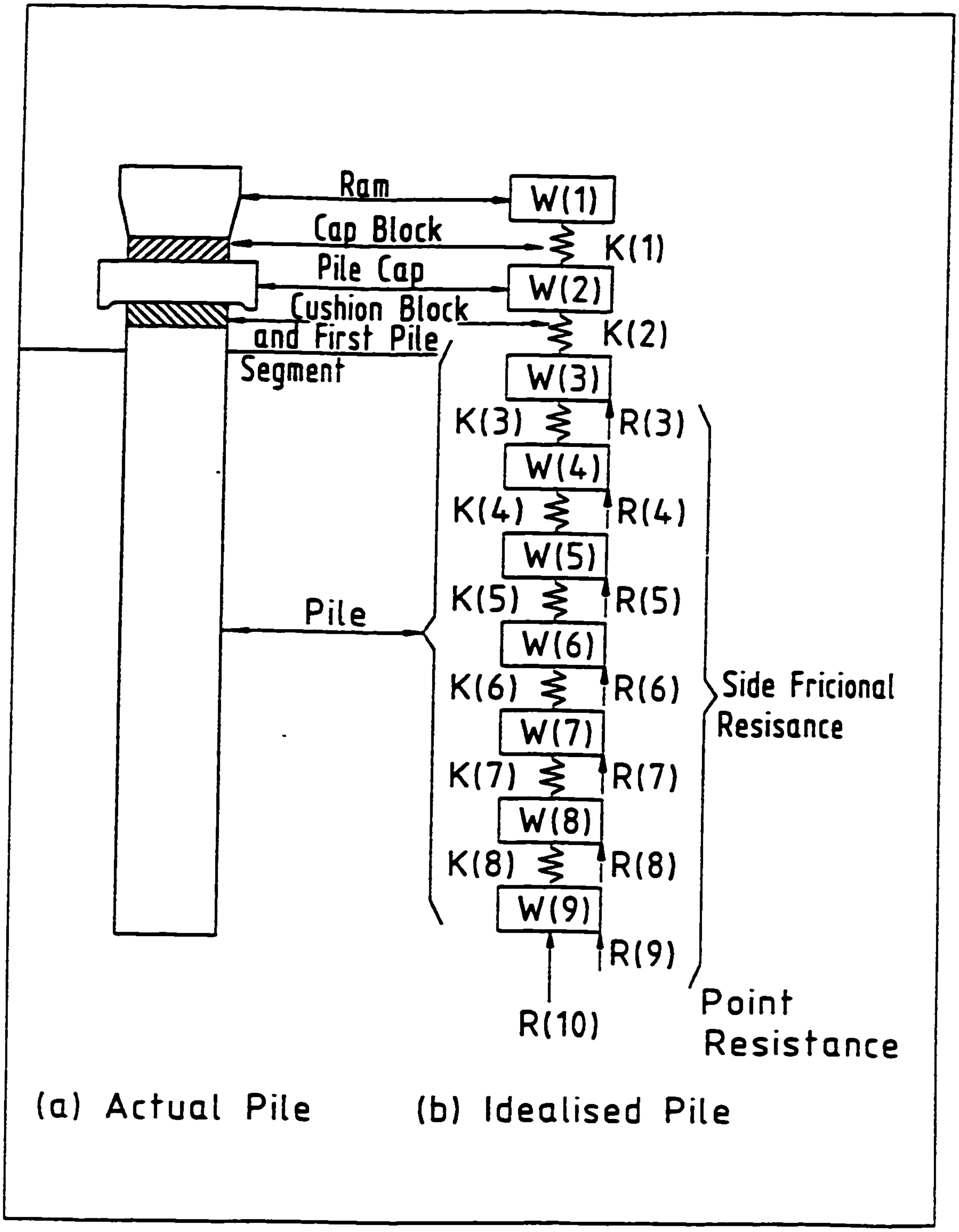

Figure 3.1 Smith Model

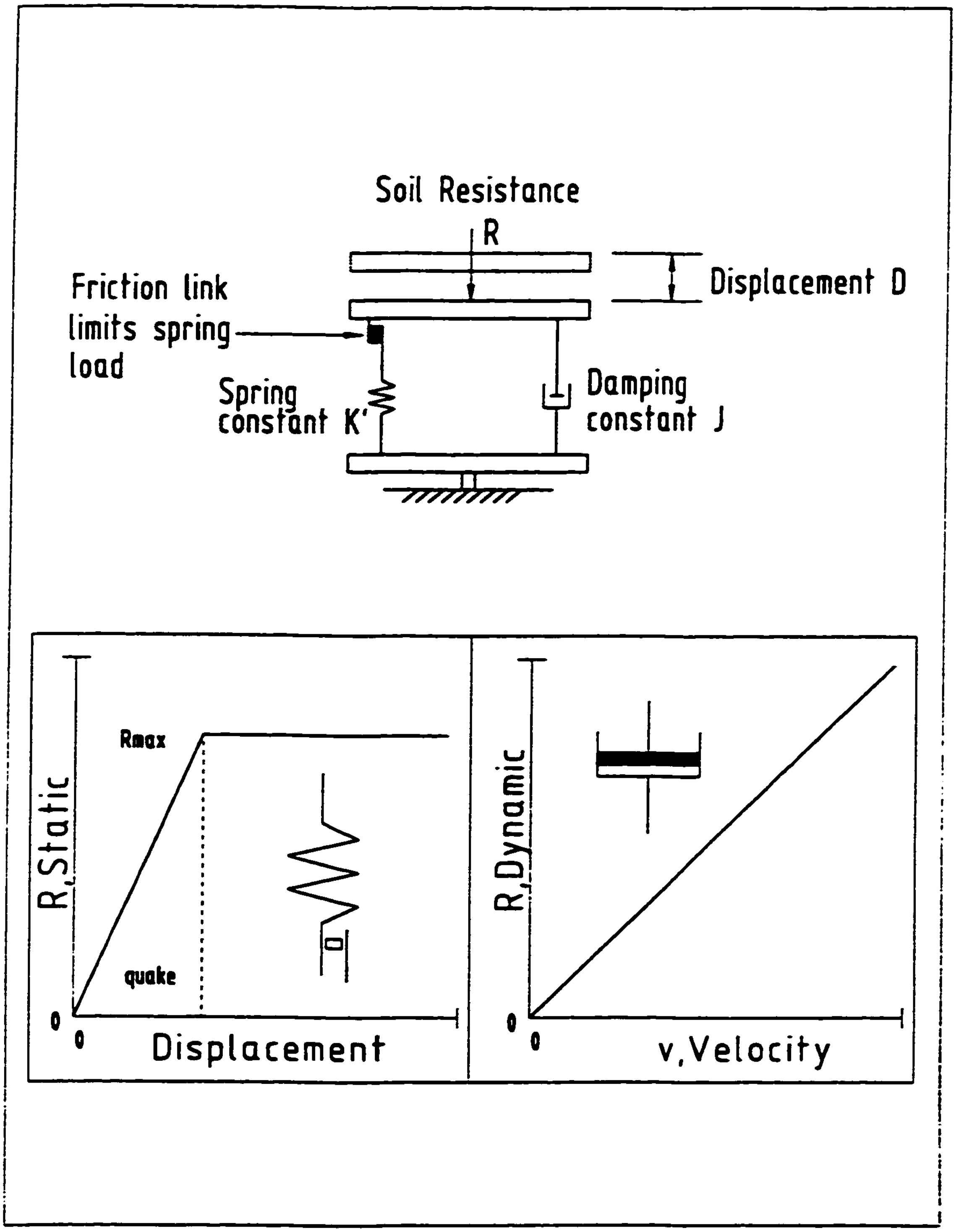

Figure 3.2 Smith Soil Model

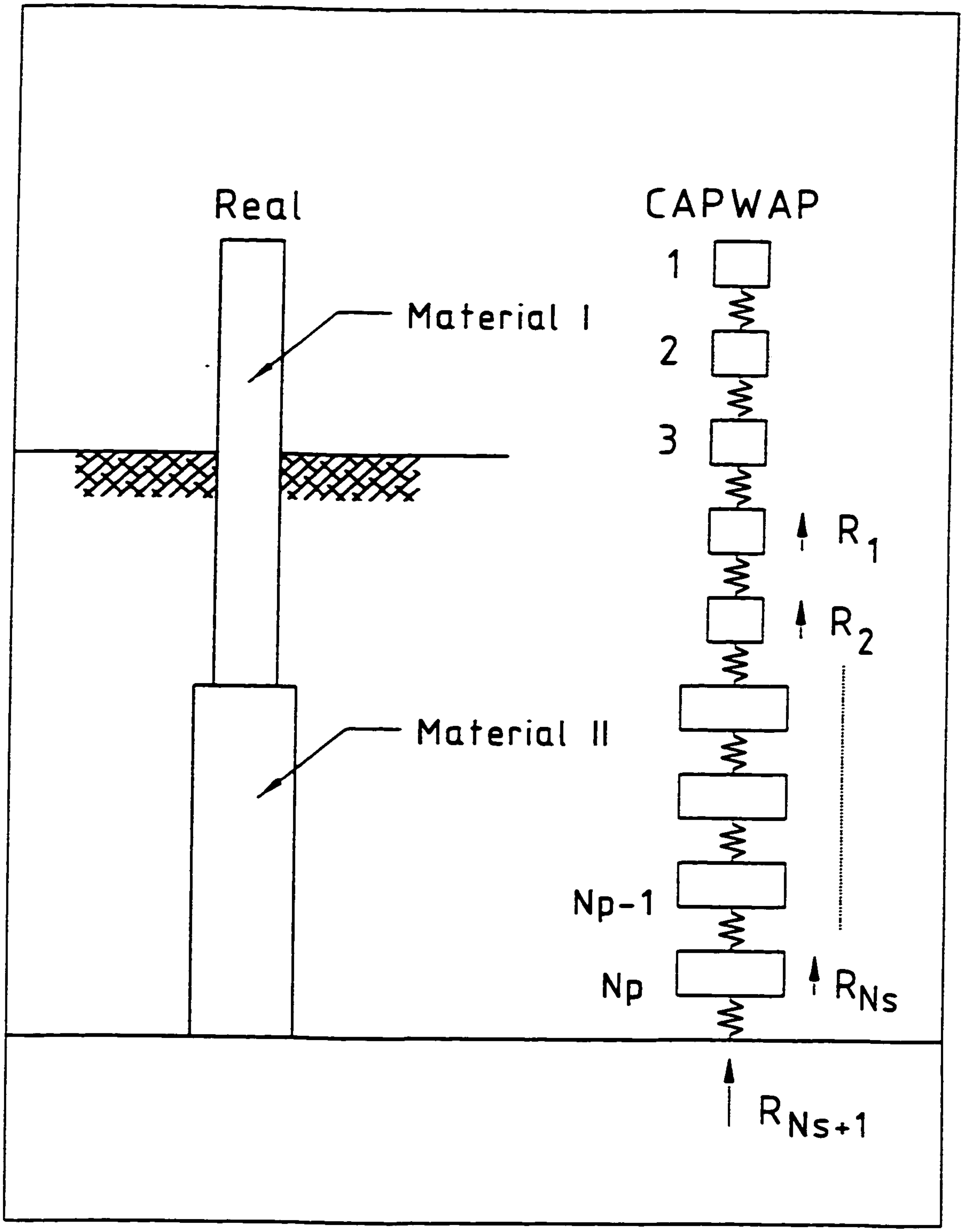

Figure 3.3 CAPWAP Model

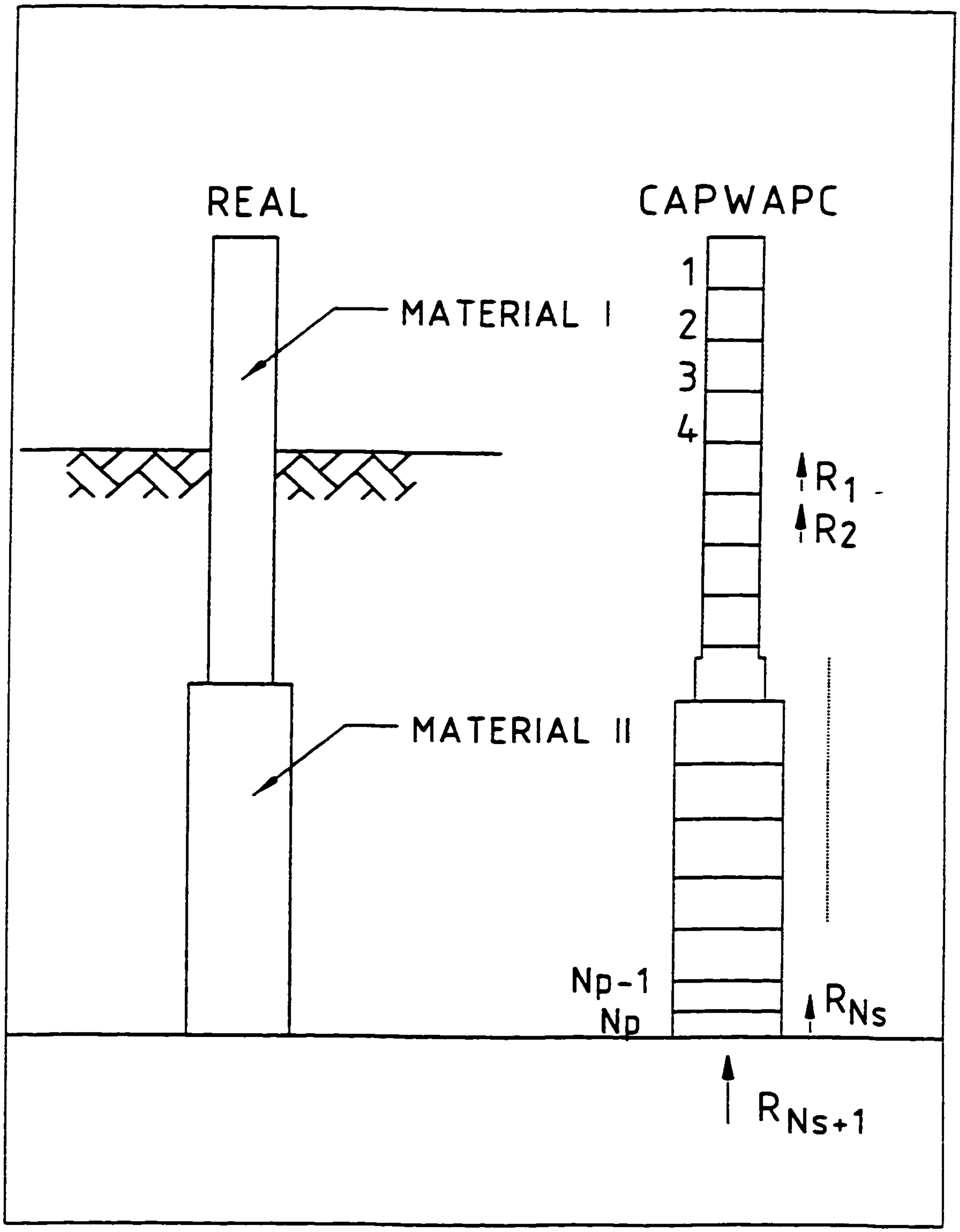

Figure 3.4 Continuous CAPWAP Model

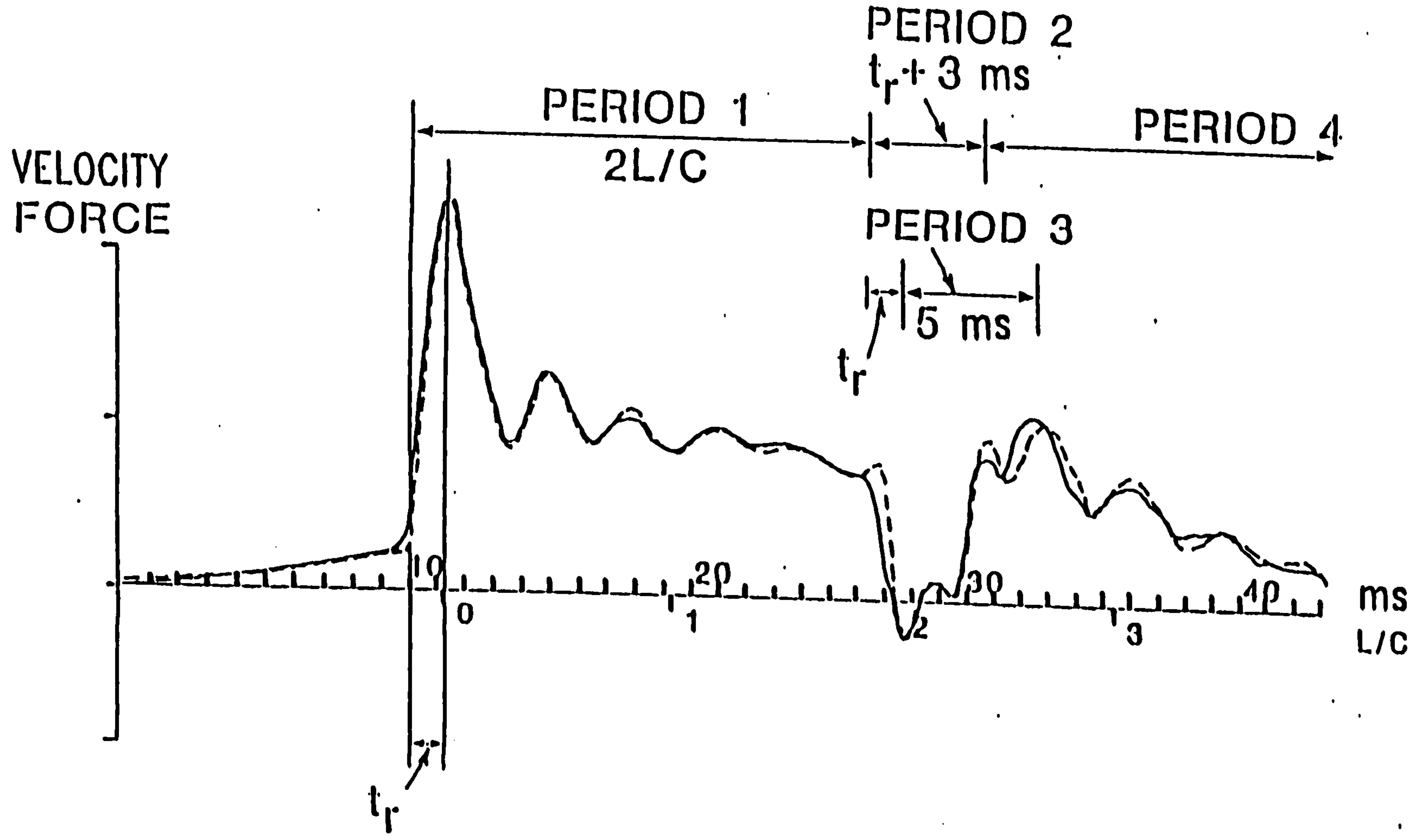

Figure 3.5 Subdivisions of a CAPWAP Trace, (after Rausche, 1986)

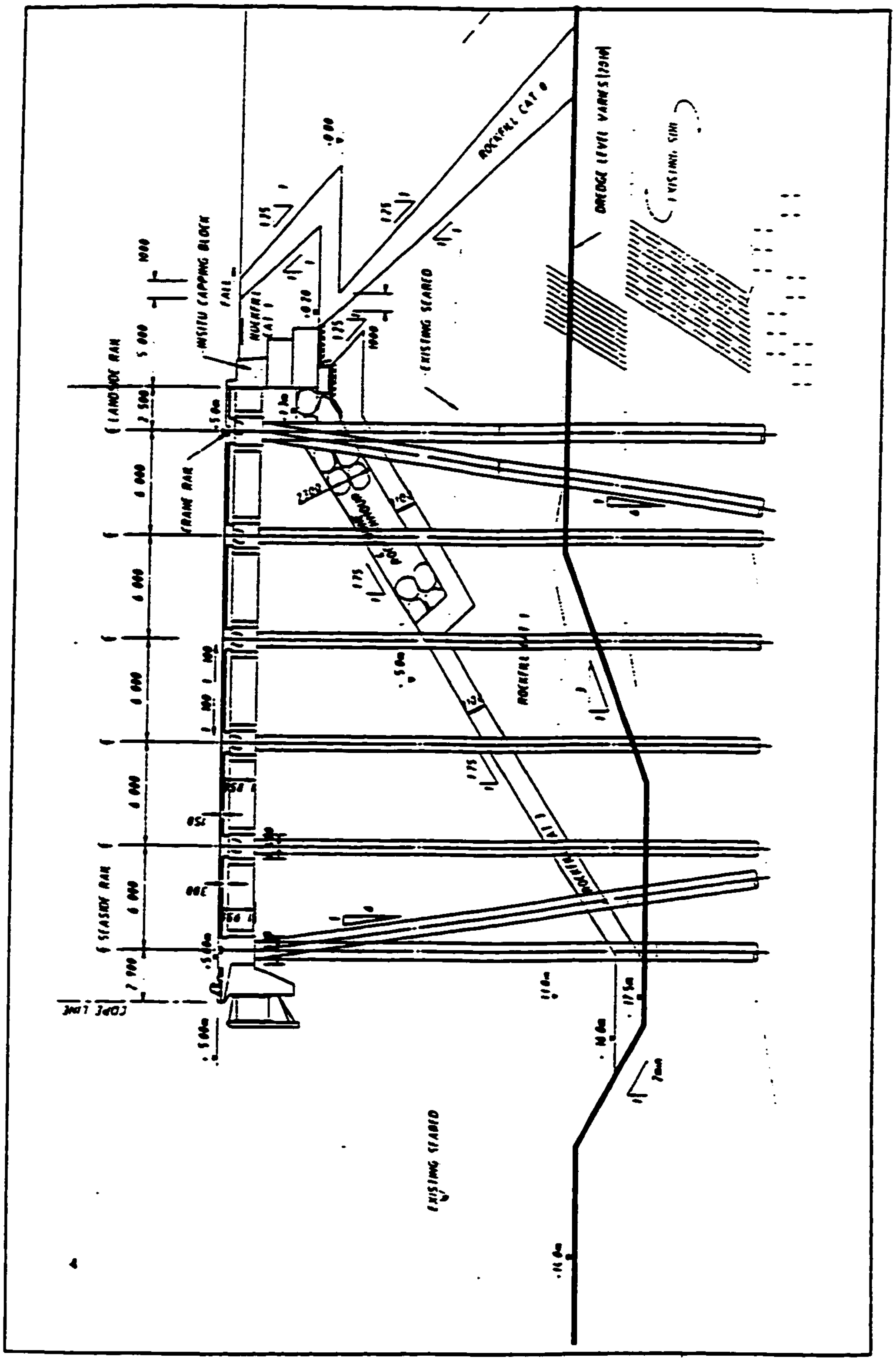

Figure 4.1 - Cross-Section of the Quay Deck Structure

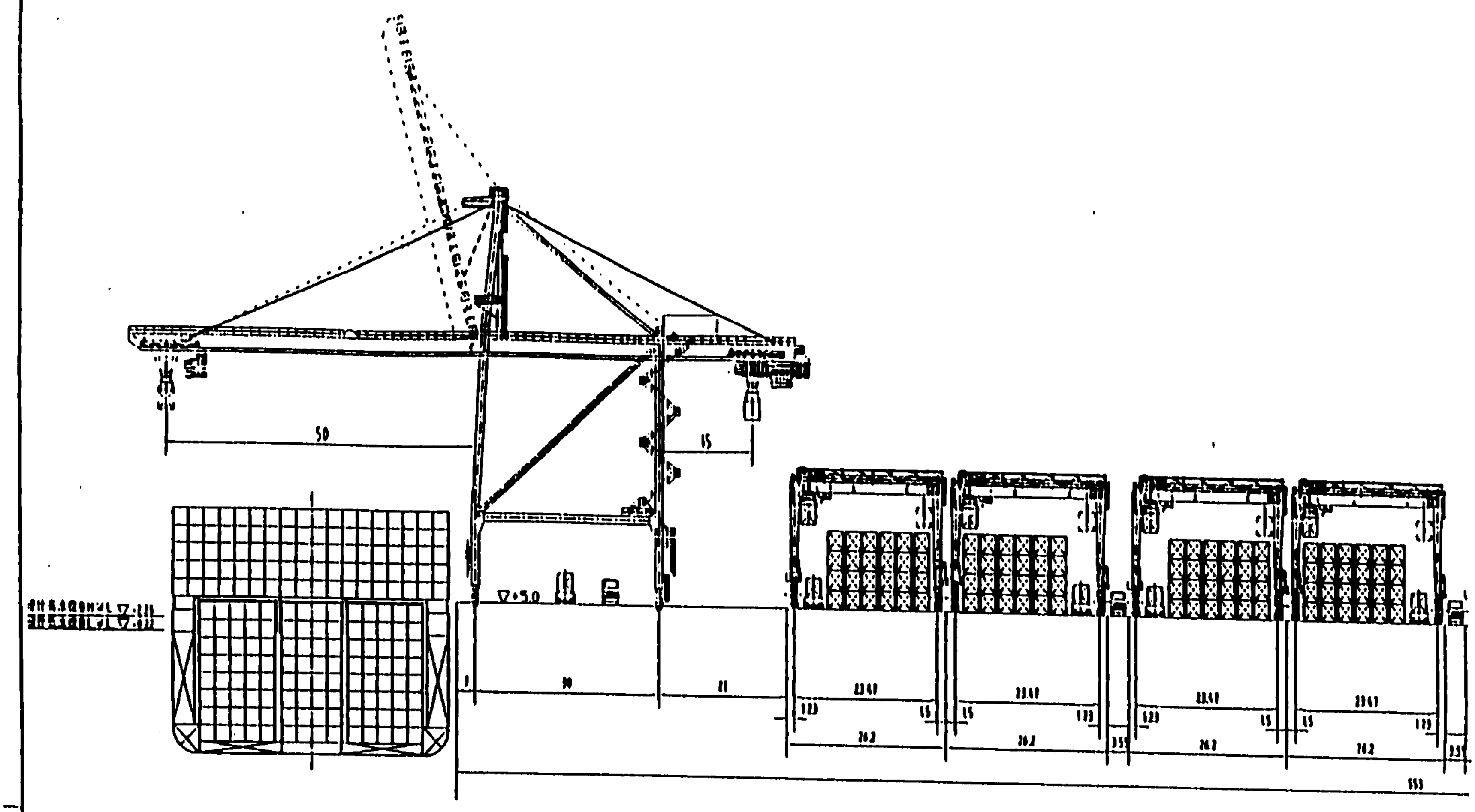

Figure 4.2 Cross-section profile of the Container Terminal

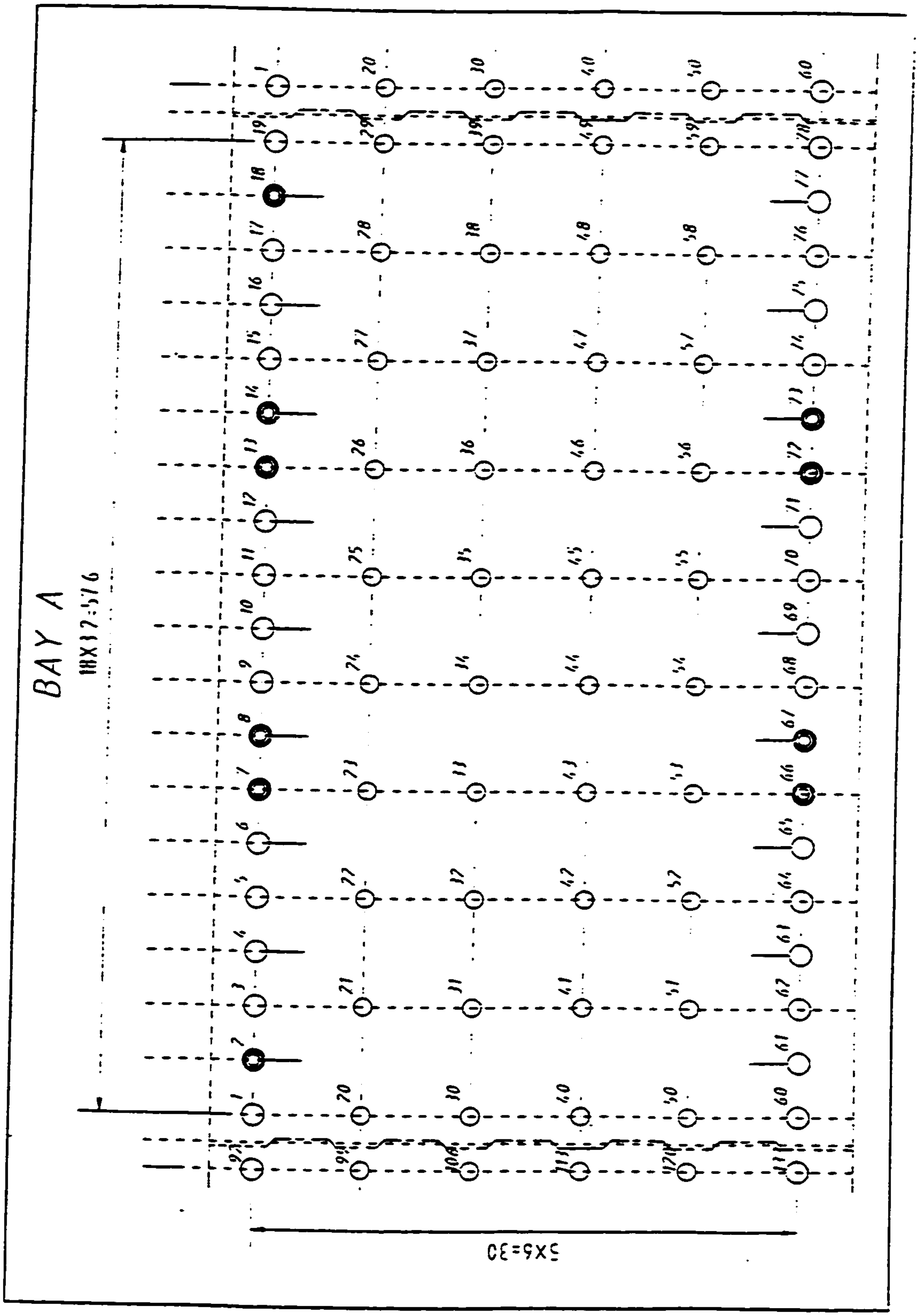

Figure 4.3 - Typical Bay of the Pile Layout

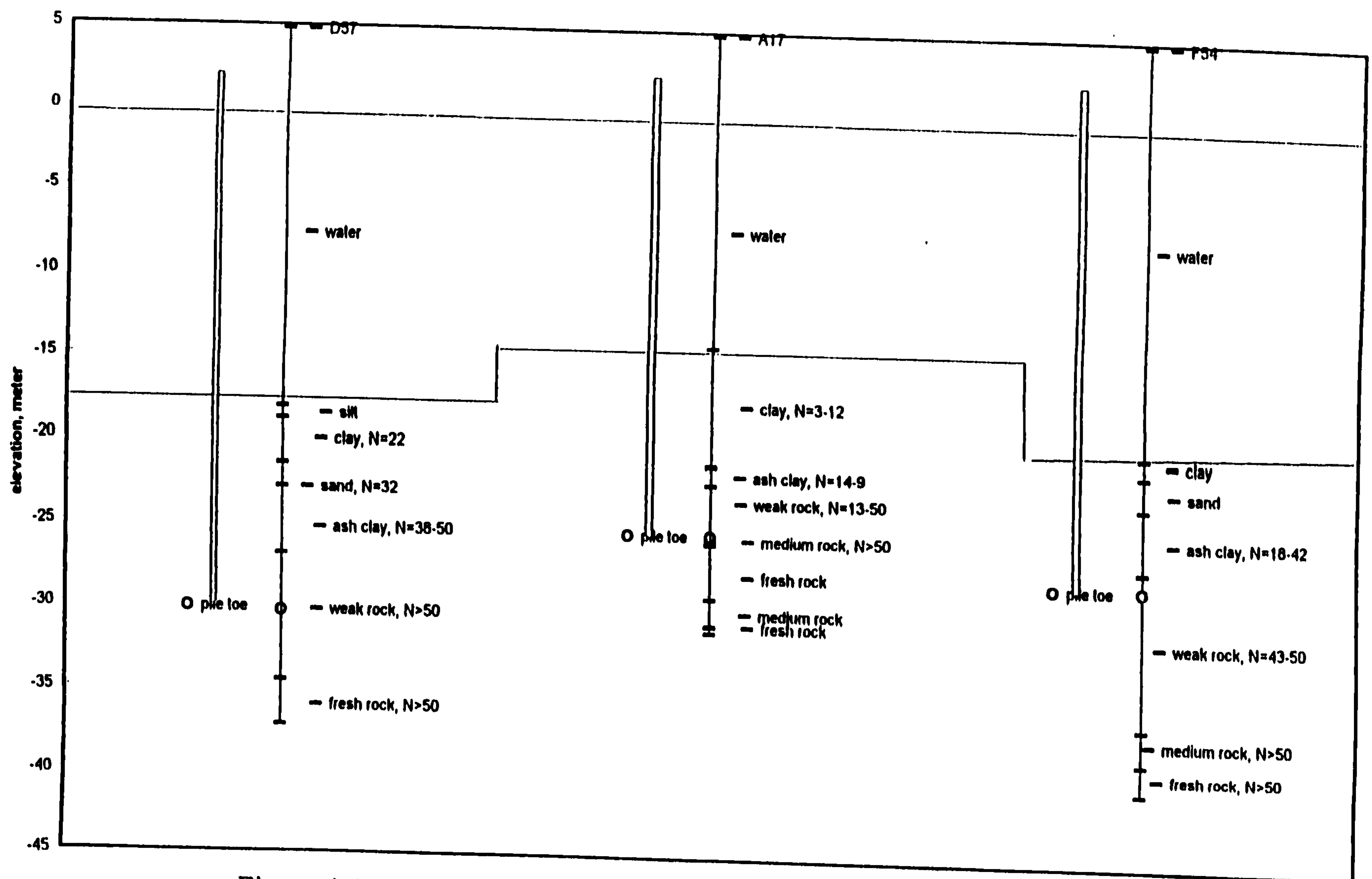

Figure 4.4 Ground Profile from Boreholes for Pile A17, F54 and D57

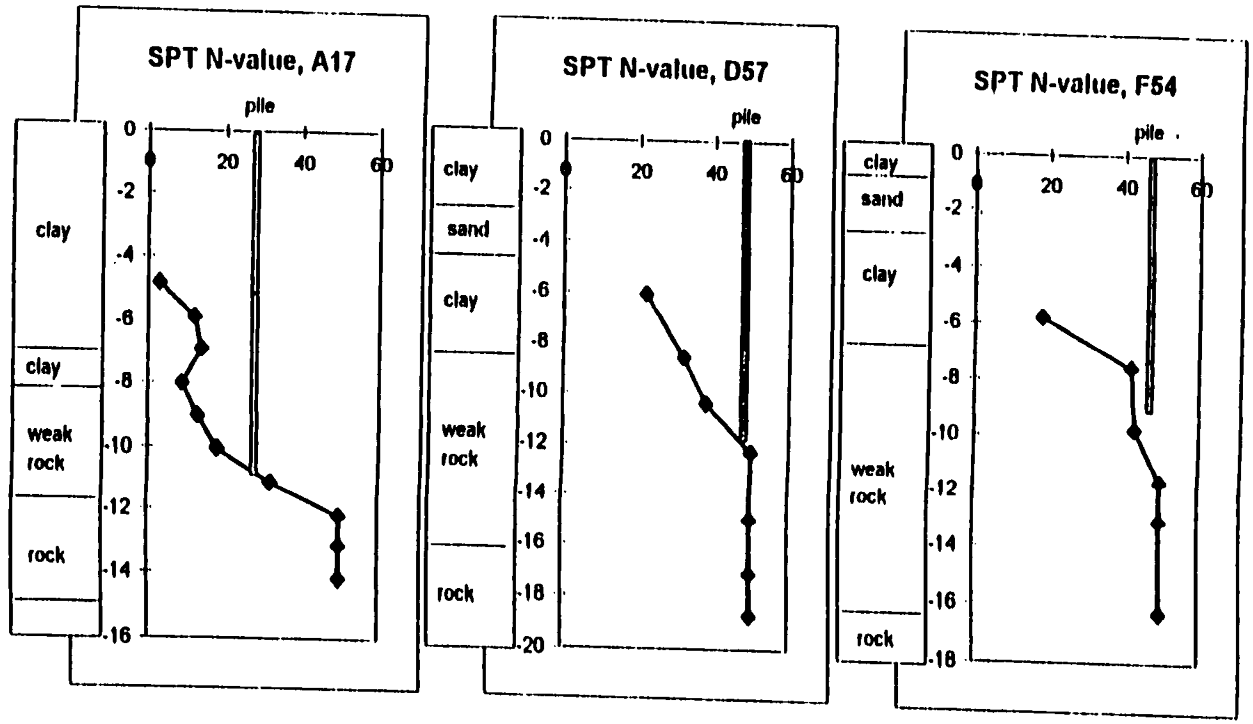

Figure 4.5 SPT for Pile A17, F54 and D57

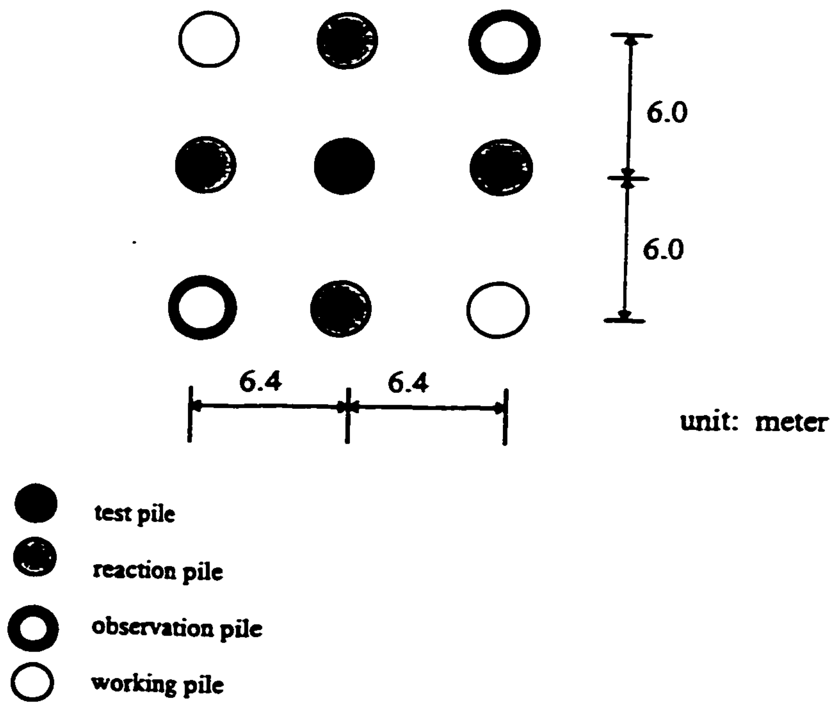

Figure 5.1 Plan of Pile Arrangement for Pile Test

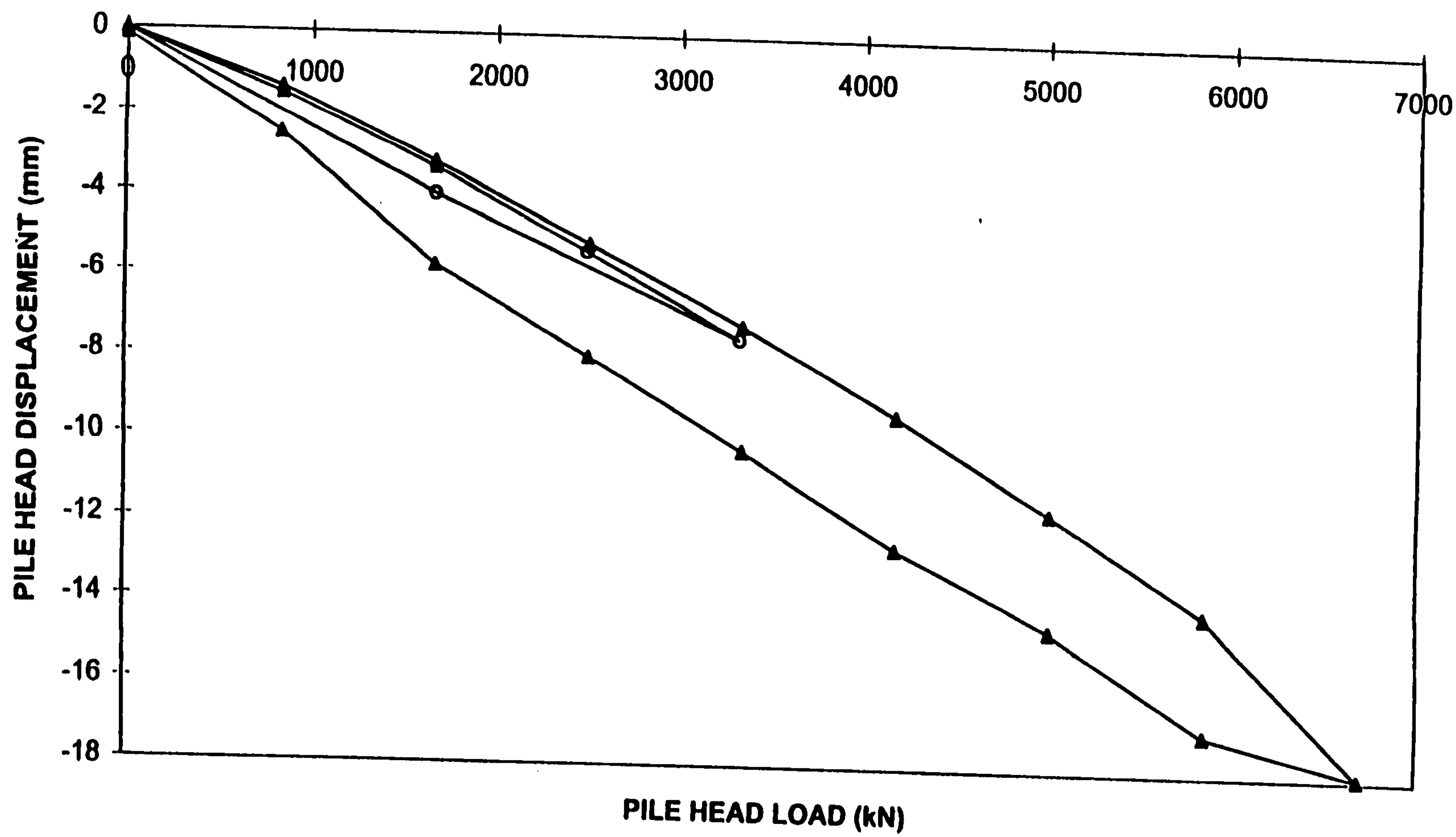

Figure 5.2 - Load-Displacement Curve under Compression Load, Pile A17

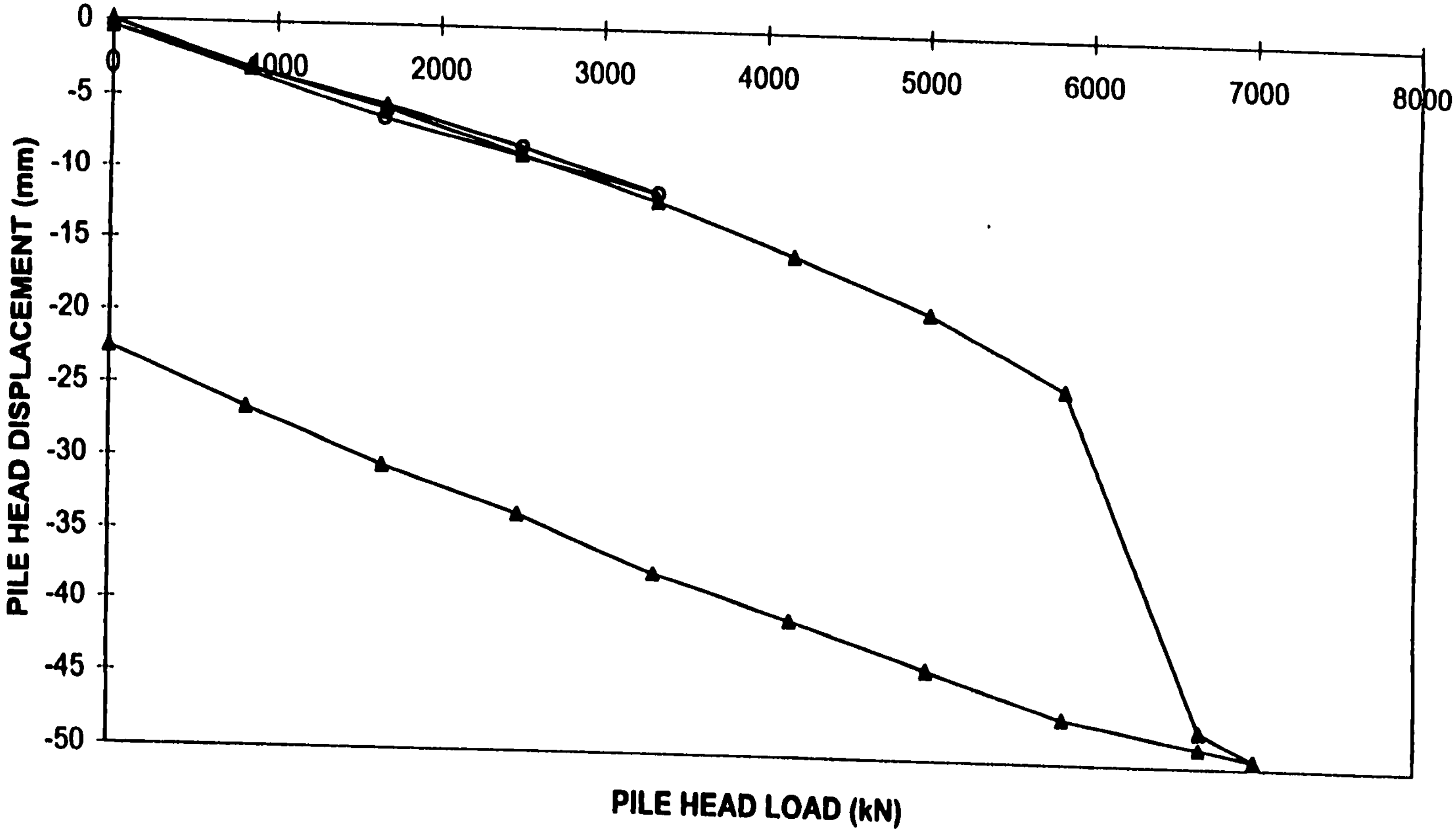

Figure 5.3 - Load-Displacement Curve under Compression Load, Pile F54

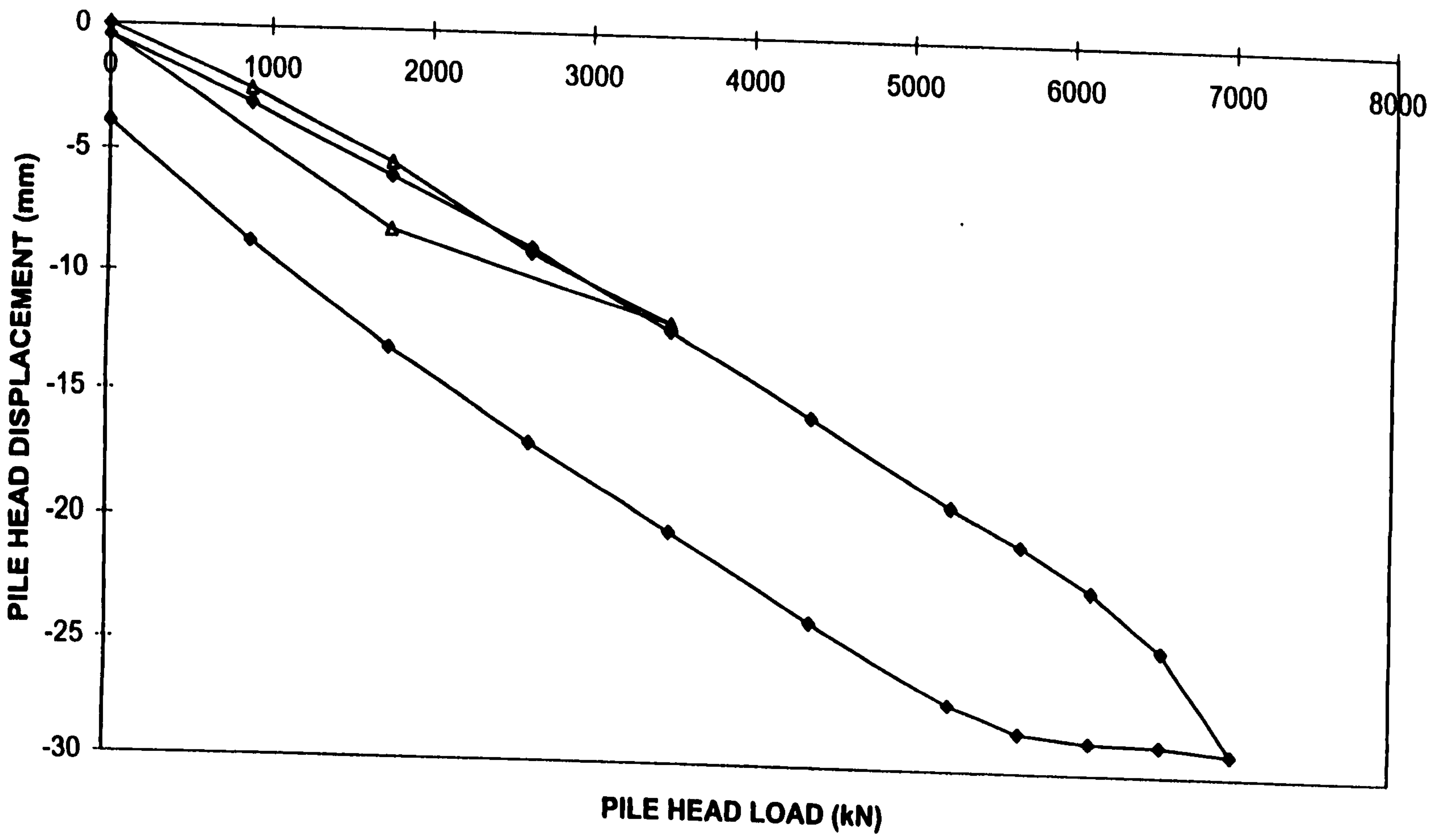

Figure 5.4 - Load-Displacement Curve under Compression Load, Pile D57

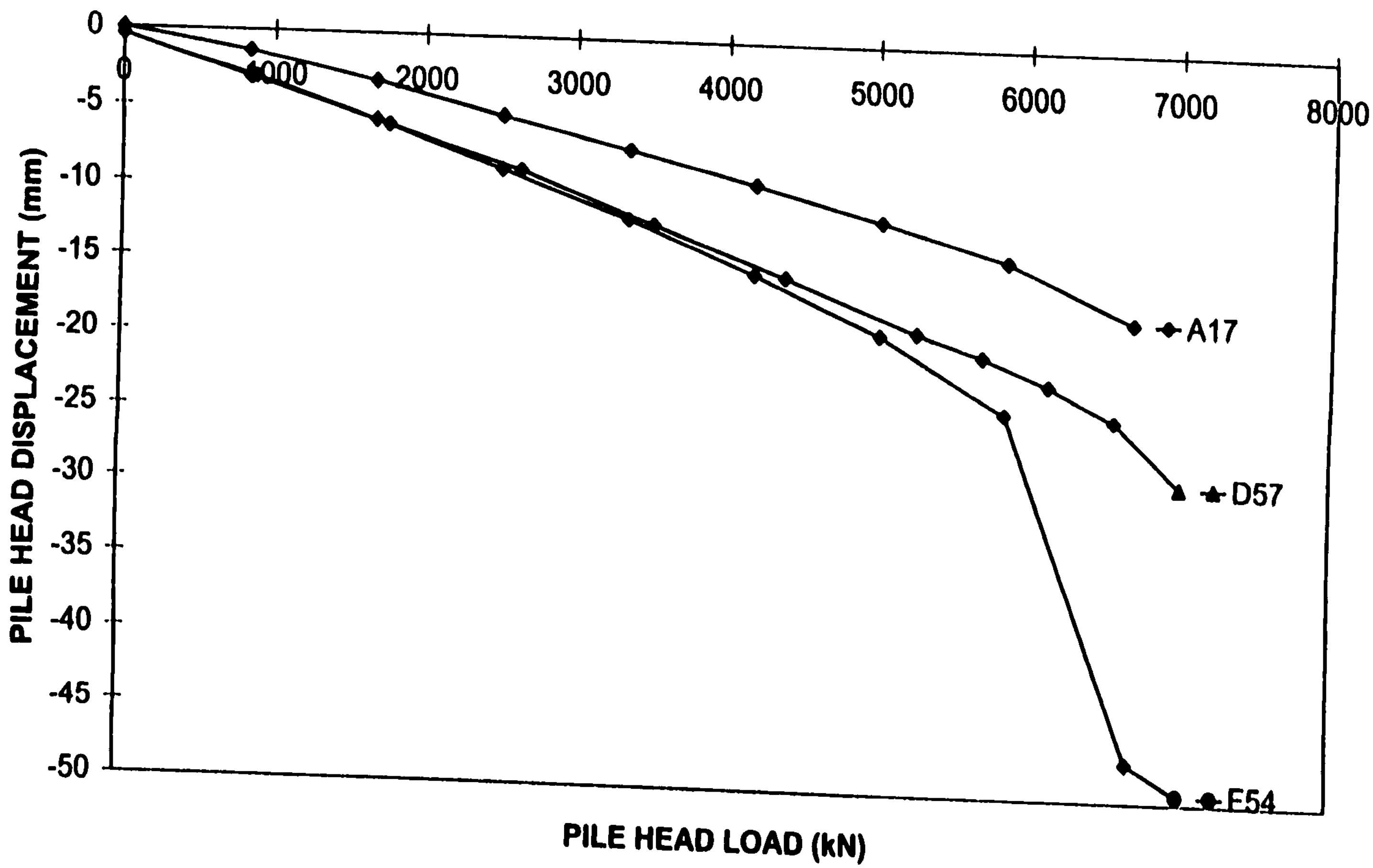

Figure 5.5 - Load-Displacement Curve under Compression Load, Piles A17, F54 and D57

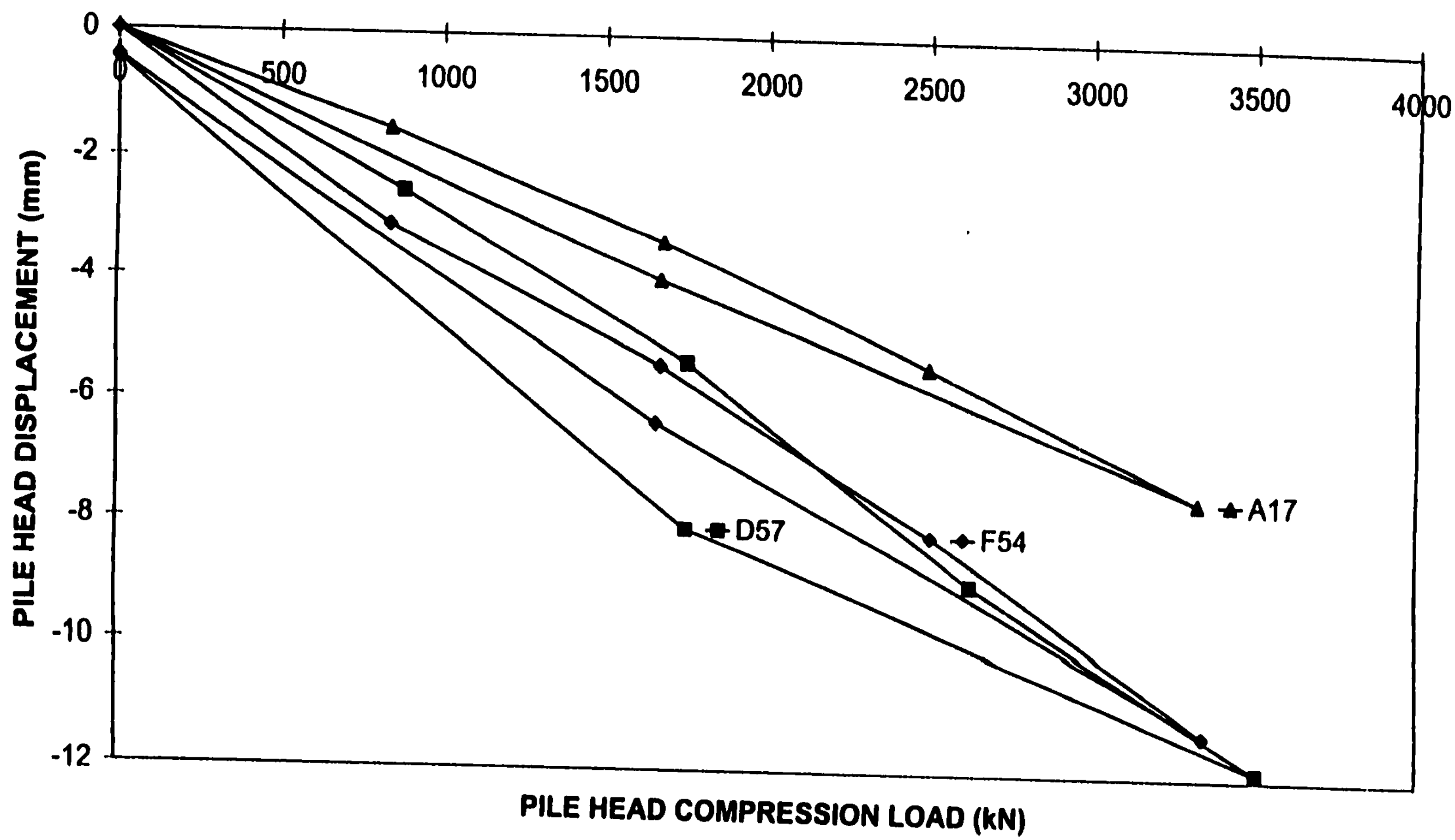

Figure 5.6 - Load-Displacement Curve under Compression, First Cycle, Piles A17, D57 and F54

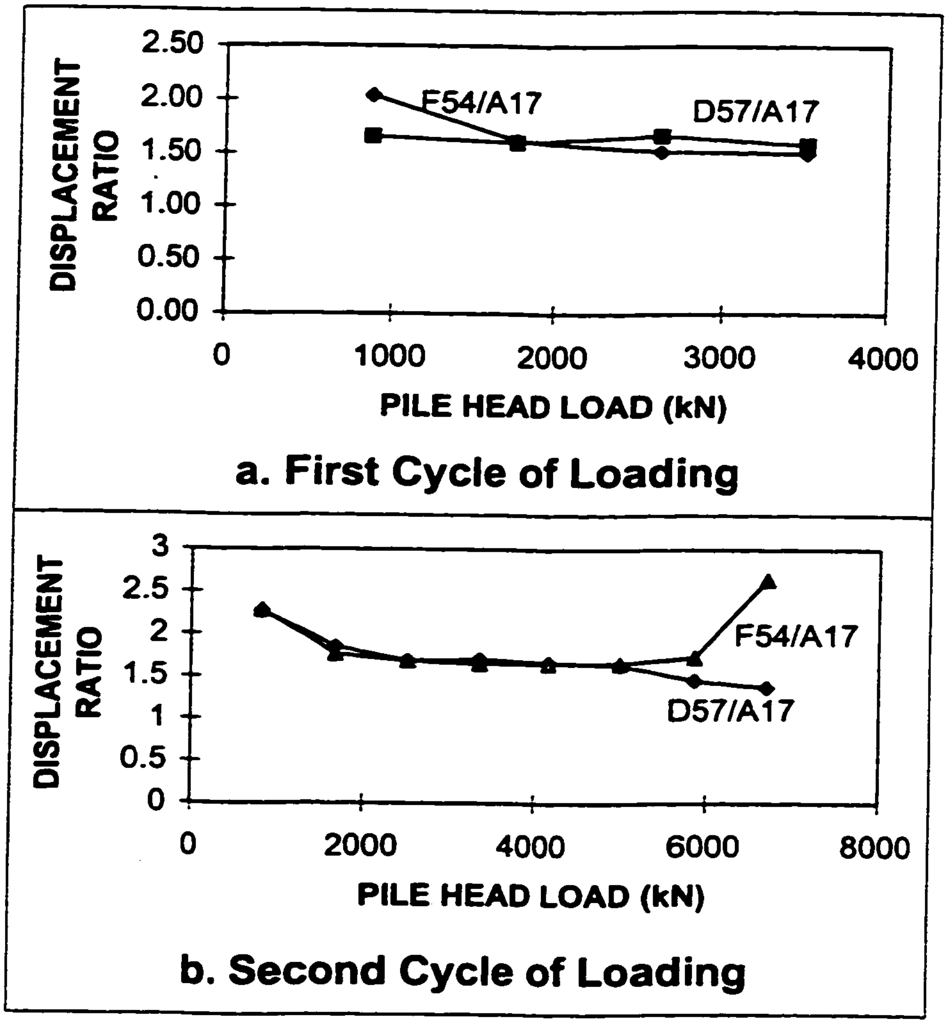

Figure 5.7 - Displacement Ratio of D57/A17

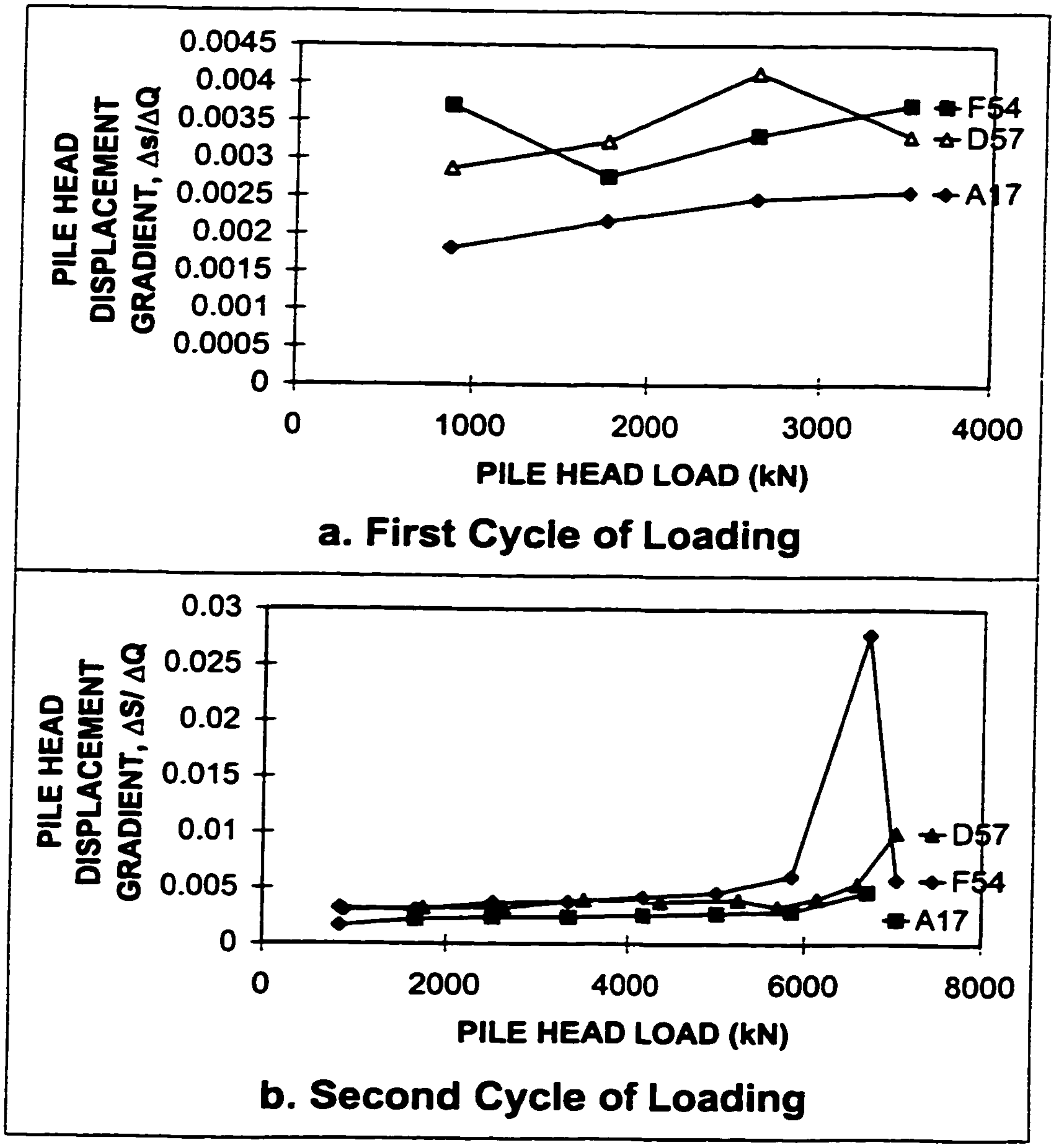

Figure 5.8 - Load-Displacement Gradient under Compression Load, Piles A17, F54 and D57

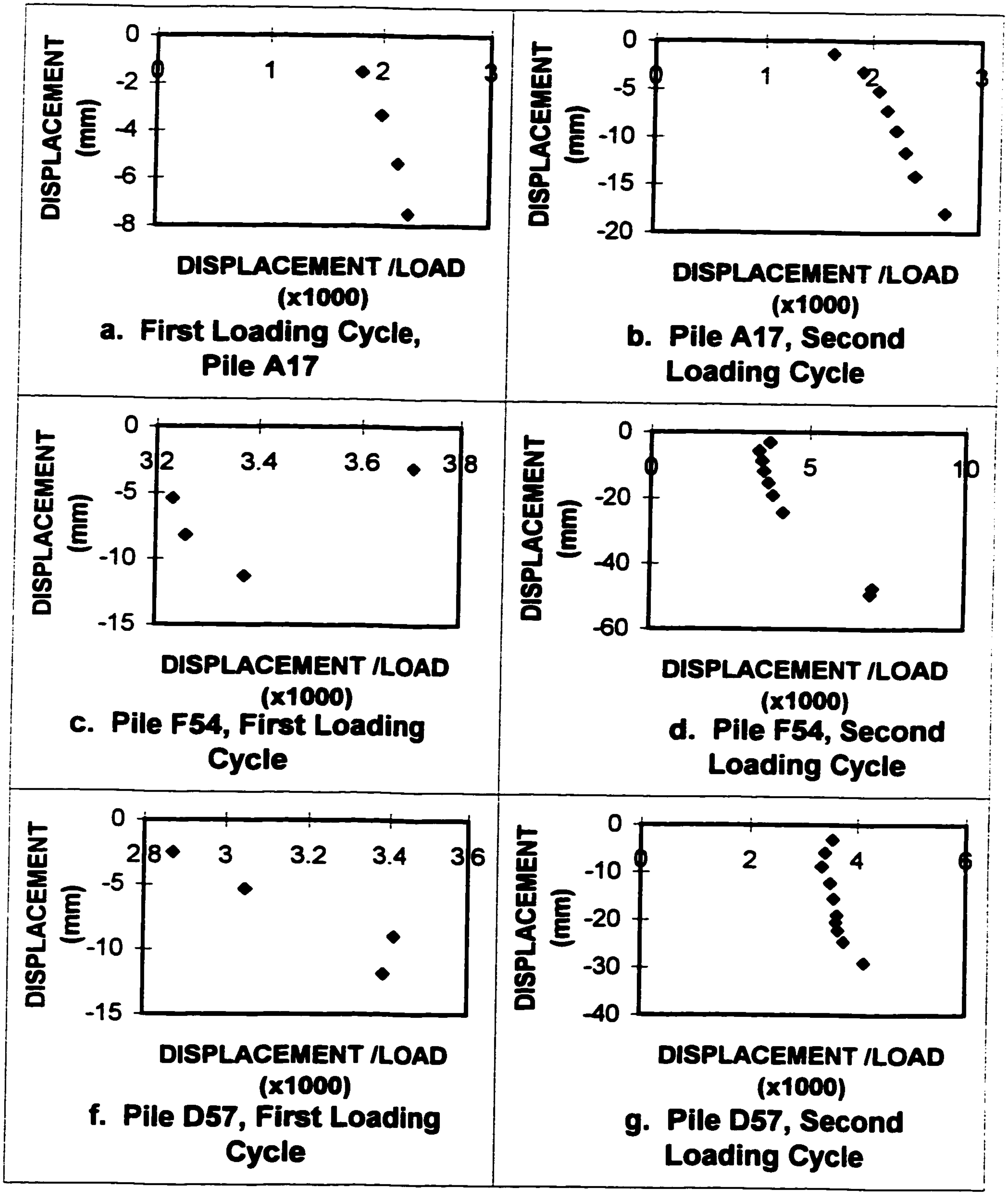

a. First Loading Cycle, Pile A17

b. Pile A17, Second Loading Cycle

c. Pile F54, First Loading Cycle

d. Pile F54, Second Loading Cycle

f. Pile D57, First Loading Cycle

g. Pile D57, Second Loading Cycle

Figure 5.9 - Displacement /Load versus Displacement

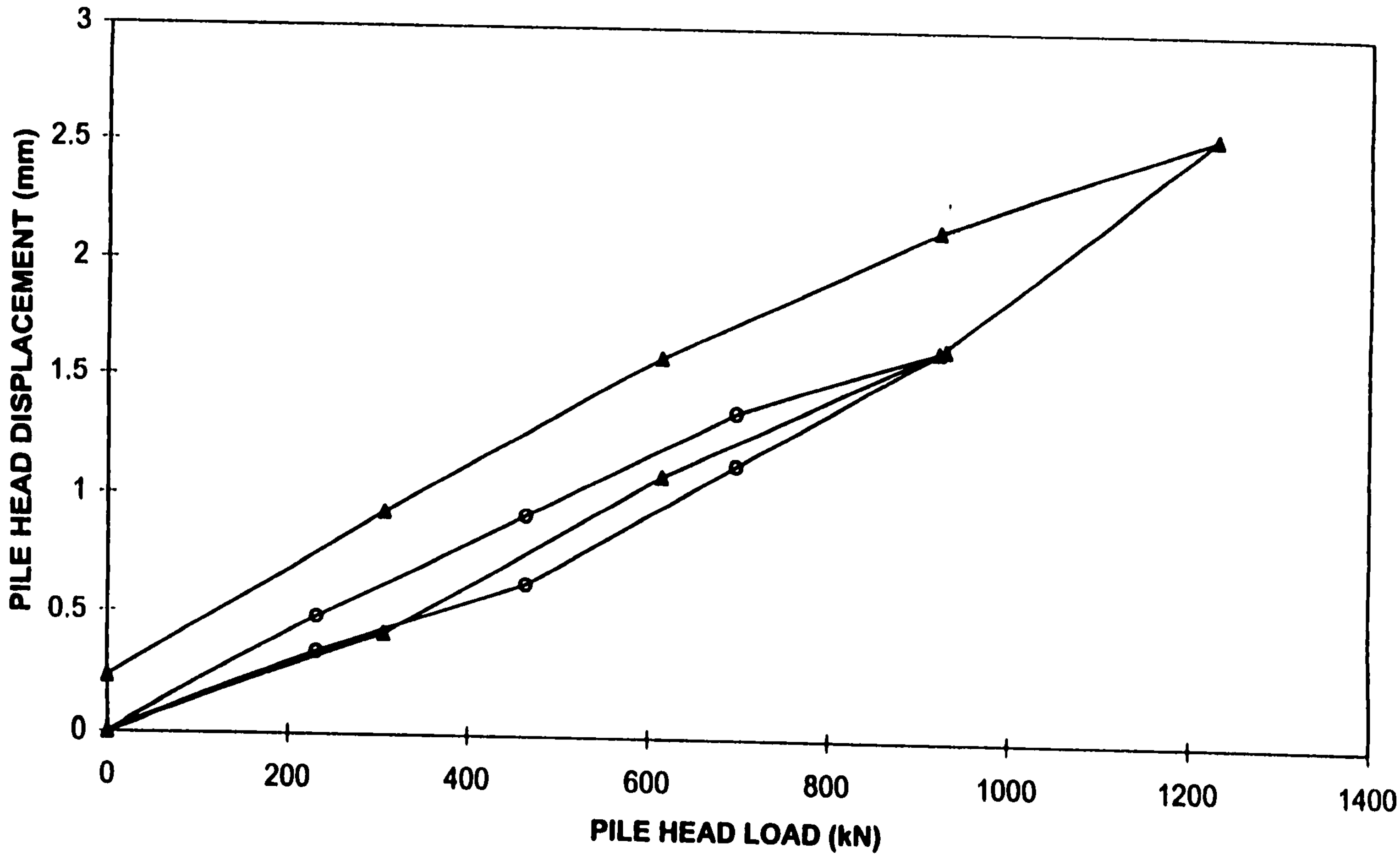

Figure 5.10 - Load-Displacement Curve under Tension Load, Pile A17

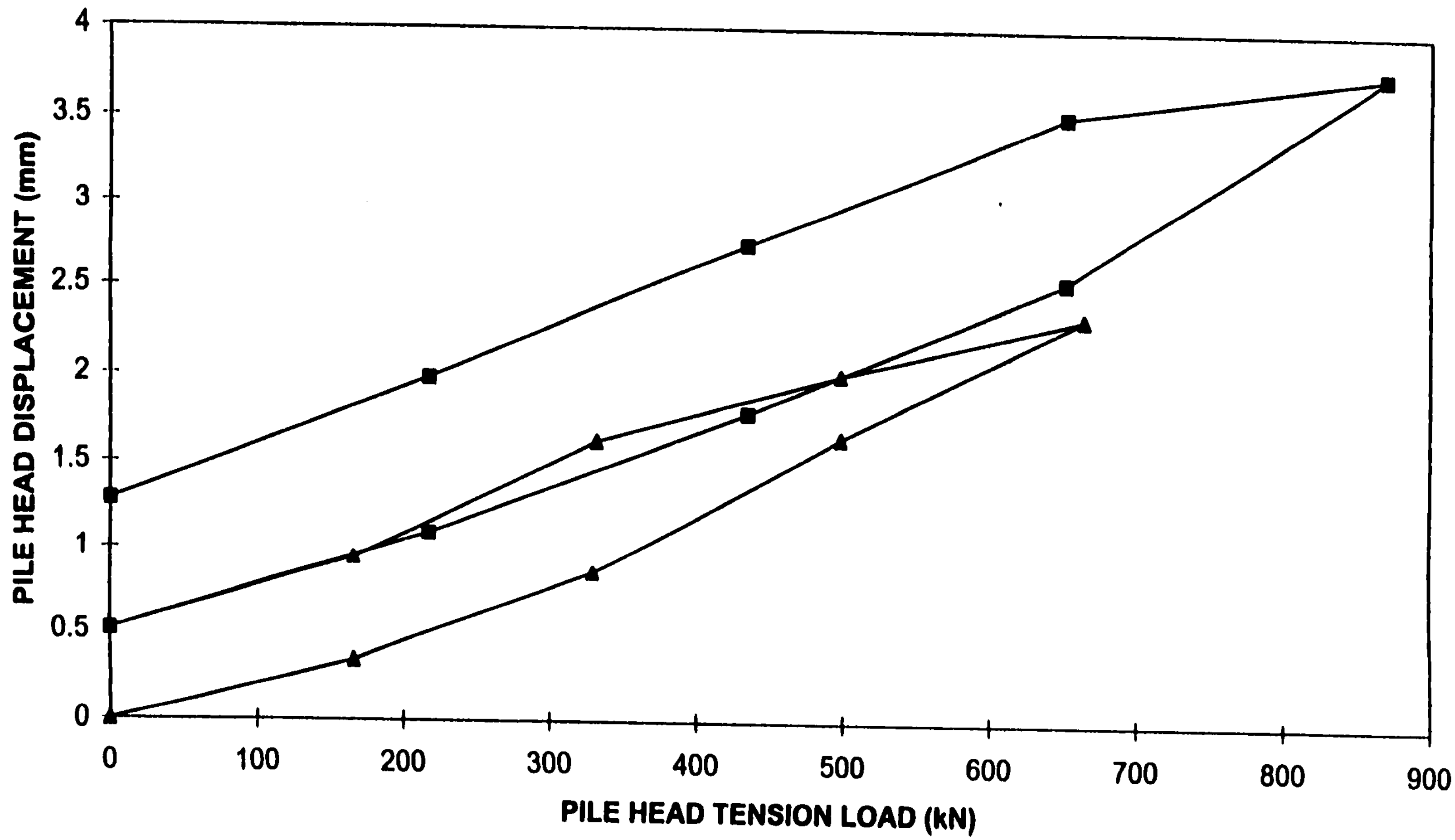

Figure 5.11 - Load-Displacement Curve under Tension Load, Pile D57

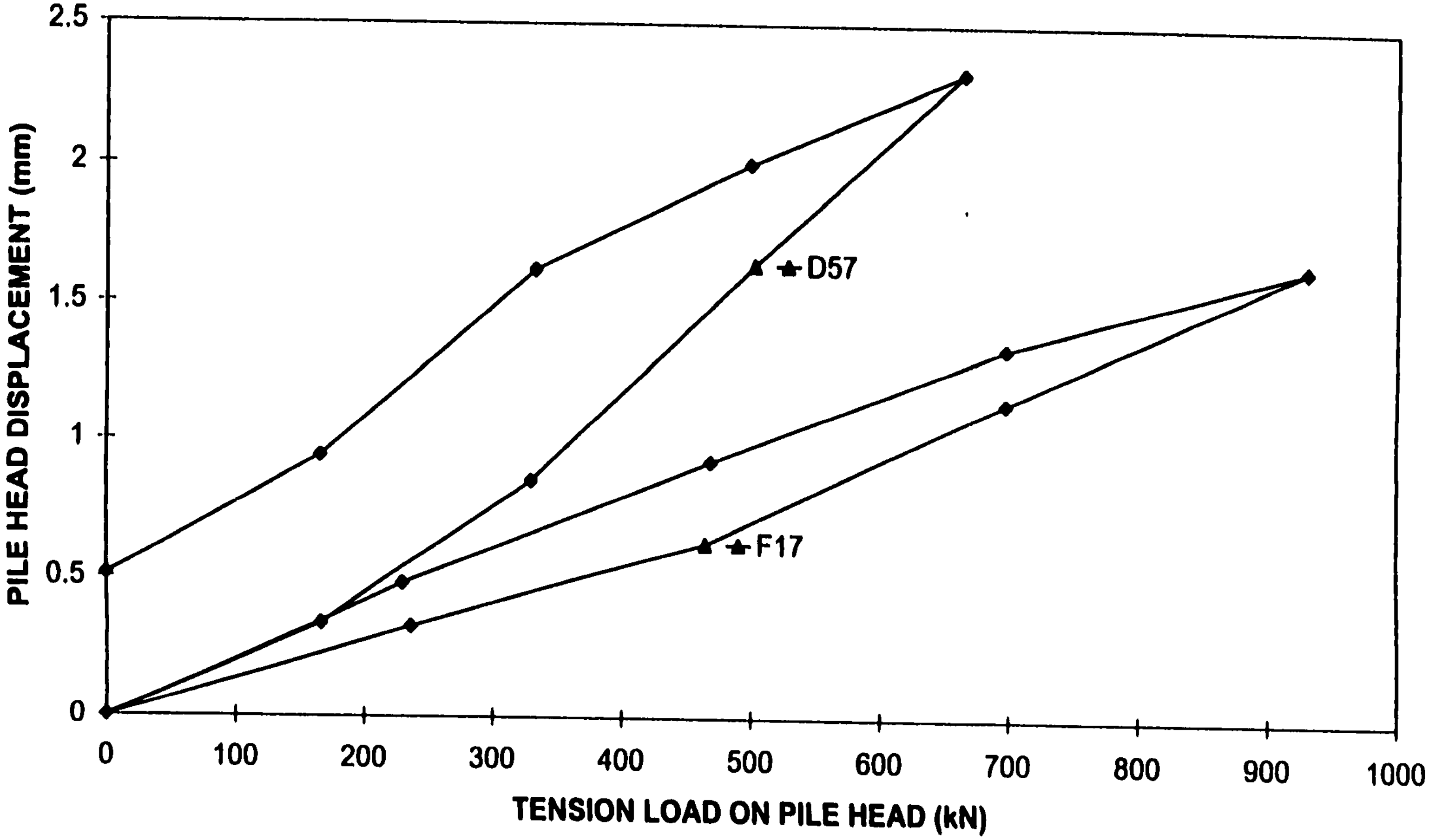

Figure 5.12 - Load-Displacement Curve under Tension, First Cycle, Pile A17 and D57

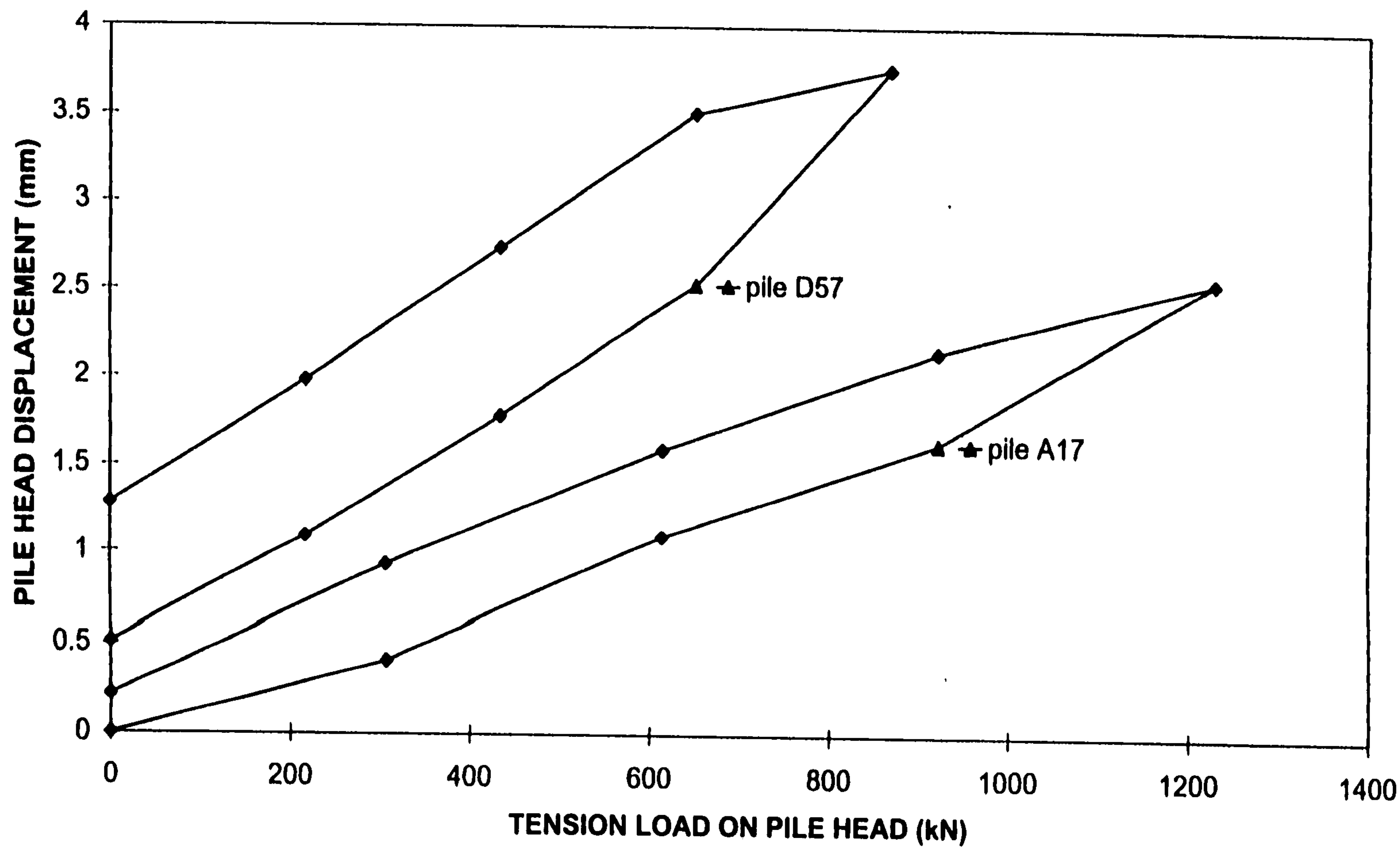

Figure 5.13 - Load-Displacement Curve under Tension Load, Second Cycle, Pile A17 and D57

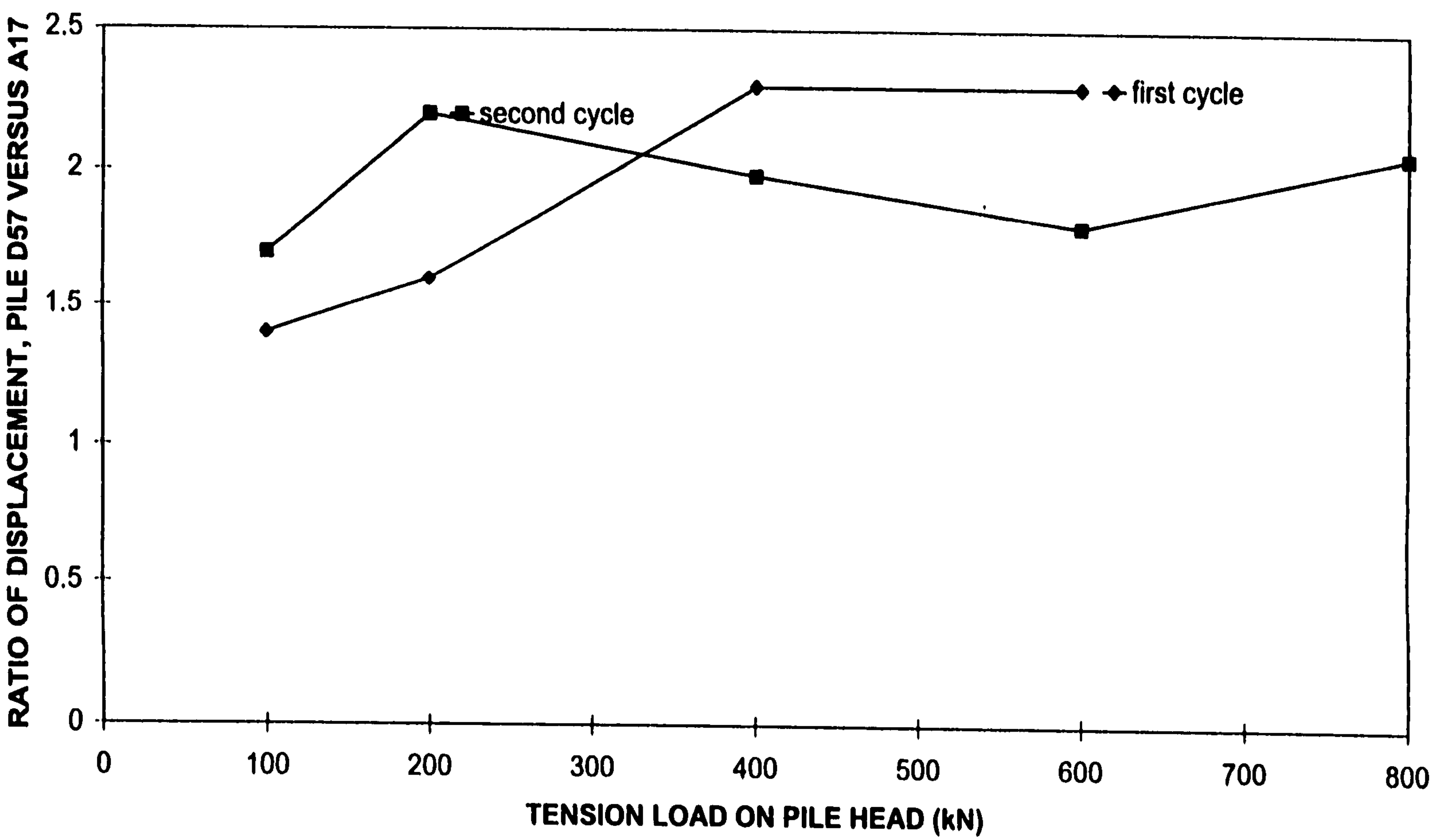

Figure 5.14 - Displacement Ratio of D57/A17 under Tension Load

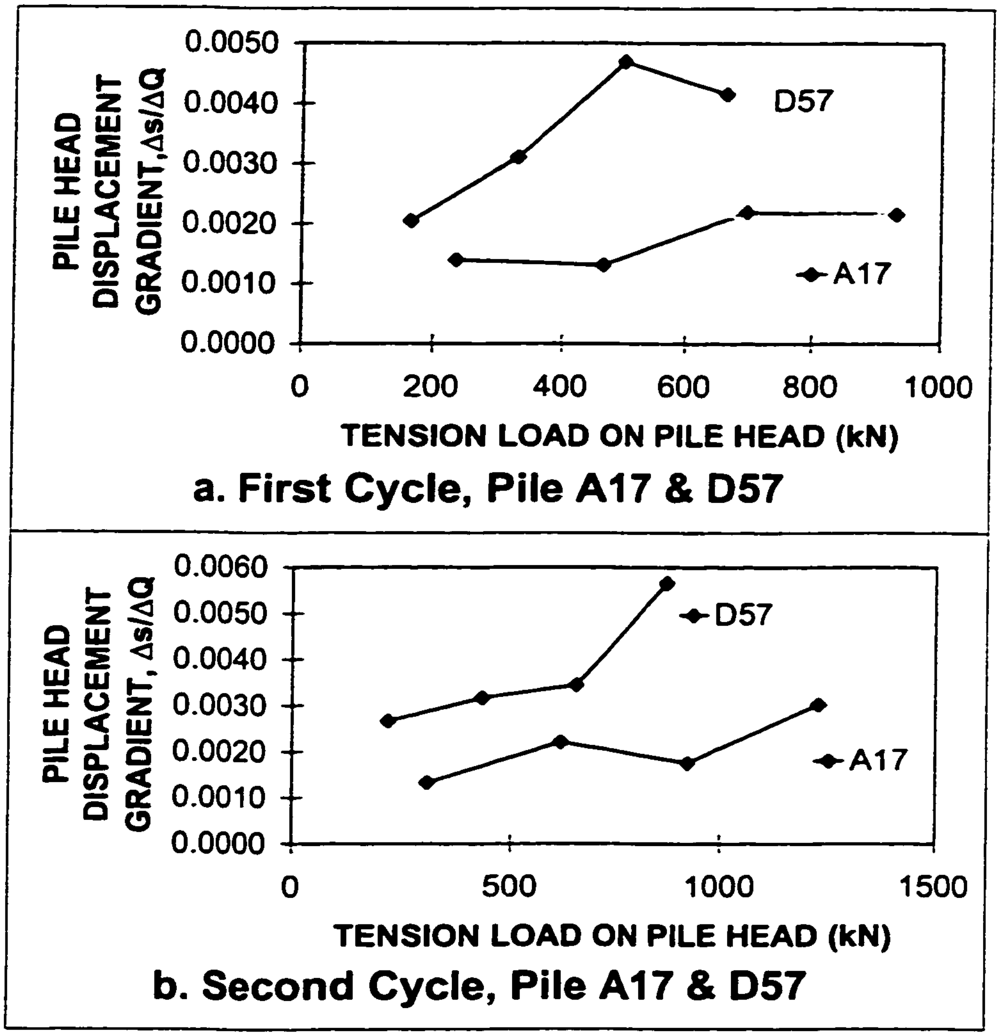

Figure 5.15 - Load-Displacement Gradient Curve under Tension Load

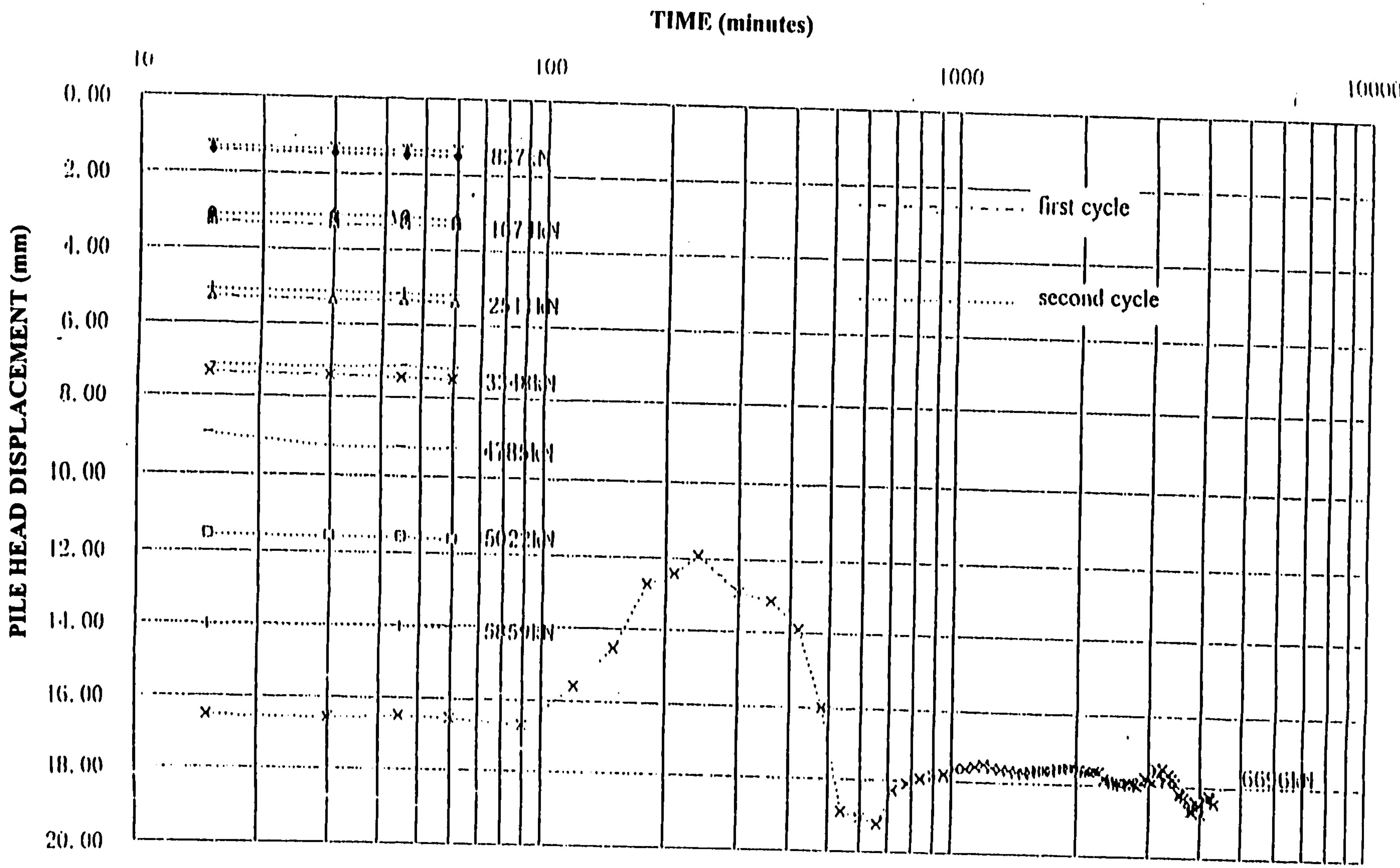

Figure 5.16 - Displacement-Time, s-lg(t), Curve, under Compression Load, Pile A17

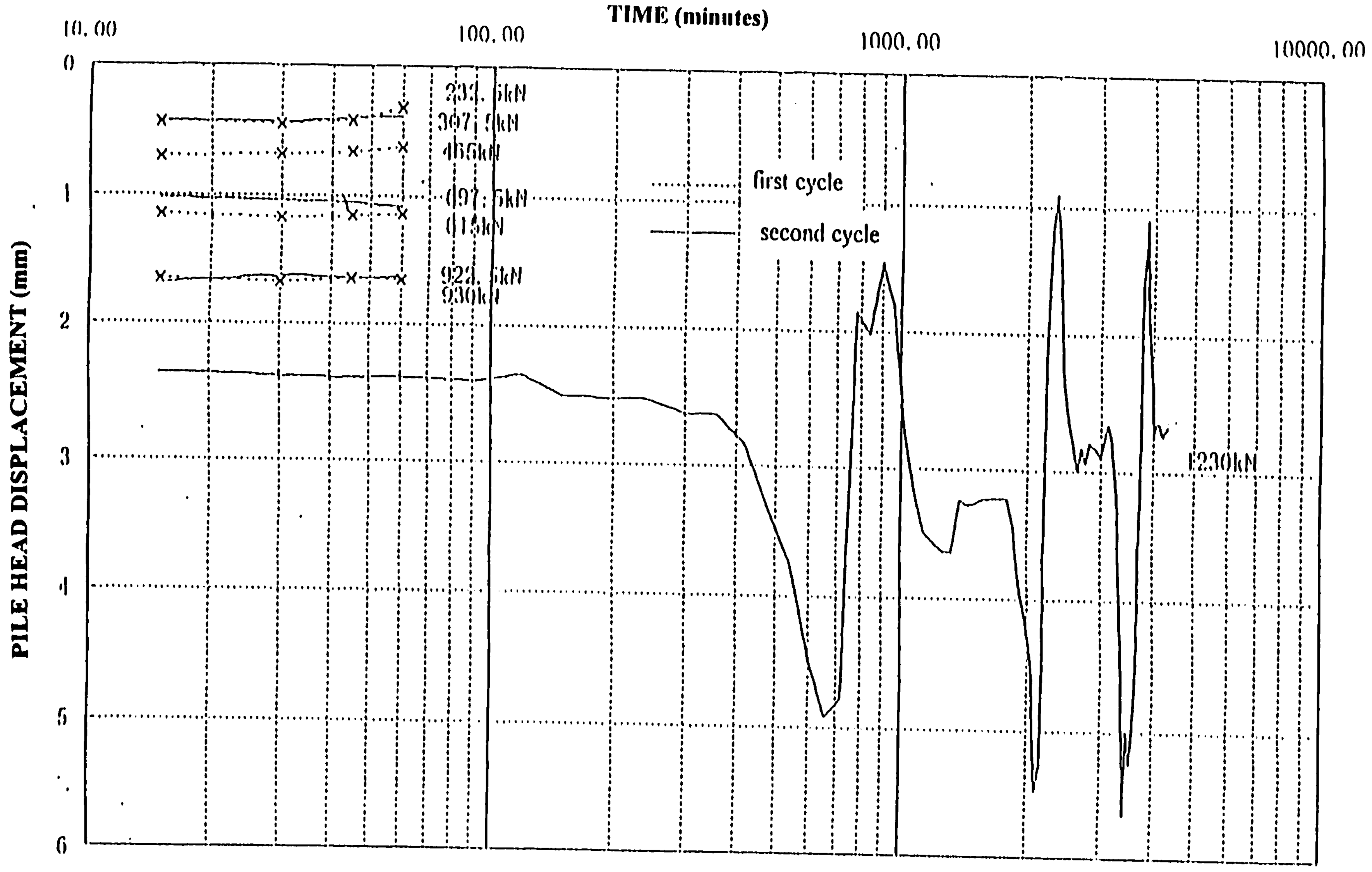

Figure 5.17 - Displacement-Time, s-lg(t), Curve, under Tension Load, Pile A17

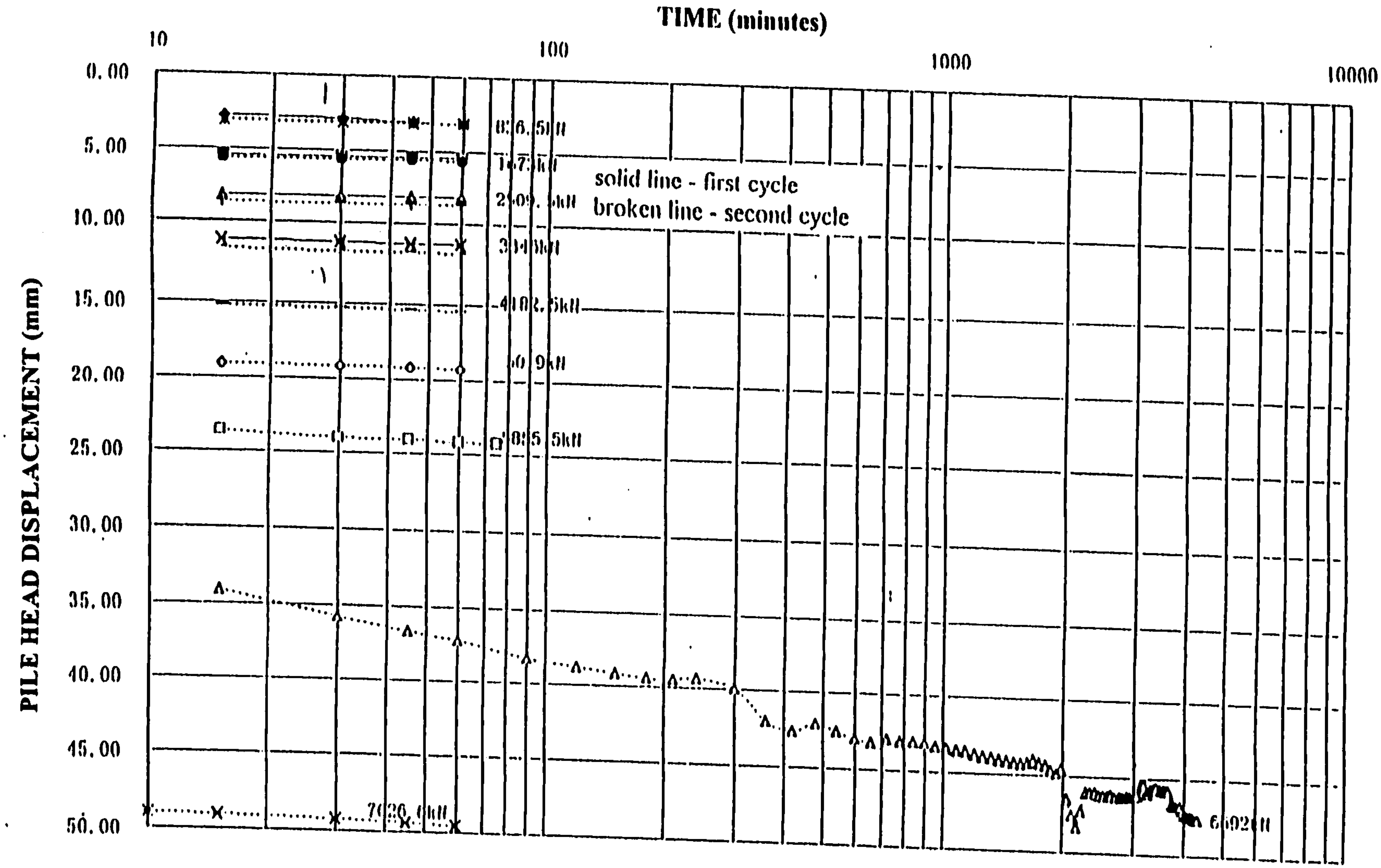

Figure 5.18 - Displacement-Time, s-lg(t), Curve, under Compression Load, Pile F54

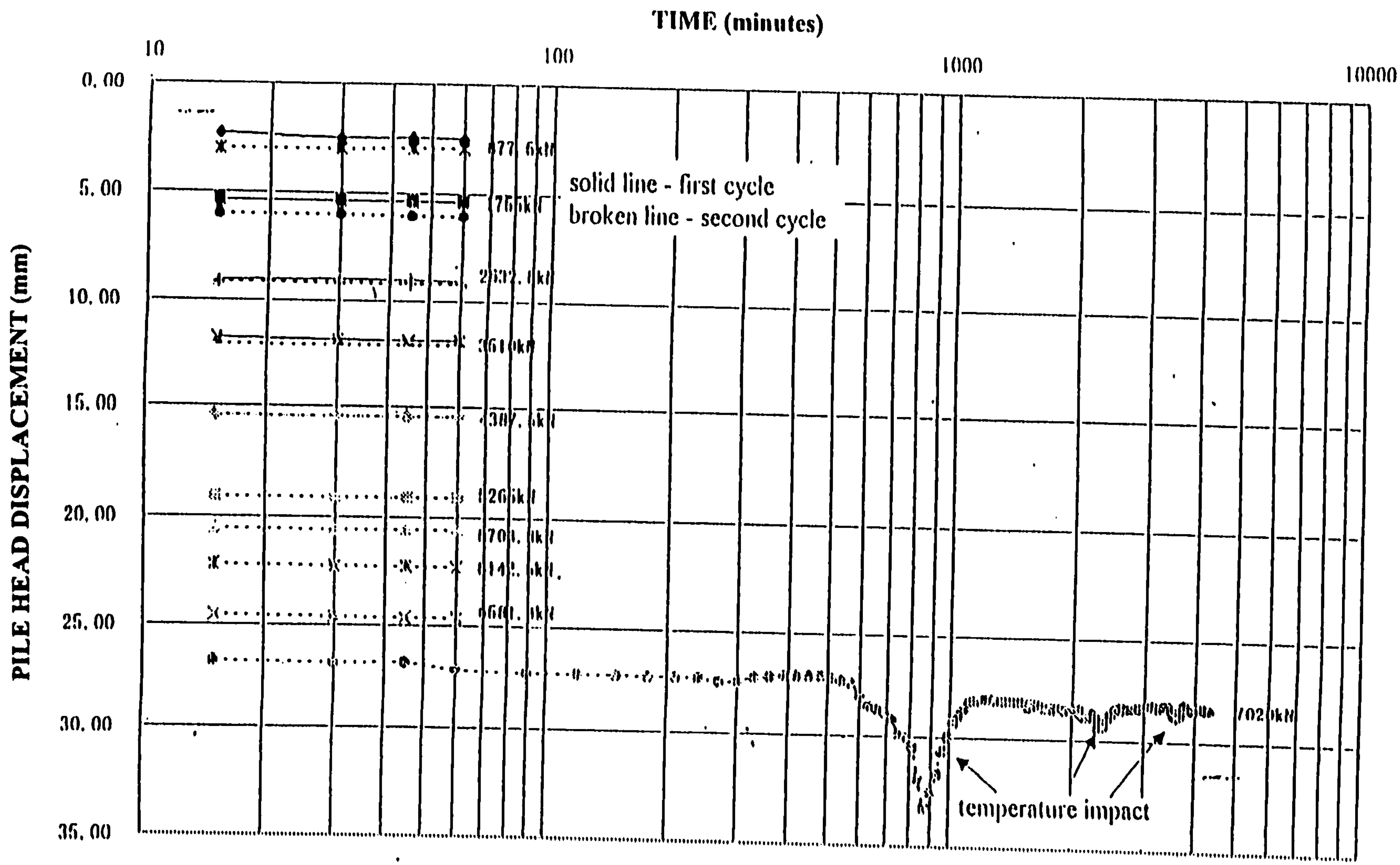

Figure 5.19 - Displacement-Time, s-lg(t), Curve, under Compression Load, Pile D57

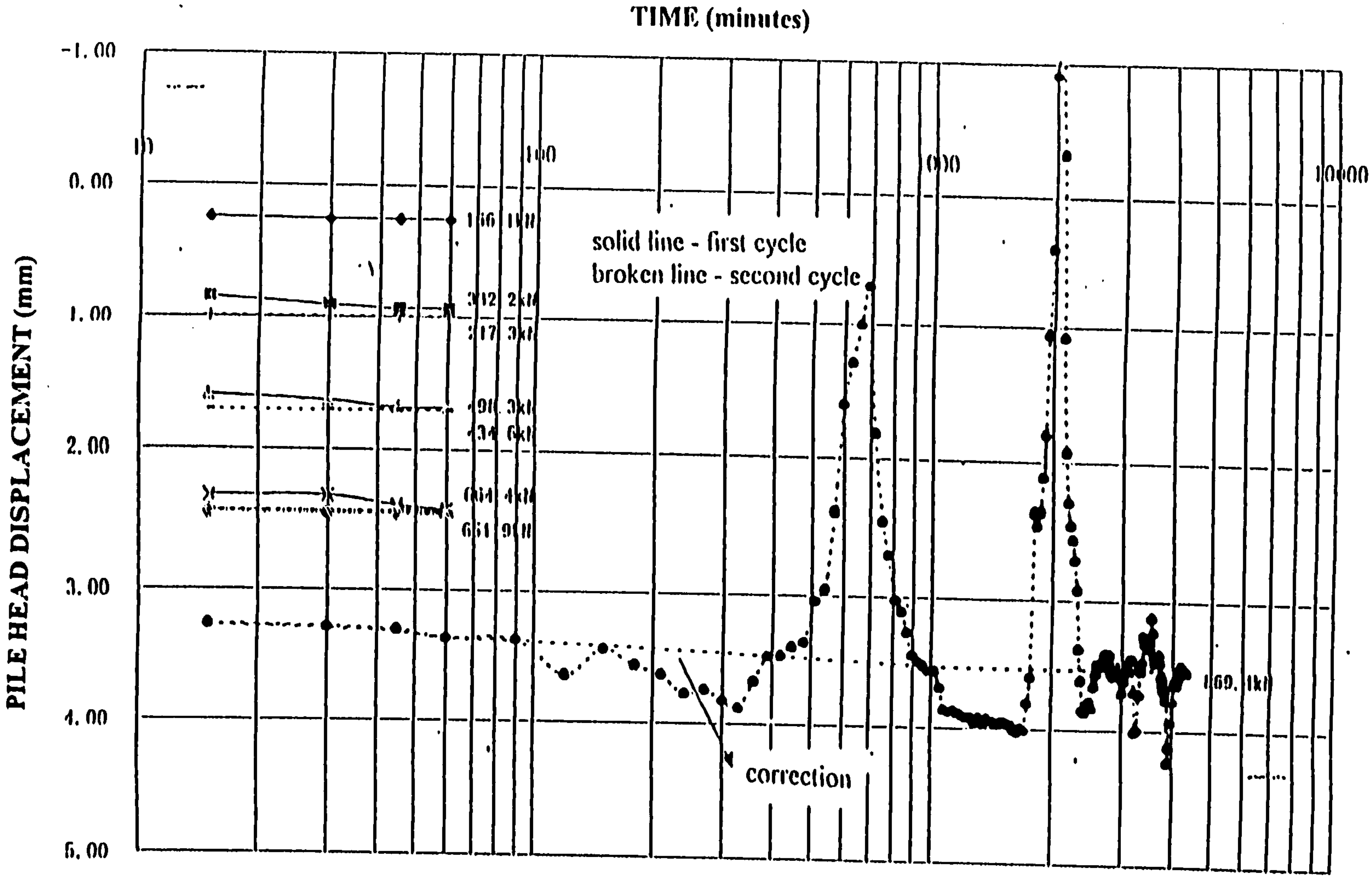

Figure 5.20 - Displacement-Time, s-lg(t), Curve, under Tension Load, Pile D57

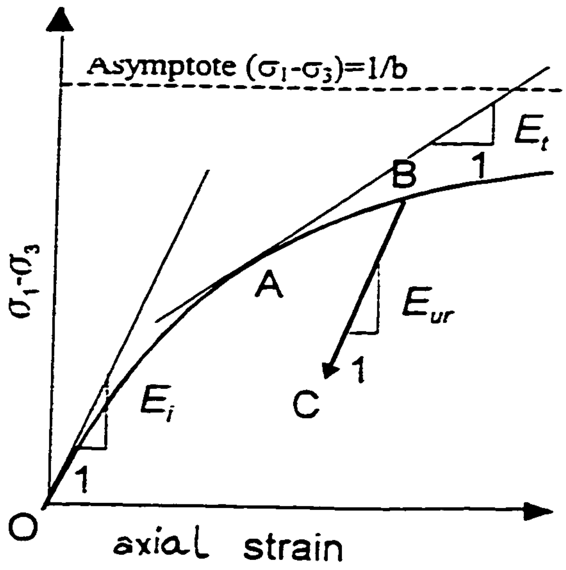

Figure 6.1 - Hyperbolic Stress-Strain Curve

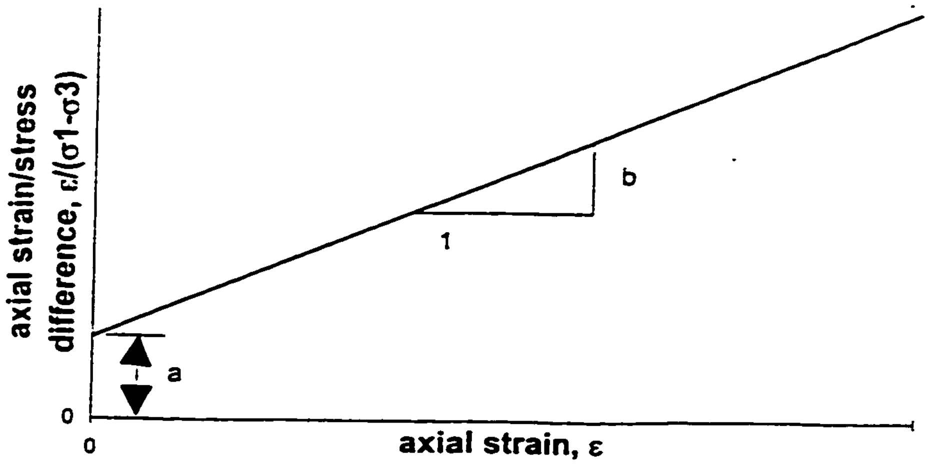

Figure 6.2 - Transformed Hyperbolic Stress-Strain Curve

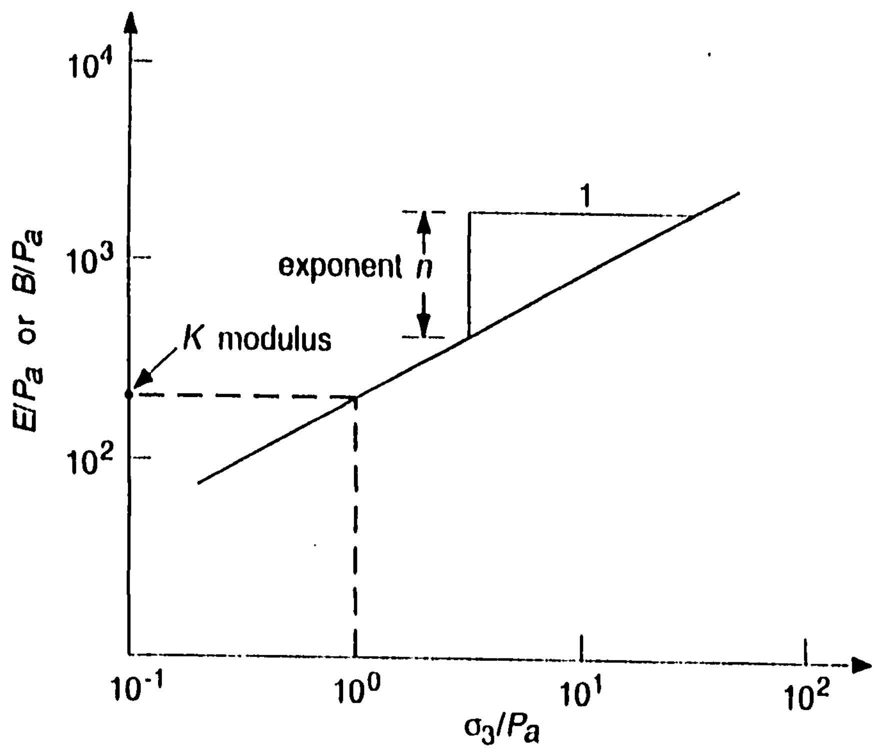

Figure 6.3 - Initial Tangent/Bulk Modulus versus Confining Pressure Relation

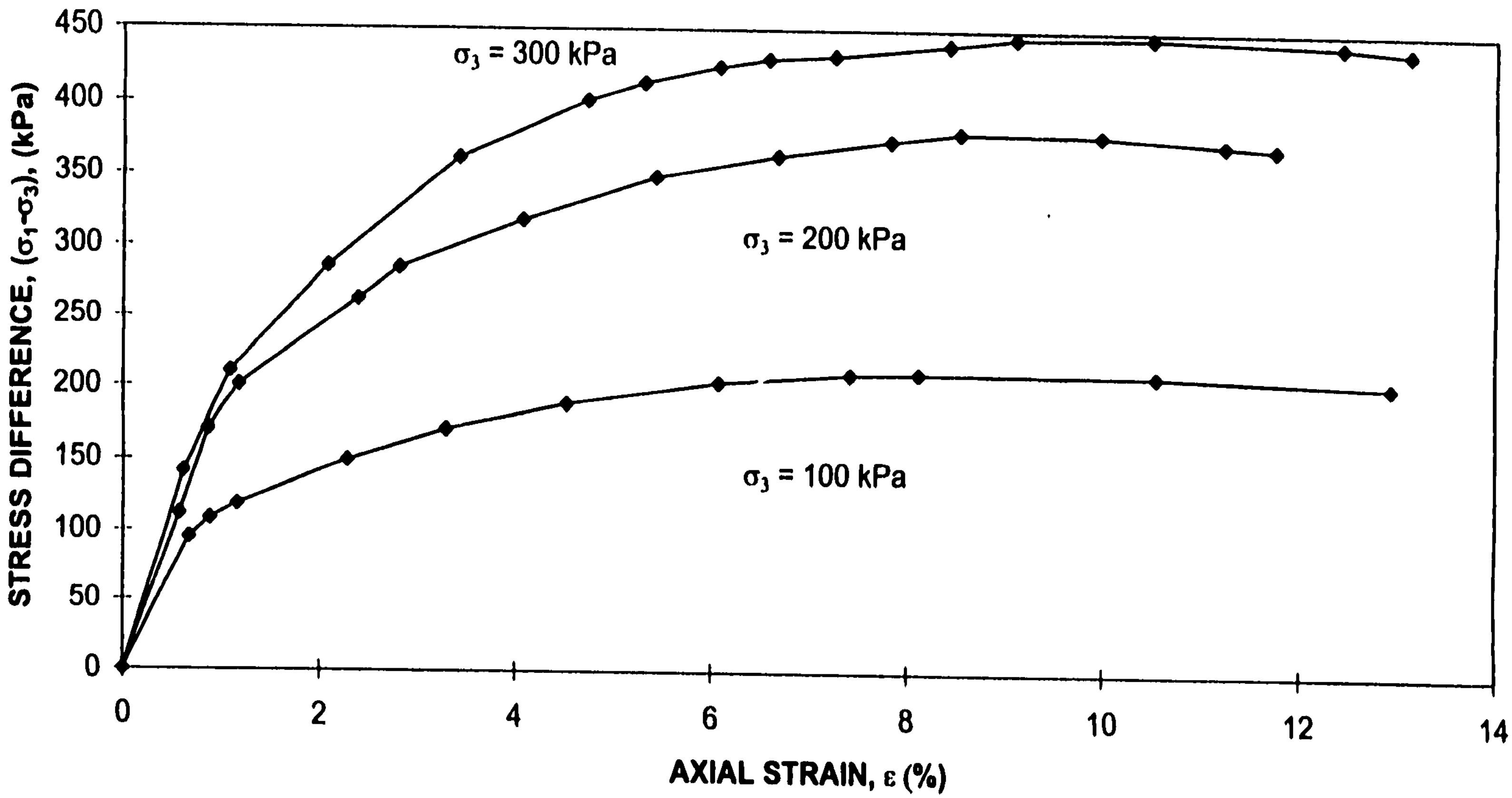

Figure 6.4 - Consolidated-Undrained Triaxial Compression Test at Different Confinements, A111-13

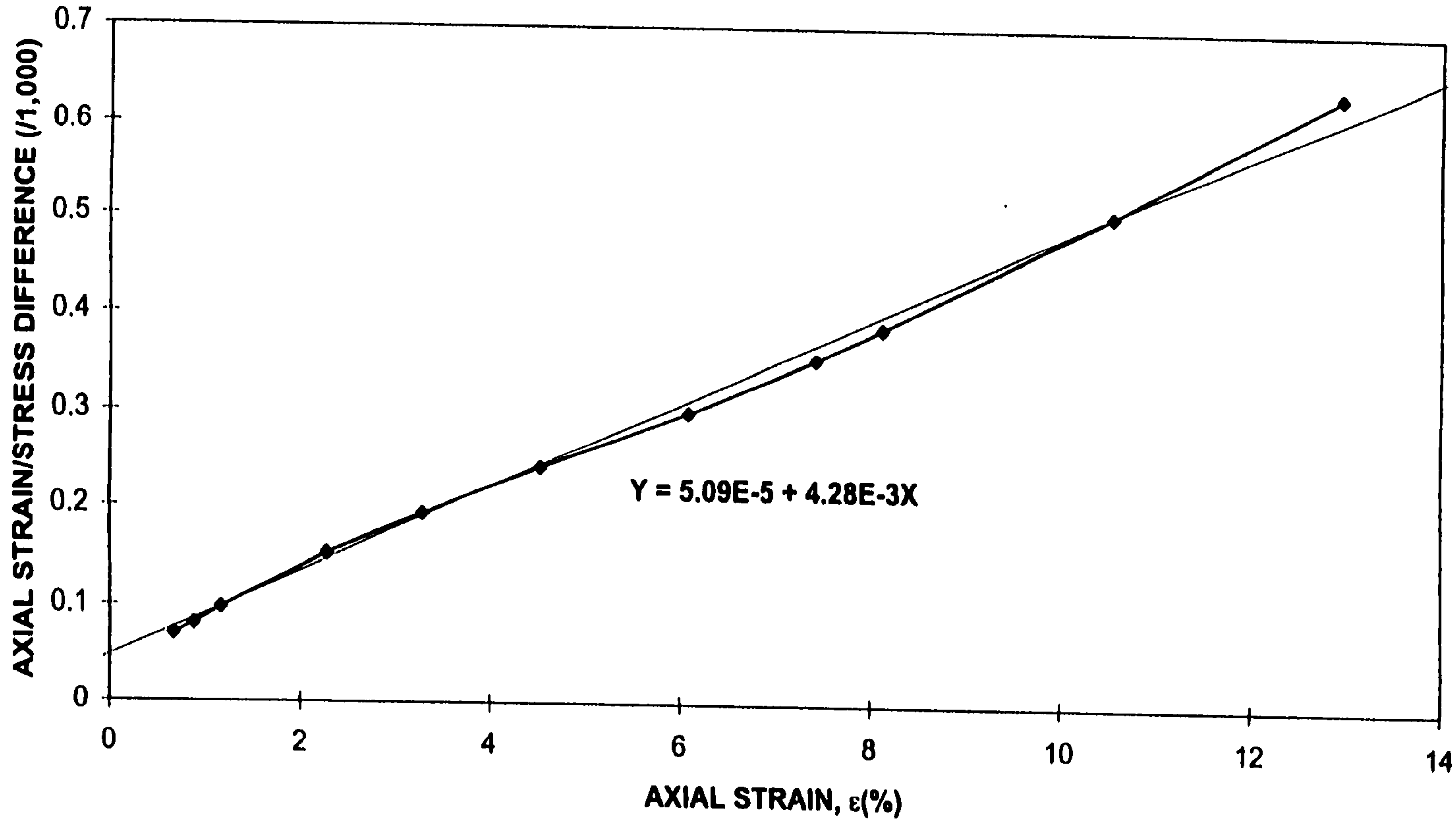

Figure 6.5 - Transformed Hyperbolic Stress-Strain Curve, 100 kPa Comfinement, A111-13

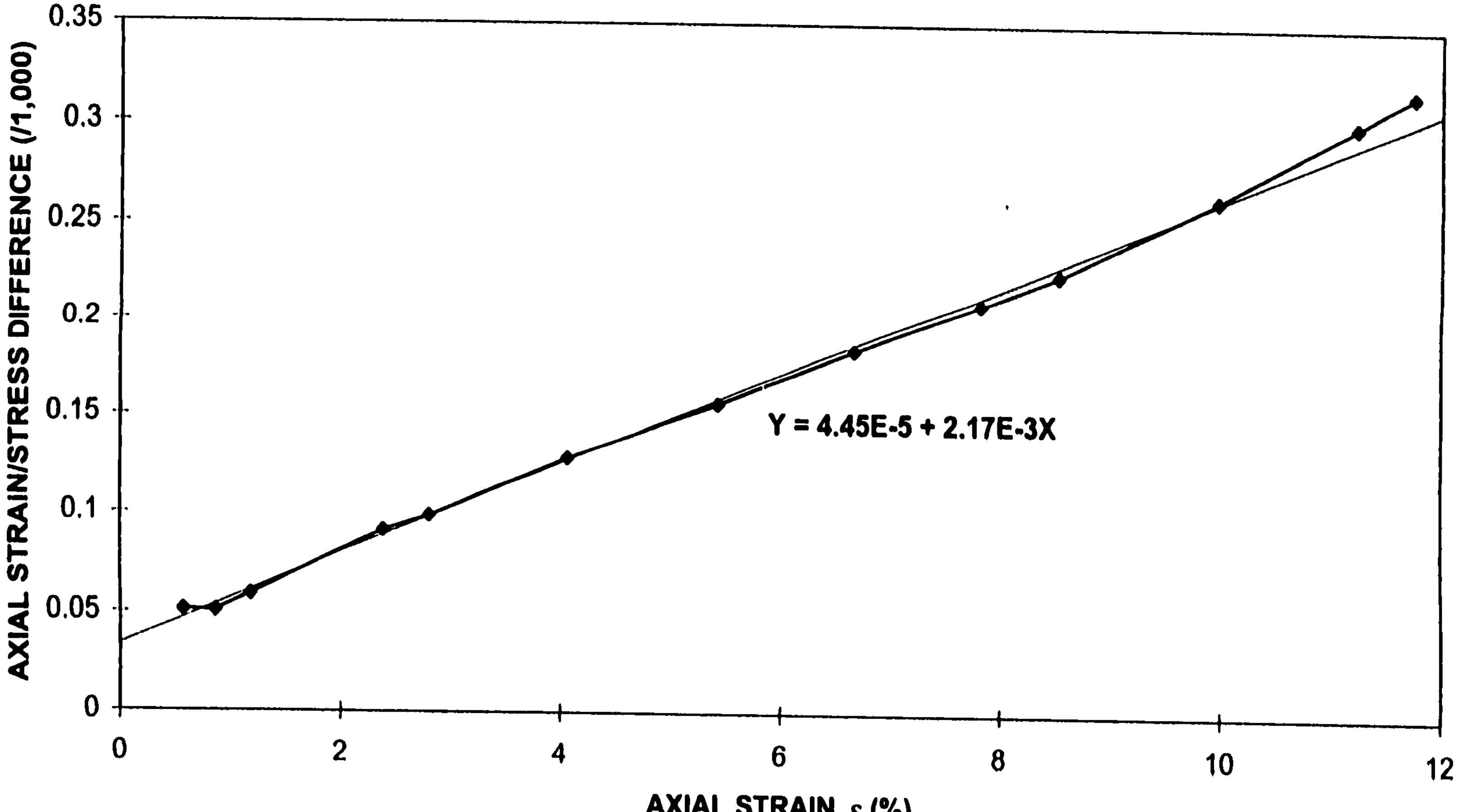

Figure 6.6 - Transformed Hyperbolic Stress-Strain Curve, 200 kPa Confinement, A111-13

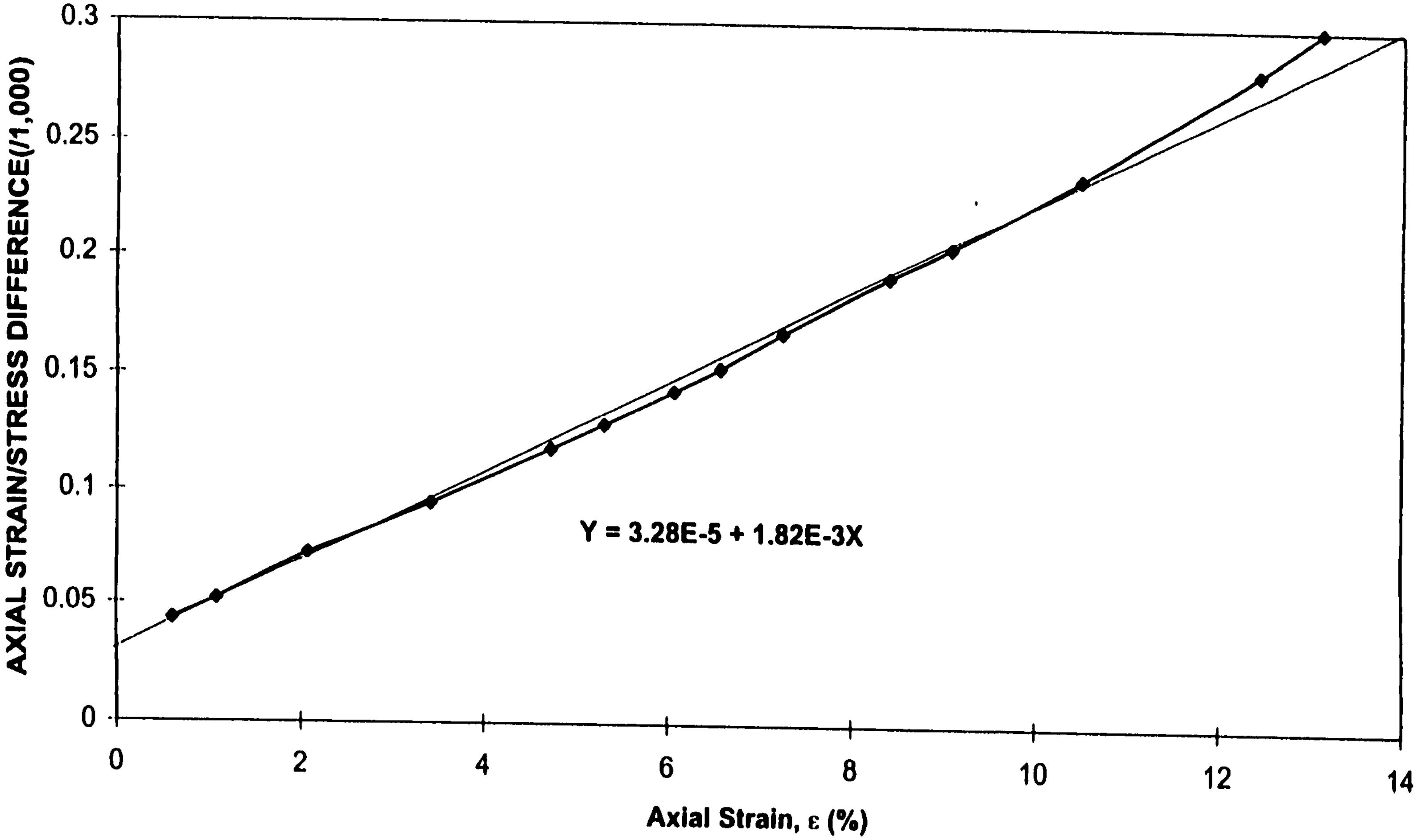

Figure 6.7 - Transformed Hyperbolic Stress-Strain Curve, 300 kPa Confinement, A111-13

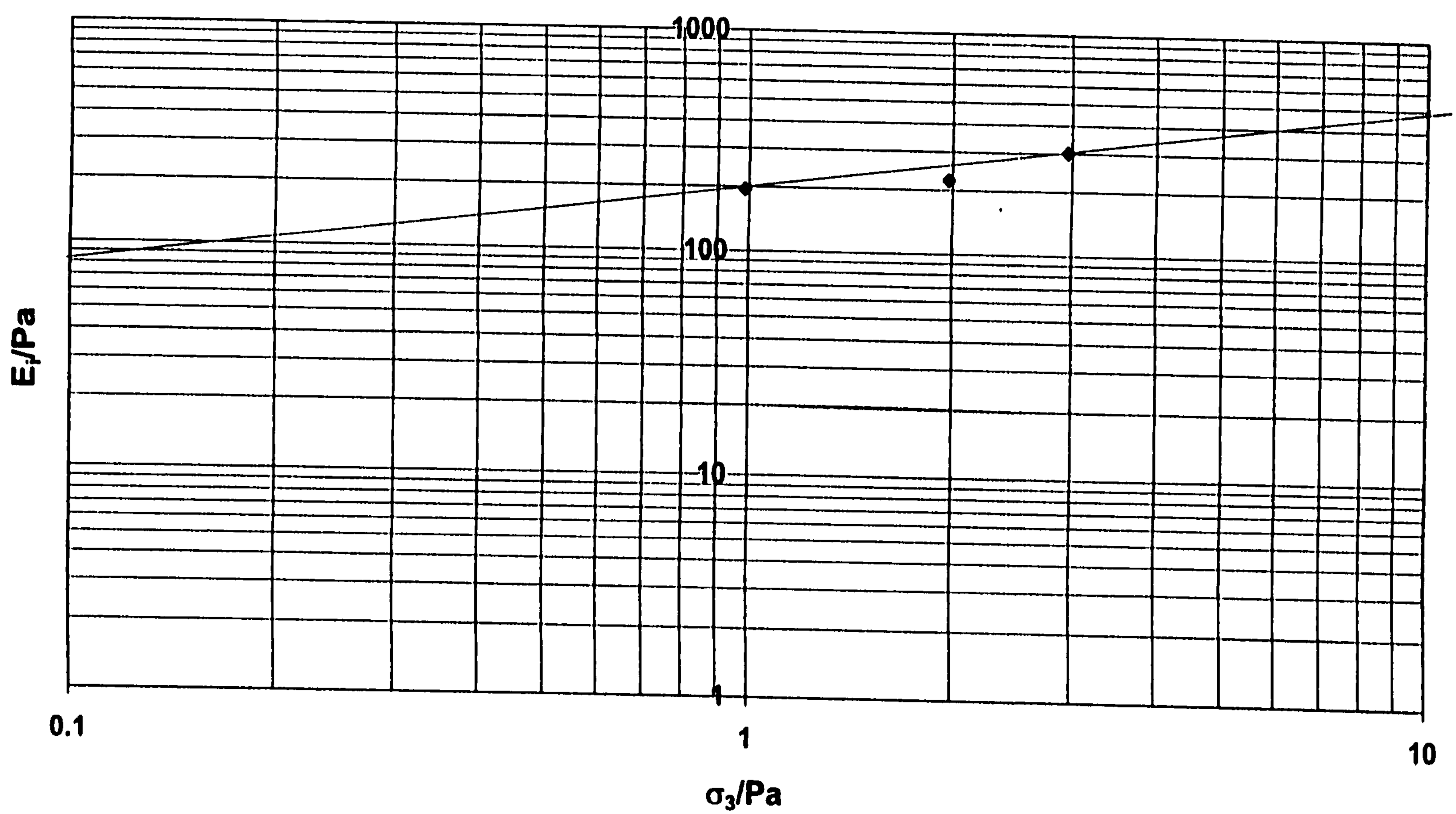

Figure 6.8 - Variations of Initial Tangent Modulus with Confining Pressure, A111-13

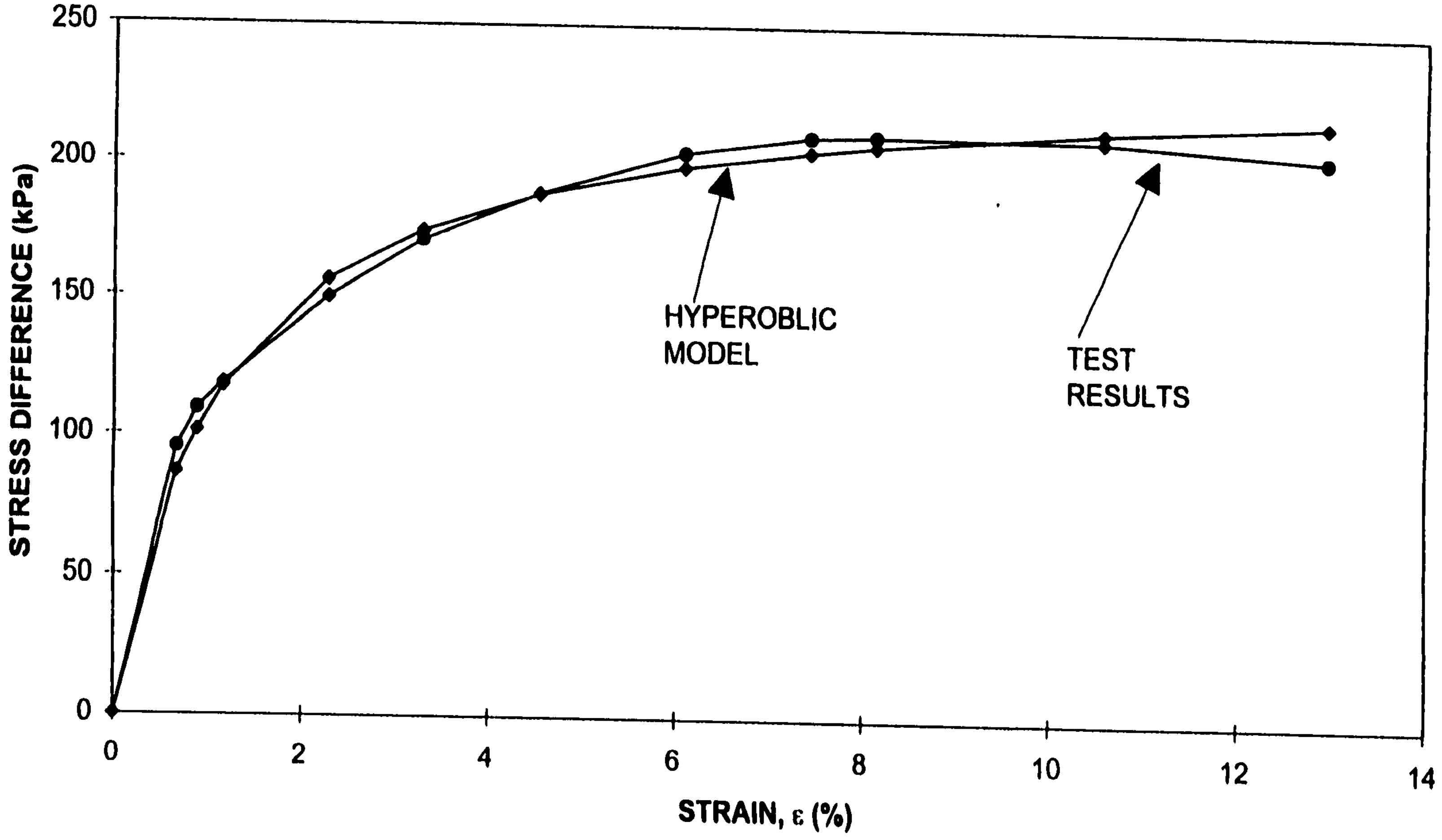

Figure 6.9 - Fitted Hyperbolic Model, 100 kPa Confining Pressure, A111-13

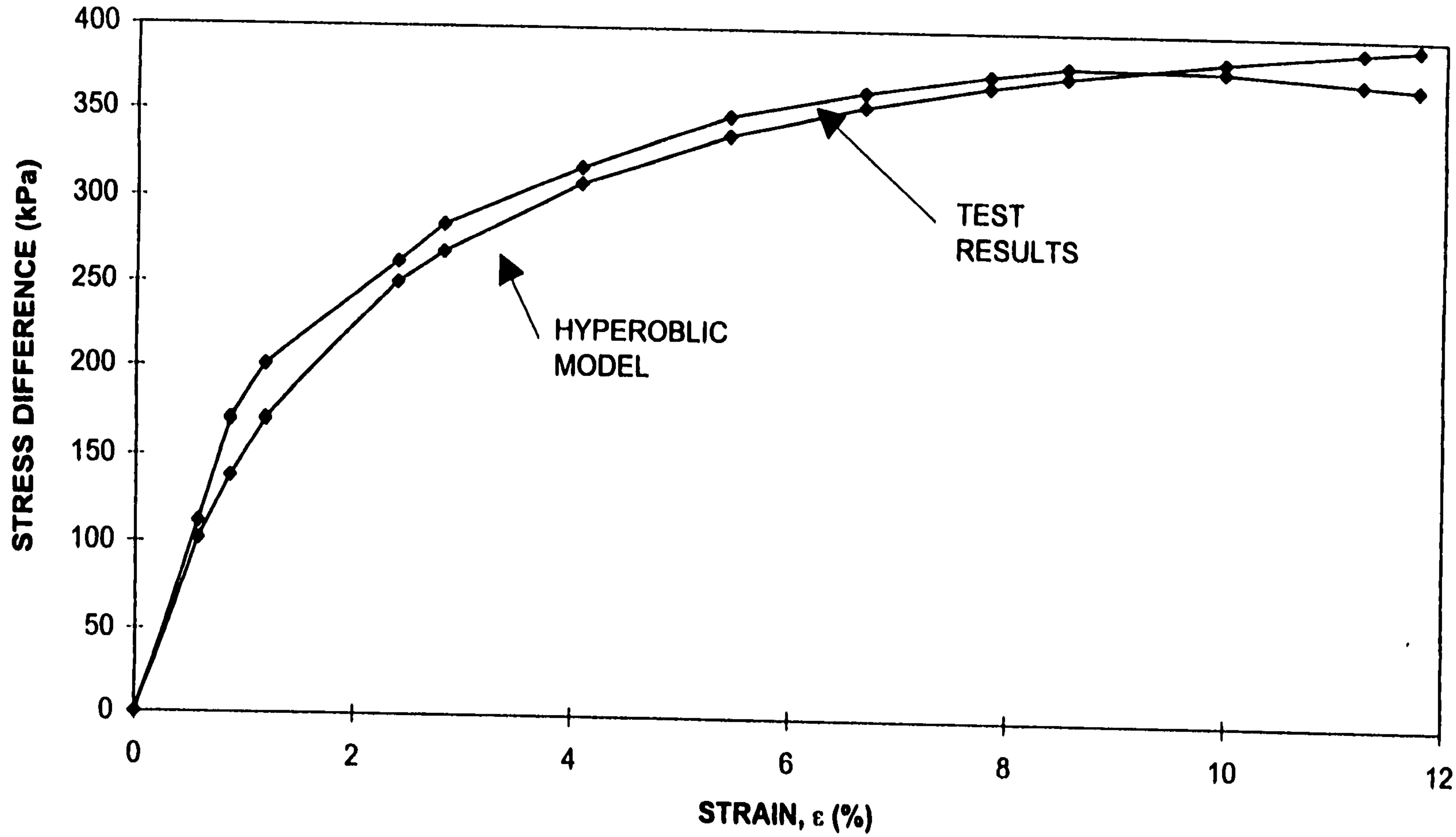

Figure 6.10 - Fitted Hyperbolic Model, 200 kPa Confining Pressure, A111-13

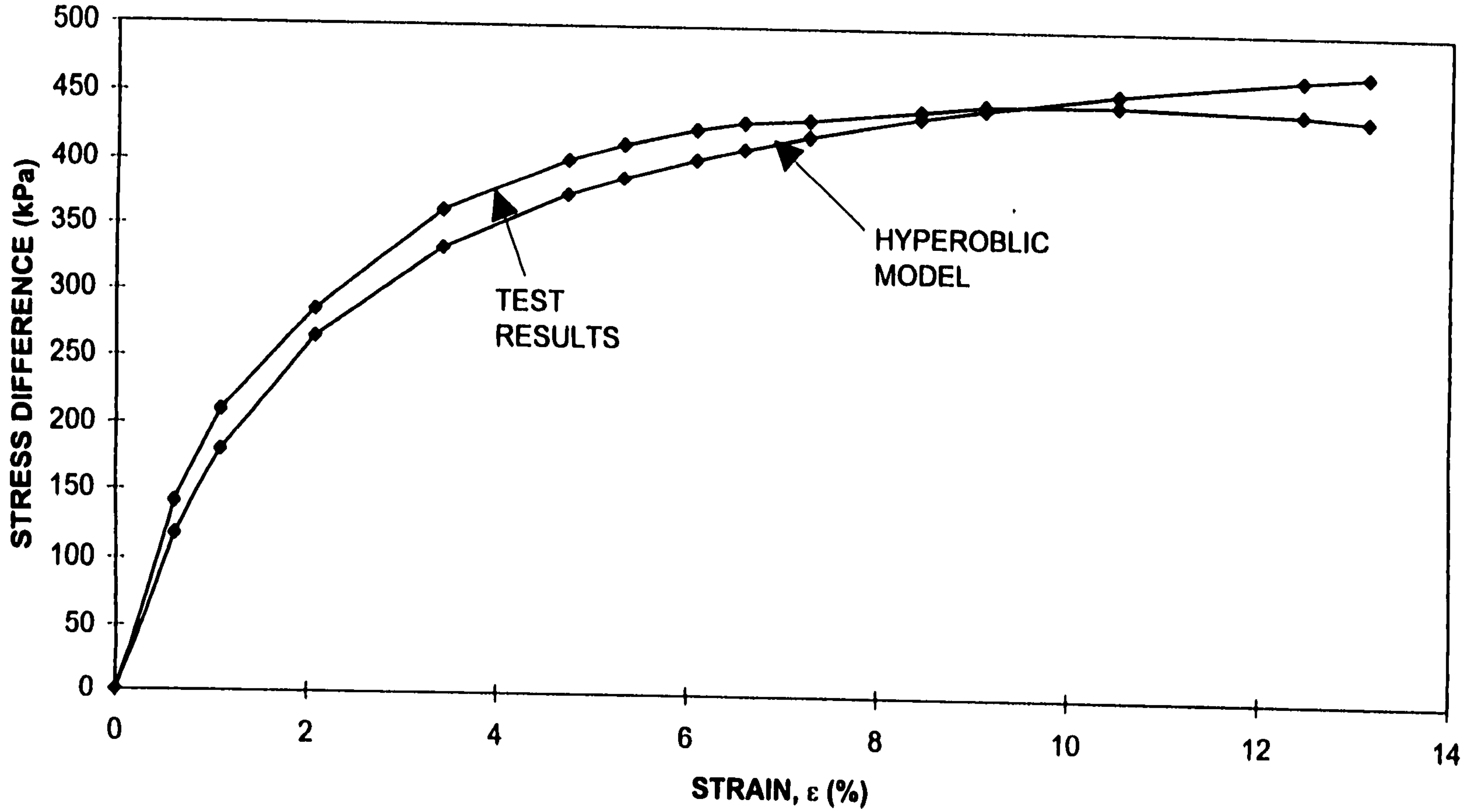

Figure 6.11 - Fitted Hyperbolic Model, 300 kPa Confining Pressure, A111-13

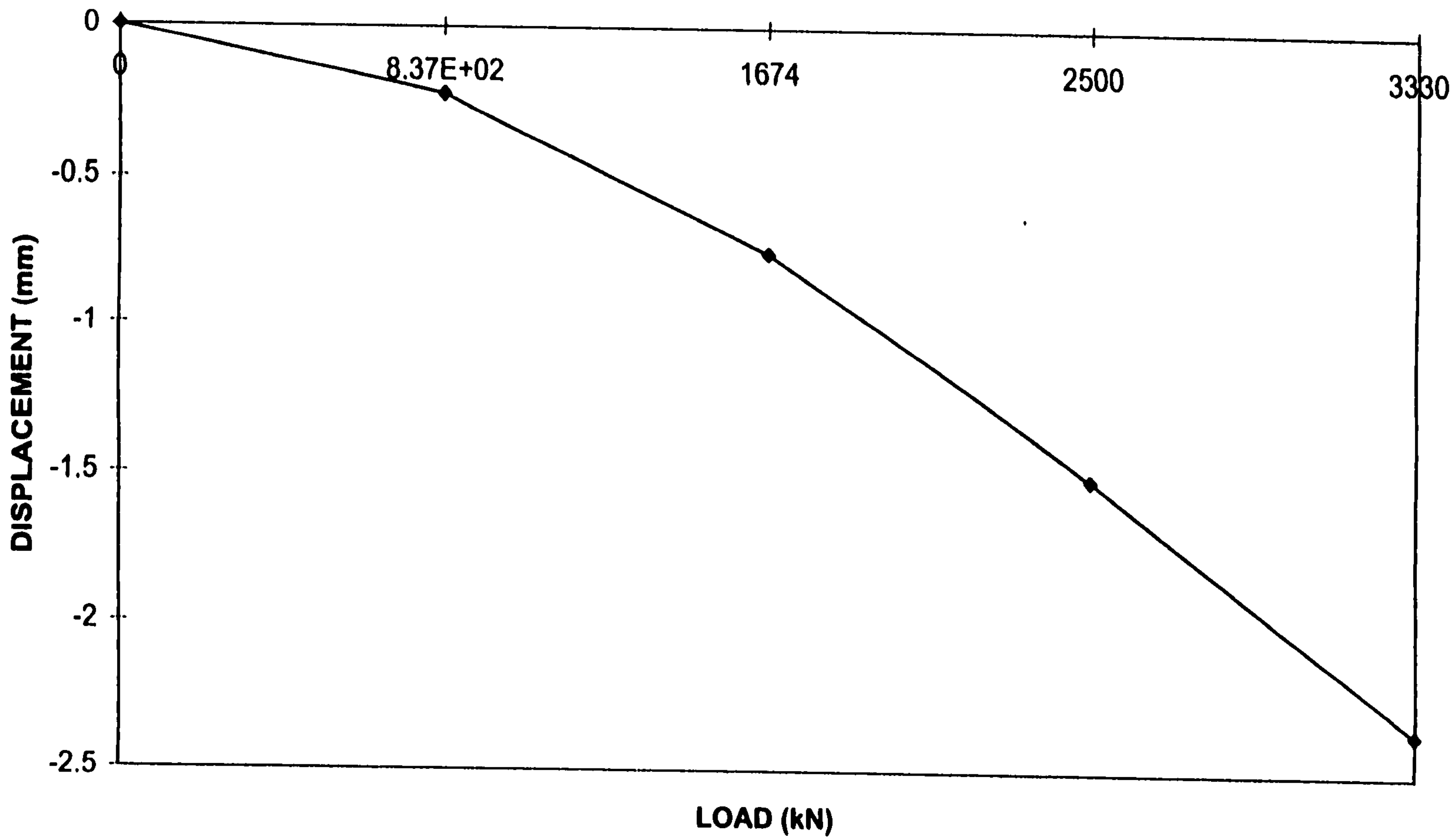

Figure 6.12 - Displacement on Pile Head for Section Buried in Soil, Compression, First Loading Cycle, A17

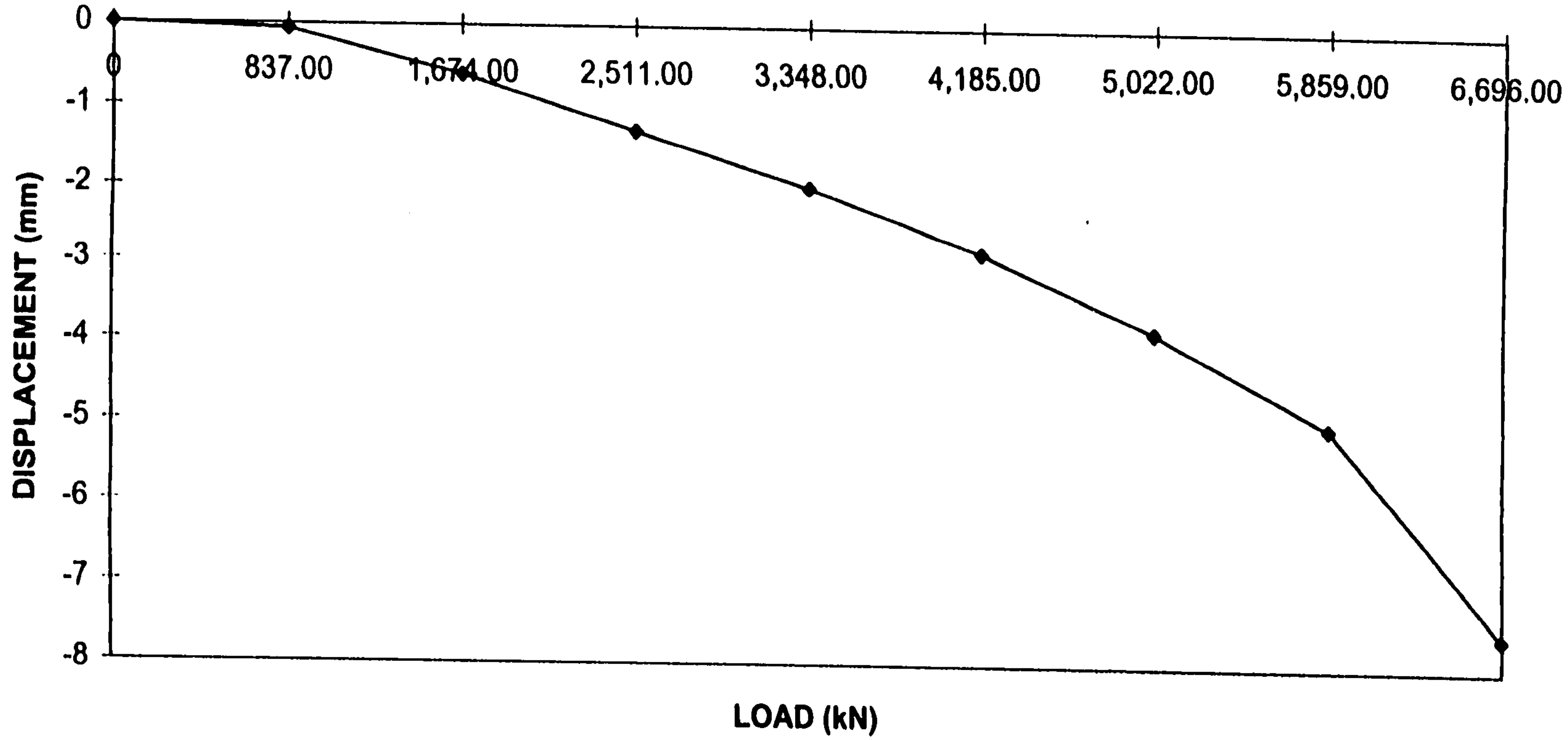

Figure 6.13 - Displacement on Pile Head for Section Buried in Soil, Compression, Second Loading Cycle, A17

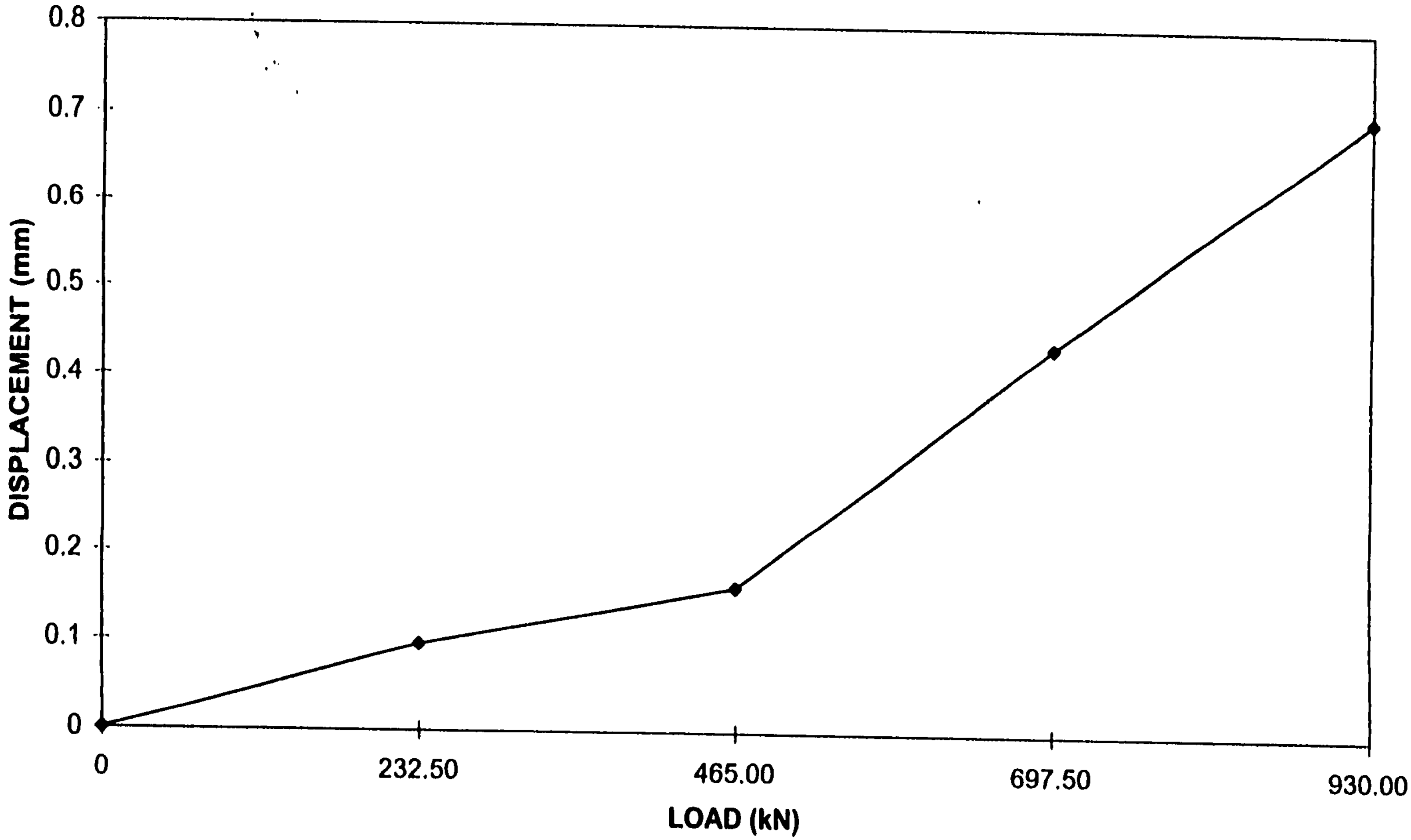

Figure 6.14 - Displacement on Pile Head for Section Buried in Soil, Tension, First Loading Cycle, Tension, A17

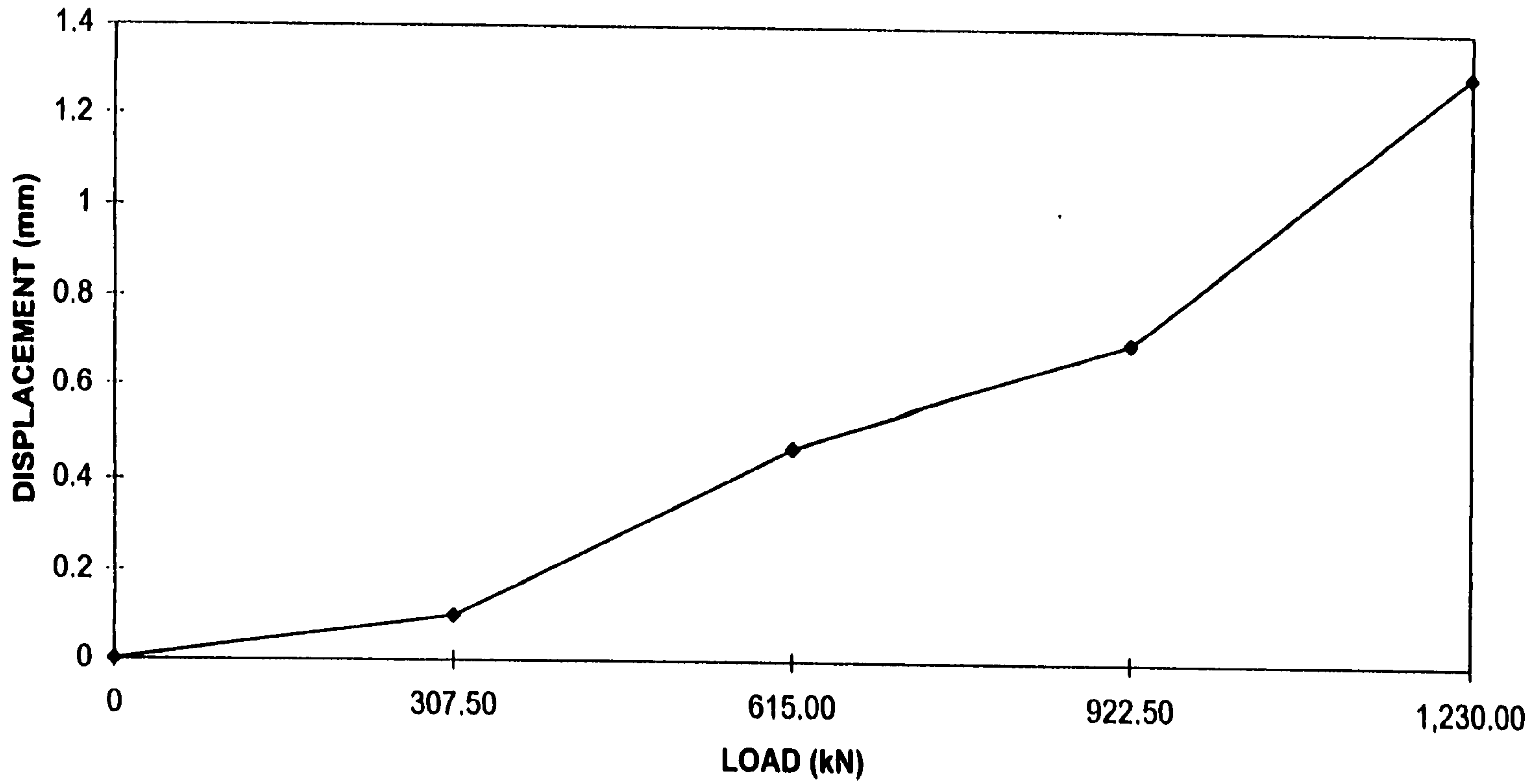

Figure 6.15, Displacement on Pile Head for Section Buried in Soil, Tension, Second Loading Cycle, Tension, A17

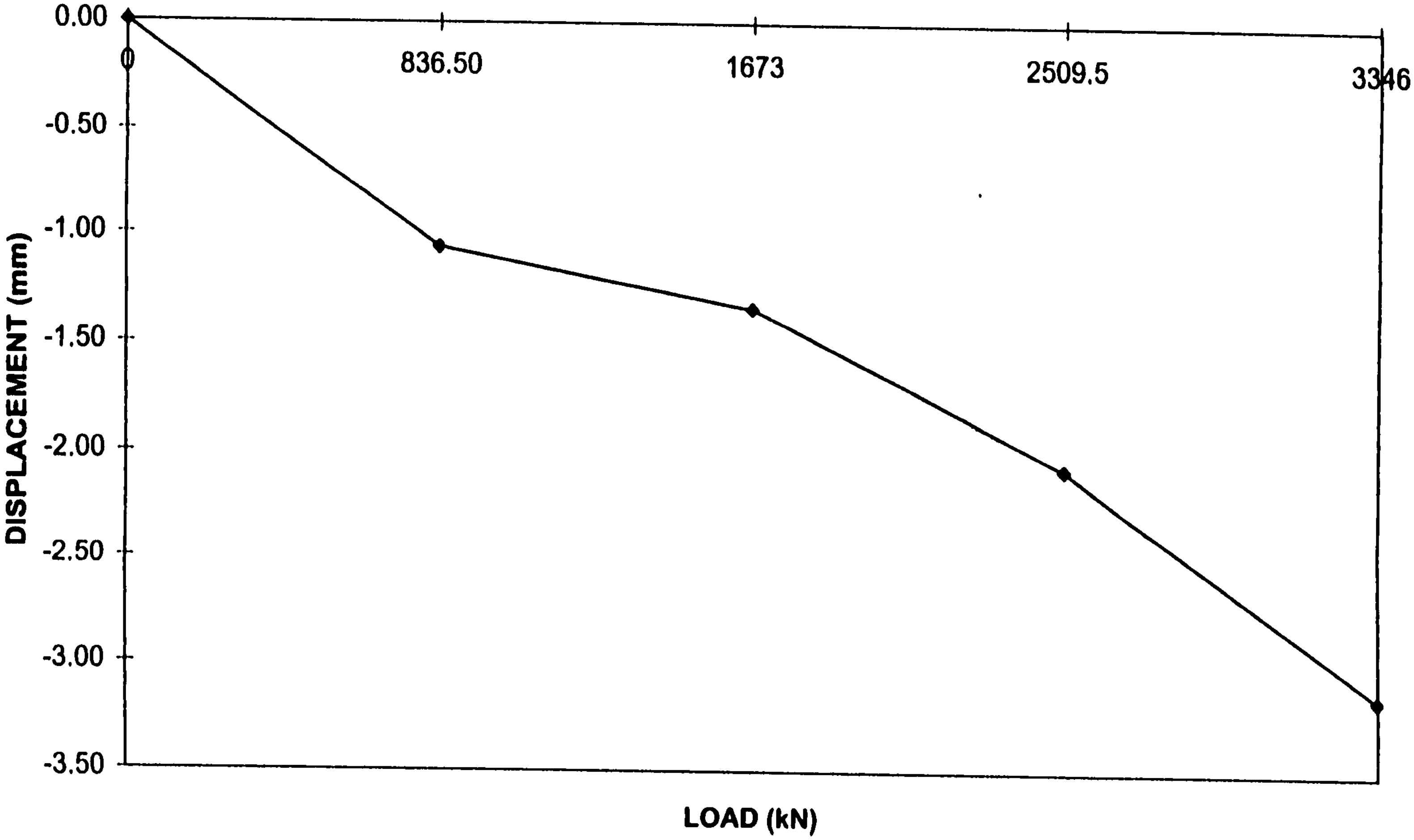

Figure 6.16, Displacment for Pile buried in Soil, Compression, First Loading Cycle, F54

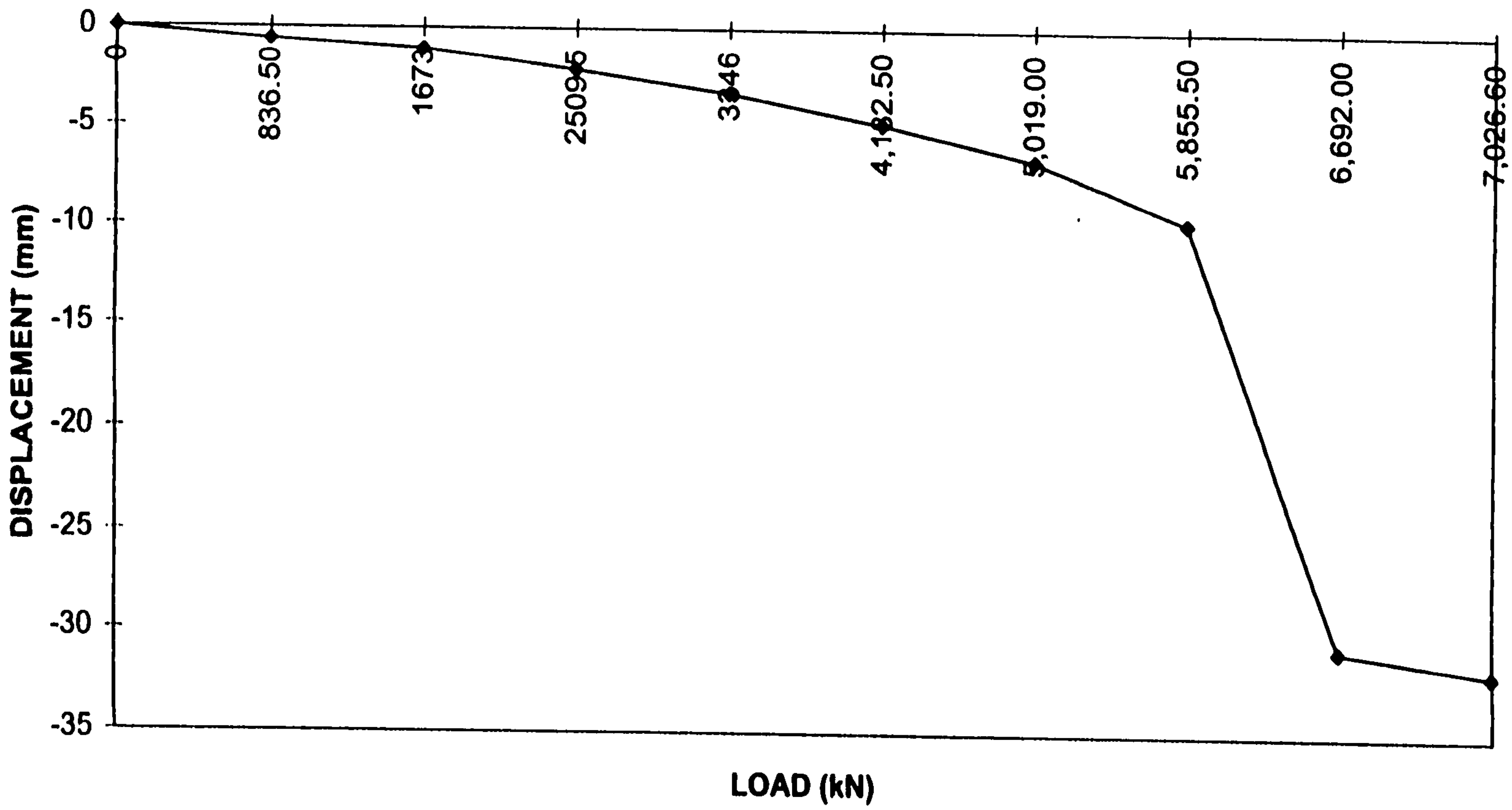

Figure 6.17, Displacment for Pile buried in Soil, Compression, Second Loading Cycle, F54

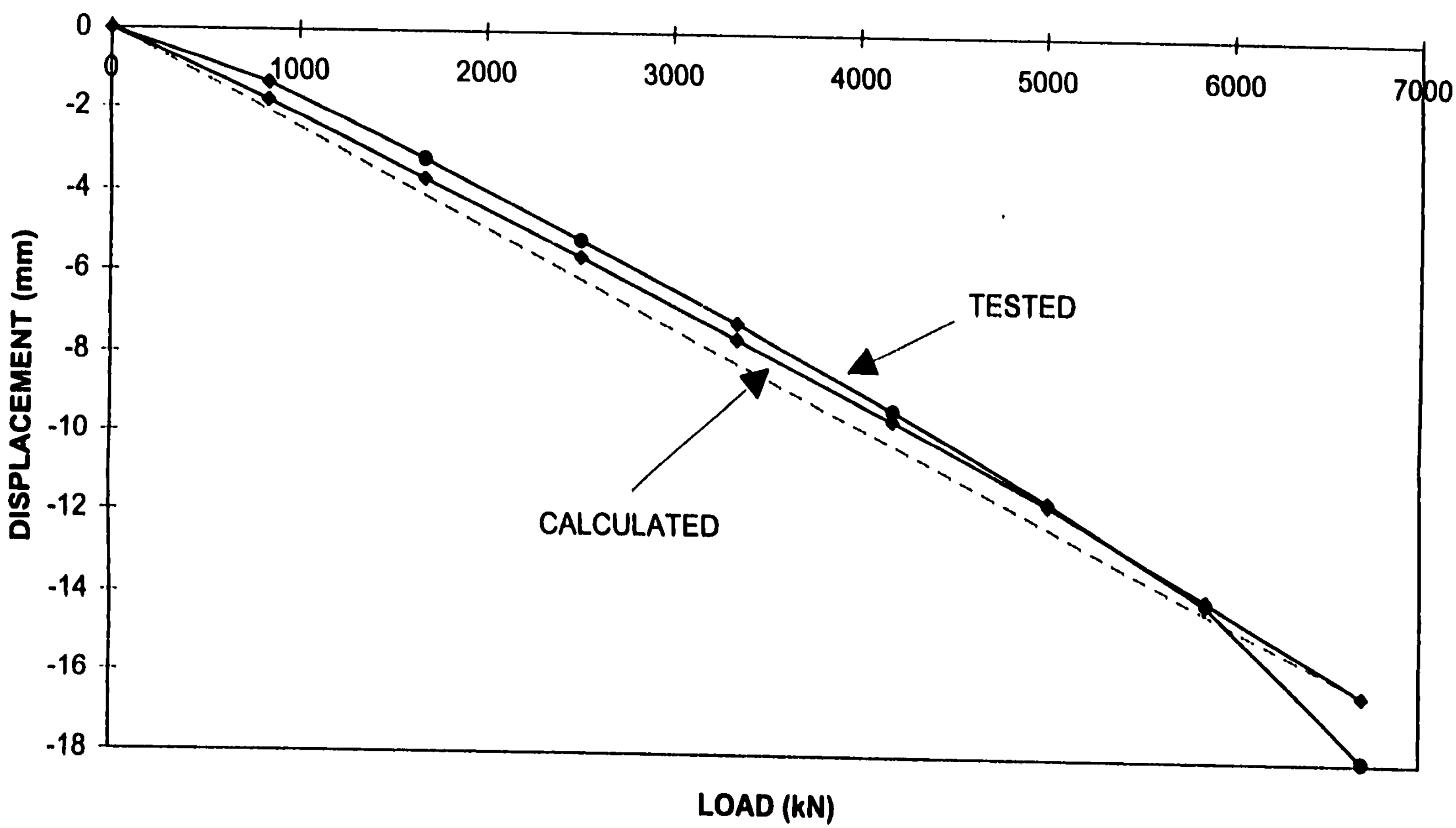

Figure 6.18 - Comparison of Results from Finite Element Analysis and Static Load Test, A17

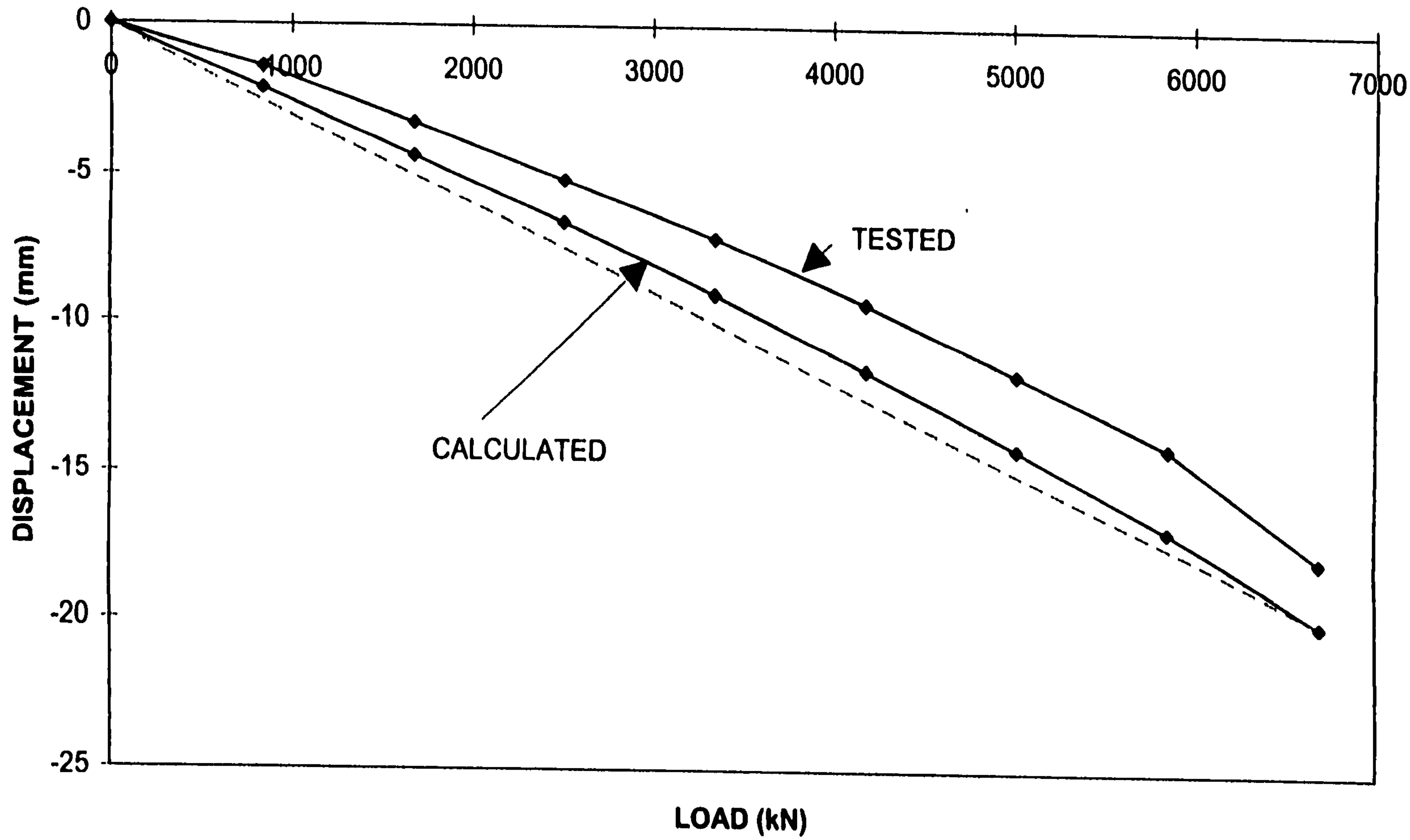

Figure 6.19 - Case 1, Comparison of Results from Finite Element Analysis and Static Load Test, A17

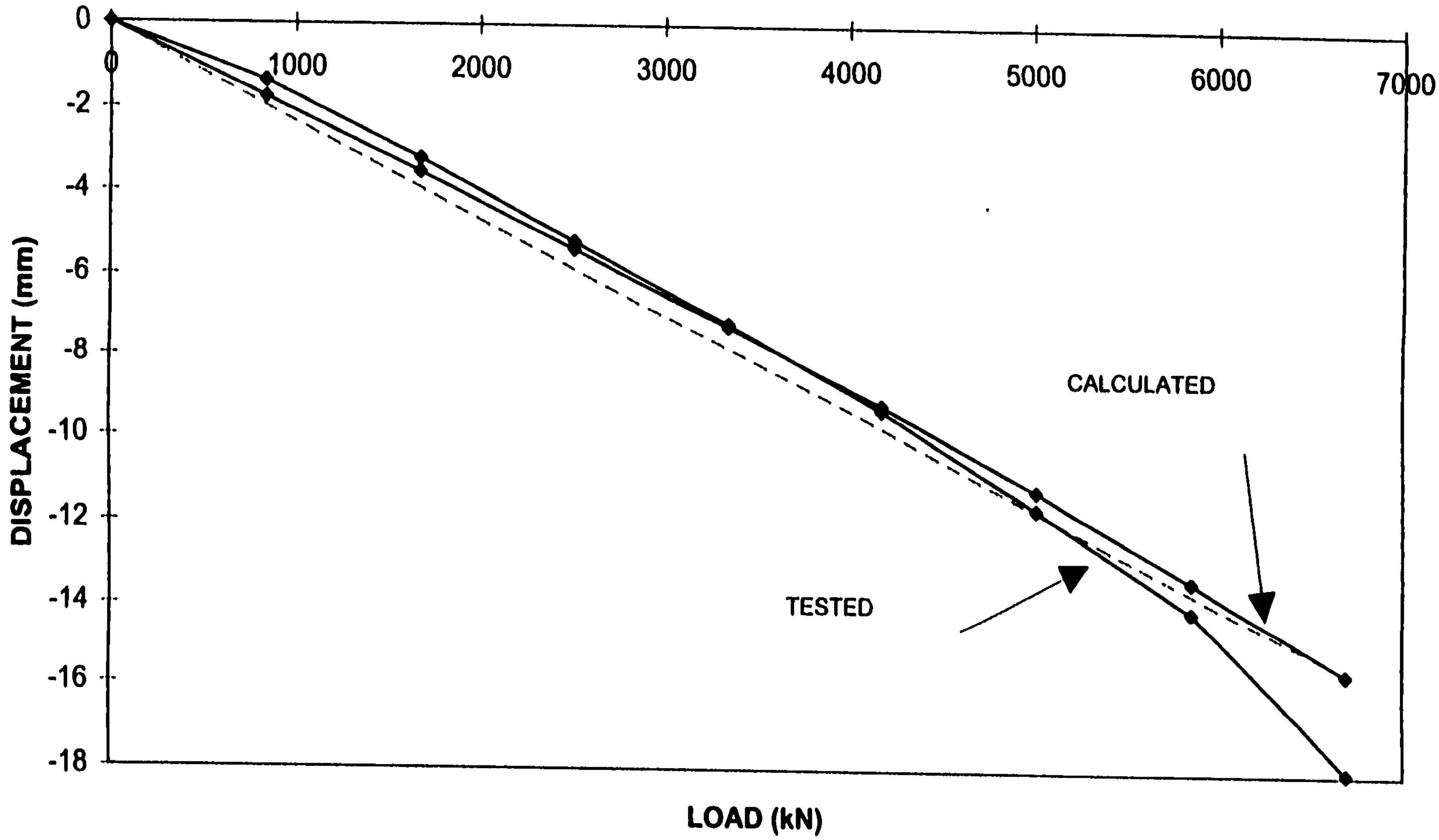

Figure 6.20 - Case 2, Comparison of Results from Finite Element Analysis and Static Load Test, A17

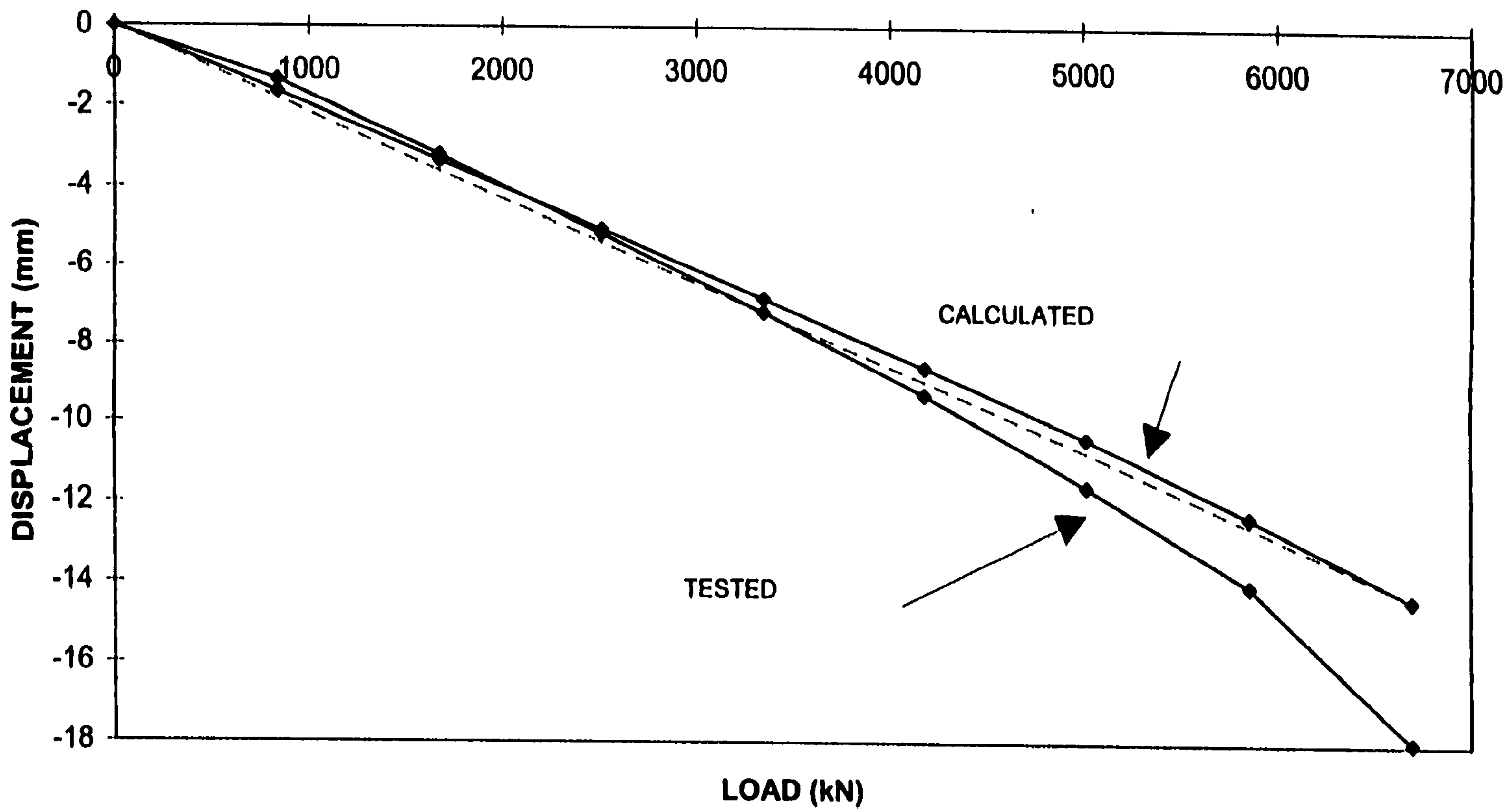

Figure 6.21 - Case 3, Comparison of Results from Finite Element Analysis and Static Load Test, A17

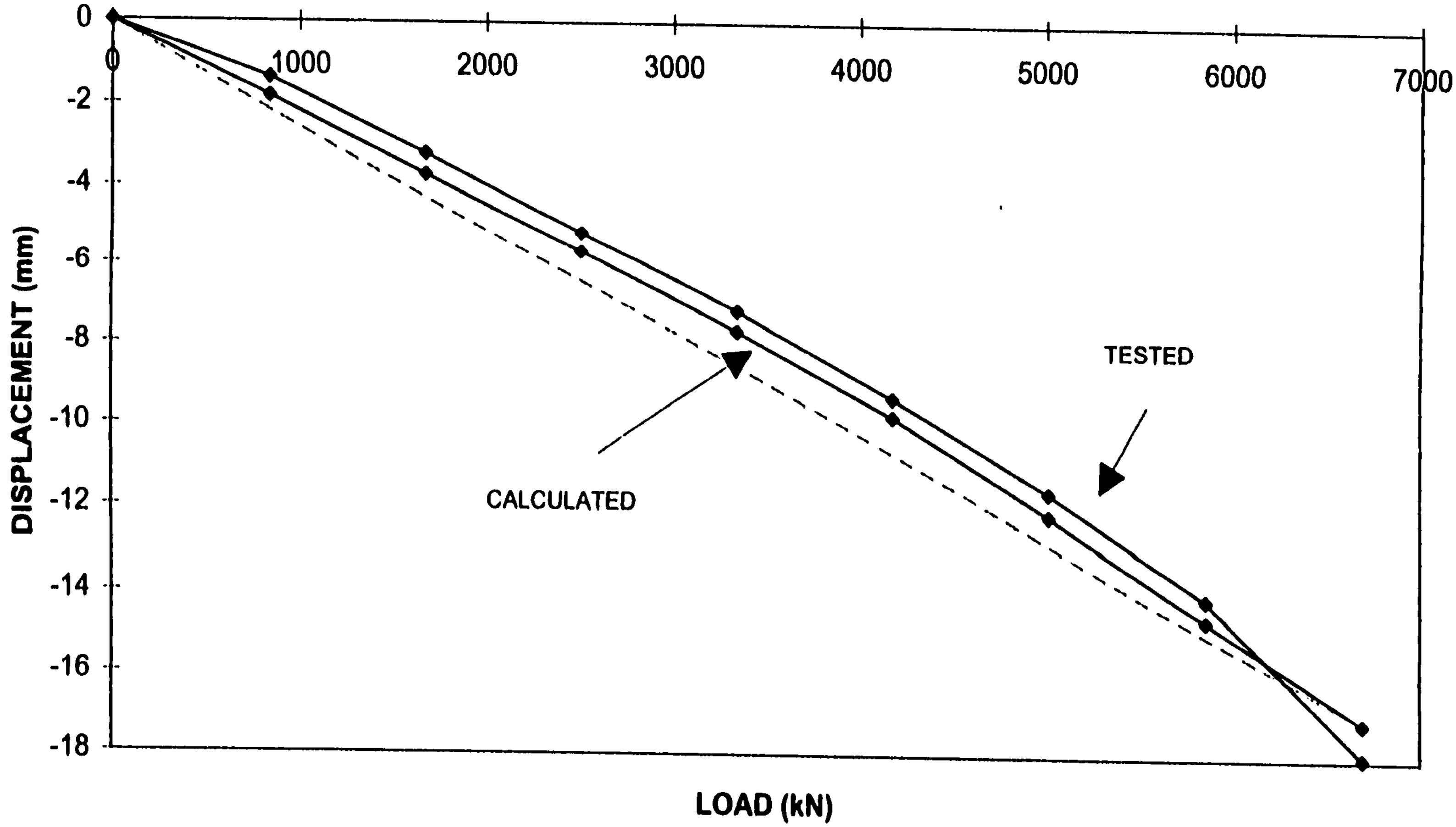

Figure 6.22 - Case 4, Comparison of Results from Finite Element Analysis and Static Load Test, A17

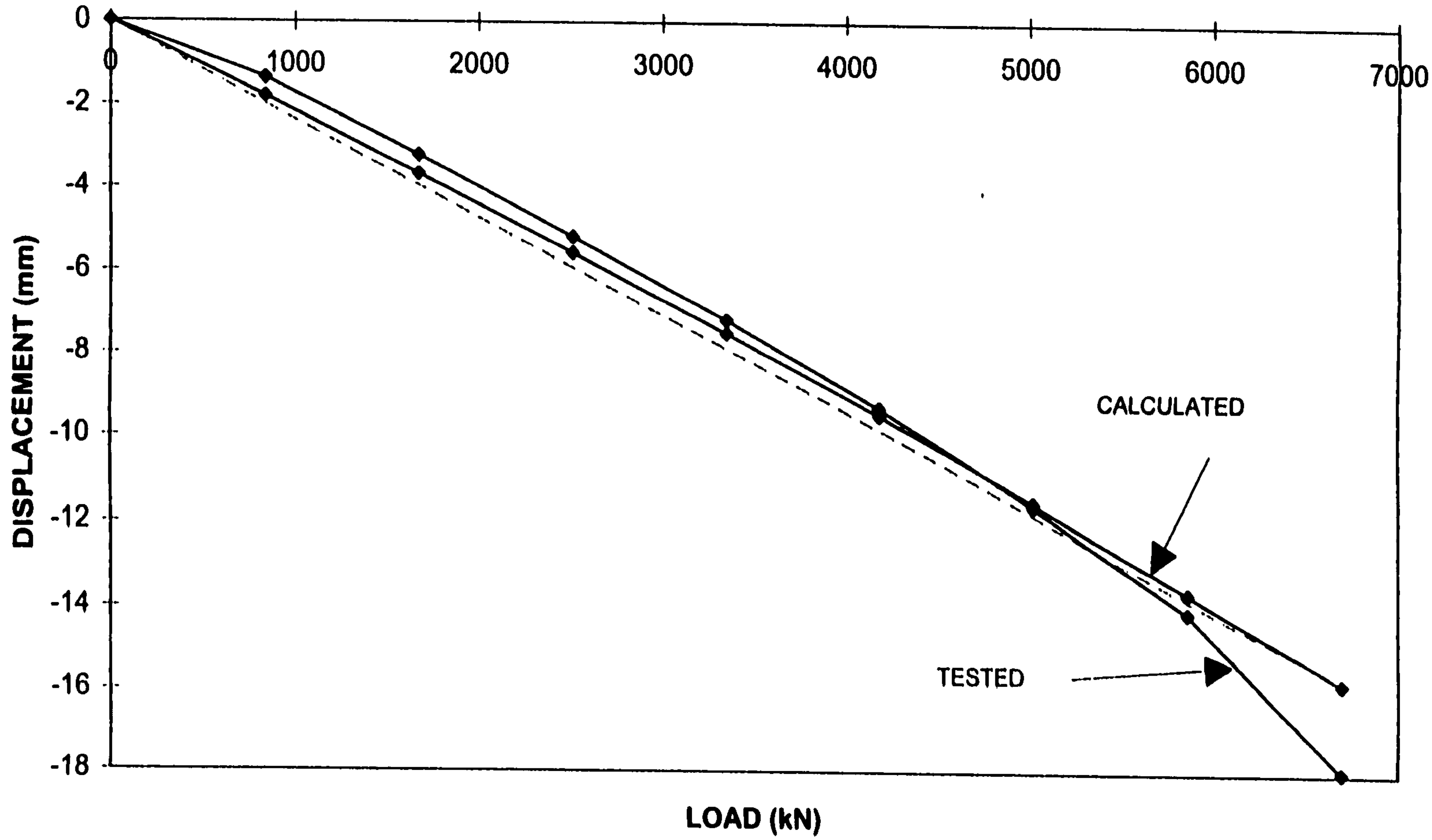

Figure 6.23 - Case 5, Comparison of Results from Finite Element Analysis and Static Load Test, A17

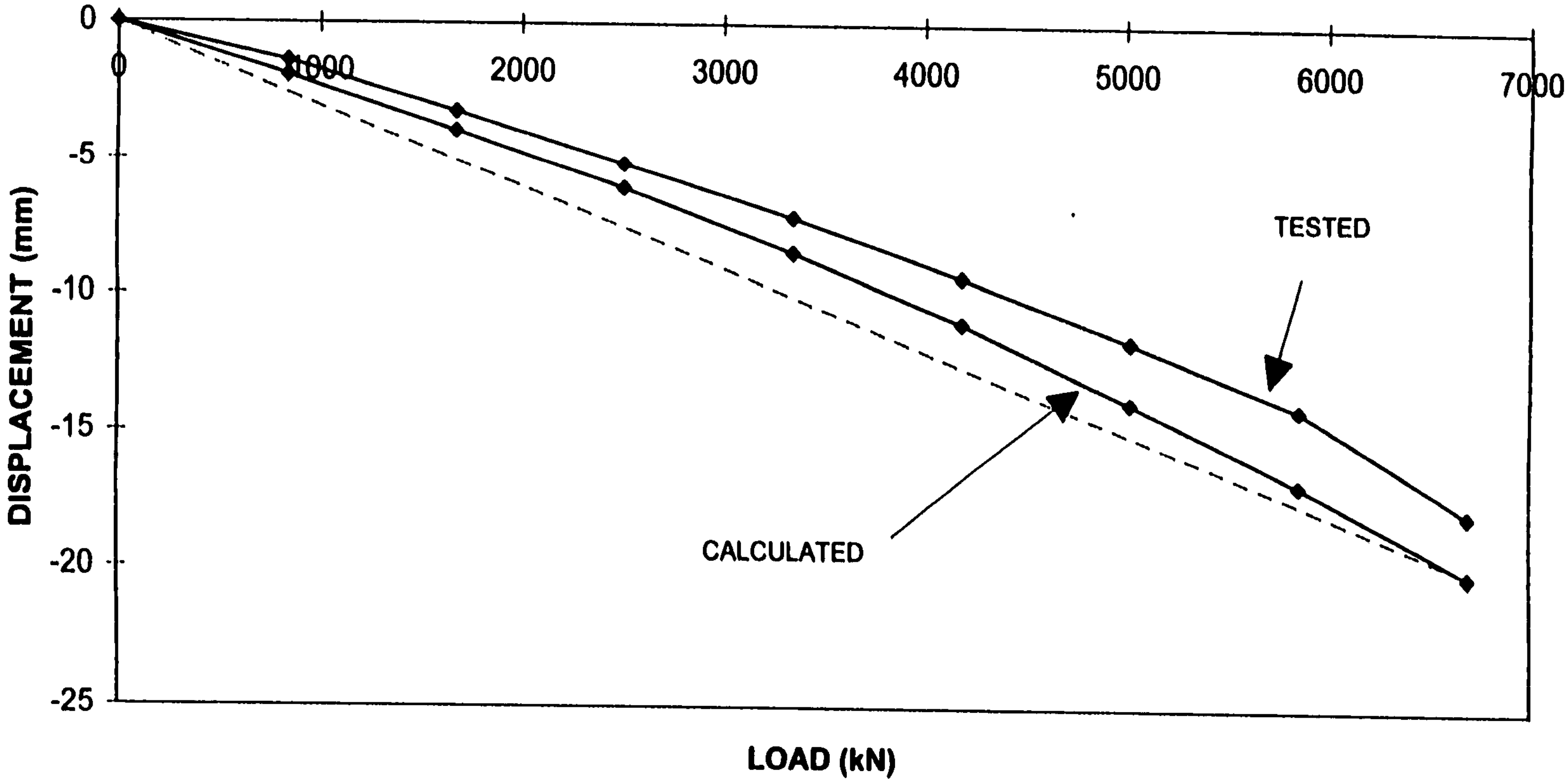

Figure 6.24 - Case 6, Comparison of Results from Finite Element Analysis and Static Load Test, A17

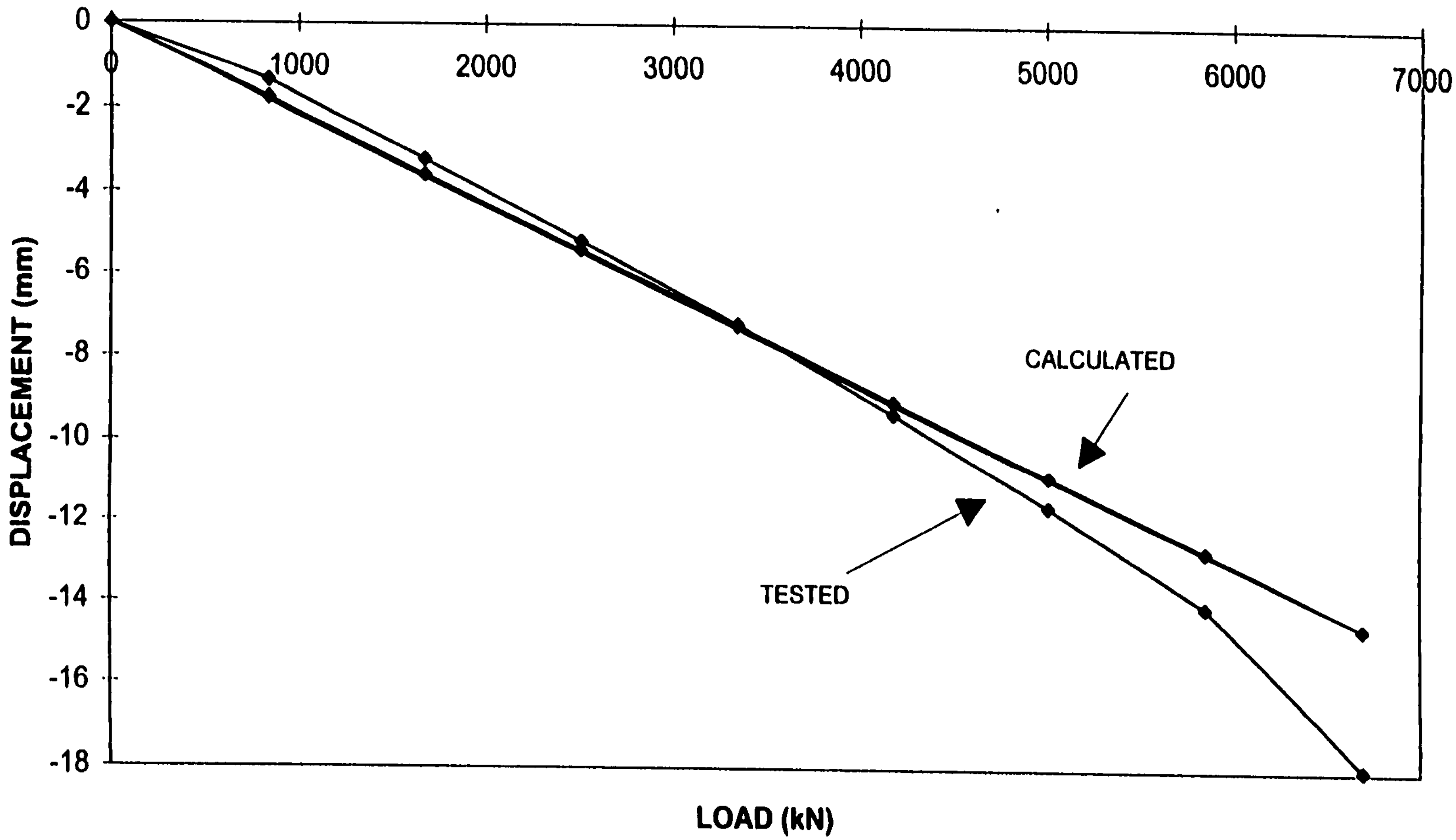

Figure 6.25 - Case 7, Comparison of Results from Finite Element Analysis and Static Load Test, A17

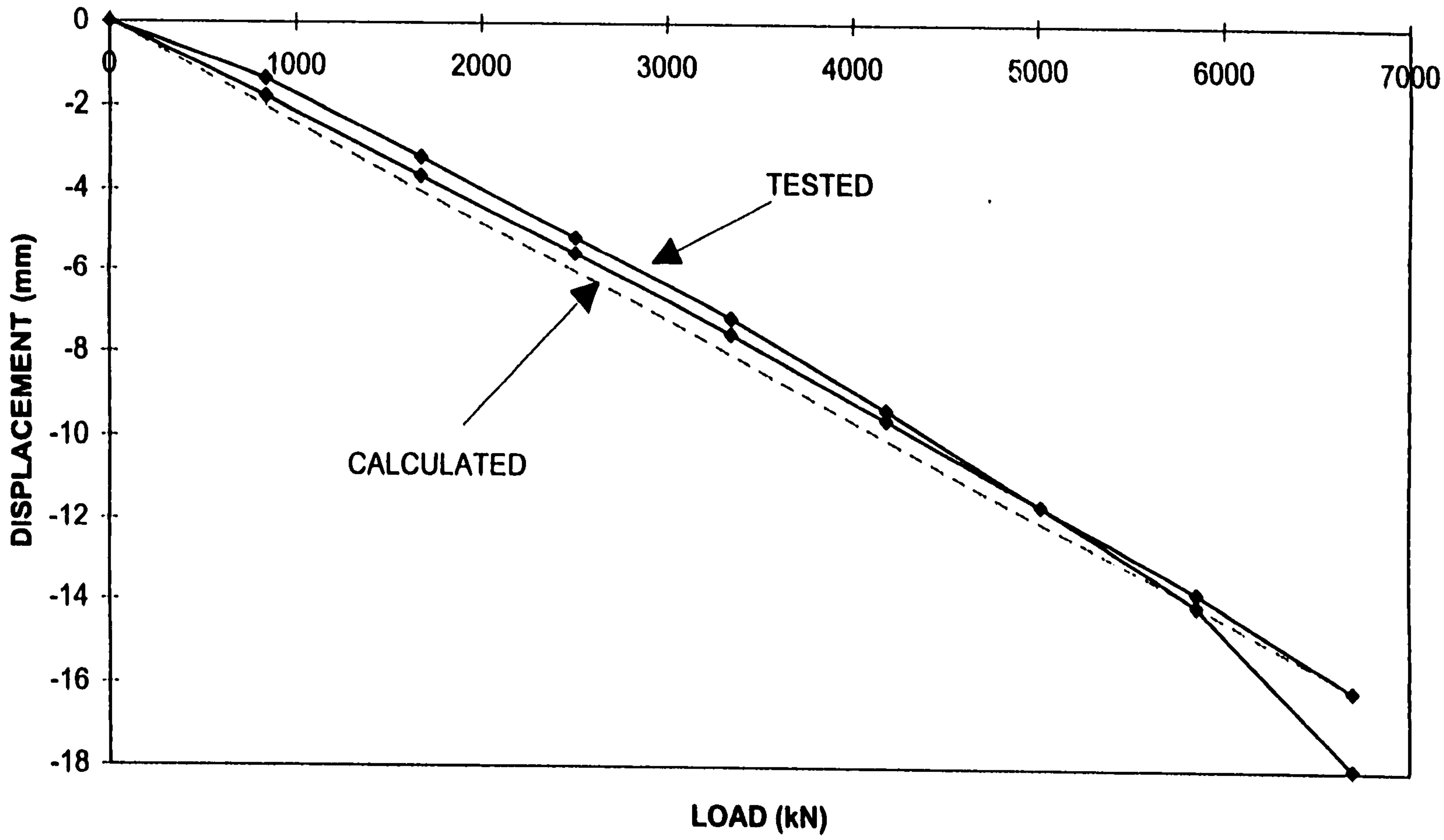

Figure 6.26 - Case 8, Comparison of Results from Finite Element Analysis and Static Load Test, A17

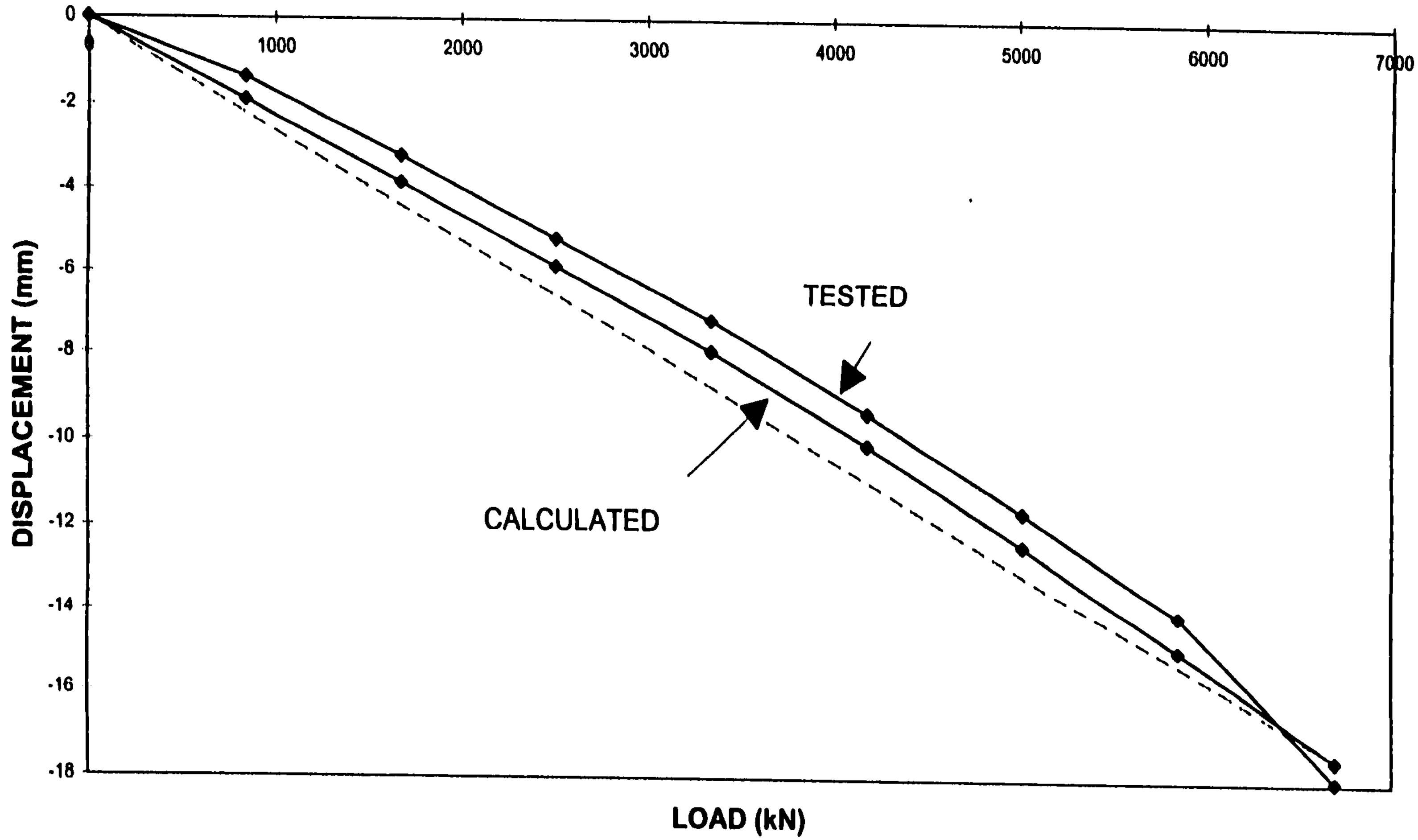

Figure 6.27 - Case 9, Comparison of Results from Finite Element Analysis and Static Load Test, A17

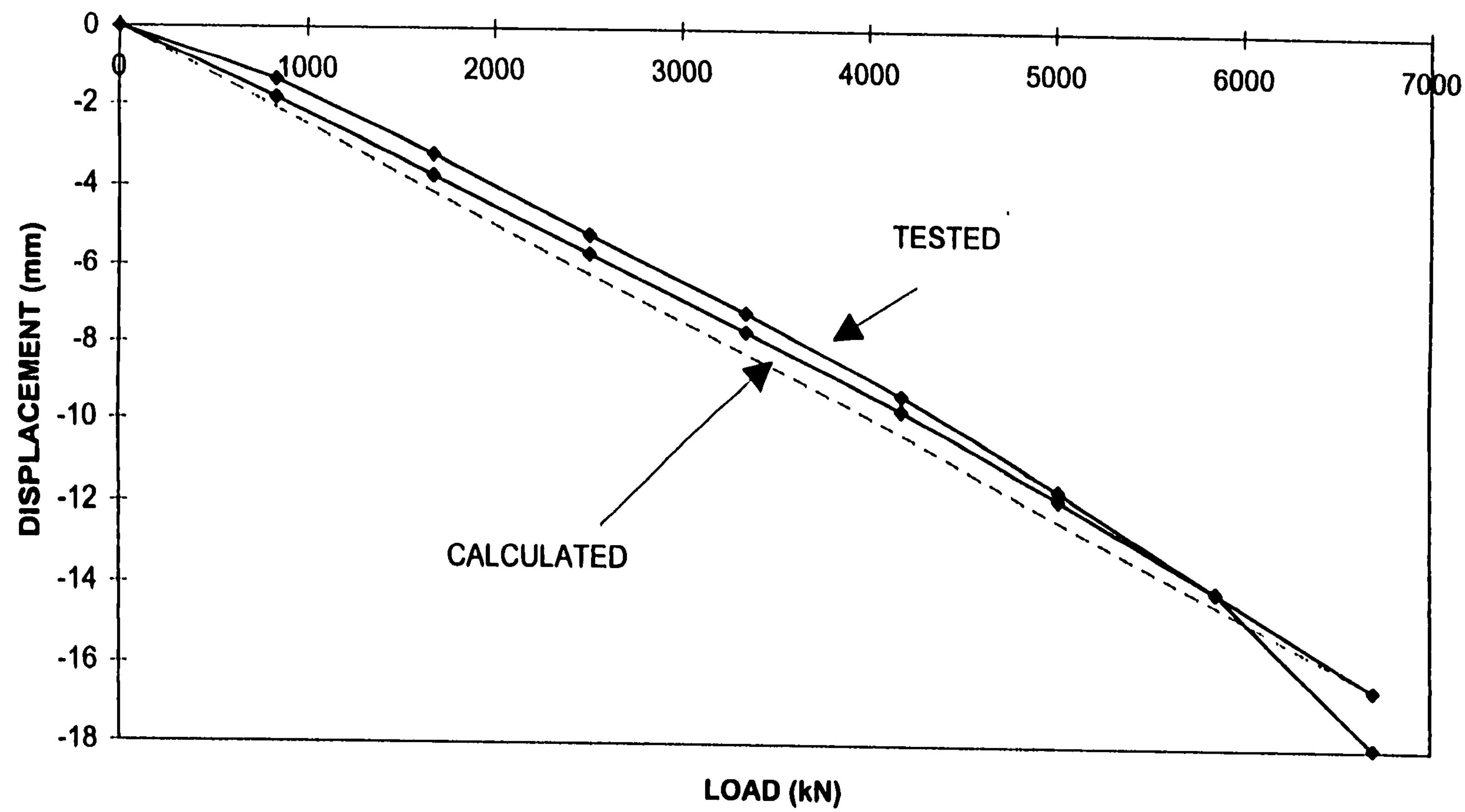

Figure 6.28 - Case 10, Comparison of Results from Finite Element Analysis and Static Load Test, A17

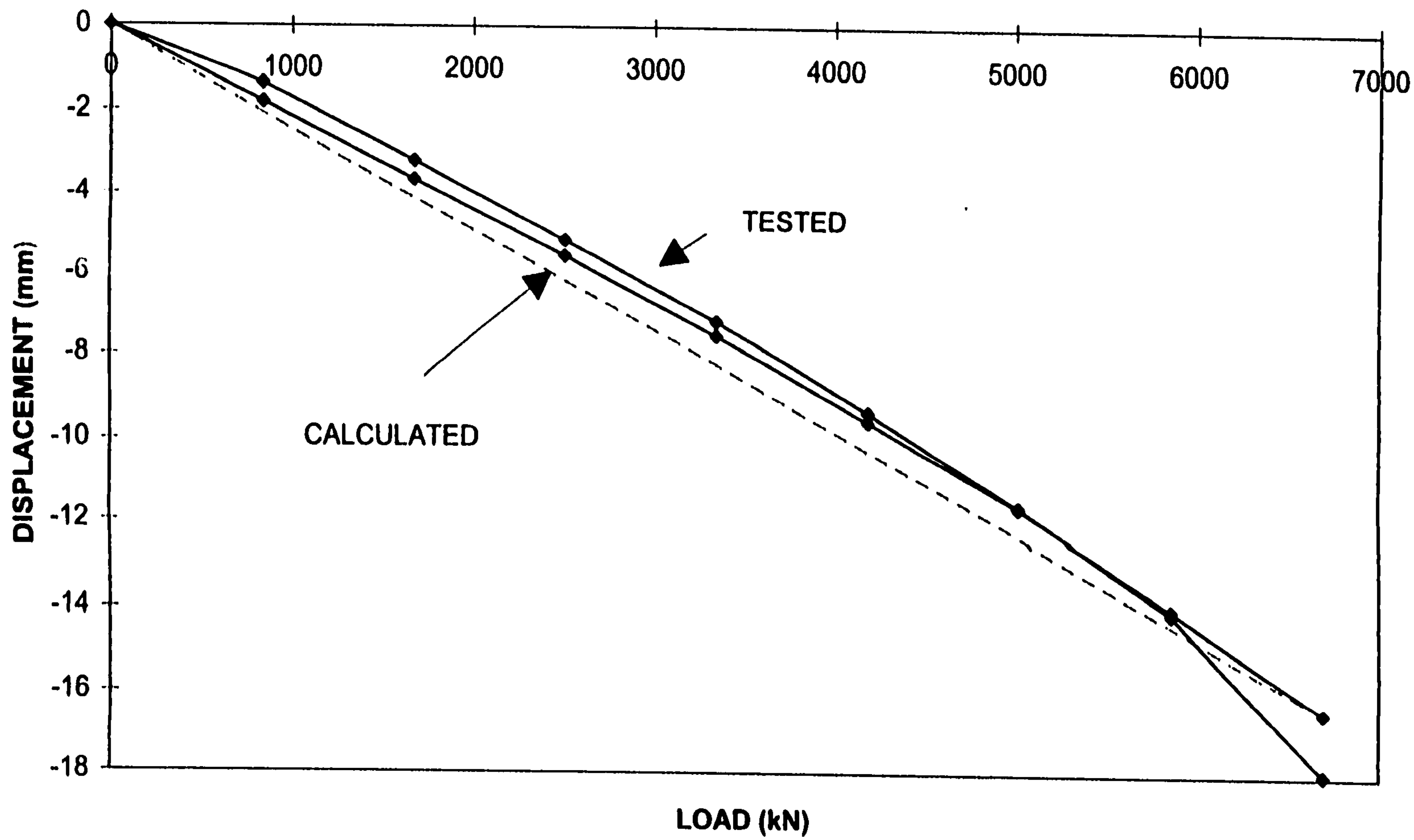

Figure 6.29 - Case 11, Comparison of Results from Finite Element Analysis and Static Load Test, A17

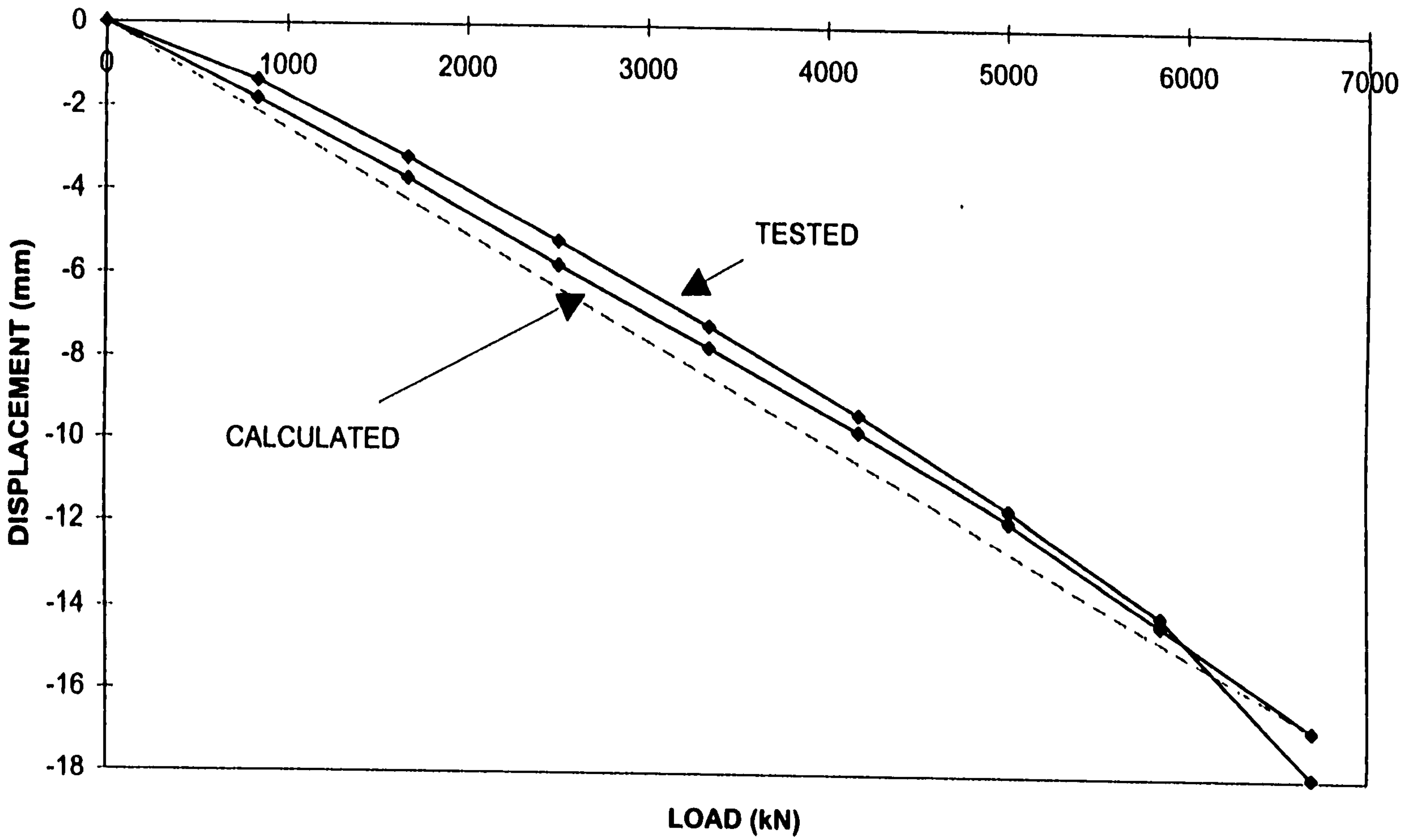

Figure 6.30 - Case 12, Comparison of Results from Finite Element Analysis and Static Load Test, A17

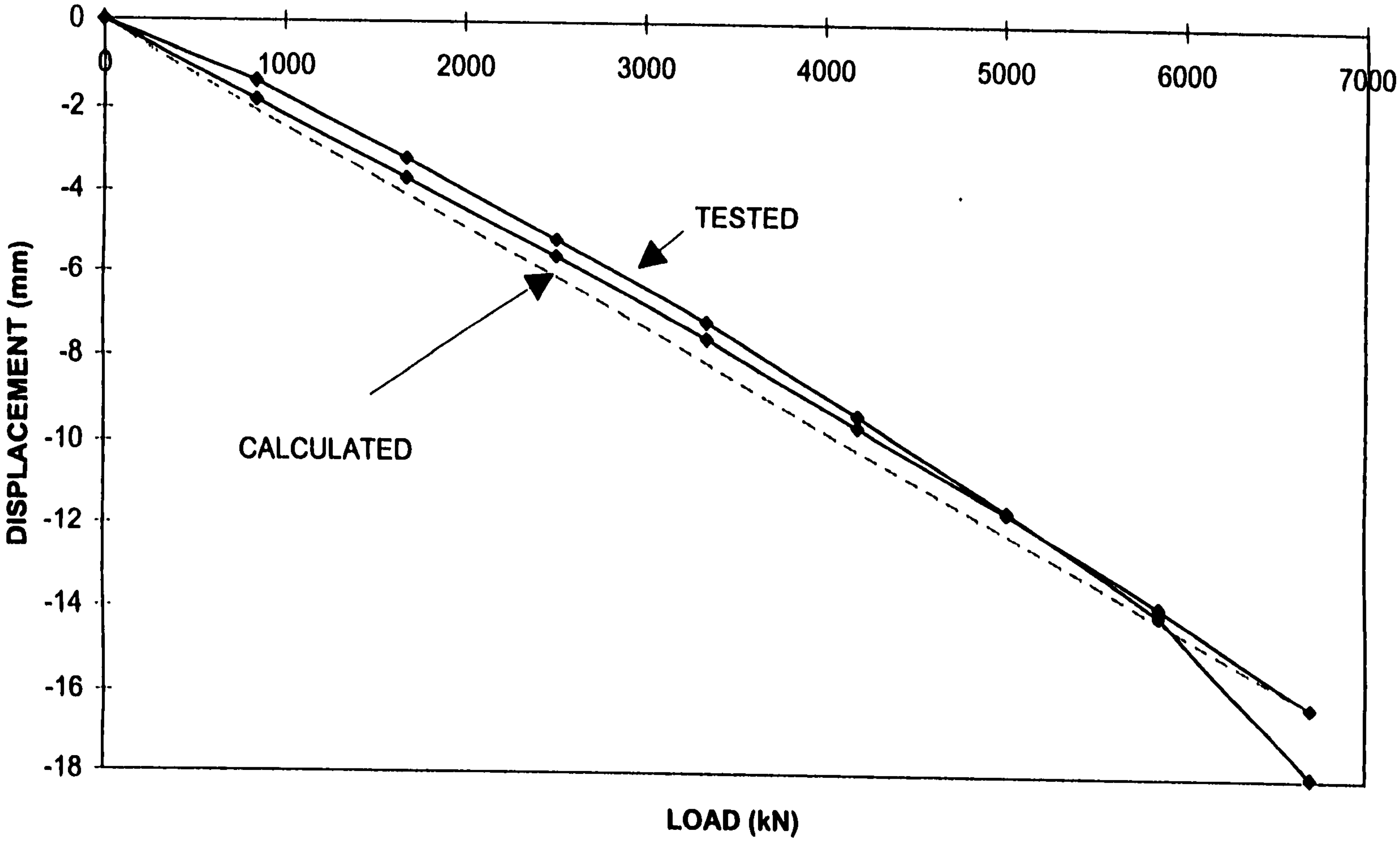

Figure 6.31 - Case 13, Comparison of Results from Finite Element Analysis and Static Load Test, A17

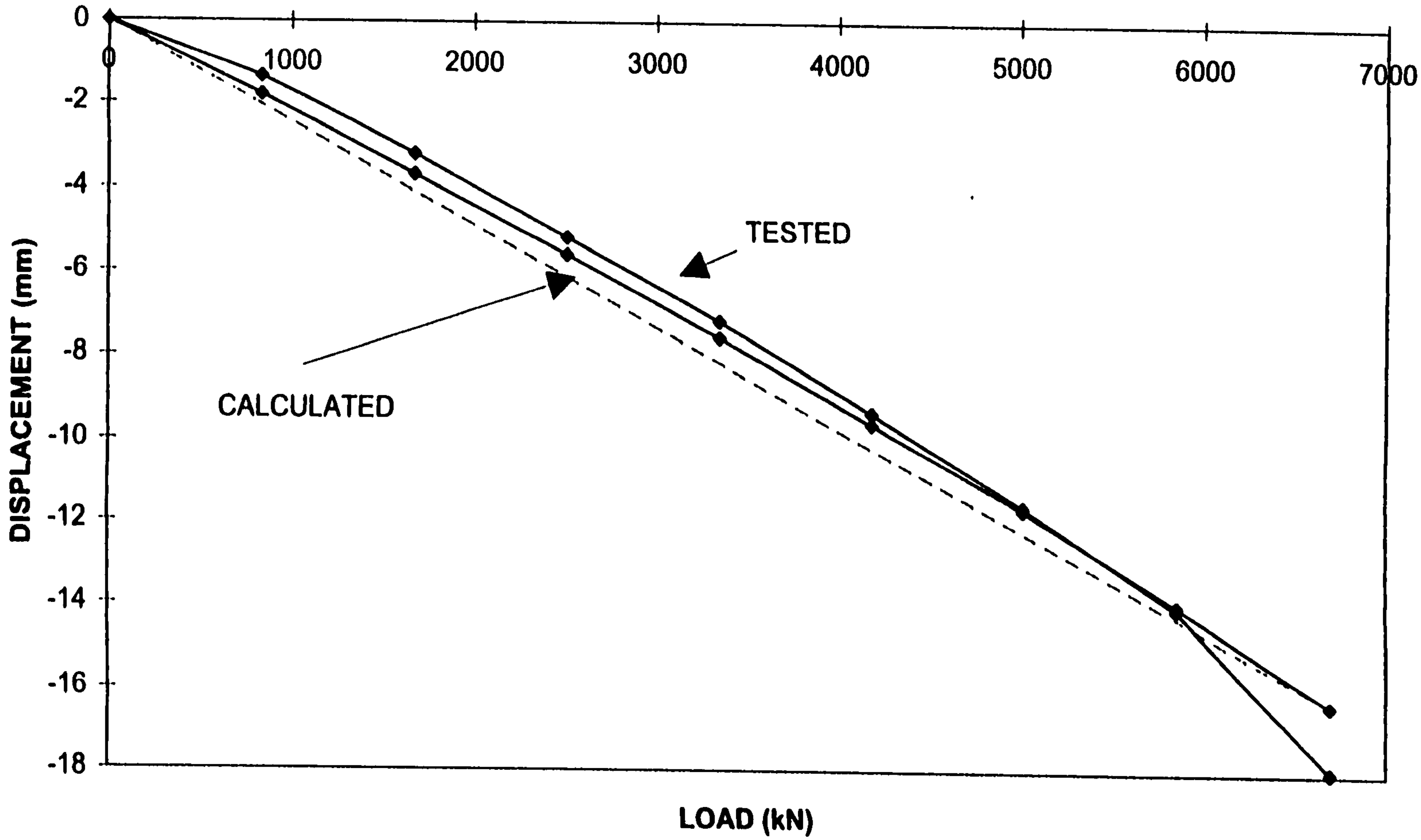

Figure 6.32 - Case 14, Comparison of Results from Finite Element Analysis and Static Load Test, A17

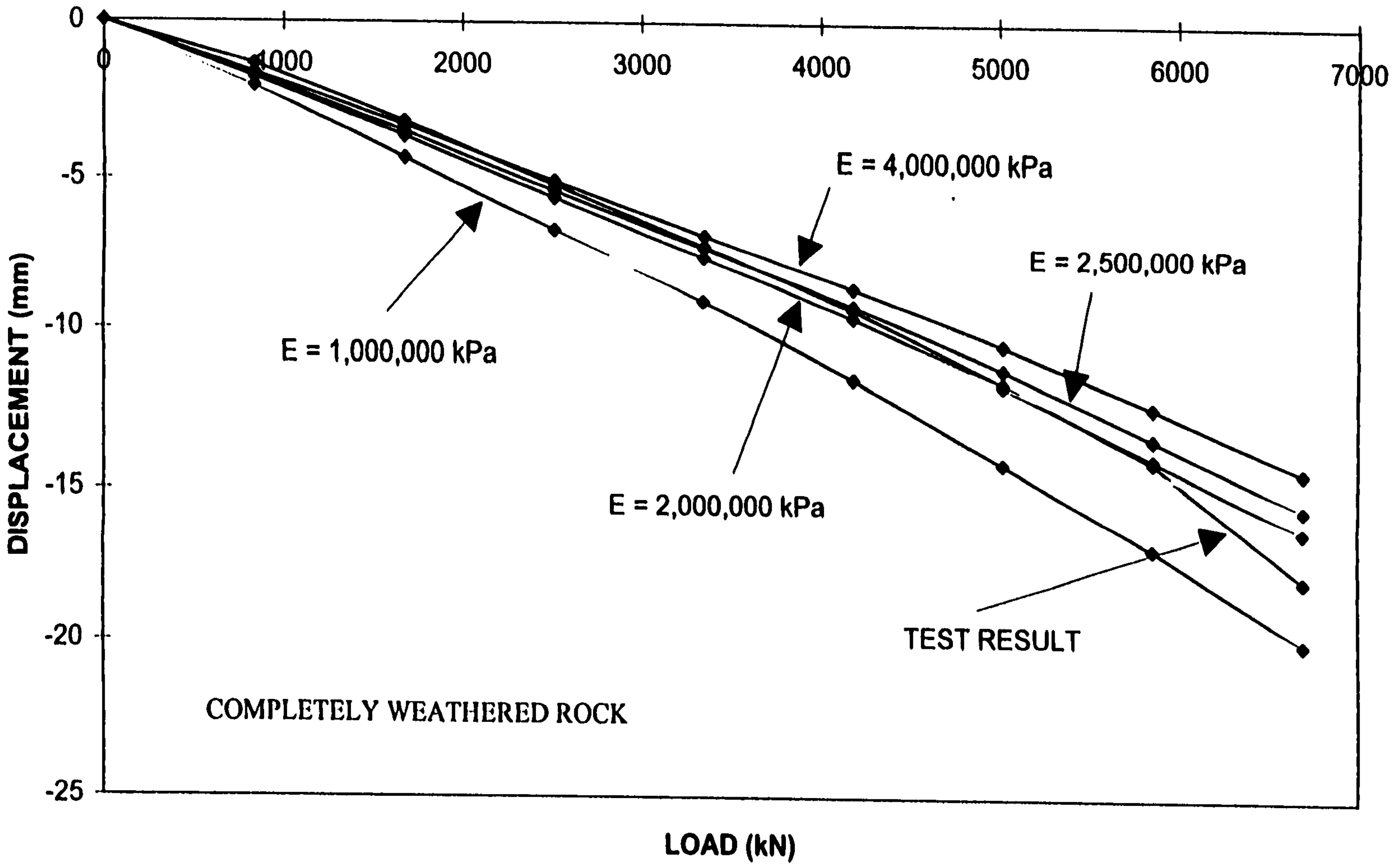

Figure 6.33 - Comparison of Results from Test and Calculation, A17

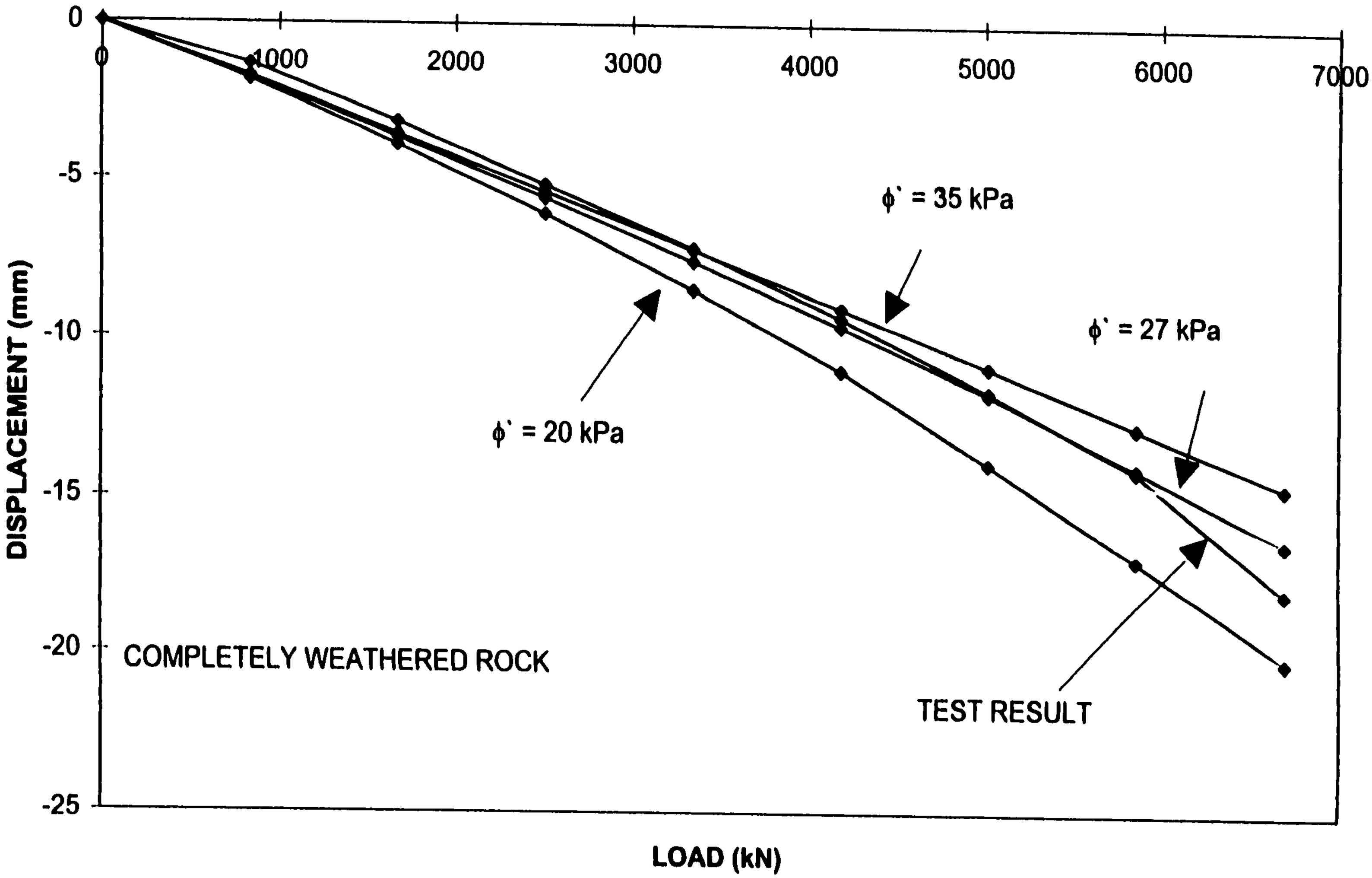

Figure 6.34 - Comparison of Results from Test and Calculation, A17

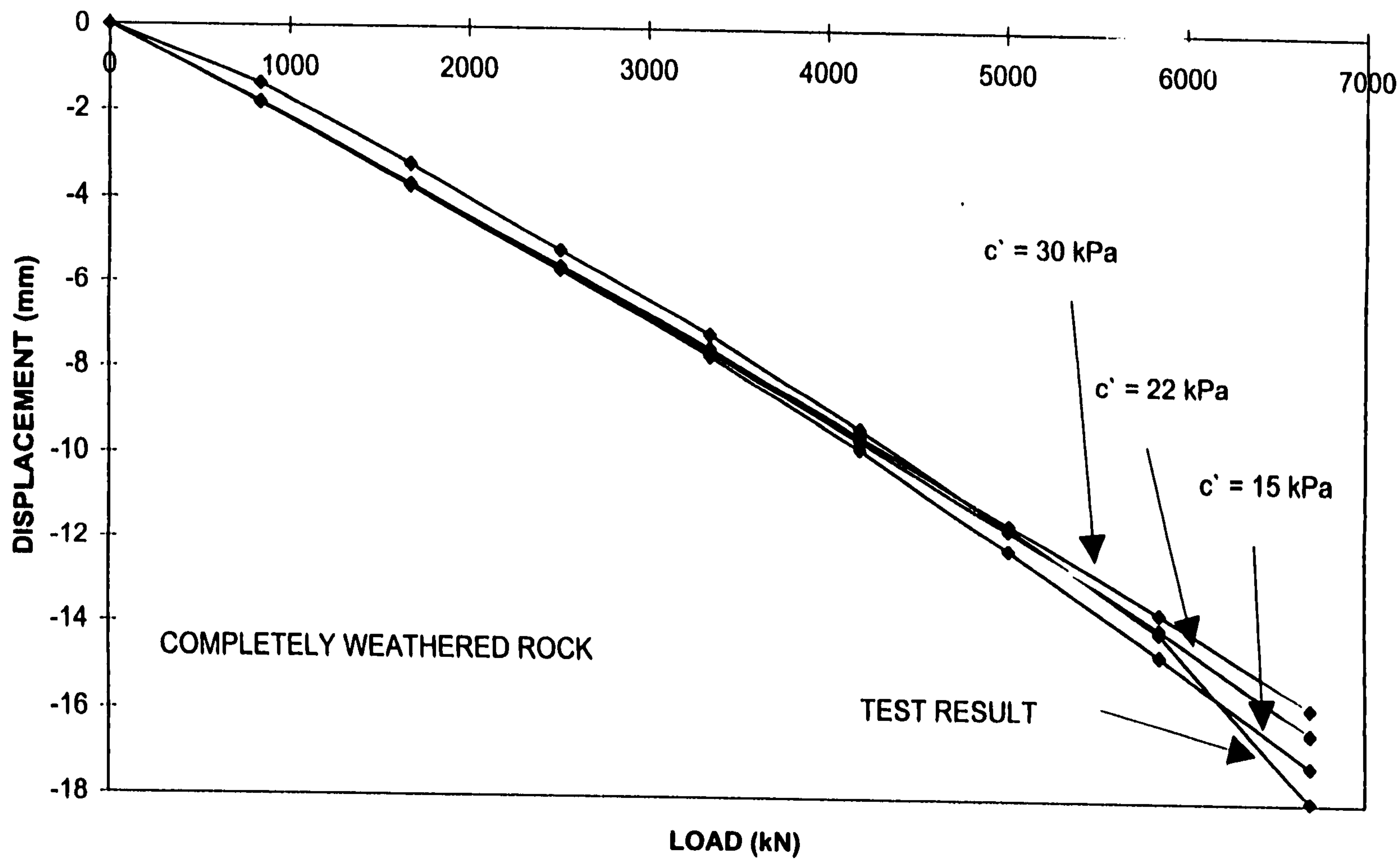

Figure 6.35 - Comparison of Results from Test and Calculation, A17

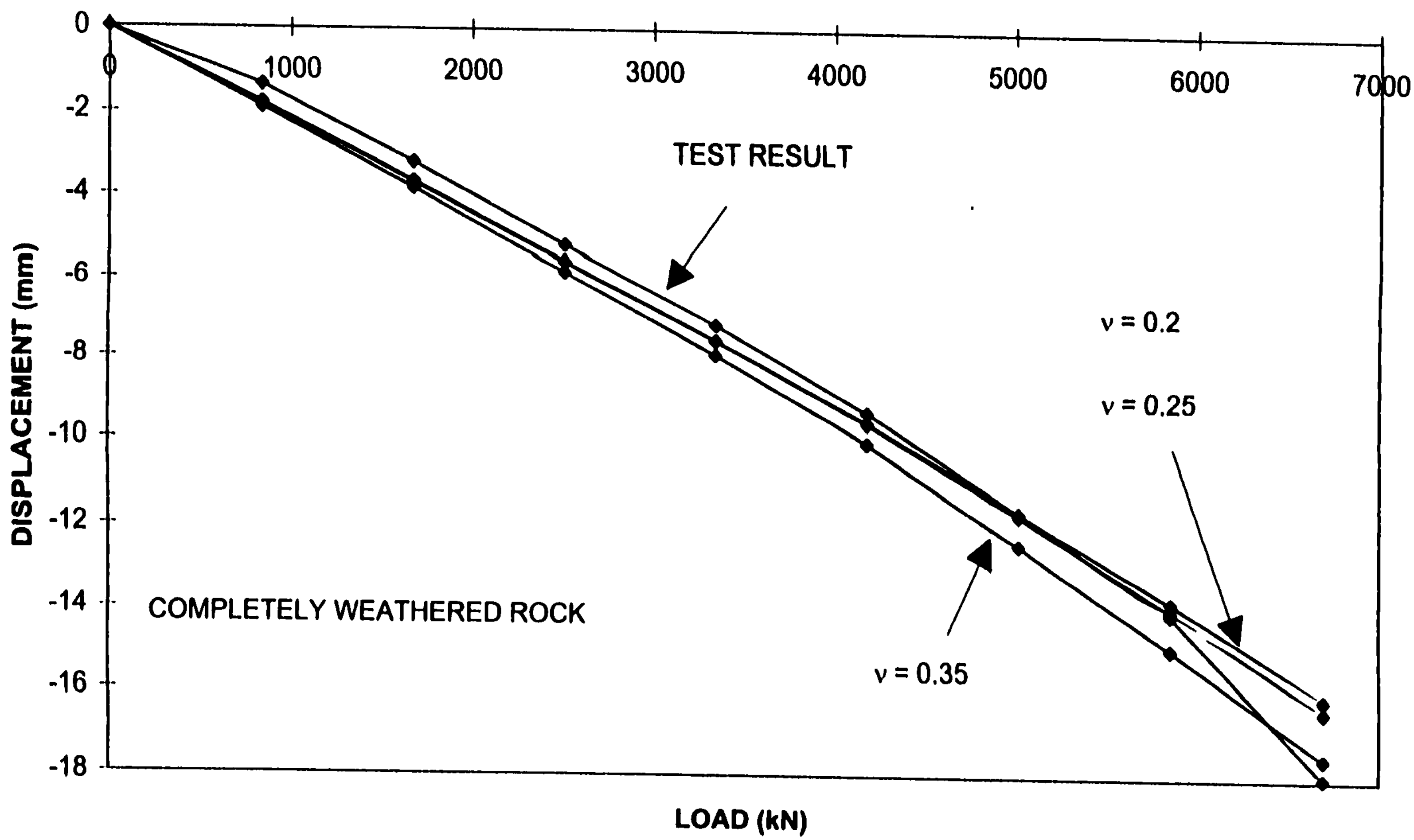

Figure 6.36 - Comparison of Results from Test and Calculation, A17

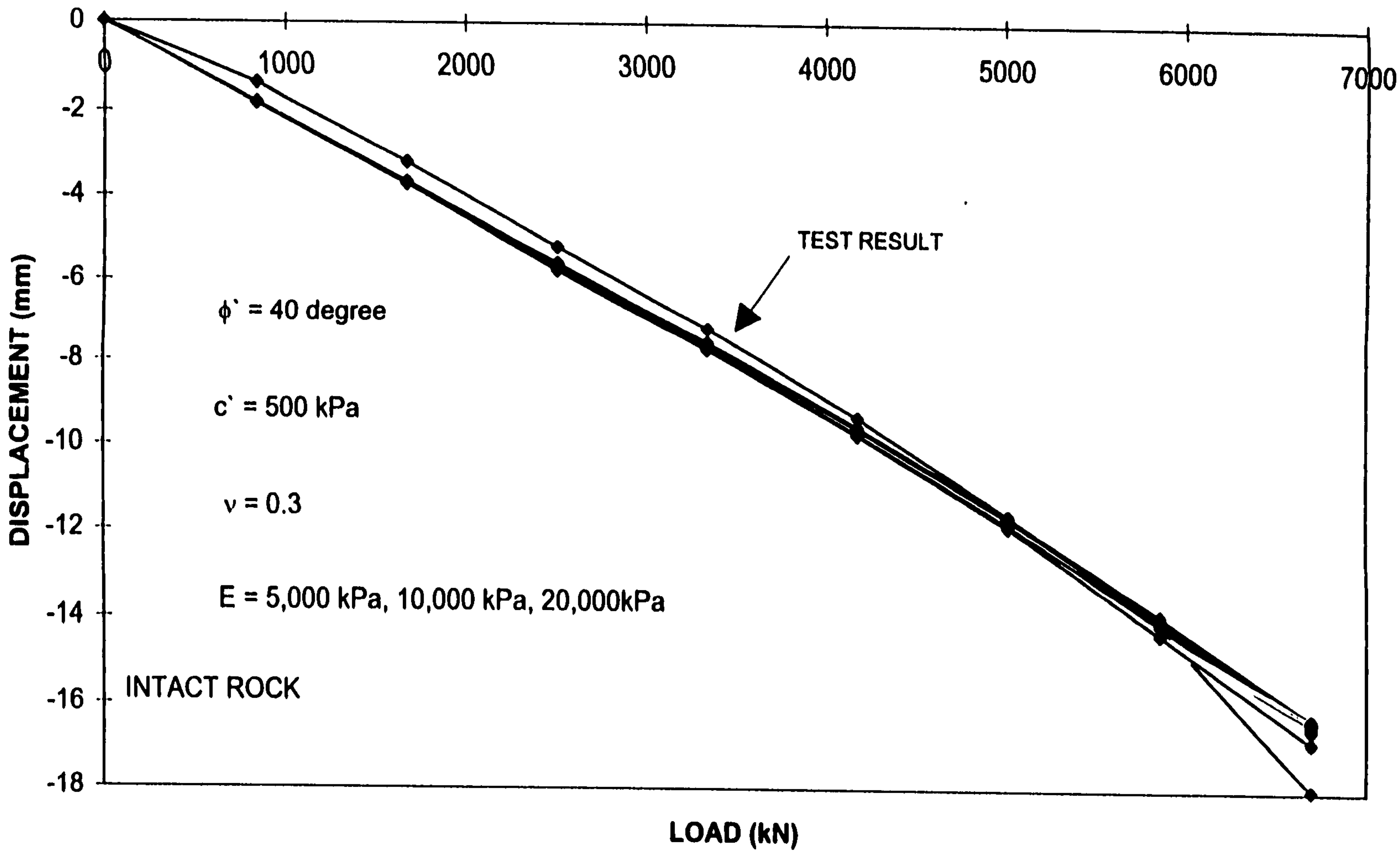

Figure 6.37 - Comparison of Results from Test and Calculation, A17

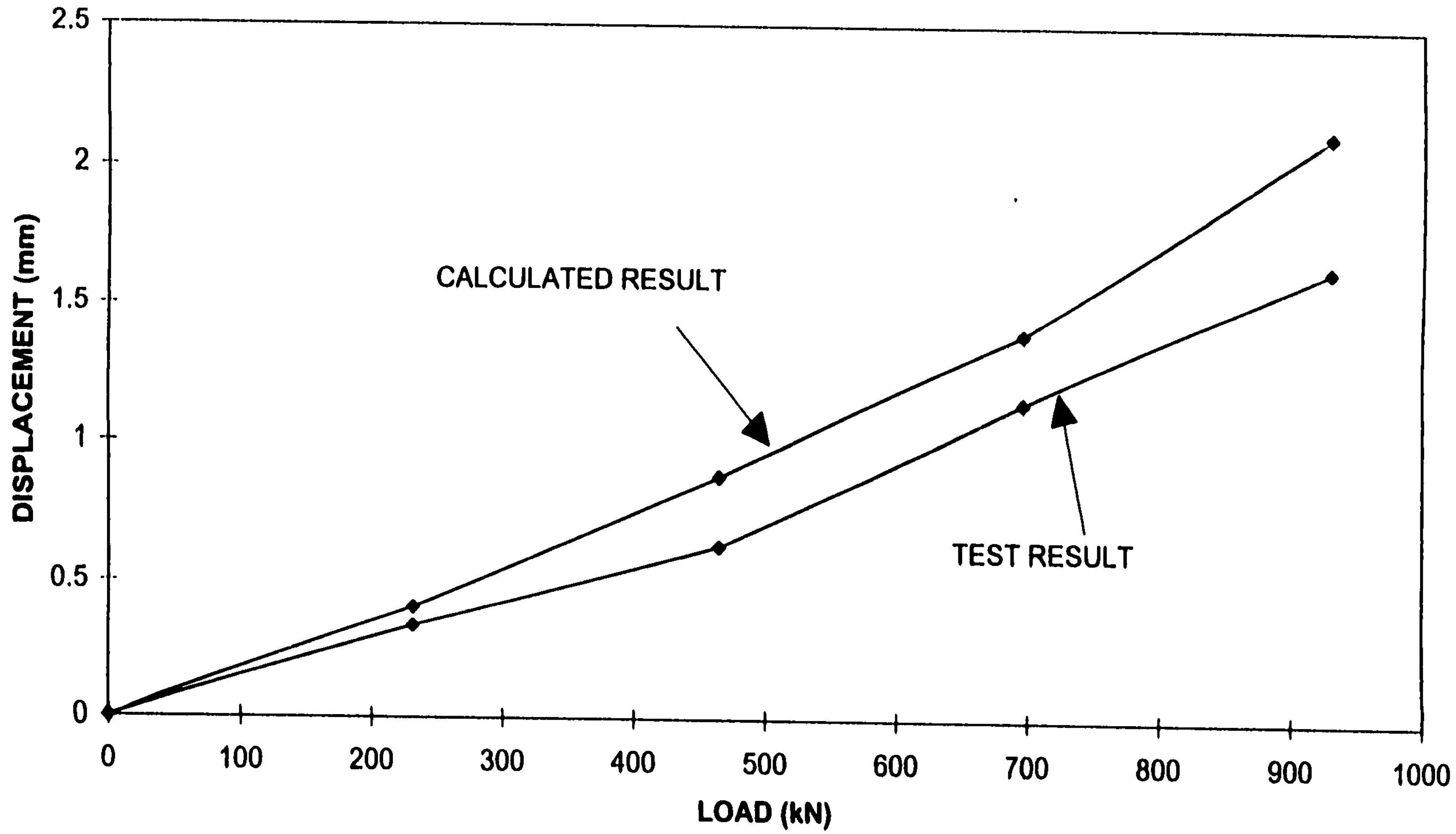

Figure 6.38 - Comparison of Results, Tension, First Loading Cycle, Pile A17

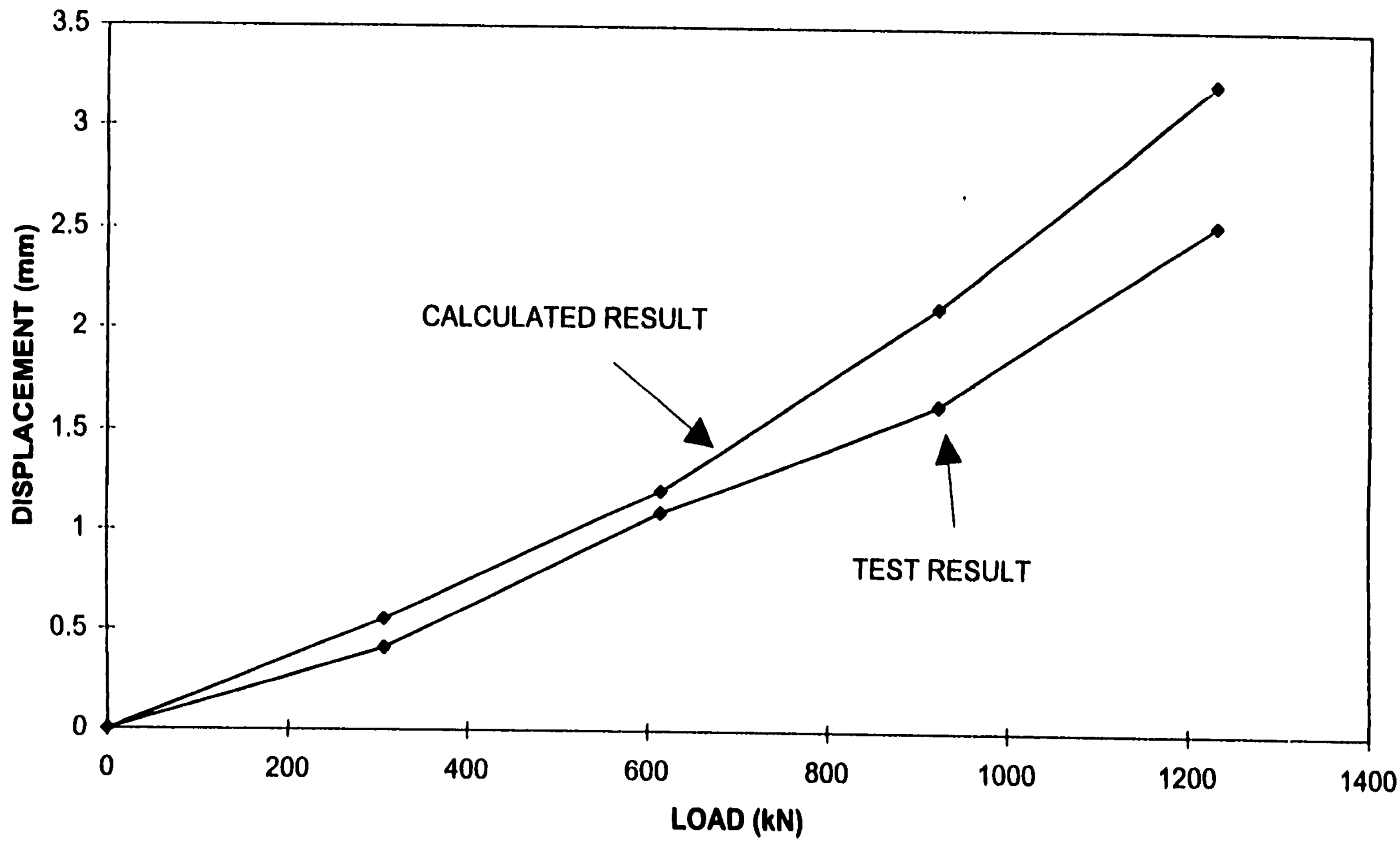

Figure 6.39 - Comparison of Results, Tension, Second Loading Cycle, Pile A17

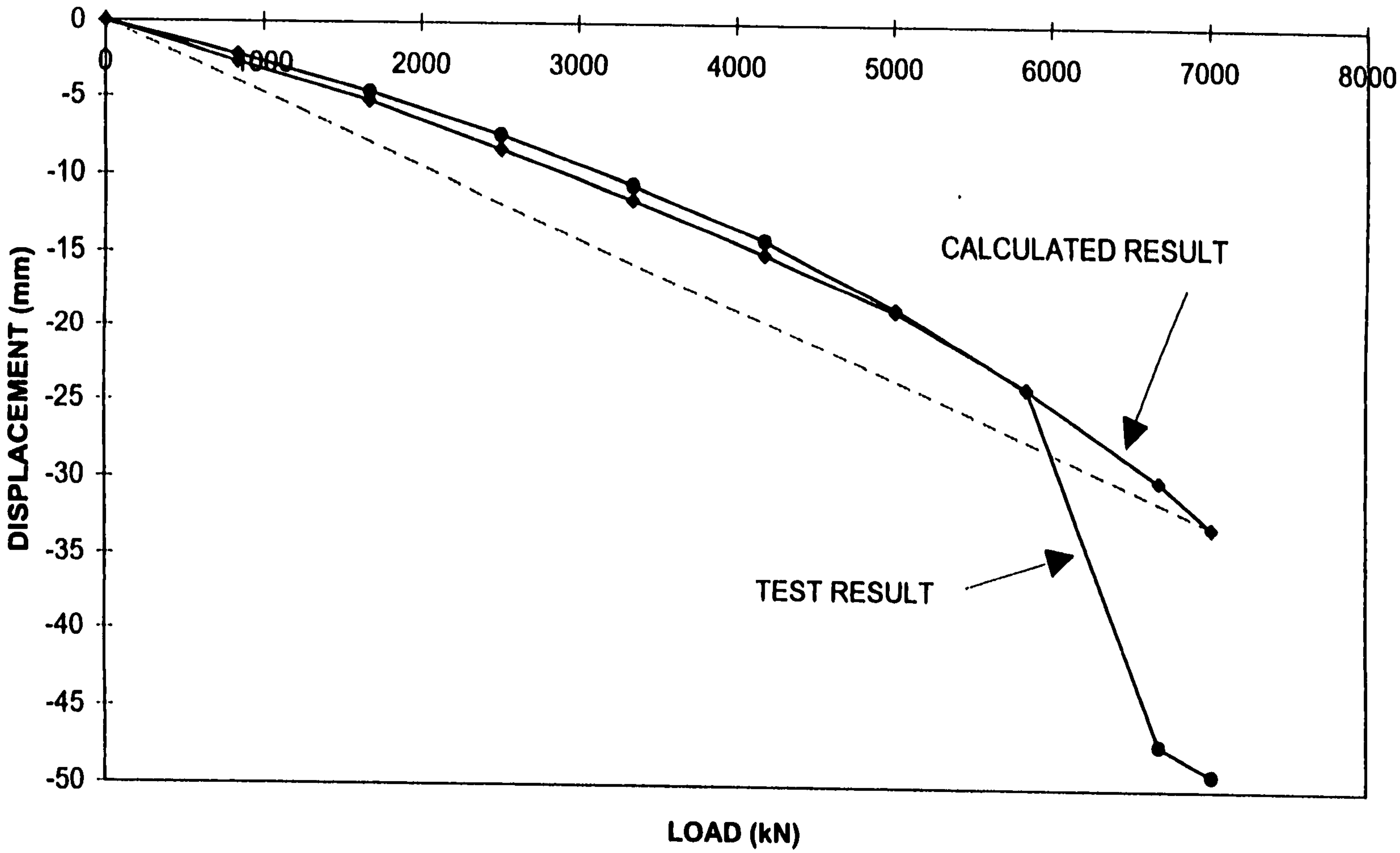

Figure 6.40 - Comparison of Results from Finite Element Analysis and Static Load Test, Pile F54

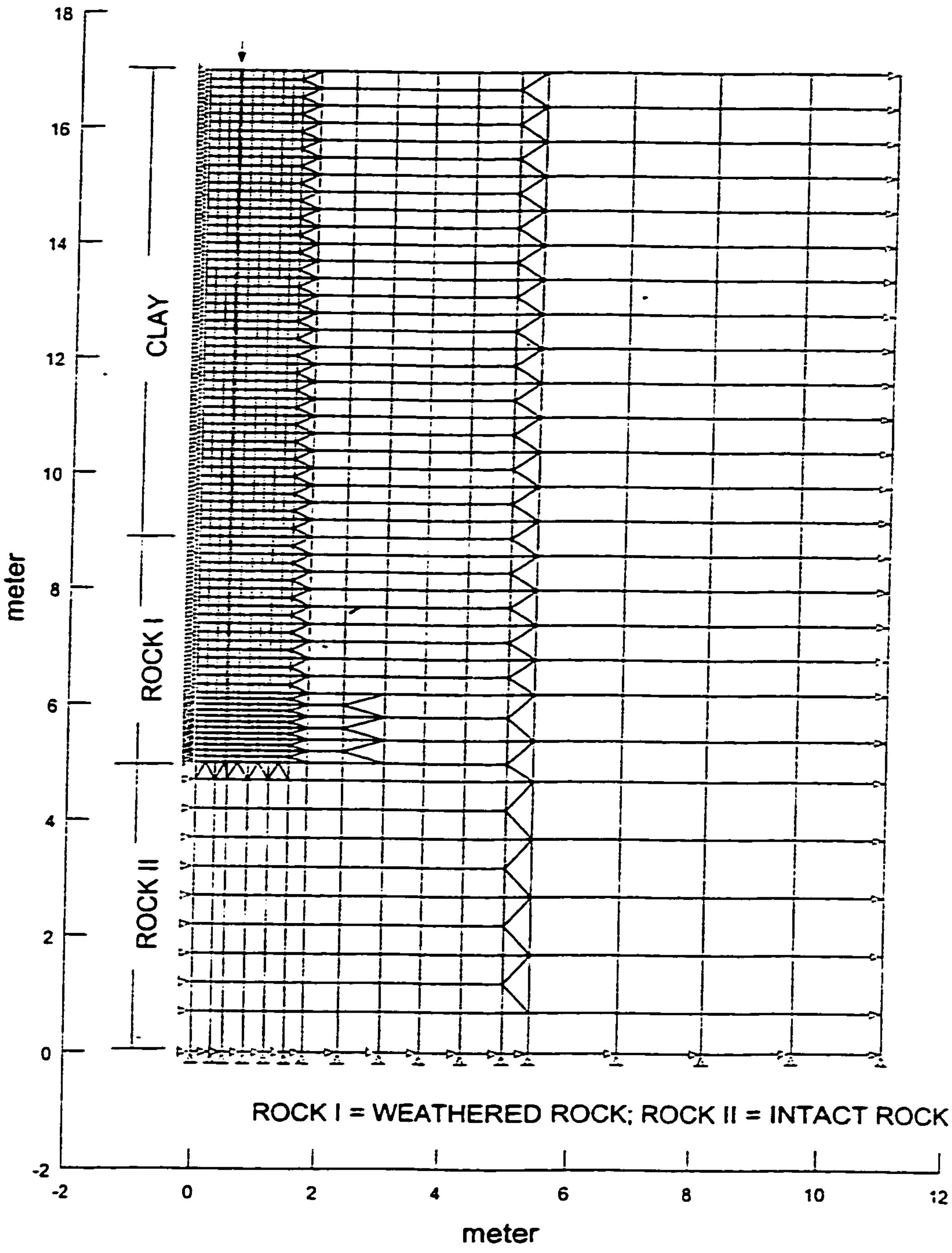

Figure 6.41a - Axisymmetric Finite Element Discretization of Pile-Soil System, A17

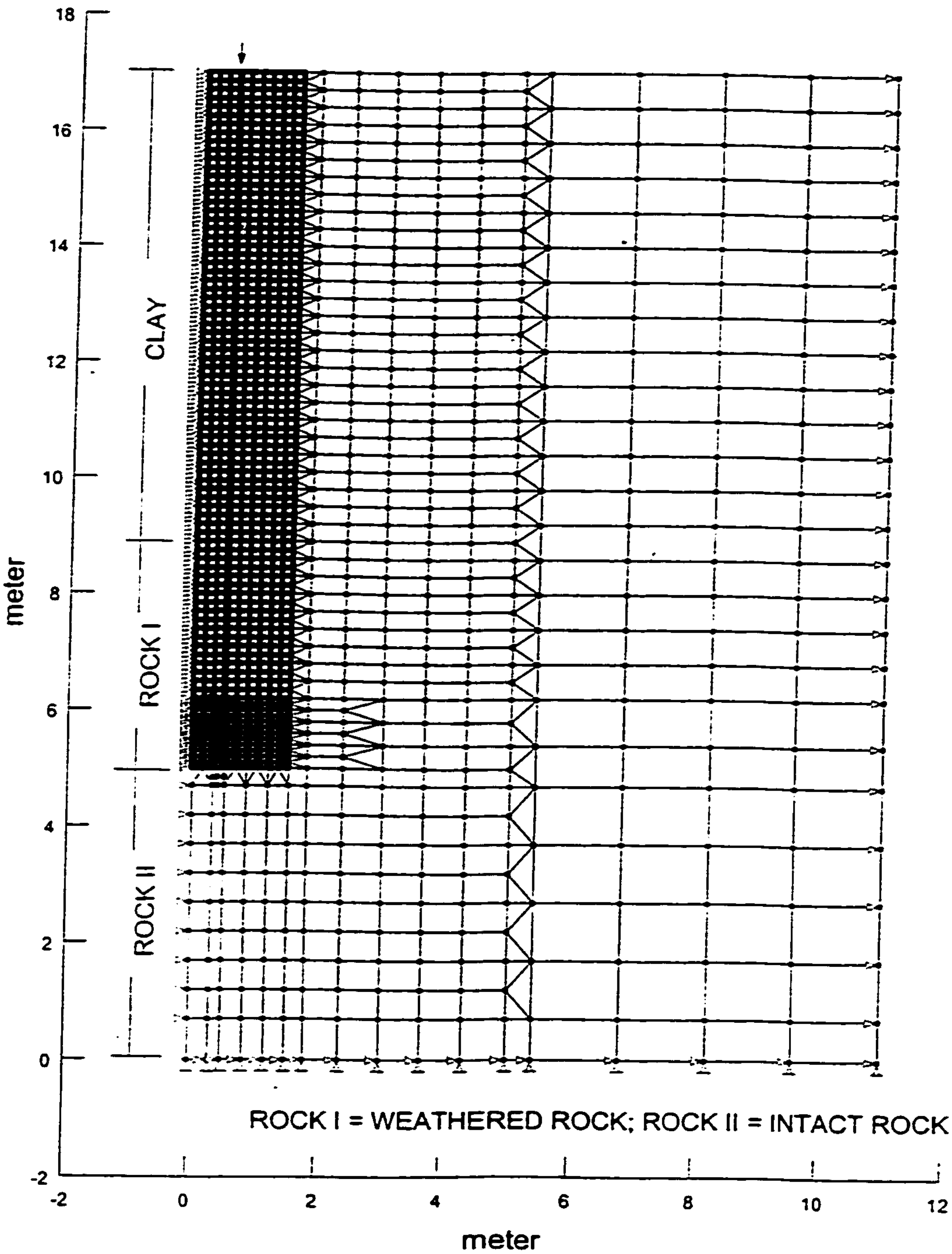

Figure 6.41b - Axisymmetric Finite Element Discretization of Pile-Soil System, A17

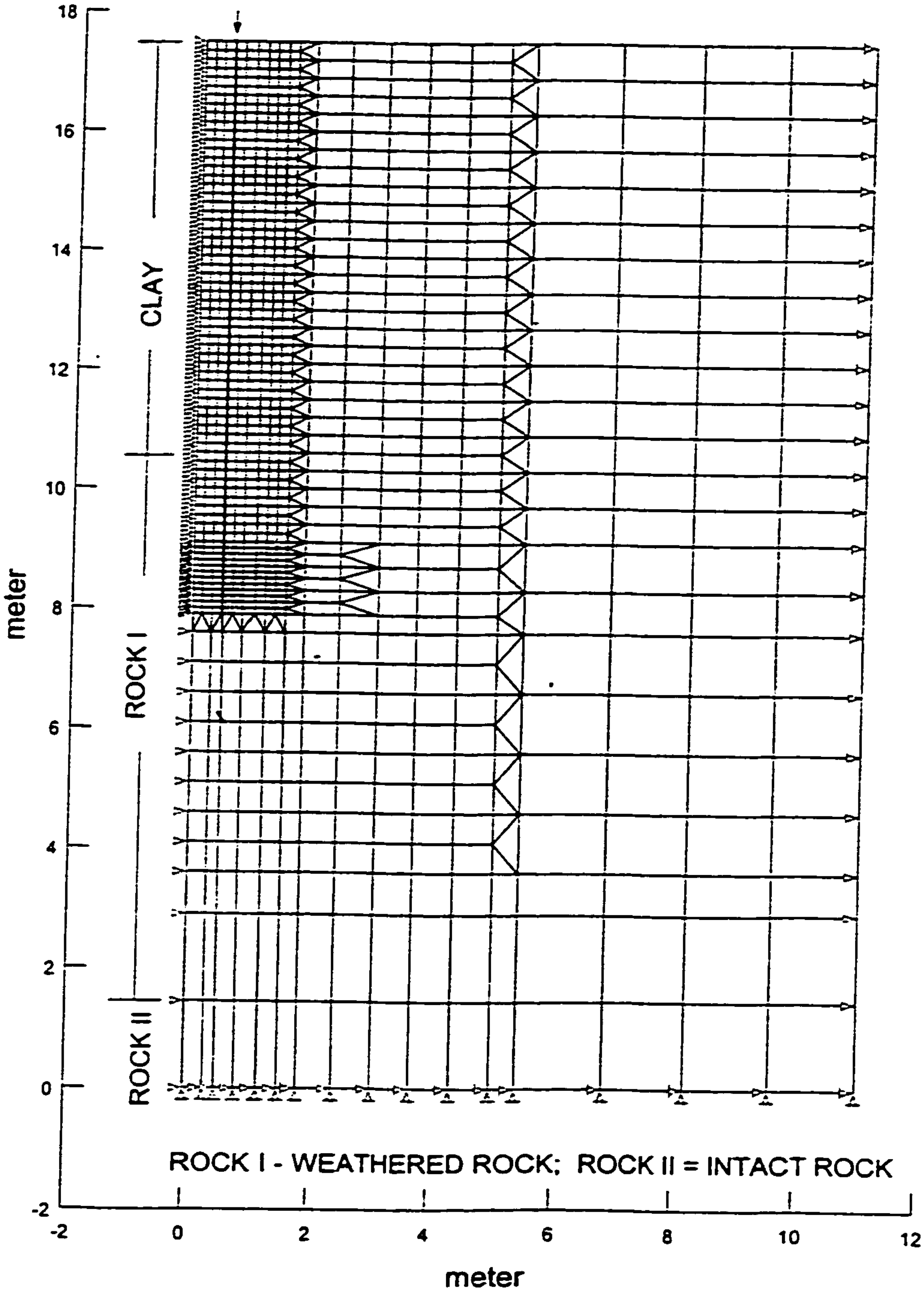

Figure 6.42a - Axisymmetric Finite Element Discretization of Pile-Soil System, F54

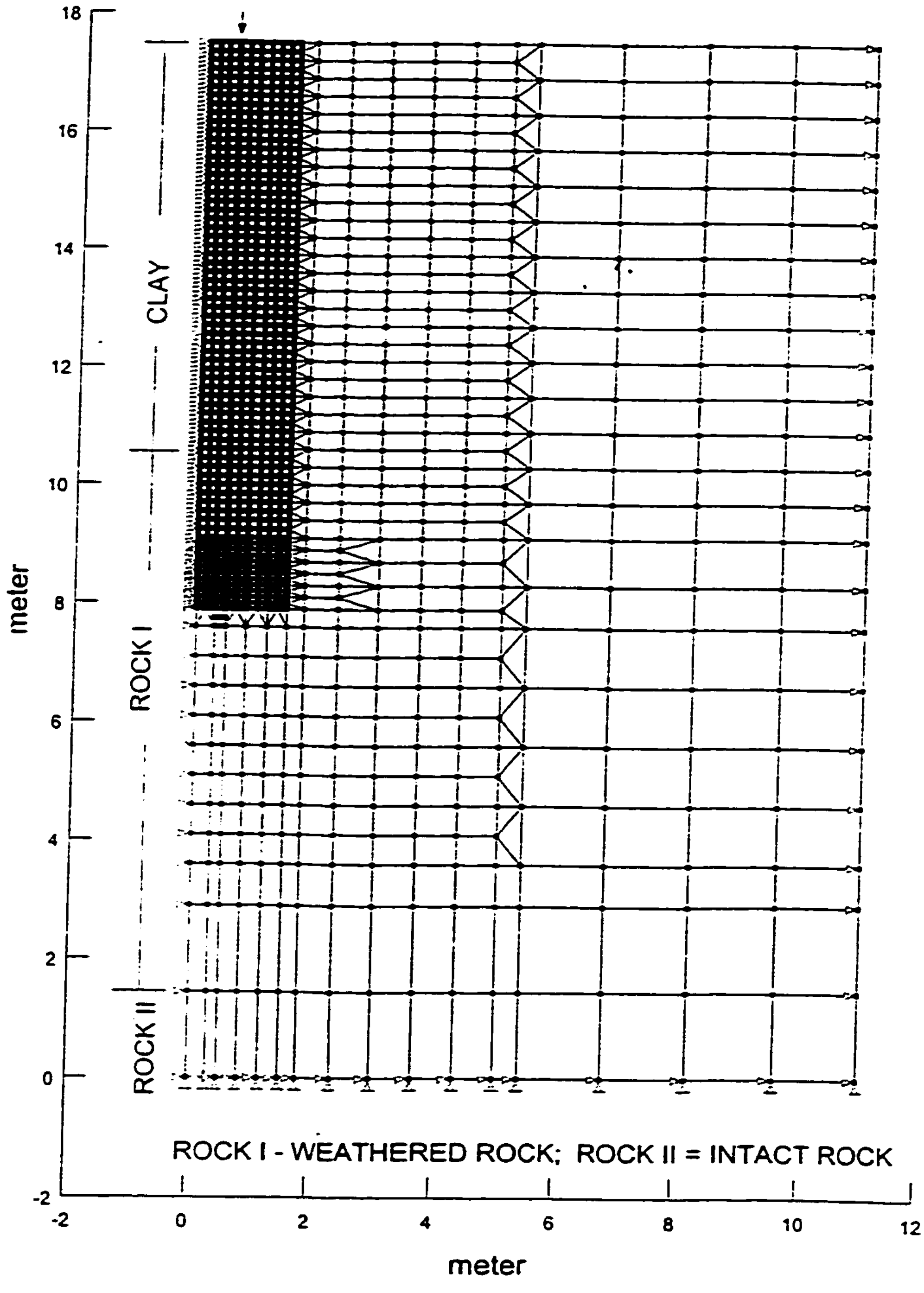

Figure 6.42b - Axisymmetric Finite Element Discretization of Pile-Soil System, F54

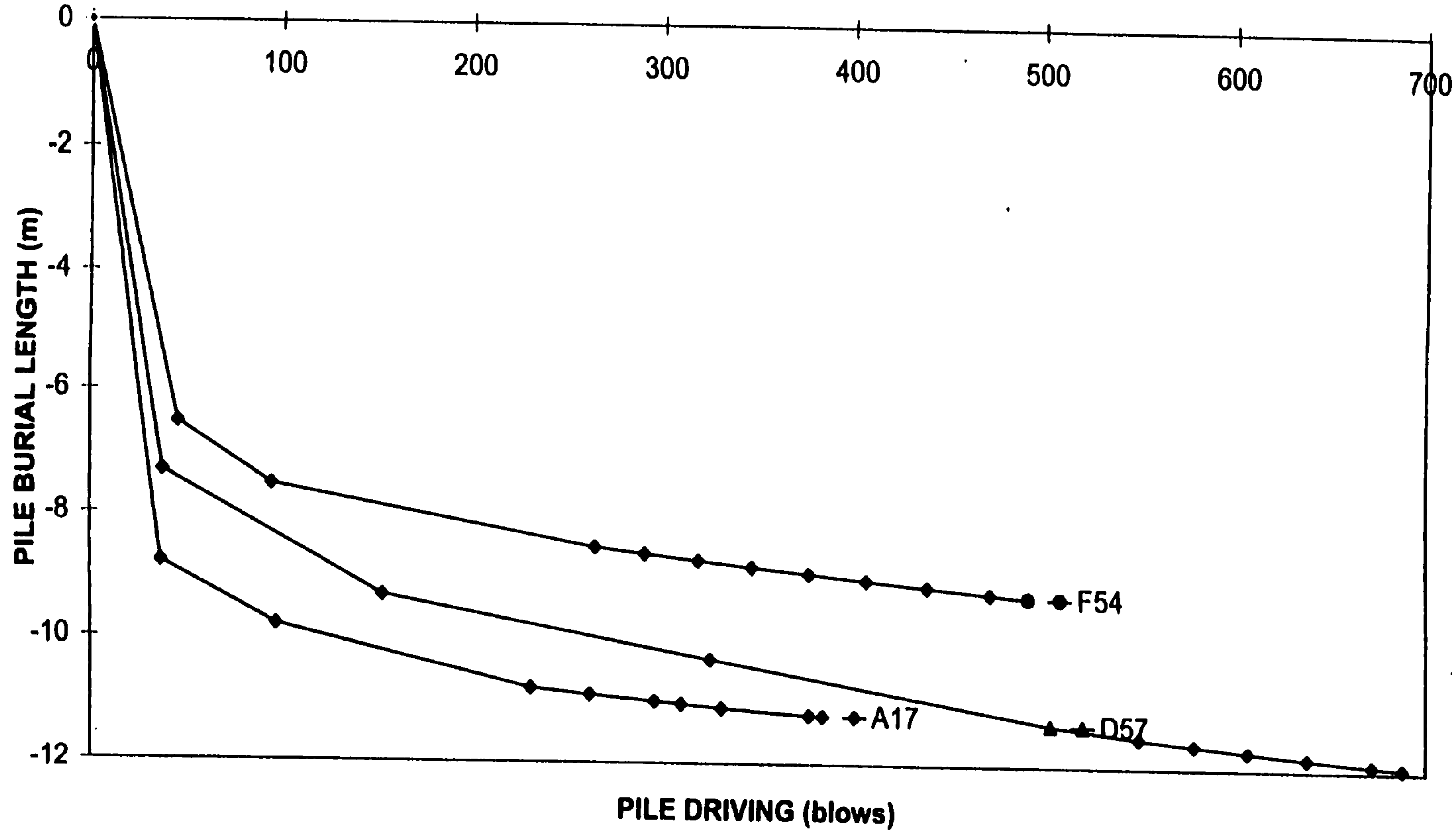

Figure 7.1 - Pile Driving Advance Curve, for three Tested Piles

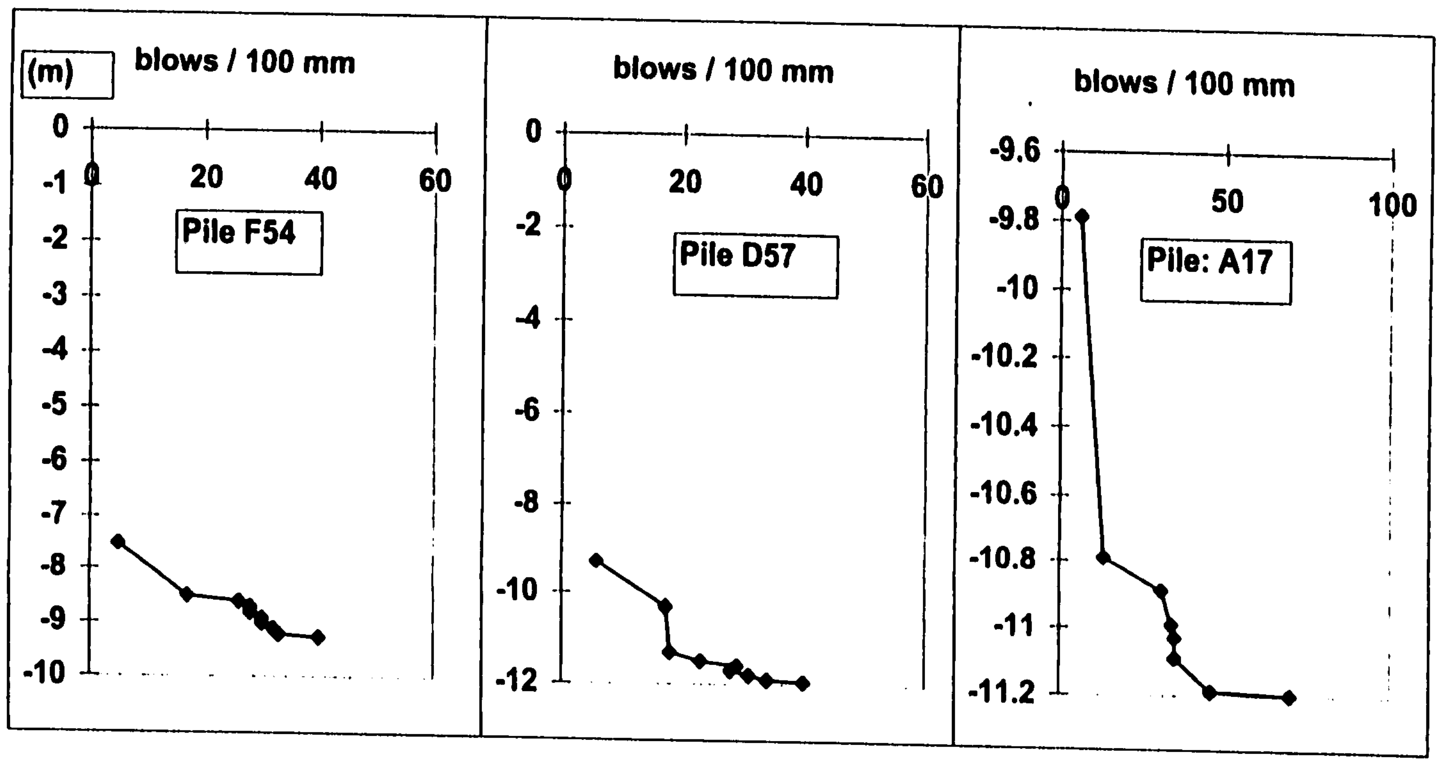

Figure 7.2 - Pile Driving Advance Curve

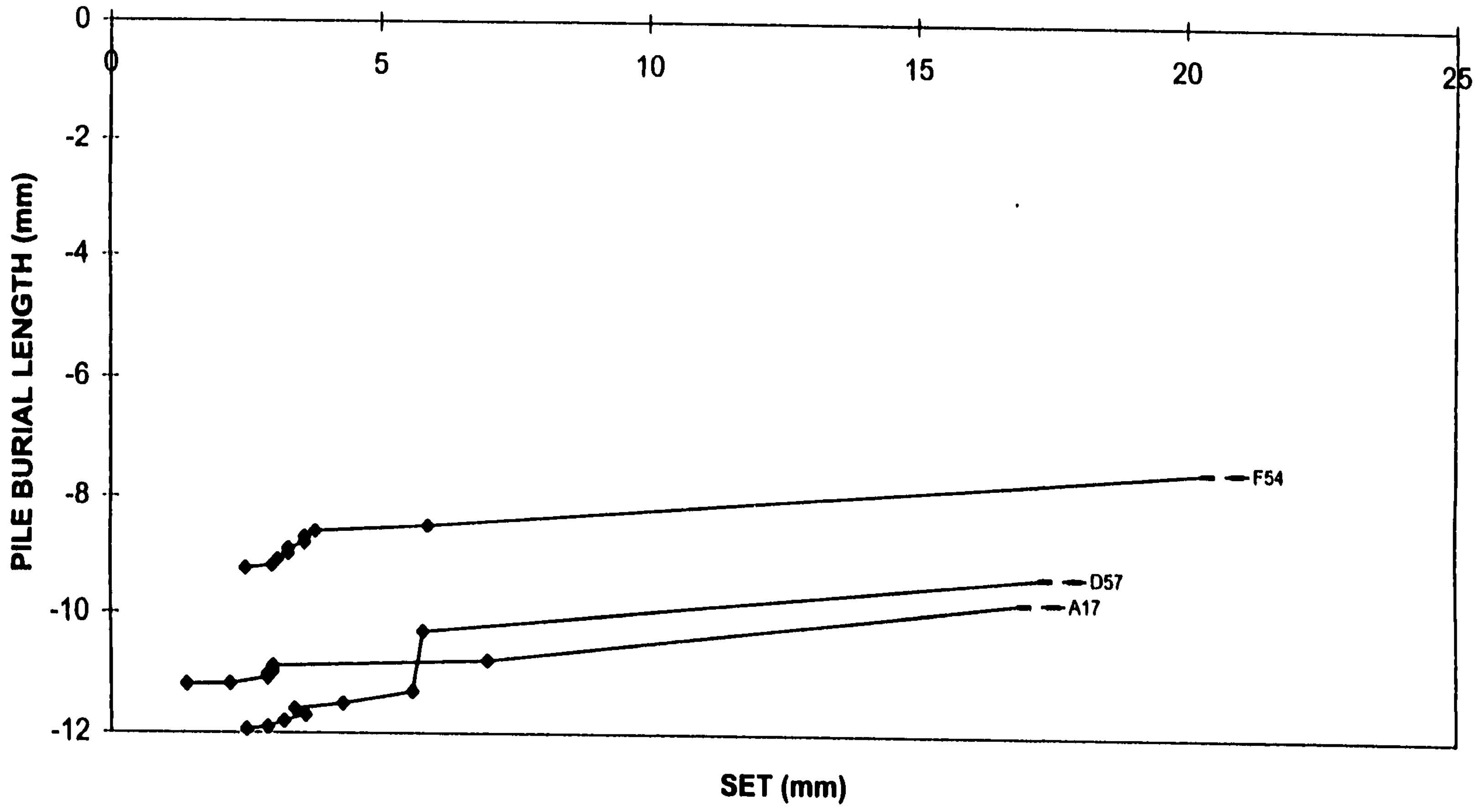

Figure 7.3 - Pile Enbeded Length-Set (Average) Curve, Pile A17, F54 and D57

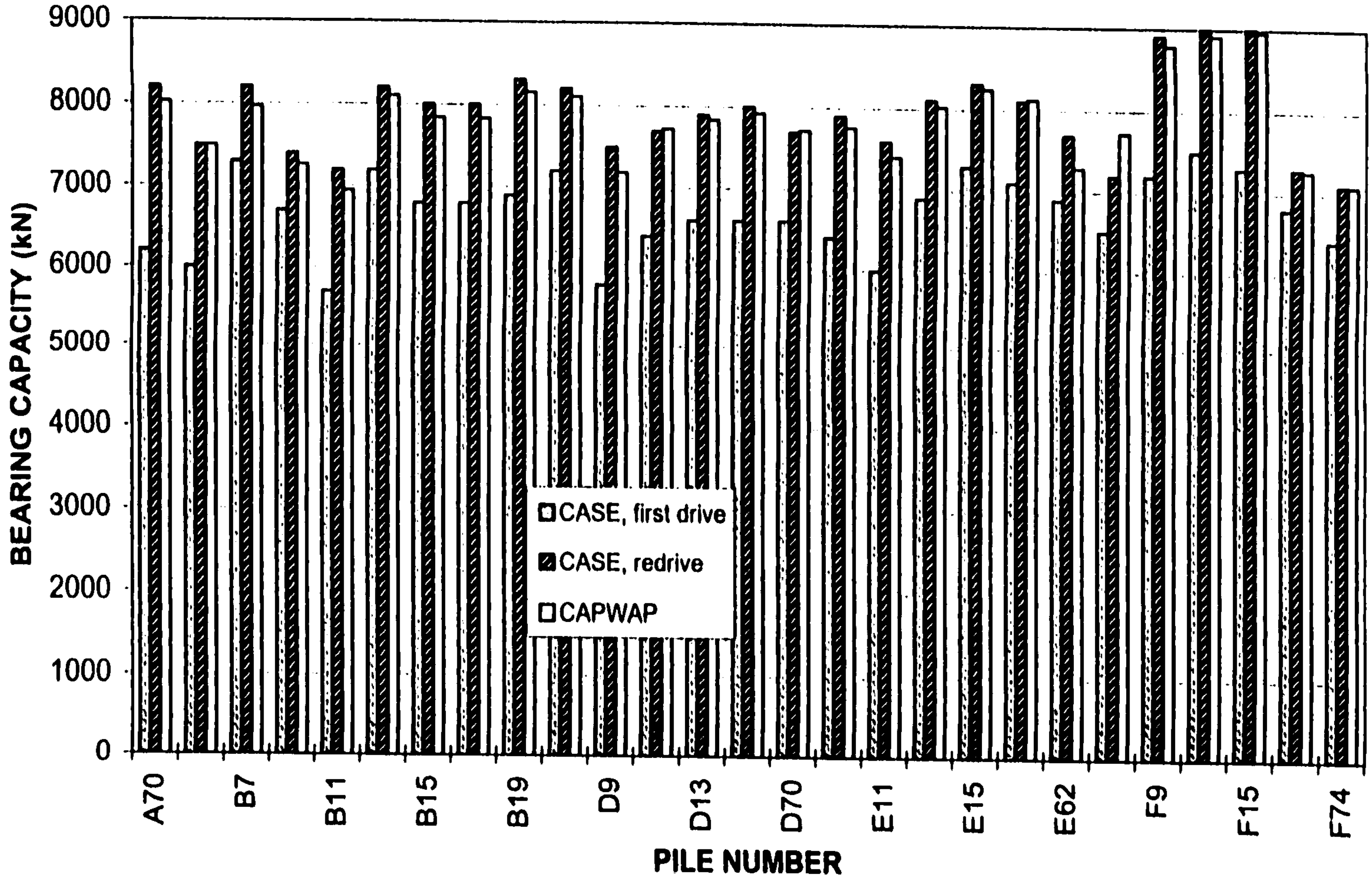

Figure 7.4 - Bearing Capacity by CASE & CAPWAP Methods, 1.0 m Piles

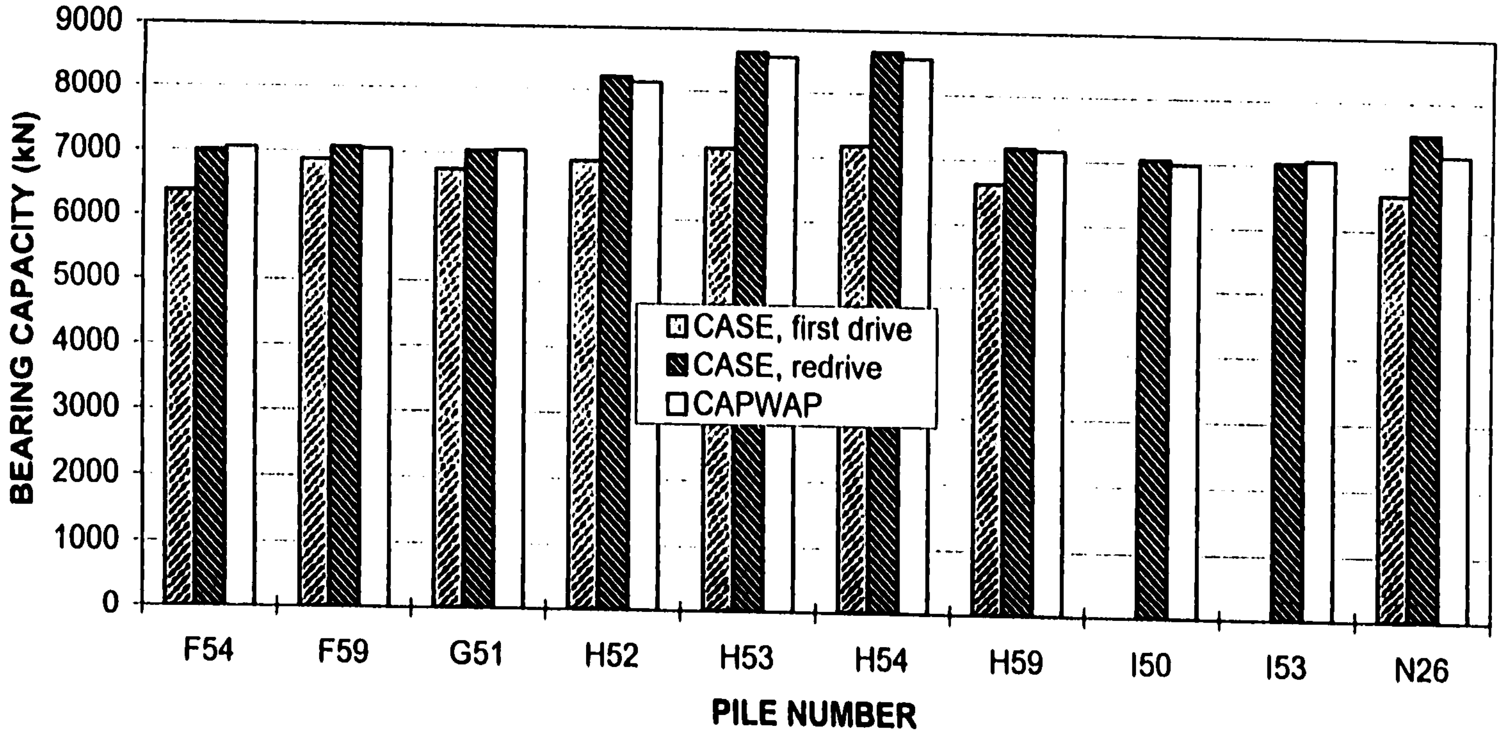

Figure 7.5 - Comparison of Bearing Capacity by CASE and CAPWAP Methods, 0.813 m Piles

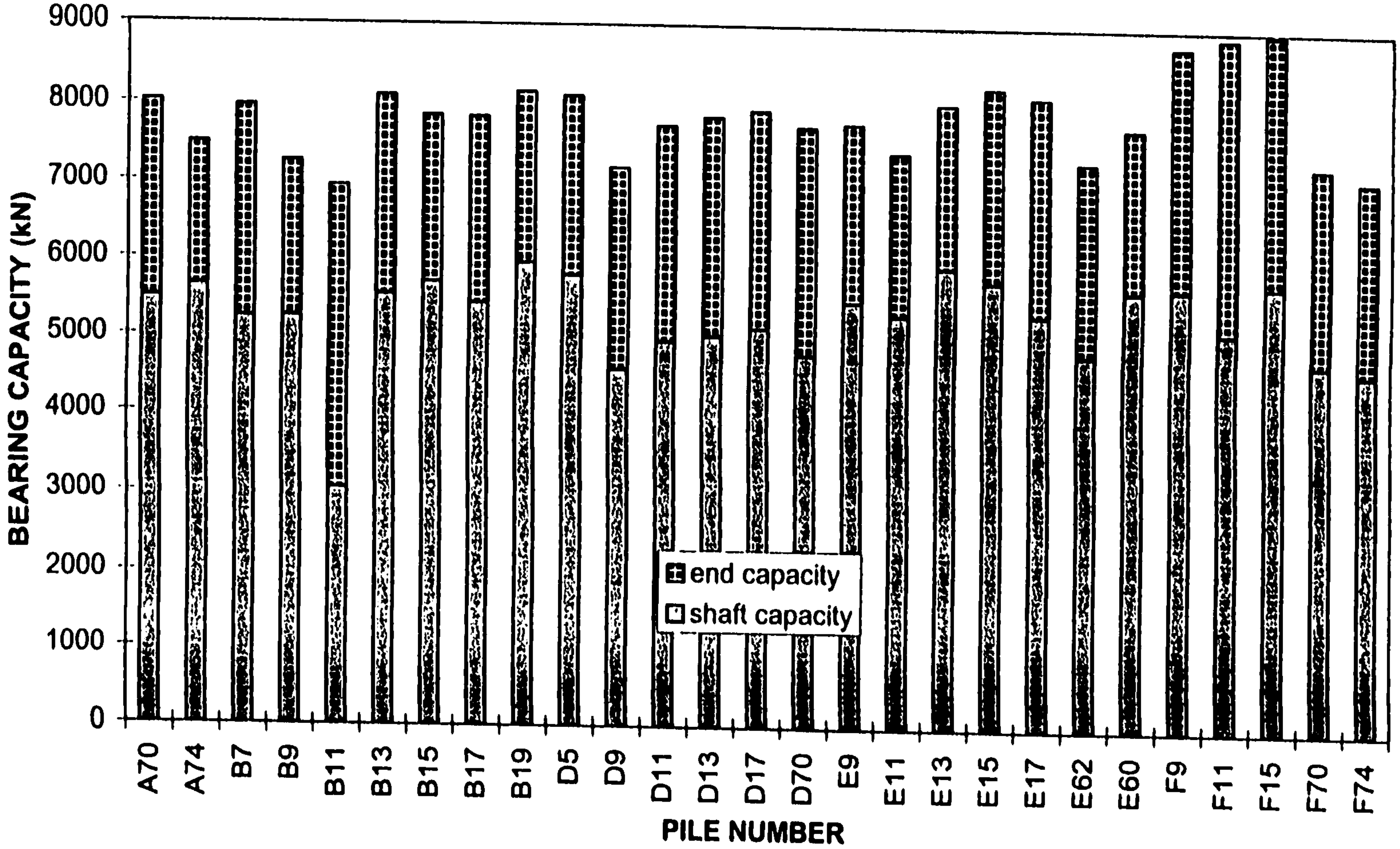

Figure 7.6 - Pile Shaft Resistance and Toe Resistance by CAPWAP, 1.0 m Pile

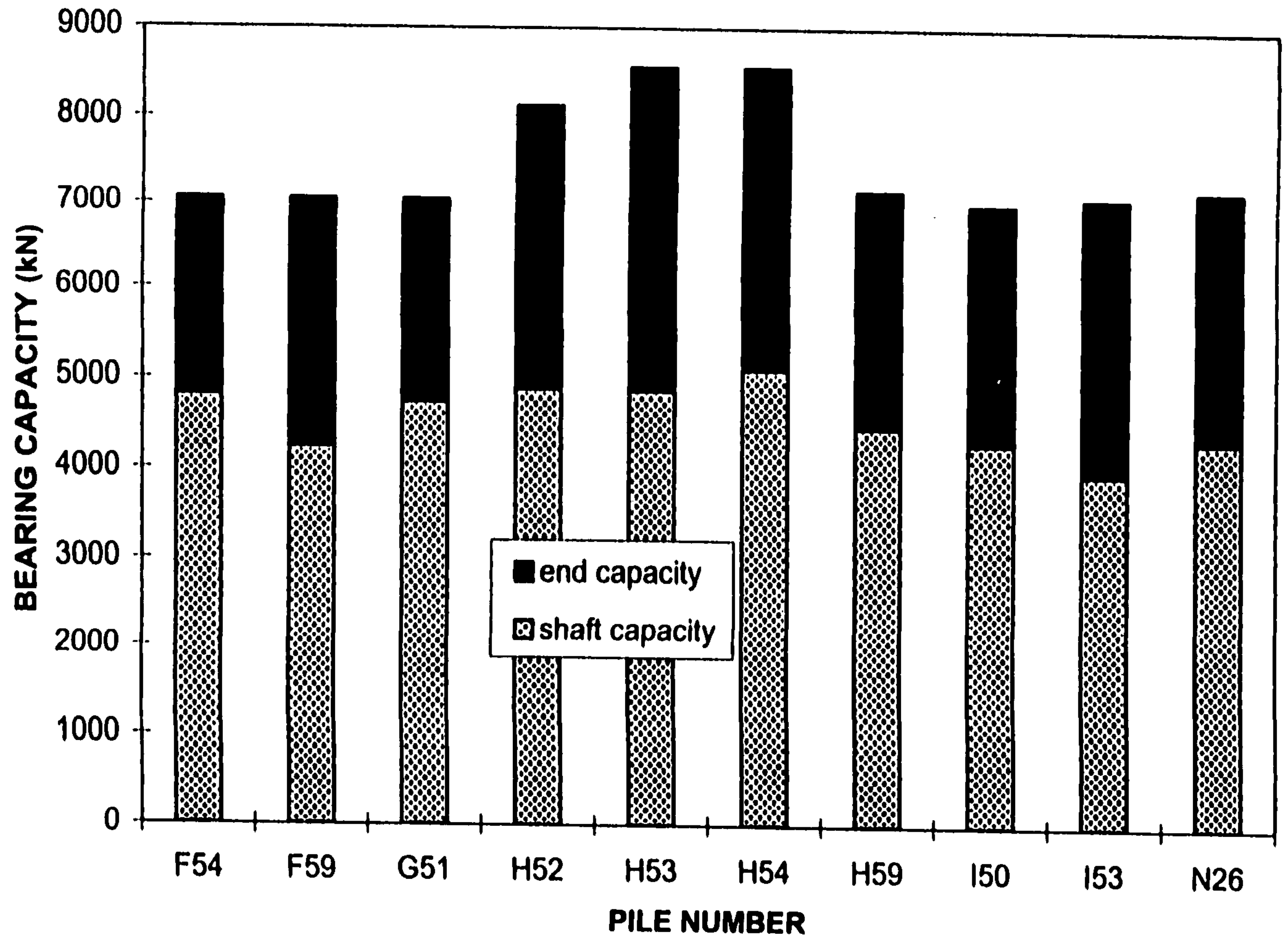

Figure 7.7 - Bearing Capacity by CAPWAP Method, 0.813 m Piles

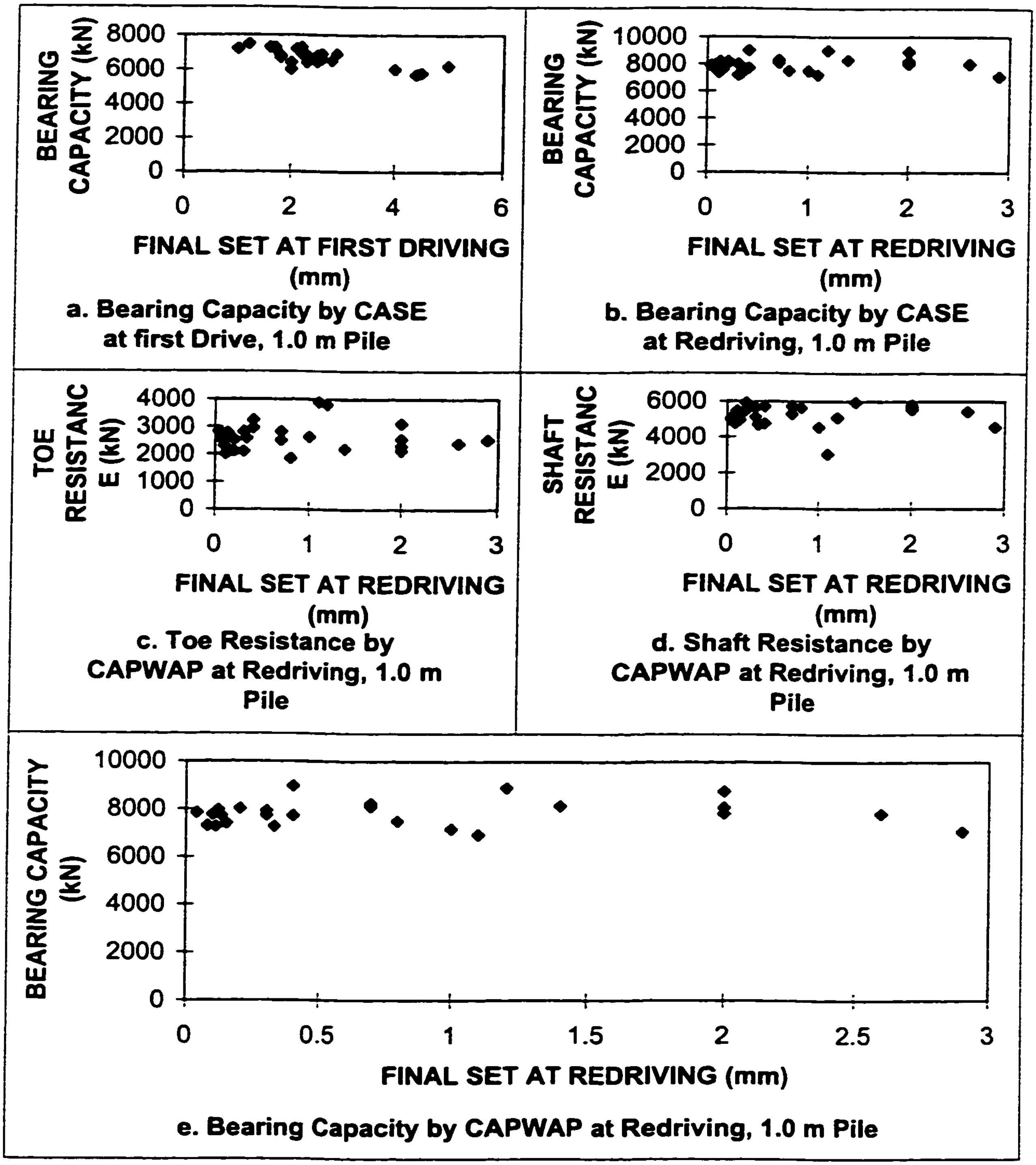

Figure 7.8 - Final Set-Bearing Capacity by CASE and CAPWAP, 1.0 m Pile

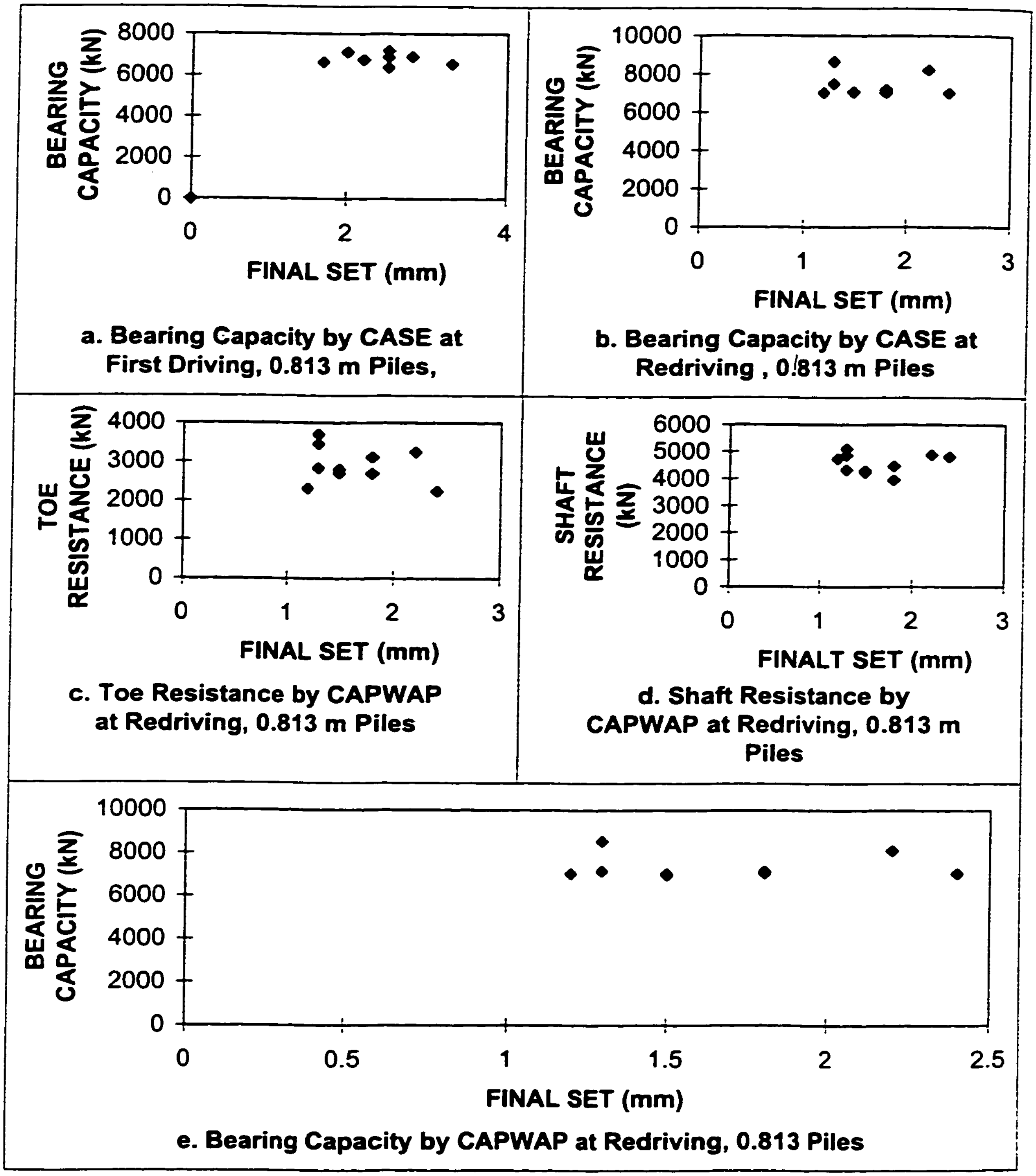

a. Bearing Capacity by CASE at First Driving, 0.813 m Piles,

b. Bearing Capacity by CASE at Redriving , 0.813 m Piles

c. Toe Resistance by CAPWAP at Redriving, 0.813 m Piles

d. Shaft Resistance by CAPWAP at Redriving, 0.813 m Piles

e. Bearing Capacity by CAPWAP at Redriving, 0.813 Piles

Figure 7.9 - Final Set-Bearing Capacity by CASE and CAPWAP, 0.813 m Pile

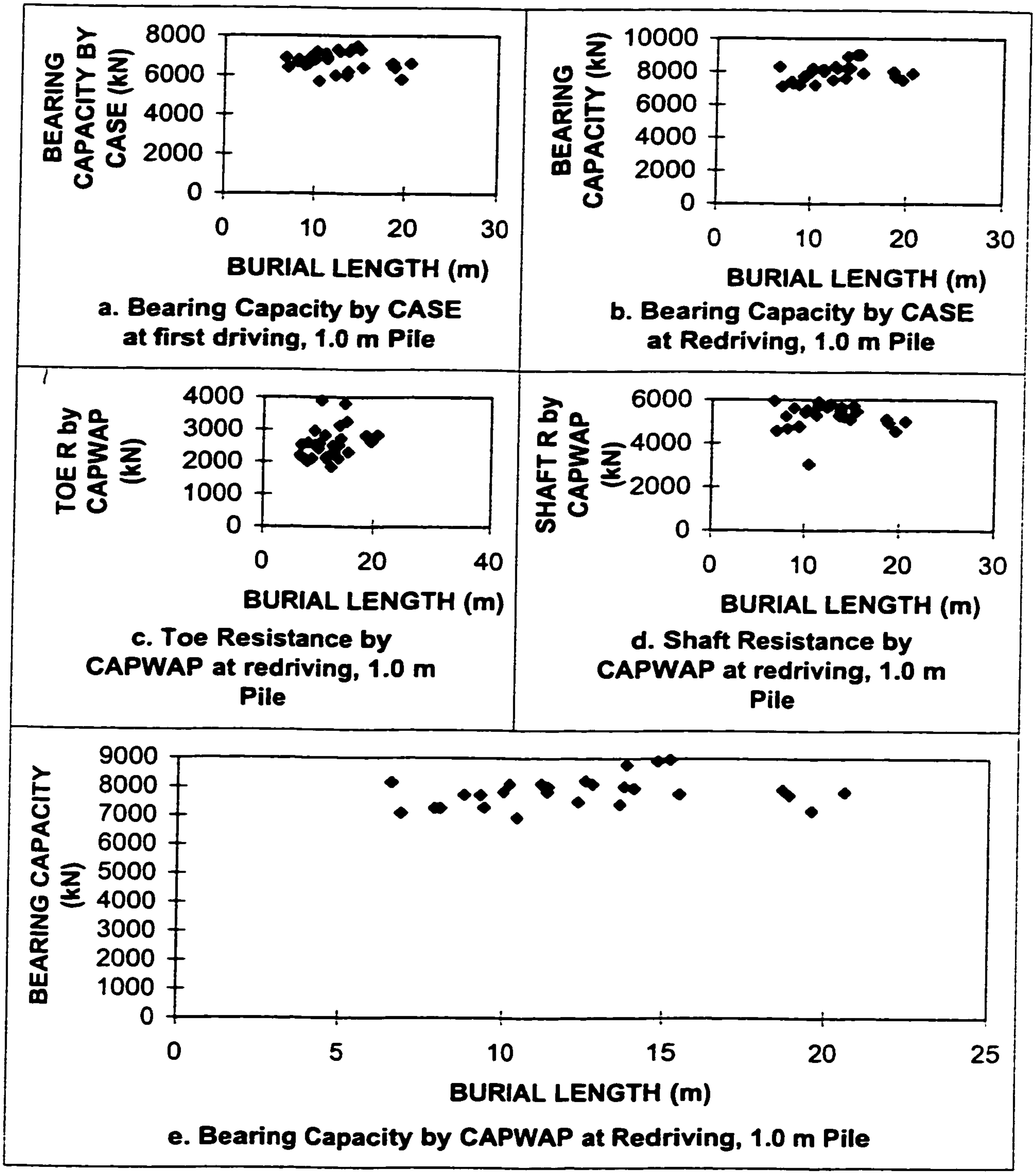

a. Bearing Capacity by CASE at first driving, 1.0 m Pile

b. Bearing Capacity by CASE at Redriving, 1.0 m Pile

c. Toe Resistance by CAPWAP at redriving, 1.0 m Pile

d. Shaft Resistance by CAPWAP at redriving, 1.0 m Pile

e. Bearing Capacity by CAPWAP at Redriving, 1.0 m Pile

Figure 7.10 - Burial Length - Bearing Capacity by CASE and CAPWAP, 1.0 m Pile

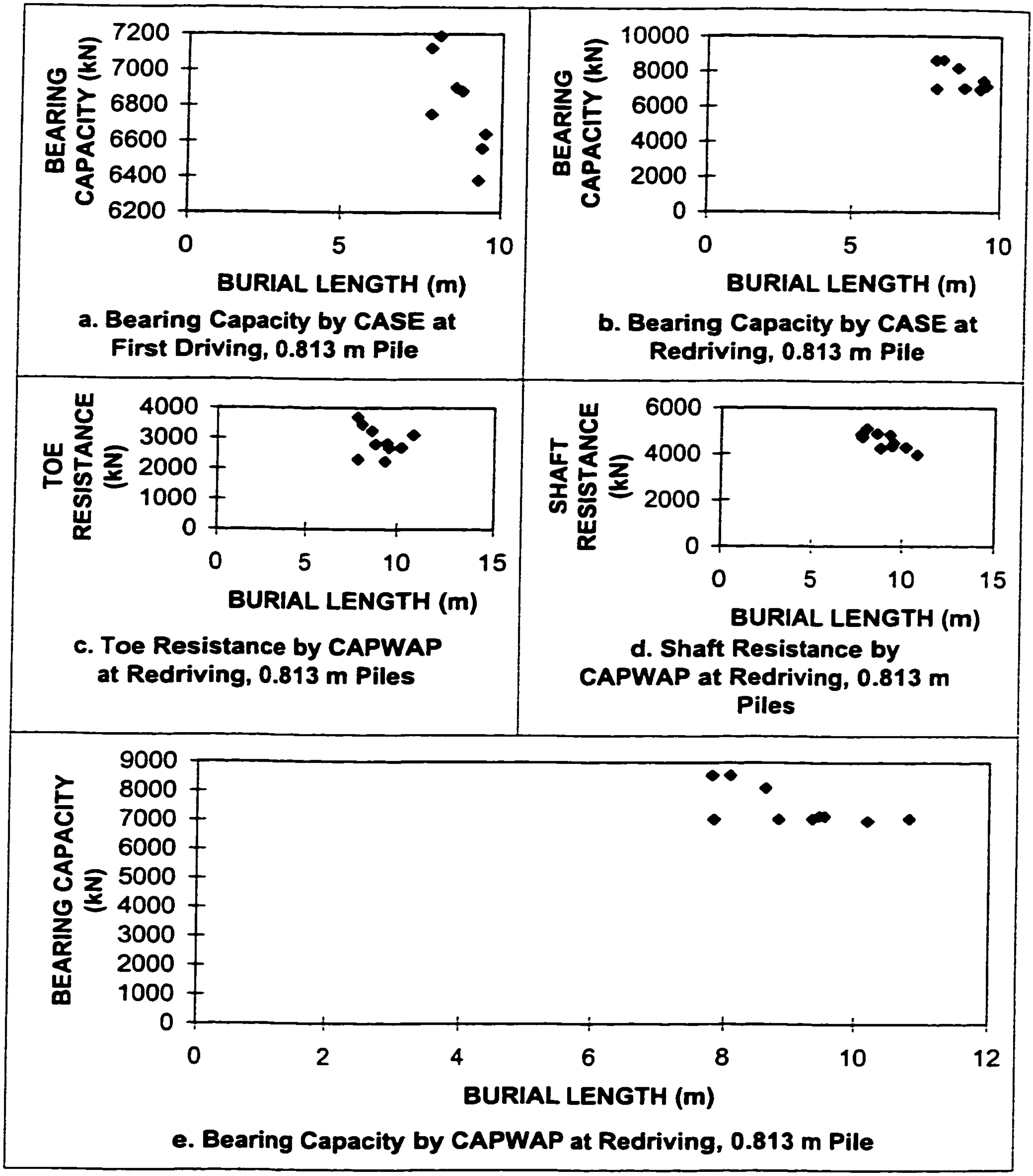

Figure 7.11 - Pile Burial Length-Bearing Capacity by CASE and CAPWAP, 0.813 m Pile

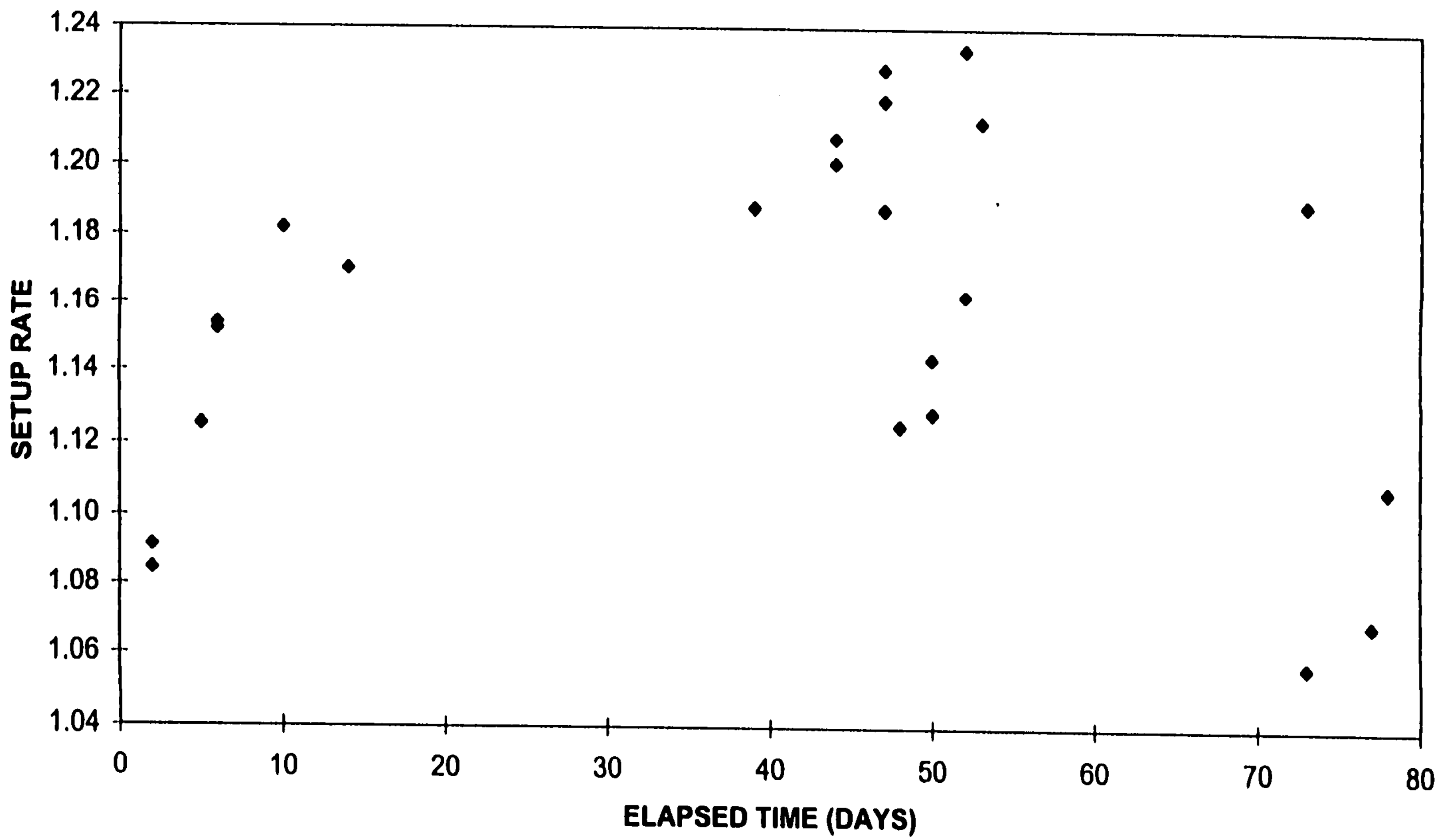

Figure 7.12 - Elapsed Time-Setup Rate, 1.0 m Pile

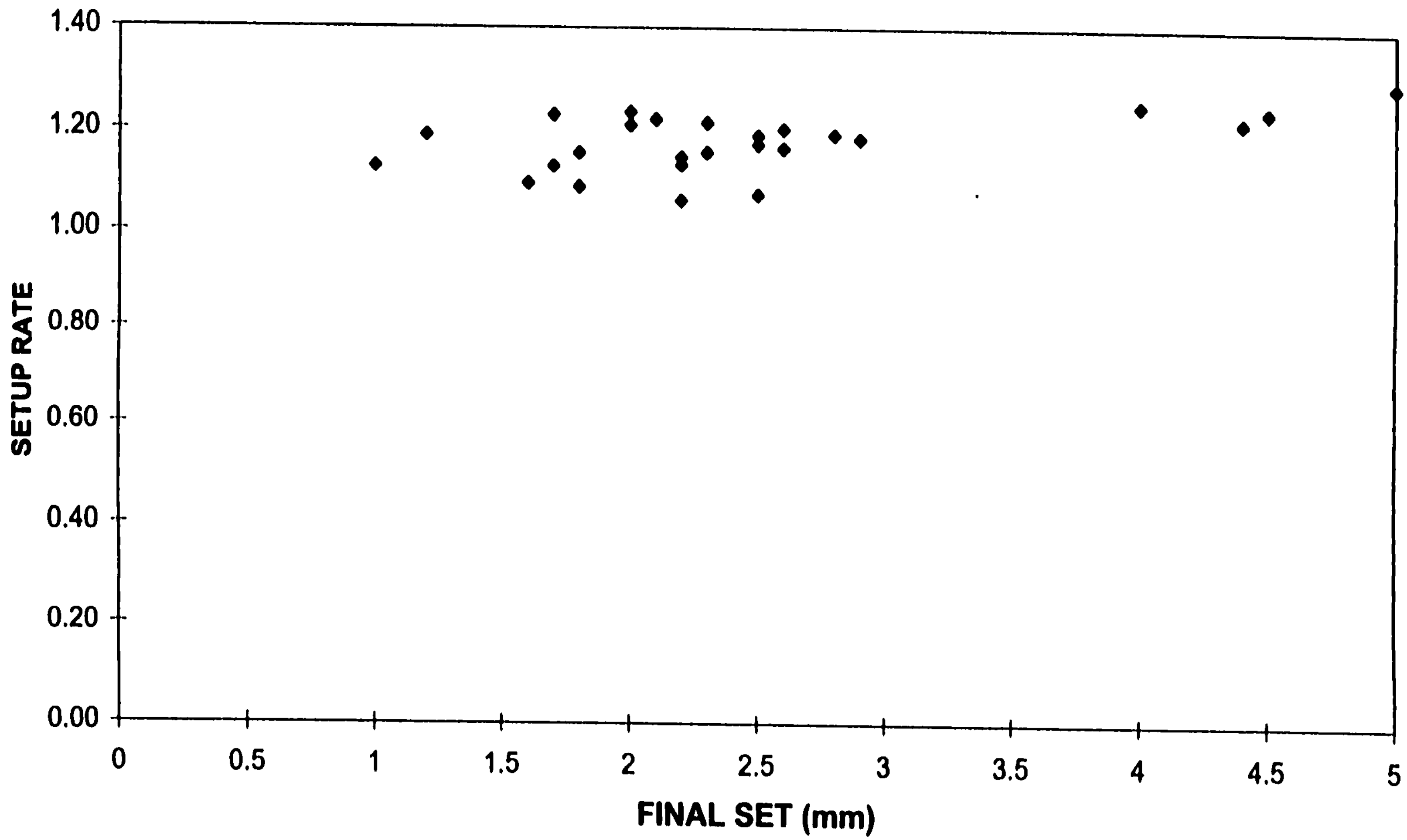

Figure 7.13 - Setup Rate-Final Set at First Driving, 1.0 m Pile

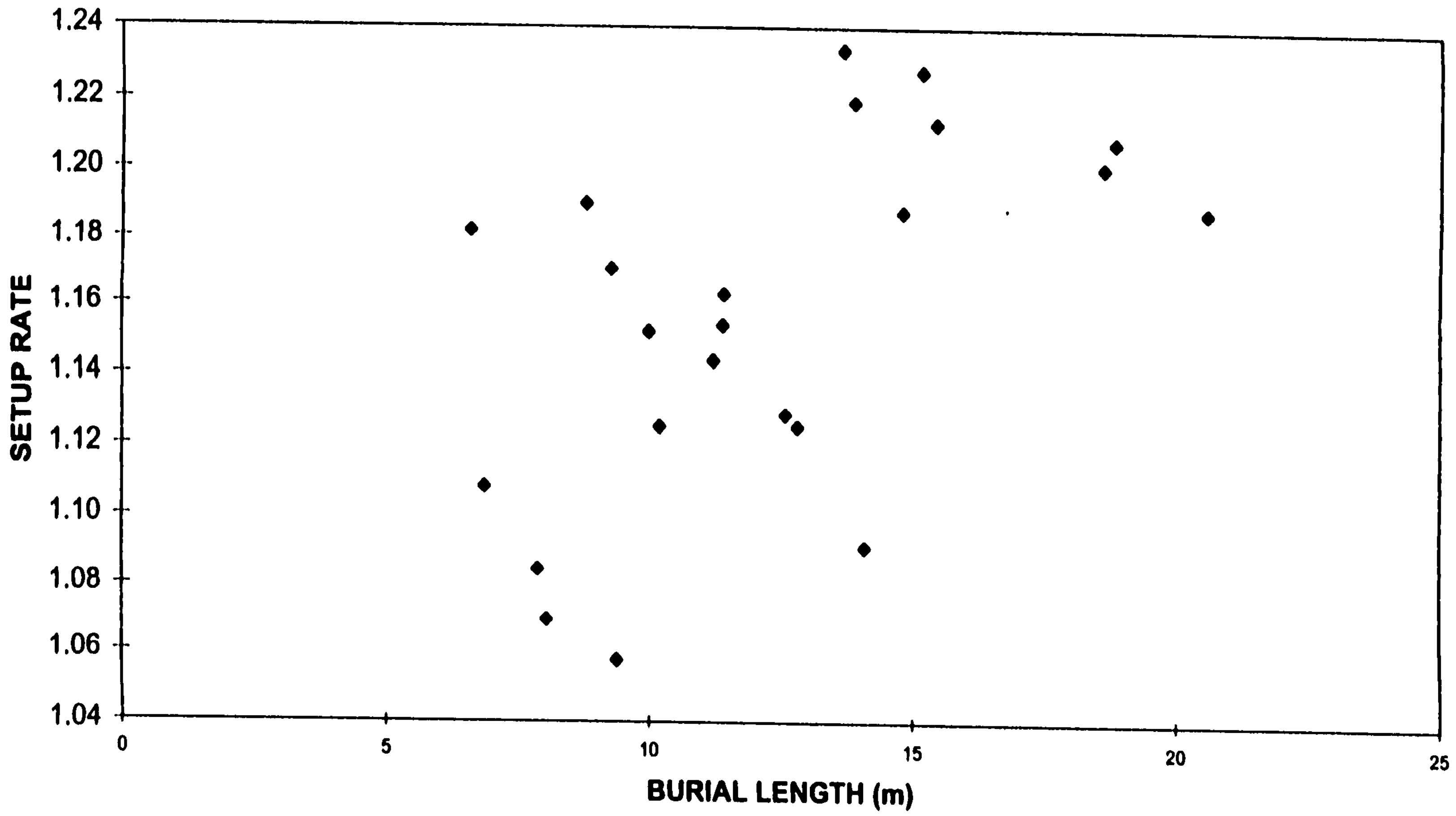

Figure 7.14 - Setup Rate-Pile Buried Length, 1.0 m Pile

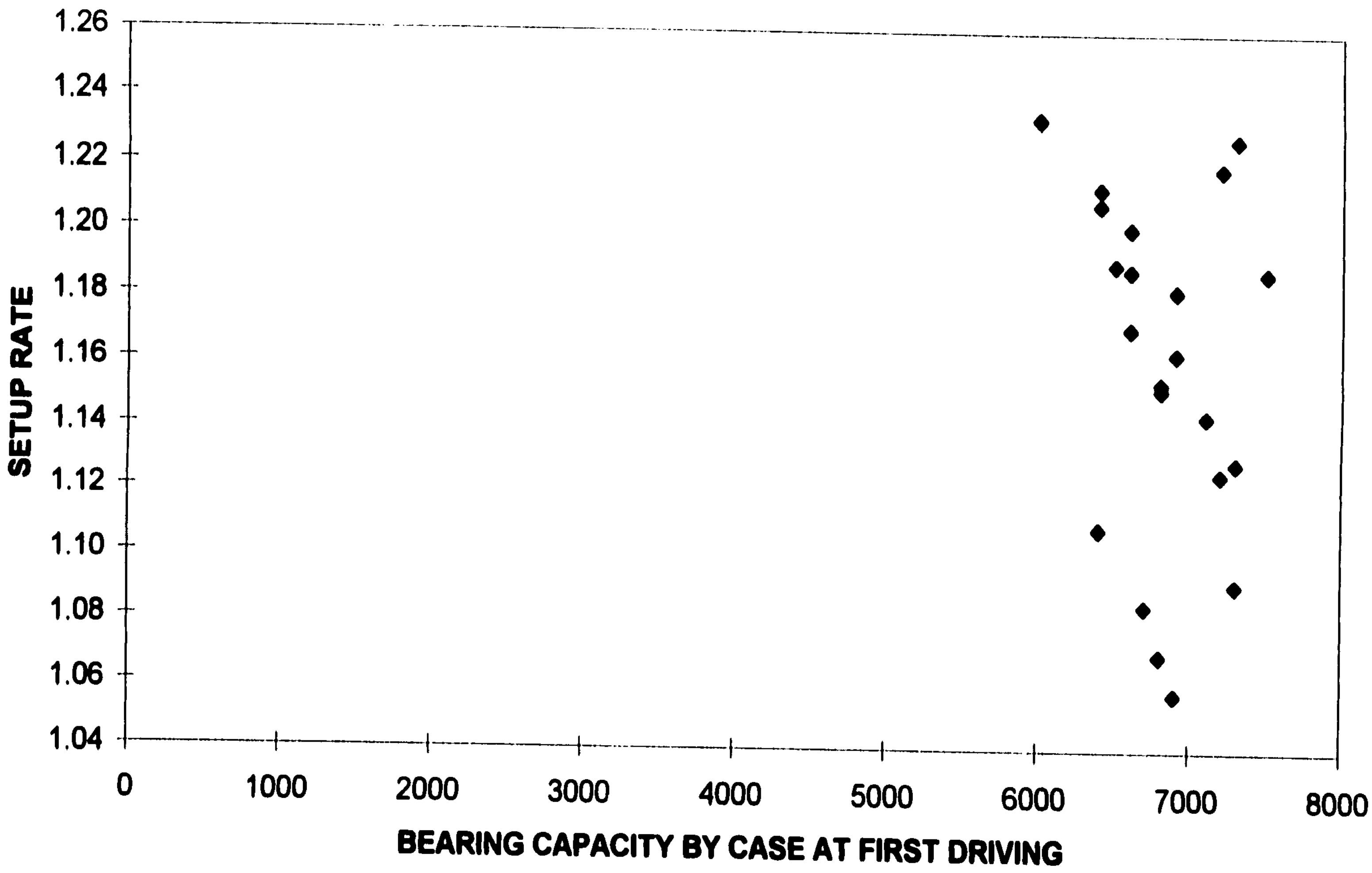

Figure 7.15 - Setup Rate-Bearing Capacity by CASE at first Driving, 1.0 m Pile

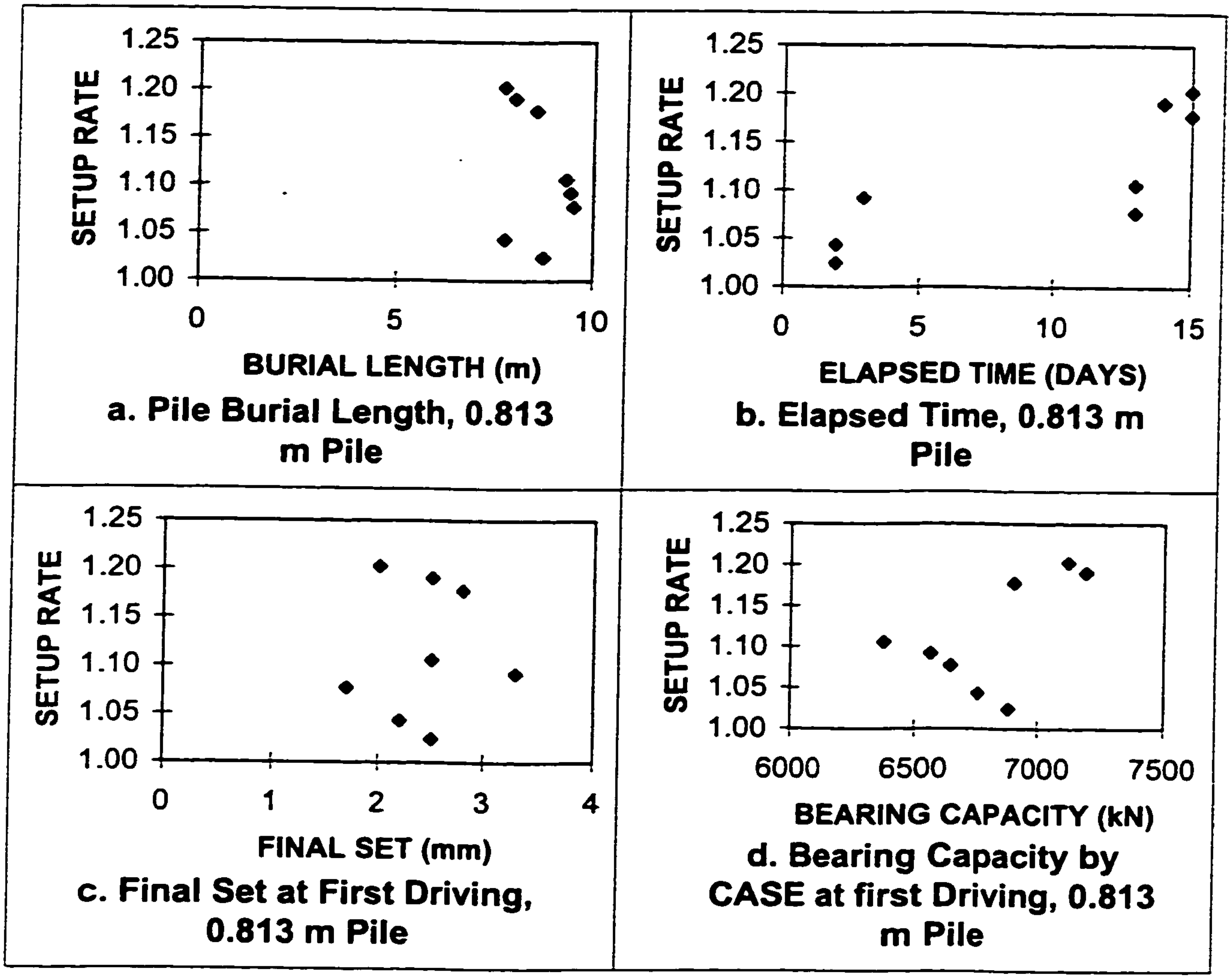

Figure 7.16 Setup Rate - effects by other factors

(Note: setup rate = bearing capacity by CAPWAP at redriving / bearing capacity by CASE at first driving)

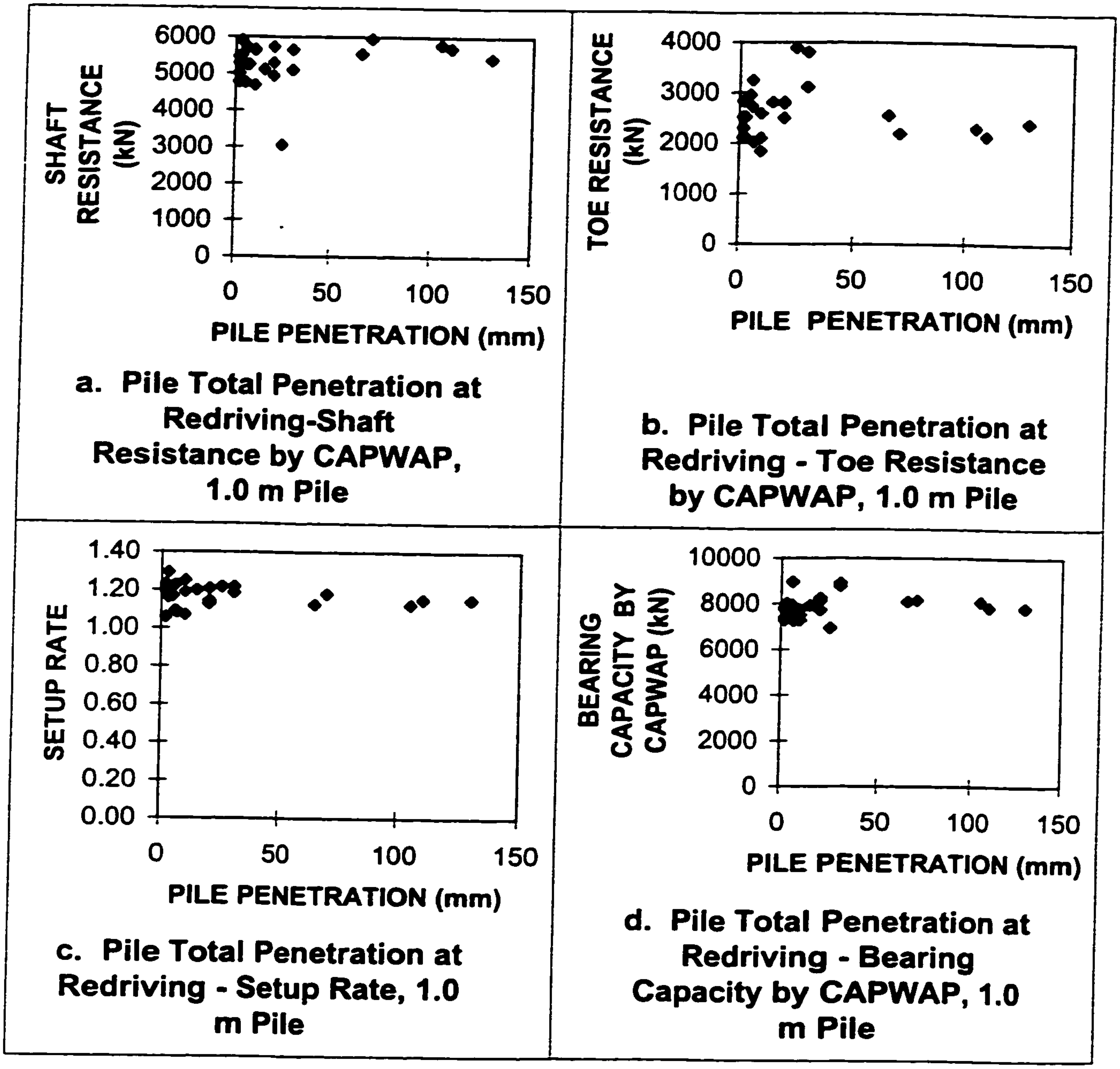

Figure 7.17 - Displacement at Redriving, 1.0 m Piles